The Dissertation Committee for Reza Ganjdanesh
Certifies that this is the approved version of the following dissertation:

Integrating Carbon Capture and Storage with Energy Production from Saline Aquifers

Committee:

Gary A. Pope, Supervisor

Kamy Sepehrnoori, Co-Supervisor

Steven L. Bryant

Mojdeh Delshad

Gary T. Rochelle

Integrating Carbon Capture and Storage with Energy Production from Saline Aquifers

by

Reza Ganjdanesh, B.E.; M.S.

Dissertation

Presented to the Faculty of the Graduate School of

The University of Texas at Austin

in Partial Fulfillment

of the Requirements

for the Degree of

Doctor of Philosophy

The University of Texas at Austin

May 2014

Dedication

To my family

Acknowledgements

I would like to express my special appreciation to my supervisors Dr. Gary A. Pope and Dr. Kamy Sepehrnoori for their constant encouragement, guidance and patience during my Ph.D. studies. I have always benefited from their expertise, brilliant ideas, and continuous enthusiasm.

I would also like to thank my research committee, Dr. Steven L. Bryant, Dr. Gary T. Rochelle, and Dr. Mojdeh Delshad, who have further enriched this dissertation with their suggestions and comments.

Special thanks go to the sponsors of the Geologic CO_2 Storage Joint Industry Project at The University of Texas at Austin. Also, I am grateful of Nigel Jenvey for his mentorship and support during my summer internship in BP. Without their support, this research would not be possible.

It has been a great pleasure working with several colleagues. I would like to thank Mohsen Taghavifar, Hamed Darabi, Behdad Aminzadeh, and Hamid Lashgari for their useful discussions and comments during my Ph.D. research. Special thanks to the outstanding departmental staff, Dr. Roger Terzian, Frankie L. Hart, Cheryl Kruzie, Joanna L. Castillo, and other administrative personnel in the Department of Petroleum and Geosystems Engineering.

Above all, I would like to thank my beloved parents, Azam and Alireza, my sister Mahdokht, and my brother Farhang, for their endless love and support through my entire life.

Integrating Carbon Capture and Storage with Energy Production from Saline Aquifers

Reza Ganjdanesh, Ph.D.

The University of Texas at Austin, 2014

Supervisor: Gary A. Pope

Co-Supervisor: Kamy Sepehrnoori

Technologies considered for separating CO_2 from flue gas and injecting CO_2 into saline aquifers are energy intensive, costly, and technically challenging. Production of dissolved natural gas and geothermal energy by extraction of aquifer brine has shown the potential of offsetting the cost of CO_2 capture and storage along with other technical and environmental advantages. The key is to recognize inherent value in the energy content of brine in many parts of the world. Dissolved methane in brine and geothermal energy are two of the sources of energy of many aquifers. For example, geopressured-geothermal aquifers of the US Gulf Coast contain sheer volume of hot brine and dissolved methane. For the same reason, the capacity of these geopressured-geothermal aquifers for storage of CO_2 is remarkable.

In this study, various reservoir models were developed from data of Texas and Louisiana Gulf Coast saline aquifers. A systematic study was performed to determine the range of uncertainty of the properties and the prospective of energy production from saline aquifers. Two CO_2 injection strategies were proposed for storage of CO_2 based on the results of simulation studies. Injection of CO_2-saturated brine showed several advantages compared to injection of supercritical CO_2. An overall energy analysis was

performed on the closed-loop cycles of capture from power plants, storage of CO_2, and production of energy.

The level of cost offset of CCS technology by producing energy from target aquifers strongly depends on the applications of the produced energy. The temperature of the produced brine from geopressured-geothermal aquifers is higher than the temperature of amine stripper column. Calculations for the strategy of injecting CO_2-saturated brine show that the amount of extracted thermal energy from geopressured-geothermal aquifers exceeds the amount of heat required for capturing CO_2 by amine scrubbing. In the process of injecting dissolved CO_2, compressors and pumps should run to pressurize the CO_2 and brine to be transported and achieve the required wellhead pressure. The preliminary estimations indicate that the produced methane provides more energy than that required for pressurization.

In the regions where the temperature gradient is normal, the temperature of the produced brine may not be high enough for using in the chemical absorption processes. Separation mechanisms driven by pressure difference are the alternatives for chemical absorption processes since the produced methane can be burned for running the compressors and pumps. Membrane process seems to be the leading technology candidate. The preliminary estimations show that the produced power by extracted methane and geothermal energy exceeds the power needed for membranes, compressors, and pumps.

Neither storage of greenhouse gases in saline aquifers nor production of methane and/or geothermal energy from these aquifers are profitable. However, designing a closed looped system by combining methods of capture, storage and production may pay off the whole process at least from the energy point of view.

Table of Contents

List of Tables

List of Figures

Chapter 1: Introduction

In the past few decades, greenhouse gases have increased in the atmosphere and aroused concerns about climate change (Herzog and et al. 2000). It is believed that greenhouse gases trap the heat radiated from air causing global warming and that carbon dioxide accounts for two thirds of the observed global warming. Methane and nitrous oxide are the other important greenhouse gases emitted into the atmosphere. In the past 150 years, the concentration of carbon dioxide in the atmosphere has surged from 280 ppm to about 400 ppm mainly as a result of burning fossil fuels.

Increasing the efficiency and developing alternative energies have been introduced as approaches to reduce the level of carbon dioxide in the atmosphere. Geological storage of carbon dioxide has been studied comprehensively in the past decade as a new solution to reduce the carbon content in the atmosphere. This idea consists of capturing carbon dioxide from sources of emission and injecting it into the deep geological formations. There are different options as storage strategies: Injecting CO_2 into mature oil and gas reservoirs, injecting CO_2 into depleted oil and gas reservoirs, injecting CO_2 in coal seams, and injecting CO_2 into deep saline aquifers. Among these candidates, deep saline aquifers have the highest estimated storage capacity.

On the other hand, it is erroneously believed that deep saline aquifers have no economic value. Some aquifers contain sources of energy such as dissolved methane and geothermal energy. Production of this energy along with the produced brine can help

offset the cost of Carbon Capture and Storage (CCS). Extraction of brine from target aquifers has been introduced as a solution to mitigate some technical and environmental issues of Carbon Capture and Storage technology. Some of these issues include pressure buildup in the aquifer, brine displacement and leakage of CO_2 through faults and abandoned wells. It seems that the extraction of brine and its energy should be considered as a way to mitigate several issues which prevent CCS from being feasible.

1.1 RESEARCH OBJECTIVES AND TASKS

The goals of this research were to investigate energy production from deep saline aquifers and its use in the capture and storage processes in order to improve the economics of CCS. Therefore, the capture and storage processes were studied at the same time. A compositional reservoir simulator was utilized to investigate this coupled process. Vikas (2002), Kumar (2004), Ozah (2005), Ghomian (2008) and Saadatpoor (2012) studied CO_2 storage in saline aquifers using a compositional simulator to better understand the carbon storage mechanisms and the best storage strategies. This research has taken into account both the carbon storage and energy extraction from deep saline aquifers.

The first task was to investigate different deep saline aquifers and the potential of production of energy from these aquifers. Methane dissolved in the brine and geothermal energy are the key sources of energy in deep saline aquifers. A comprehensive study was performed to find the formations containing these sources of energy and also the main aquifer parameters that help to maximize the extraction of energy from these aquifers. Geopressured-geothermal aquifers of US Gulf Coast were selected as the most promising reserves of energy from aquifers. Several different aquifer properties and development

strategies take part in the recovery of energy from these aquifers. Uncertainty analysis shows that significant amount of reservoir simulation and sensitivity analysis should be performed to find the favorable aquifer properties and development strategies. Therefore, statistical analysis by experimental design was performed to reduce the number of required simulation runs. Also, response surface methodology was used to correlate the objective functions with parameters.

The second task was to combine energy extraction and CO_2 storage into one coupled process. The main goal of this task was to co-optimize the production of energy and storage of CO_2. Different CO_2 injection strategies including injection of supercritical CO_2 or CO_2-saturated brine as well as various development strategies for injection and production were studied. The interaction between CO_2 and in-situ fluids is one of the important factors in the amount of stored CO_2 and produced energy. Injected CO_2 acts as injected fluid to improve the recovery of energy. Therefore, a phase behavior model was needed to model the interaction between CO_2, brine and dissolved gases under both aquifer and surface conditions. Since methane forms the majority of the in-situ gas, only CH_4 was used as representative of natural gas to model the phase behavior. Horizontal and vertical wells were utilized for both injection and production and the results were compared. Finally, a simplified energy balance was performed to compare the produced energy and the energy required for capture of CO_2 from coal-fired power plants and storage in deep saline aquifers.

The third task was to integrate the production and storage with CO_2 capture methods. Two prominent capture methods were introduced for separation of CO_2 from flue gas. The energy cost for separation of CO_2 by different capture methods and the energy cost of the pressurization of fluids up to wellhead pressure were provided. Also, the energy revenue from geopressured-geothermal aquifers and hydrostatically-pressured

aquifers were estimated. The energy costs and revenue for different capture methods and different aquifers conditions were scaled up for CO_2 emission rate from a 500 MW power plant. The energy balance analysis was performed for two aquifer conditions and two capture methods. Finally, a comparison was performed between all methods based on the results of the energy balance analysis.

1.2 METHODOLOGY

The first step in performing this research was to review the literature related to this work. During 70's and 80's, the Department of Energy (DOE) conducted a comprehensive research on the energy content of geopressured-geothermal aquifers in the Gulf Coast of the United States and also the feasibility of energy production from these aquifers. This has been the only study on the economic value of deep saline aquifers. In addition, literature related to CO_2 capture and storage methods as well as constraints and hazards regarding to storage technology were reviewed.

Numerical simulation was utilized as a tool to better understand the effect of different fluid and formation parameters. Several phase behavior and geologic models were built using the data from the reviewed literature. Since many parameters were involved in the models, a large number of numerical simulations were required. Therefore, experimental design and response surface methodology were used to minimize the number of simulations.

Different combined cycles of energy production and CCS were designed in this study. Since improving the economics of CCS was the main goal of this research, an overall economic study of different cycles was necessary. However, these cycles consist of numerous components. Gathering the data of capital and operating costs of these parts

were beyond the scopes of this study. Instead, a simplistic energy balance analysis was performed for each cycle. In fact, the amount of produced energy was compared to the amount of energy consumed for capture and storage processes. Finally, the overall energy balance was used to compare the cycles with each other.

1.3 REVIEW OF CHAPTERS

This dissertation is organized into seven chapters. Chapter 2 contains the literature review related to this research. This chapter has been divided into three sections. These sections are about energy production from deep saline aquifers, CO_2 storage, and CO_2 capture from power plants.

Chapter 3 describes the numerical model used to simulate the energy production from deep saline aquifers and geologic storage of CO_2. All of the specifications of the model, including petrophysical properties, fluid properties and rock-fluid properties are explained in this chapter. Also, the applied wellbore model and numerical methods are described in this chapter.

Chapter 4 deals with the first objective of this research, which is about the production of energy from deep saline aquifers. This chapter mainly focuses on production of energy from geopressured-geothermal aquifers.

Chapter 5 deals with how production of energy from geopressured-geothermal aquifers can be combined with storage of CO_2 in these aquifers. It describes the effect of injecting CO_2 on recovery of energy and effect of produced energy on overall economy of CCS.

Chapter 6 introduces the idea of injecting CO_2 in hydrostatically-pressured aquifers. The CO_2 capture methods are integrated with energy production and CO_2

storage. The overall energy balance of coupled energy production and CO_2 storage are discussed for various scenarios.

Chapter 7 presents a summary of the results of the chapters. It also discusses the proposed ideas and strategies of coupled energy extraction and CCS. Finally, recommendations for future works are presented.

Chapter 2: Literature Survey

Three different technologies have been used in this research to develop a new idea. The first technology is the production of energy from deep saline aquifers. The second technology is the geologic storage of greenhouse gases. The last one is the technology of capture of CO_2 from coal-fired power plants. Since the material used in this study consists of a wide range of information, the literature review was organized into three sections along these same lines.

2.1 ENERGY PRODUCTION FROM GEOPRESSURED-GEOTHERMAL AQUIFERS

The production of energy from deep saline aquifers has been mainly focused on production from geopressured-geothermal aquifers of US Gulf Coast. During 70's and 80's, Department of Energy funded several comprehensive studies on these aquifers. Therefore, the majority of available literature on this topic is related to the DOE program.

Formations of abnormally high pressure and temperature at depths exceeding 10,000 feet are called geopressured-geothermal aquifers. According to Jones (1976), geopressured aquifers have pressures exceeding the hydrostatic pressure of water column with salinity of 80,000 ppm that can be estimated by a pressure gradient of 0.465 psi/ft.

Dickinson et al. (1953) discuss the geology of the geopressured aquifers of the Gulf Coast. It is stated that the pressure gradient of the sediments above the geopressured

formations is about 0.465 psi/ft which is the normal hydrostatic pressure exerted by the column of brine. Below these formations, units of sand and shale at abnormal pressures exist. These high pressured zones are known as geopressured formations. It is believed that the formation of geopressured aquifers is the result of compaction phenomena. The weight of the overburden tends to decrease the volume and porosity of the underlying sediments. Since the compressibility of sand and water is very low, the only shrinking mechanism is water expulsion, which is controlled by the permeability of the surrounding rocks. If the water cannot escape through the overlying rocks, a portion of the overburden load will be carried by the underlying load. Therefore, the pressure of both formation and fluid increases abnormally. This pressure gradient may approach the lithostatic pressure gradient of 1.0 psi/ft.

After the energy crisis of the 1970's, the United States began to explore for new unconventional hydrocarbon sources. Geopressured-geothermal aquifers were a priority for research because they had significant amounts of dissolved natural gas and potentially recoverable heat. Estimates by different investigators of dissolved natural gas in geopressured sandstones in Gulf of Mexico cover a wide range. Hise (1976) estimate of the in-place natural gas was 3,000 trillion SCF while Jones (1976) estimate was 49,000 trillion SCF. Wrighton (1981) estimated that the geopressured-geothermal resource of the northern Gulf of Mexico could exceed 1,000 trillion SCF of recoverable natural gas. These numbers are significant and several times bigger than conventional natural gas resources. However, the recovery factor was estimated to be less than three percent (Wallace et al., 1978).

At the beginning of 1970's, the Department of Energy commenced to explore the unconventional hydrocarbon resources. DOE funded several studies related to the development of the geopressured-geothermal reservoirs as prospective sources of both

heat and natural gas. Several "wells of opportunity" were tested to assess the amount and quality of the natural gas associated with the geopressured-geothermal waters. Production of the Pleasant Bayou No. 2 well located in Brazoria County, Texas is an example of a detailed investigation of geopressured-geothermal energy (Riney, 1991). The goal of the project was to provide the information necessary to assess the production characteristics of geopressured-geothermal reservoirs and their economic potential. The Pleasant Bayou No. 2 well produced 330 million SCF of natural gas from 1979 to 1983. Reservoir simulation development and simulation case studies were performed at The University of Texas at Austin (Isokrari, 1976, Knapp et al., 1977, Ohkuma et al., 1979a, Ohkuma et al., 1979b and MacDonald et al., 1981). Another well included in this study was Gladys McCall No. 1, which is located in Cameron Parish, Louisiana. This well produced over 676 million SCF of natural gas and 27 million STB of hot brine from 1983 to 1987 without any significant pressure decline (Riney, 1988). John (1988) reviewed the geology of the Gladys McCall in detail.

Gregory et al. (1980) discuss the quality of the geopressured formations of the Gulf Coast. They explained that the original porosity and permeability of the formations are compromised as a result of diagenesis. Thus, the permeability of geopressured sandstones, especially in South Texas, would not be expected to exceed 100 md. However, permeabilities higher than 100 md are not unlikely, especially in Louisiana. The core and pressure build-up data from Pleasant Bayou No. 2 indicate permeabilities greater than 150 md.

Knapp et al. (1976) categorize the drive mechanisms in geopressured reservoirs into four groups. These mechanisms are (1) reservoir fluid expansion (2) reservoir rock compaction (3) surrounding shale water influx and (4) ex-solution of natural gas from brine.

Geer et al. (1978) claim that natural gas in geopressured aquifers may exist as a continuous gas phase, as a dispersed gas phase or as gas dissolved in the brine. It is concluded that all three types of natural gas in geopressured aquifers can be produced. The pressures of the aquifers are high enough to allow the water flow to the surface. Thus, the solution gas is produced along with produced water. In the case of watered-out geopressured natural gas reservoirs, the expansion of natural gas as a result of declining pressure may lead to a higher gas saturation and mobility of gas phase. The gas cap not produced during conventional production may be coned into the production well as the pressure declines in the aquifer.

Griggs (2005) summarizes several successful producing wells which were drilled and tested in the DOE study. Also, he carried out a comprehensive study of the cost of production and surface facilities and claimed that by increase in natural gas price in 2000's and improvement in technology of production and methane extraction from brine, geopressured-geothermal resources could be a viable alternative for conventional hydrocarbon sources.

Taggart (2010) proposed the idea of injecting supercritical CO_2 into the aquifer to expel methane from the brine. He states that when the CO_2 mixes with the brine in the aquifer, the methane will come out of solution and flow upward where it can be captured and produced from a production well at a higher elevation in the aquifer.

The other available source of energy from deep saline aquifers is geothermal energy. Geothermal energy is a small contributor to the energy supply of the United States. The geothermal resources mainly exist in the western regions of the United States. In addition to these areas, geothermal energy exists at the large depths of geopressured-geothermal aquifers of the United States Gulf Coast. The water of these aquifers contains dissolved natural gas. Therefore, after lowering the pressure to extract the dissolved

methane, hot water can be used to generate electrical energy. An advantage of geothermal resources is that the temperature of the resource drops very slowly. Dorfman et al. (1974, 1976) estimate that the energy content of geopressured-geothermal aquifers of Texas may be about 20,000 MW excluding the natural gas.

Knapp et al. (1977) express that the temperature gradient in the hydrostatic pressured sediments of the Gulf Coast is about 1.5°F/100ft. In the geopressured zones, this gradient exceeds over 3°F/100ft. Temperature at the depth of 10,000 ft ranges between 225 to 300 °F and below 15,000 ft, exceeds 300 °F.

There is vast amount of reservoir data available about Frio and Wilcox formations of the Texas Gulf Coast (Bebout, 1982 and 1983). Figure 2-1 illustrates the well-suited identified fairways in these formations.

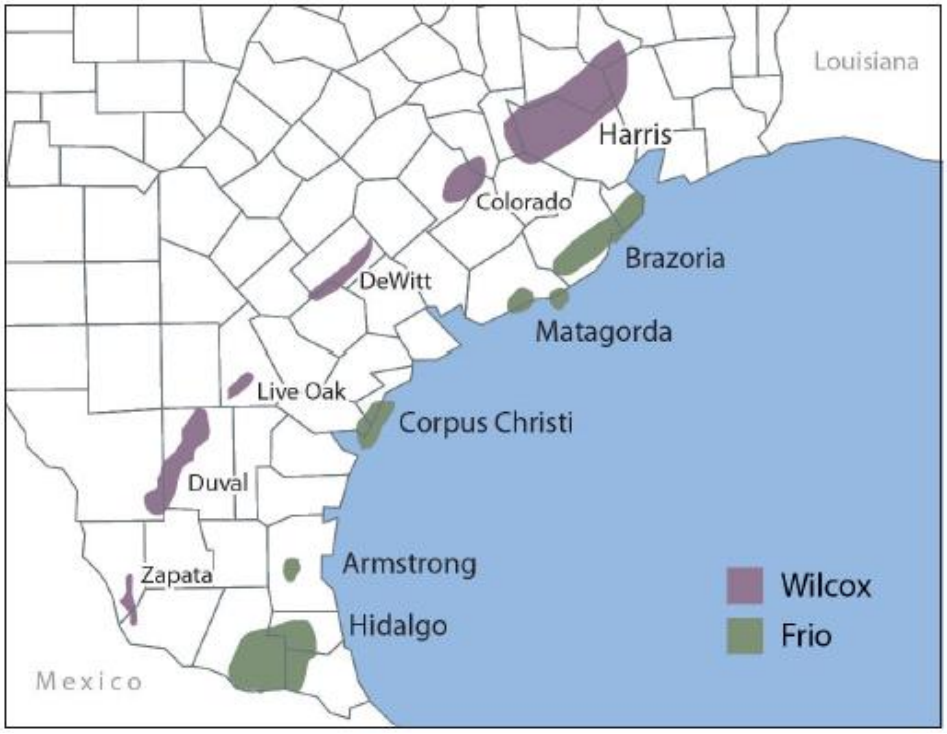

Figure 2-1: Geopressured-geothermal fairways within Frio and Wilcox (Esposito, 2011).

Esposito et al. (2011) investigated the energy resource from the fairways of Frio and Wilcox formations of the Texas Gulf Coast using the available data from the studies of the Bureau of Economic Geology (BEG) at The University of Texas at Austin. Tables 2-1 and 2-2 represent their estimate for the Wilcox and Frio formations, respectively. In another study (Esposito et al., 2012), they estimate the amount of recoverable energy by determining the amount of methane and thermal energy that can be produced during a 20-year production period. Also, they compare the energy sources of Texas and Louisiana. Table 2-3 summarizes the total thermal energy in place as well as recoverable energy from natural gas and potential electricity from thermal energy from Louisiana and Texas. Five geopressured-geothermal formations have been identified in Texas: Lower Wilcox, Lower Frio, Vicksburg-Jackson, Lower Claiborne, and Upper Claiborne. It is concluded that the southern Vicksburg-Jackson has the highest quality geothermal resource because of high sand thickness and temperatures. Also, the estimate of Louisiana resources is considerably high though the temperature of resources is lower than Texas ones.

Table 2-1: Total resource estimate for Wilcox fairways.

Wilcox Fairway	Area (mi^2)	Total Thermal Energy (BTU)	Total Methane (MMSCF)
Zapata	92.31788	9.86E+16	4.72E+07
Duval	550.4309	5.55E+17	2.52E+08
Live Oak	79.57106	9.67E+16	3.61E+07
De Witt	244.5072	1.98E+17	9.65E+07
Colorado	316.3529	3.00E+17	1.21E+08
Harris	1732.795	2.10E+18	1.10E+09
Total	3015.975	3.36E+18	1.65E+09

Table 2-2: Total resource estimate for Frio fairways.

Frio Fairway	Area (mi^2)	Total Thermal Energy (BTU)	Total Methane (MMSCF)
Hidalgo	1146.441	1.83E+18	4.85E+08
Corpus Christi	256.0952	2.36E+17	6.10E+07
Matagorda	199.7002	1.54E+17	5.19E+07
Brazoria	637.341	6.99E+17	1.72E+08
Armstrong	74.93585	1.43E+17	5.19E+07
Total	2314.513	3.06E+18	8.22E+08

Table 2-3: Thermal energy in place and recoverable energy from Texas and Louisiana.

Formation	Recoverable Natural Gas (Tcf)	Thermal Energy in Place (BTU)	Electricity Generation (MW)
Louisiana	95.2	4.7E+18	2,620
Lower Wilcox	13.7	1.7E+18	939
Lower Frio	6.92	1.6E+18	429
Vicksburg-Jackson	6.82	2.5E+18	1,032
Upper Claiborne	1.98	1.8E+17	46
Lower Claiborne	0.95	1.0E+17	54
Total	125	1.1E+19	5,120

Natural gas dissolved in brine has been an important energy source in Japan (Marsden, 1979). This gas is produced from shallow aquifers which is formed from sandstone and siltstone usually found at depths of 500 to 1000 m. Therefore, they should not be confused with the much deeper abnormally pressured aquifers of Gulf Coast area. Japan has faced drastic land subsidence as a result of reservoir depletion caused by brine production. Ohkuma (1986) suggested that the reinjection of produced brine could

prevent or minimize land subsidence and also improve the ultimate recovery of dissolved natural gas. Quitzau (1981) and Quong (1982) claimed that the brine reinjection would be economically infeasible. However, it seems that they did not take into account the possible additional natural gas recovery with reinjection.

2.2 GEOLOGIC CARBON STORAGE

During the past forty years, the annual global emission of carbon dioxide has increased from 21 to 38 Gigatonnes (IPCC, 2007). In order to stabilize the CO_2 level in atmosphere, new technologies are required in addition to more efficient use of energy. Capture and storage of CO_2 is a technology that can contribute to mitigating this problem.

2.2.1 Options for geologic storage of CO_2

Parson et al. (1998) and Gale (2004) introduced three options for geologic storage of CO_2. These three options are oil and gas reservoirs, deep saline aquifers and deep unmineable coalbeds. Orr (2004) reviews these three options and their estimated CO_2 storage capacities. These estimates are summarized in Table 2-4.

Table 2-4: Estimated CO_2 storage capacities of geologic formations (Gigatonnes).

Geologic Formation	Parson and Keith	Gale
Oil and gas reservoirs	740-1850	920
Deep saline aquifers	370-3700	400-10,000
Unmineable coalbeds	370-1100	40

These estimates show that these formations are large enough to store significant amounts of CO_2.

2.2.1.1 Oil reservoirs

Oil reservoirs are known for having structural seals that trap hydrocarbons for millions of years. Also, regulations have been set for gas injection in these structures. Therefore, oil fields seem to be the first candidate for storing captured CO_2. During the past four decades, a vast amount of experience has been acquired regarding injecting CO_2 into mature oil reservoirs. SACROC (Hawkins et al., 1996) and North Cross (Mizenko, 1992) were among the first successful projects where the CO_2 separated from the natural gas produced from southwest Texas fields was injected to improve the oil recovery. But, most CO_2 injection projects have been using the CO_2 extracted from the natural reservoirs. For example, Permian Basin projects of West Texas have been using the CO_2 transported by pipeline from New Mexico and Colorado (Tanner et al., 1992, Stein et al., 1992, Lambert et al., 1996).

Another ongoing gas injection project in which the injected stream contains a large fraction of CO_2 is Prudhoe Bay project (McGuire et al., 1995). Injecting the solvent containing CO_2 and light hydrocarbons allows the multi-contact miscibility throughout the reservoir. The objective for most of these gas injection projects is to improve the oil recovery. In fact, all the efforts have been to minimize the amount of injected CO_2 to assist the economics of the process. Ghomian (2008) discusses the operating conditions for maximizing oil production and for maximizing CO_2 storage, which are not the same. Thus, the engineering design objectives should be modified for co-optimization of oil recovery and CO_2 storage. Jessen et al. (2005) discuss that injection of CO_2 into the

capillary pressure zone or injection into the aquifer below the water-oil contact might be alternative strategies for co-optimization. Many more oil reservoirs would be candidates for CO_2 injection if sufficient volumes of CO_2 were available by minimizing the cost of CO_2 capture or by offering incentives for CO_2 storage. Kovscek (2002) discusses the criteria for reservoir characteristics that might be the candidates for CO_2 storage.

The first large field for CO_2 storage in an oil reservoir is the Weyburn field in Saskatchewan (Malik et al., 2000). The source of CO_2 in this project is a coal-gasification plant in North Dakota. This CO_2 is transported to the Weyburn field through a pipeline. Also, a monitoring plan is performed to detect the potential leakage of CO_2 from the reservoir (Moberg et al., 2002).

2.2.1.2 Gas reservoirs

CO_2 injection into gas reservoirs has never been performed because of economic shortcoming. Oldenberg et al. (2002, 2004) proposed the injection of CO_2 into gas reservoirs for pressure maintenance or condensate vaporization. In gas reservoirs with condensate saturations, CO_2 can vaporize the condensate and improve the hydrocarbon recovery. CO_2 could be used as a multi-contact miscible flood to recover natural gas and condensate (Jessen et al., 2003).

Orr (2004) claims that a greater mass of CO_2 from burning the CH_4 produced from a natural gas reservoir could be stored in the same reservoir at the same pressure and temperature because one mole of CO_2 is produced by burning one mole of methane and the density of CO_2 is higher than the density of methane at the same pressure and temperature. The higher density of CO_2 provides the opportunity to inject a mixture of CO_2 and N_2. In fact, separation of all of N_2 from CO_2 would not be necessary to match

the injected and produced volumes. He also discusses that the mixing of injected gas and in-situ methane would be another issue of injecting CO_2 into the natural gas reservoirs resulting in lower quality of the produced natural gas. Presence of high concentrations of CO_2 in produced natural gas would require the costly separation of CO_2 from CH_4. For reservoirs with good vertical communication, Oldenberg et al. (2002) suggest that the denser CO_2 can be injected in lower layers of reservoir and methane can be produced from the top. It is possible that higher density of CO_2 would assist to avoid significant mixture of CO_2 and CH_4.

2.2.1.3 Deep saline aquifers

Orr (2004) reported that the sources of anthropogenic CO_2 are distributed geographically in many places. Finding oil and gas reservoirs in the vicinity of all of CO_2 emission sources may be unlikely. But, deep saline aquifers are widely distributed.

Pope et al. (2003) performed a reservoir simulation study to better understand the aspects of storage of CO_2 in deep saline aquifers. This study concluded that the injected CO_2 would move more likely through high permeability paths. Since producers would not be present, the flow pattern would not be affected by the pressure gradient between injectors and producers. Gravity segregation as a result of the density difference between injected CO_2 and in-situ brine is a technical issue. It is suggested that injecting at the bottom of the aquifer can partially mitigate the gravity segregation. Pressure buildup in the aquifer is another technical issue. It is suggested that larger aquifers, with high permeability and thickness and good vertical and lateral pressure communication are better candidates to overcome the pressure buildup. The injected CO_2 will dissolve in brine and the CO_2-saturated brine is slightly denser than the brine alone. Thus, the

heavier mixture flows downward and the replaced fresh brine will become in contact with the CO_2 phase. This may result in further dissolution of CO_2. Trapping of CO_2 phase by brine may immobilize another portion of injected CO_2 as residual gas. Finally, slow chemical reactions may store some of the CO_2 as minerals (Ozah, 2005).

The most famous large-scale aquifer-storage project is being performed at the Sleipner gas field in the North Sea (Torp et al., 2002). Approximately a million tons of CO_2 are separated from produced natural gas each year. The separated CO_2 is injected into an overlying aquifer. An extensive monitoring program shows that the injected CO_2 remains within the sand in which CO_2 is injected, although vertical migration within the sand occurs. Injected CO_2 flows horizontally below the shale layers until it reaches a break in a shale layer, where it then migrates upward toward the caprock. This behavior is identical to the one in the injection of gas in oil reservoirs. Sleipner project has been performed in high permeability sand with relatively high porosity in vicinity of the CO_2 source. Thus, it has been a significant step to prove the feasibility of storage in aquifers.

Several field tests have been conducted to better understand the mechanisms involved in CO_2 storage in saline aquifers. A field test was conducted in the Frio sand in South Texas (Hovorka et al., 2006). Approximately, 1600 tons of CO_2 were injected into the Frio formation. Several measurements were performed to observe the dissolution of CO_2 and migration of CO_2 and brine. Global CCS Institute announced that as of 2011, eight CCS projects were under operation all around the world and six others were under construction. Besides Sleipner, In Salah in Sahara desert in Algeria and Snohvit in Barents Sea are three industrial-scale projects in deep saline aquifers. Vast amounts of monitoring data have been gathered including time-lapse seafloor gravity survey, 3-D seismic survey, Controlled Source Electromagnetic (CSEM), and inSAR satellite data (Arts et al., 2008; Mathieson et al., 2010). These data have been used in several reservoir

modeling and simulation studies (Singh et al., 2010; Alnes et al., 2011) for history matching and performance prediction.

CO_2 injection project at Cranfield, Mississippi is another example of large-scale projects (Hovorka et al., 2013). Approximately four million tons of CO_2 have been injected into the fluvial Tuscaloosa formation as of the beginning of 2013. Several tests have been conducted in the shallow groundwater, above the injection formation, and within the injection zone to assess the feasibility, operation and sensitivity of monitoring. Hosseini et al. (2013) utilized the data from Cranfield to build static and dynamic reservoir models to predict the CO_2 plume size and reservoir pressurization. These data include well test data, gas saturation, temperature and pressure in and above the injection zone, and U-tube samples from bottomhole fluids. All of these projects have demonstrated the feasibility of CO_2 storage in deep saline aquifers.

2.2.1.4 Coalbeds

Unlike oil and gas reservoirs and saline aquifers which store CO_2 as a separate gas phase or dissolved in oil or water, deep unmineable coalbeds store CO_2 by a different mechanism. CO_2 and CH_4 adsorb on the surface of coal particles at high pressures. Coal adsorbs much more CO_2 than CH_4 and N_2 at similar pressure and temperature. Moreover, the adsorption hysteresis curve shows that even by dropping the pressure, most of the CO_2 remains adsorbed. Ogha et al. (2002) experiments demonstrate that at a given pressure, CO_2 adsorbs on coal three times more than CH_4 and six times more than N_2.

Ogha et al. (2002) suggest that flow in coalbeds occurs in the fracture network. Injected CO_2 flowing through fracture network, diffuses the matrix blocks and replaces the adsorbed CH_4. Therefore, CO_2 helps to enhance CH_4 recovery. This displacement

process, which is similar to adsorption chromatography, can be used to separate a mixture of CO_2 and N_2. Pekot and Reeves (2002) suggest that as CH_4 is removed from coal, the coal permeability increases. On the contrary, coal permeability decreases as CO_2 adsorbs on the coal. Thus, modeling the displacement processes in coalbeds seems to be much more complicated than that of other geological formations.

Field experience of CO_2 storage in coalbeds is limited (Stevens et al., 1998; Reeves, 2001). The main objective has been enhanced recovery of coalbed methane. CO_2 from a pipeline providing CO_2 for Permian Basin is being injected in the Allison Unit in the San Juan basin. Production of CH_4 from this unit demonstrates response to CO_2 injection. Results show minimal CO_2 breakthrough, which supports the idea that injected CO_2 can replace adsorbed CH_4. The experience form these field-test projects provide information for future storage projects. The potential for offsetting the cost of storage by extraction of CH_4 is the motivation for more investigation of this approach.

2.2.2 Trapping mechanisms

CO_2 injection into geologic formations causes pressure buildup near the wellbore. Oruganti et al. (2009) claimed that the amount of pressure buildup depends on the injection rate, formation permeability, thickness of the interval, and injection well pattern. Security of storage depends on a combination of physical and geochemical trapping mechanisms. The major trapping mechanisms are

- Structural and stratigraphic trapping: trapping below an impermeable, confining rock. The injected CO_2 is less dense than the in-situ brine. The buoyancy of the injected CO_2 is the driving force for vertical migration of CO_2 toward the top of formation. The buoyant CO_2 may be prevented from rising back to the surface by

an impervious layer which is called structural or hydrodynamic trapping (Bachu et al., 1994). Folds or faults may form structural traps above the storage formations. Salvi et al. (1999) explain that faults can act as permeability or capillary barriers. If the barrier has insufficient integrity, the injected CO_2 may rise up into the shallow water or to the surface.

- Solubility trapping: dissolution in the in-situ brine. Dissolution of CO_2 in brine commence from the injection period. Ennis-King et al. (2002) state that the amount of dissolution during the injection phase depends on the residual water saturation. After the injection, diffusion of CO_2 in aqueous phase and reaction between dissolved CO_2 and formation minerals facilitate further dissolution (Gunter et al., 1993). Ennis-King et al. (2005) state that convective mixing is the dominant long-term mechanism. Dissolution of CO_2 in the formation brine slightly increases the density of brine, which causes the convective mixing due to gravitational instability. In another work, Ennis-King et al. (2005) estimate that the scale for the onset of convective mixing ranges from one year to decades or centuries depending on the permeability of the formation.
- Geochemical trapping: reacting with the minerals in formation and caprock: The dissolved CO_2 in brine reacts with other dissolved species and also with the rock minerals. This reaction results in precipitation or dissolution of minerals leading to more storage of CO_2 as minerals. Several numerical simulation studies have been conducted by modeling this complex process. Pruess et al. (2003) demonstrate that under favorable conditions, the amount of CO_2 that can be stored by precipitation is comparable to the amount of stored CO_2 by dissolution. Xu et al. (2004) report that the accumulation of carbonates as a result of precipitation leads to a considerable decrease in porosity. This phenomenon adversely affects

the permeability of formation. On the contrary, Ozah et al. (2005) claim that the amount of stored CO_2 by precipitation even after thousands of years is small compared to capillary trapping and dissolution. Also, they report that the effect of precipitation on porosity and permeability is not large.

- Residual gas trapping: Retention as an immobile phase in pore spaces of formation. Kumar (2004) and Kumar et al. (2005) conducted a reservoir simulation study of CO_2 storage in deep saline aquifers. They used a Land-type model for relative permeability and concluded that the effect of residual gas trapping on CO_2 storage can be more significant than dissolution and precipitation. Flett et al. (2004) included the hysteresis effect in the gas-water relative permeability to investigate gas trapping during their reservoir simulation study. They used the Land hysteresis model. They reported that the residual gas trapping has a constructive effect on the sequestration process. Ozah et al. (2005) utilized a compositional reservoir simulator to study strategies for optimizing several trapping mechanisms involving in geological storage of waste gases. They state that hysteresis in relative permeability is very effective in gas trapping and large volume can be stored without the need for long-term seal integrity because CO_2 never reaches the caprock. Juanes et al. (2006) study the effect of hysteresis in relative permeability and conclude that residual gas trapping plays an important role in the storage process, but mostly after the initial injection phase. Hesse et al. (2006) examine the effect of residual gas trapping on CO_2 plume migration and conclude that residual gas trapping is very effective in sloping aquifers and may be the dominant trapping mechanism.

2.2.3 Challenges of aquifer disposal

Many studies have been conducted on technical and economic feasibility of aquifer disposal of CO_2. Pruess et al. (2003) summarizes some technical and environmental issues as engineering challenges:

- The rate at which CO_2 can be injected
- The available storage capacity
- The presence of an impermeable caprock and the potential for CO_2 leakage through it
- Identification of suitable aquifer formations and caprock structures
- Uncertainty and possibility of failure because of incomplete knowledge of aquifer conditions and processes
- Corrosion of materials that are used in injection facilities

Gunter et al. (1998) investigate three different CO_2 sources and express that deep saline aquifers can hold large amounts of CO_2. In contrast, storage of CO_2 in deep saline aquifers has the following environmental issues:

- CO_2 leakage from aquifer
- Dissolution of formation rock
- Devaluation of mineral sources
- Effect on groundwater quality

They conclude that injectivity of CO_2 can be maximized by locating injectors in locally high permeability zones surrounding low permeability zones. This strategy prevents the excessive pressure buildup near wellbore to reduce the risk of rock fracturing, which may cause CO_2 leakage through vertical conduits. Law and Bachu (1996) present the same conclusion.

If a large volume of CO_2 is injected at near the top of the formation, then the CO_2 will accumulated below the caprock. Even if it is injected at the bottom of the formation, some of it may migrate to the top depending on how much is trapped. Therefore, the faults and fractures as well as abandoned wells which penetrate the top seal are potential conduits for escape of CO_2 from the storage formation. In order to assess the risk of leakage, several analytical and numerical models have been developed, and numerical simulation studies have been performed. Pruess (2004) presented a model for simulating the scenario of leaking CO_2. Nordbotten et al. (2005) developed a semi-analytical solution for predicting the rate of leakage from abandoned wells. Woods and Farcas (2009) presented a model to anticipate the migration of CO_2 along an inclined low-permeability seal layer. This model includes the leakage into this layer as a capillary barrier.

In order to minimize the risk of leakage from the aquifer, Ozah et al. (2005) proposed using horizontal disposal wells low in the aquifer so that all of the injected gases are dissolved, trapped or precipitated in the formation before they reach the top seal. They estimated that for their base case conditions seven times more CO_2 can be stored without reaching the top seal with a horizontal well compared to a vertical well. Another advantage is that higher injection rates can be achieved.

Bryant et al. (2008) investigated the strategy of "inject low and let rise". In this strategy, CO_2 is injected in the bottom part of the formation. When injection ends, CO_2 migrates upward due to buoyancy and will be contacted by uninvaded rock. Some CO_2 remains as residual gas in its upward pathway due to imbibition of brine into the volume which is previously occupied by mobile gas. Also, some CO_2 dissolves in previously intact brine. The CO_2-saturated brine which is slightly heavier than uncontacted brine, will sink downward and be replaced by fresh brine. They present a threshold value for the

amount of injected gas at which the CO_2 will just reach below the top seal and no gas cap will form. This value depends on several factors such as uniformity of the displacement front, and saturation of CO_2 below the front.

Solubility trapping is a crucial mechanism in geological storage. When CO_2 fully dissolves in aquifer brine, there is no tendency for it to migrate upward and escape since it is denser than brine. Tao and Bryant (2012) explain that the injection of supercritical CO_2 without extraction of brine includes the following risks:

- The buoyancy of CO_2 increases the risk of leakage through the faults, fractures and abandoned wells.
- Bulk injection of CO_2 increases the aquifer fluid pressure. Elevated pressure has the potential to cause long-term environmental effects (Nicot, 2008; Birkholzer et al., 2009). Excessive injection rates may induce fractures in formation and seismic activities (Luo et al., 2010; Zoback, 2012).
- Groundwater resources may be contaminated due to migration of CO_2 toward shallow waters and displacement of native high-salinity brine (Benson et al., 2007; Price et al., 2007).

These risks result in higher monitoring costs (Bryant, 2007).

Burton and Bryant (2009) introduced the surface dissolution process. This process is to dissolve CO_2 in the extracted brine from the disposal aquifer, then inject the CO_2-saturated brine in the same formation. This strategy mitigates the risk of buoyant migration of CO_2 since the CO_2-saturated brine is denser than brine. It also decreases the pressure buildup in aquifer, mitigates pressure interference between storage projects, and eliminates the risk of brine displacement. In addition, the cost of monitoring or insurance decreases substantially, though the capital and operating costs increases.

Jain and Bryant (2011) continued the investigation to develop an optimal design of injection and extraction strategy. They suggested that if all of the CO_2 is supposed to be dissolved in the brine, then the pressure contour representing the bubble-point pressure of the brine distinguishes the usable portion within the storage aquifer. They also presented an analytical model for an ideal aquifer to optimize well count and placement, areal extent of CO_2 and required pore volume.

Ganjdanesh et al. (2013a) proposed the idea of coupled CO_2 sequestration and energy production from geopressured-geothermal aquifers in order to overcome the economic challenges of CO_2 capture and storage. They pointed out that geopressured-geothermal aquifers of the Gulf Coast contain about 25 to 45 standard cubic feet of dissolved methane per barrel of brine. Also, the temperature of these aquifers can exceed 300°F. They suggested that brine containing dissolved CO_2 can be extracted from these aquifers to use the geothermal energy and produced methane. The revenue from extraction of methane and thermal energy can help offset the cost of CO_2 capture and storage. They proposed two strategies for injection: injecting supercritical CO_2, and injecting along with the extracted brine. They concluded that injecting a mixture of CO_2 and extracted brine provides higher revenue per ton of stored CO_2.

In another study, Ganjdanesh et al. (2013b) suggested applications for produced methane and thermal energy. They explained that the produced methane can be burned to run the compressors and pumps used for pressurizing CO_2 and brine. Also, geothermal energy can be used for the amine stripping process in CO_2 capture from coal-fired power plants after being extracted in a heat exchanger. They estimated that the amount of energy generated by produced methane exceeds the amount of energy required for pressurization of CO_2 and brine. Also, the amount of energy extracted from hot brine exceeds the amount of heat required for amine stripping process.

2.3 CARBON CAPTURE TECHNOLOGIES

The first step of CCS technology is the separation of CO_2 from combustion stack gases. The separation and compression steps, which are called capture, are considerably more costly than transportation and storage steps. During the past decade, various studies have been conducted to reduce the capture costs. Several CO_2 capture options exist including absorption by solvents, adsorption by molecular sieves, membranes, and cryogenic (low temperature) processes. To date, only amine-based absorption process has been used commercially. However, because of high capital and operating costs of amine-based separation of CO_2 from flue gas, and also degradation of conventional amines in presence of contaminants found in flue gas, this technology has not been applied widely.

Carbon capture technologies can be summarized as follows:

- Chemical and physical absorption. For low CO_2 concentrations such as found in flue gas from power plants, chemical solvents such as monoethanolamine (MEA) (Plaza et al., 2010) or solid sorbents (Atwater and Holtsnider, 1991) are favored. For higher CO_2 concentrations, physical solvents are preferred (Chakravarti et al., 2001).
- Chemical and physical adsorption. Alumina, Zeolite or activated carbon which are high surface area adsorbents, can be used for separation (Rao et al., 2002).
- Separation by membranes. For low temperature separation, solubility selective polymers can be used, while for high temperature, ceramics can be used.
- Low temperature (cryogenic) distillation. For sources of high-concentration CO_2 (>90%), purification can be done by liquefaction (Chakravarti et al., 2001).
- Advanced processes such as CO_2 separation in an Integrated Gasification Combined Cycle (IGCC) plant (Deppe et al., 2002) or capture by ionic liquids (Bates et al., 2002).

The choice of CO_2 capture technology depends on the fuel and technology of the power plant. Two potential technologies for commercial-scale CO_2 capture from power plants are discussed as follows.

2.3.1 Amine-based absorption process

Post-combustion capture by absorption with Alkanolamine solvents is a state-of-the-art technology for carbon dioxide capture from coal-fired power plants. This technology has had prior application in acid gas treating. Chemical adsorption by amine-based solvents has been the only commercially-used technology for CO_2 capture from power plants (Van Wagener, 2011).

The general idea includes exposing the flue gas to an amine solution that reacts with CO_2 in the stream to form a soluble carbonate salt (Liang, 2003):

$$2RNH_2 + CO_2 + H_2O \leftrightarrow (RHN_3)_2CO_3$$

This is a reversible reaction. It means that CO_2 can be released by heating the CO_2-rich solution in a stripping column. The common amines that are used for absorption are monoethanolamine (MEA), diethanolamine (DEA), methyldiethanolamine (MDEA) and diisopropanolamine (DIPA).

Flue gas from coal-fired power plants should be pretreated before stripping process to reach the tolerable levels of SO_x, NO_x and other impurities. First, the pretreated flue gas passes through a blower to overcome the pressure drop in the absorber. Then it goes through the absorption column to contact the lean amine solution counter currently. The temperature at top of the column is 40 to 45 °C and 50 to 60 °C at the bottom. The CO_2 from flue gas will be absorbed by lean amine solution by a chemical reaction. The CO_2-rich amine solution will be pumped to the rich/lean heat exchanger.

The transferred heat increases the temperature of the solution to about 105 °C. Then, this solution enters the top of stripper. Operating temperature of stripper is about 110 °C at the top and 120 °C at the bottom. The operating pressure at the bottom of stripper is about 30 psi and the pressure drop along the stripper column is about 3 psi. Saturated steam at a pressure of 45 psi heats the amine solution in the reboiler at the bottom of stripper column. This energy from steam helps desorb CO_2 from the rich amine solution. The CO_2-rich vapor rises in the stripper column and is partially condensed in a condenser. The product is a mixture of CO_2 and water vapor at 25 psi. This product is dried and compressed to the pressure required for transportation and storage. The lean solvent from the bottom of the stripper is pumped to the rich/lean heat exchanger and finally back to the top of the absorber column.

The technology of chemical absorption with amine is capable of removing 75 to 90 percent of CO_2 from flue gas emitted from coal-fired power plants. To date, it is the least costly technology for directly achieving a purity of more than 99 percent CO_2 in one step.

However, the cost of amine-based CO_2 capture process is high due to very low partial pressure of CO_2. Also, the absorption capacity of amine solution decreases significantly in the presence of flue gas contaminants such as SO_x, NO_x, O_2, HCl, Hg, hydrocarbons and particles. High rate of degradation of amines is another issue in the way of commercializing this technology.

Van Wagener et al. (2011a) investigated the energy requirement of MEA-based solvent regeneration in stripper. They studied several different configurations with different levels of complexity to find the most reversible and energy efficient configuration. For instance, interheated multi-stage stripper columns significantly improve the efficiency of the stripping process.

The CO_2 absorption rate is affected by kinetics of the reaction. The kinetic rate constant of a solution mixture of piperazine and MEA (PZ/MEA) with CO_2 is an order of magnitude higher than that of just MEA and CO_2. Thus, the mixture of PZ/MEA/Water absorbs CO_2 much faster than MEA/Water.

Freeman et al. (2010) investigated the application of concentrated, aqueous PZ as an amine solvent for CO_2 absorption. They compared an 8 m PZ solvent with a 7 m MEA. They conclude that the absorption rate of PZ solution is more than double that of MEA. Also, thermal degradation of PZ is almost negligible up to 150 °C. Their initial modeling shows that 8 m PZ requires 10 to 20 percent less energy than 7 m MEA. Therefore, faster absorption, lower degradation and lower energy consumption imply that aqueous PZ is the preferred solvent for CO_2 capture.

Van Wagener et al. (2011b) estimated the energy requirement for five different stripper configurations using 8 m PZ and 9 m MEA. They concluded that higher complexity of configuration improves the efficiency of the absorber due to better reversibility of the more complex process. Moreover, 8 m PZ requires less energy than 9 m MEA.

2.3.2 Membrane separation process

The membrane separation process operates by passing the gas mixture over a CO_2 selective membrane with a pressure difference across the membrane. This pressure difference can be achieved by compressing the flue gas or by using vacuum pumps on the permeate side or a combination of both. The main advantage of membranes is their lower energy requirement for operation compared to other CO_2 capture methods. The flue gas containing CO_2 is fed along one side of the porous, polymeric membrane. CO_2 diffuses

through the gas-filled pores of the membrane and is absorbed by a liquid solution on the other side of the membrane (Feron, 2002). The combination of membrane and absorption liquid is critical. The membrane material should allow the pores to remain gas-filled and does not let the liquid leak through the membrane.

Xu et al. (2001) summarizes the advantages of membranes over conventional amine scrubbing. These advantages are low energy consumption, high removal efficiency, large contact areas per volume, larger treatment capacity, and no foaming or flooding phenomena. The most significant issue against the commercialization of membranes for CO_2 capture is the low selectivity and low permeability. Research on CO_2 capture by membrane has been focused on increasing both selectivity and permeability. In general, improving selectivity reduces permeability and vice versa.

Merkel et al. (2010) report that conventional amine scrubbing can consume up to 30% of the power plant output at a cost of $40-100 per ton of CO_2 for capturing 90 percent of CO_2 from flue gas. While, they estimate that membranes can capture 90 percent of CO_2 using only 16 percent of plant output at a cost as low as $23 per ton of CO_2.

Rochana et al. (2013) introduced nitrogen-selective membranes as a promising technology for post-combustion capture of CO_2 from coal-fired power plants. They point out that the CO_2 concentration is not high enough for CO_2-selective polymer membrane process. The nitrogen-selective membranes benefit from the high driving force of N_2 in flue gas (>70 wt. %). If H_2 is used as sweep gas on the permeate side, ammonia will be formed as a byproduct of the N_2 separation process. Thus, this technology has the potential for indirect capture of CO_2 and ammonia synthesis.

Chapter 3: Modeling the Carbon Storage Process

In this chapter, the numerical models and reservoir simulator are reviewed. After a brief discussion on the simulator features, aquifer model and initializations are presented. Then, fluid properties and phase behavior are explained. Petrophysical properties and rock-fluid properties, including relative permeability, hysteresis and capillary pressure are reviewed. Finally, the wellbore model and numerical methods are discussed.

3.1 SIMULATOR FEATURES

A powerful numerical reservoir simulator is required to model the complexities of a deep saline aquifer. GEM (Generalized Equation-of-state Model) developed by Computer Modeling Group Ltd (CMG) was used in this study. GEM is a three-dimensional numerical simulator that can be used to model three-phase multi-component flow of fluid mixtures. The finite difference method of GEM is based on adaptive implicit formulation. In adaptive implicit formulation, it is decided for each gridblock in each time step whether IMPES (Implicit Pressure Explicit Saturation) or fully implicit methods should be used. This method makes the simulator faster and more stable. GEM is a compositional simulator. The Peng-Robinson (Peng and Robinson, 1976) equation-of-state is utilized to take into account the interaction between oil and gas phases. Also,

aqueous and gas phases can be modeled by the equation-of-state. Another option for modeling phase behavior of gas and aqueous phases is Henry's law model. The mass transfer of components between different phases is an important trapping mechanism which is called solubility mechanism. This simulator has the option of different gridblock systems such as Cartesian and corner-point. Several PVT models and rock types can be defined for different regions of reservoir. Also, GEM includes a wellbore model coupled to the reservoir model to estimate surface conditions or exert specific surface operating conditions. In this chapter, features of the reservoir simulator used in this study are reviewed.

3.2 AQUIFER MODEL

In this study, a specific aquifer is not modeled. Instead, ranges of properties from the aquifers of interest were used to prepare typical aquifer models. These models were used to do a feasibility study on the proposed ideas. GEM has several options for gridding to prepare the aquifer model: rectangular Cartesian grid; variable depth/variable thickness grid; radial-angular cylindrical grid; and corner point grid. Shape of the aquifer or fault blocks is one parameter among many other parameters involved in the results of the study. For preliminary studies, a rectangular cuboid is sufficient for the aquifer model. Therefore, rectangular Cartesian grid which has uniform depth/uniform thickness layers was selected to build aquifer model.

3.3 FLUID PROPERTIES

Compositional reservoir simulators utilize an equation-of-state (EOS) to predict the properties of hydrocarbon phases. GEM has two equations of state: Peng-Robinson

(PREOS); and Soave-Redlich-Kwong (SRK). These EOS models estimate phase compositions at equilibrium and the densities of hydrocarbon phases. Also, GEM provides various models for calculating properties of hydrocarbon phases such as viscosity, enthalpy, heat capacity and interfacial tension between phases.

GEM models up to three phases. The aqueous phase is not included in the EOS calculation. Instead, properties of aqueous phase such as density and viscosity can be calculated using correlations. There is no interaction between the aqueous phase and hydrocarbon phases. However, solubility of components in aqueous phase can be computed by Henry's law. Also, vaporization of water can be added to the calculations.

Based on the capabilities of GEM, two methods can be used to model the solubility of components in brine:

1. Modeling brine as "oil" phase and predicting the interaction between brine and components by an equation-of-state. In this method, S_w is zero since the EOS is used to do the flash calculations for the aqueous and gas phases. The flash calculation determines how water and other components such as CO_2, CH_4 and N_2 partition into "gas" and "oil" phases. The EOS should be tuned to experimental data for solubility and density at temperature, pressure and salinity of aquifer.
2. Modeling brine as "aqueous" phase and estimating the solubility of components in brine by Henry's law. In this method, Henry's law is utilized to calculate the solubility of components in "aqueous" phase. Also, an equation-of-state is used to predict the properties of the hydrocarbon phase. Both, Henry's law and EOS should be tuned to experimental data of aquifer conditions.

In this study, the first method is used and described here. Solubility determines how much of each component dissolves in brine and density predicts the buoyant

migration of phases. Also, two methods for calculating phase viscosities are introduced and compared.

3.3.1 Solubility of components

Solubility trapping plays a significant role in storage of CO_2 in aquifers. Also, dissolved CH_4 in aquifer brine is a source of energy in the brine extraction process. Therefore, solubility of gas components in brine should be modeled accurately. Solubility of components depends on temperature, pressure and salinity of brine. In Peng-Robinson equation-of-state, solubility can be controlled by binary interaction coefficients (BIC) between gas components and water. Empirical correlations have been suggested to predict BIC's between hydrocarbon-hydrocarbon component pairs. But, standard databases are not available for predicting the BIC's between water and gas components such as CO_2, CH_4 and N_2. Kumar (2004) introduced a correlation for BIC's between brine and CO_2 for pressures up to 10,000 psi and temperatures up to 100 °C. However, the predicted results are not applicable for higher pressures and temperatures which are discussed in this study. Thus, binary interaction coefficients have been tuned for the specific conditions of the studied aquifers.

Duan and Sun (2003) presented a thermodynamic model for solubility of CO_2 in aqueous NaCl solutions for wide ranges of temperatures, pressures and salinities. Comparison of predicted solubility from this model and experimental data shows high accuracy of this model. In this study, the predicted solubility from this model has been used to tune the interaction coefficients for PREOS. Figure 3-1 shows the solubility of CO_2 in pure water over wide ranges of pressures and temperatures. This plot shows that CO_2 solubility increases by increasing pressure. Most of this increase occurs from 0 to

2000 psi. Also, at pressures below 3000 psi, solubility always decreases by increasing temperature, while above 3000 psi, the minimum solubility occurs at about 200 °F. Figures 3-2 through 3-4 illustrate the CO_2 solubility in brine for a salinity of 1, 2 and 4 m (molality), respectively. Also, Figure 3-5 shows that the solubility decreases by increasing the salinity at a fixed temperature. Binary interaction coefficient between H_2O and CO_2 has been tuned for PREOS at salinity of 2 m (105,000 ppm) and temperatures of 194 and 302 °F. The tuned BIC's are -0.0214 and 0.0496 for 194 and 302 °F, respectively. Figures 3-6 and 3-7 compare experimental solubility data and calculated solubility by PREOS. Solubility is calculated for both temperatures with two different BIC values. At 194 °F, PREOS matches the experimental data using a BIC of -0.0214, while at 302 °F, a BIC of 0.0496 gives the best match. Comparison with experimental data shows that results are very sensitive to temperature. It is concluded that if temperature changes in the aquifer, the previously tuned BIC cannot be used anymore. In GEM, different sets of EOS data can be defined for different regions, but the option for defining different set of EOS data for different temperatures is not available.

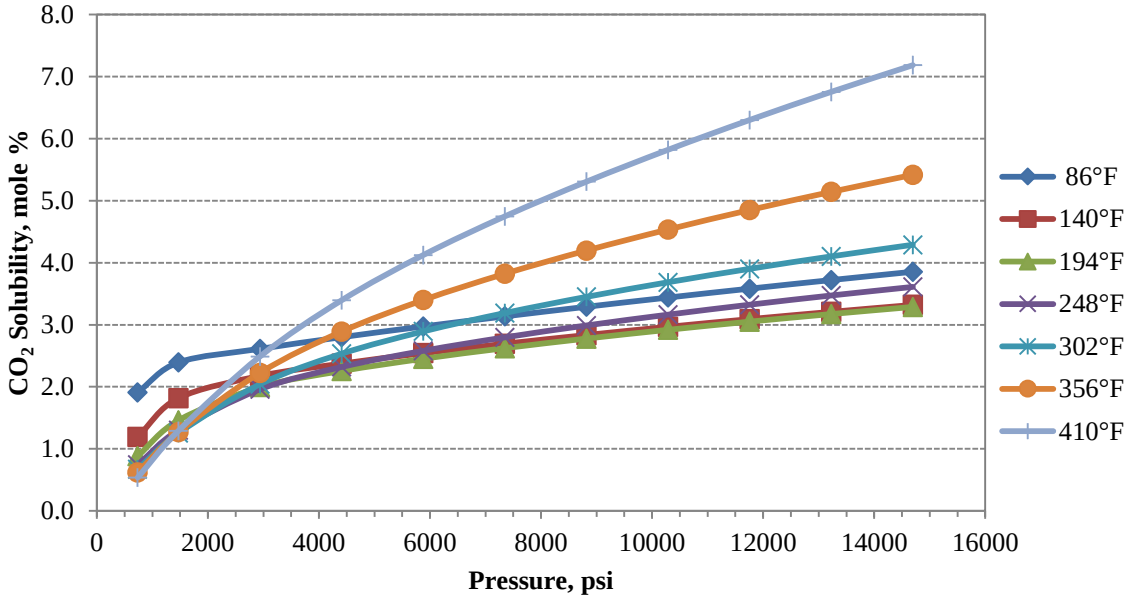

Figure 3-1: CO_2 solubility in pure water.

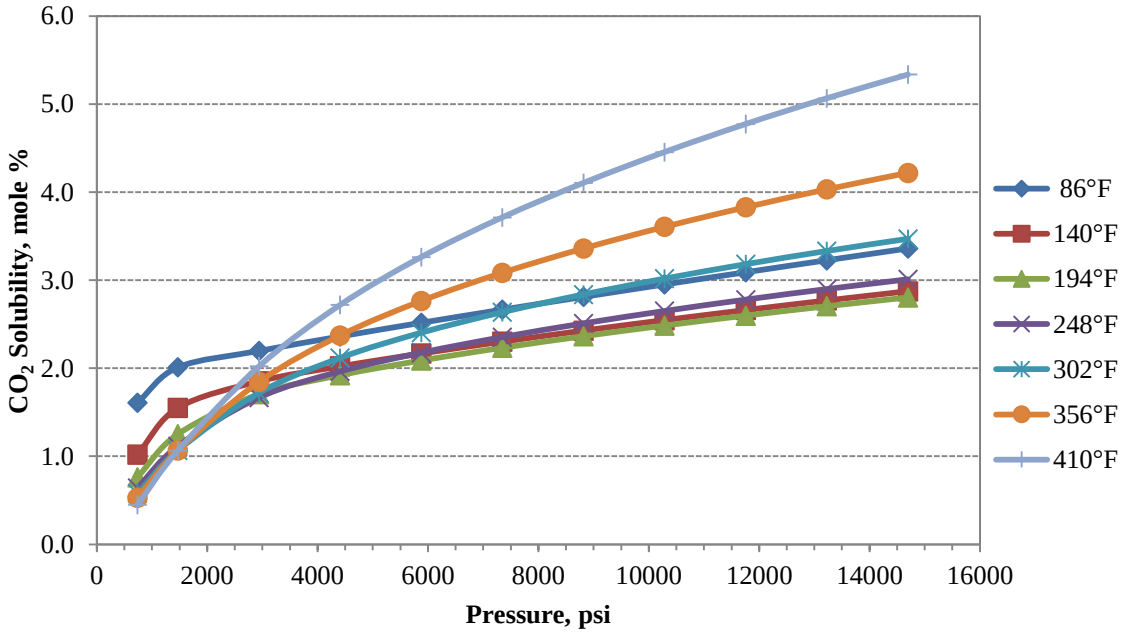

Figure 3-2: CO_2 solubility in 1 m brine (55,000 ppm).

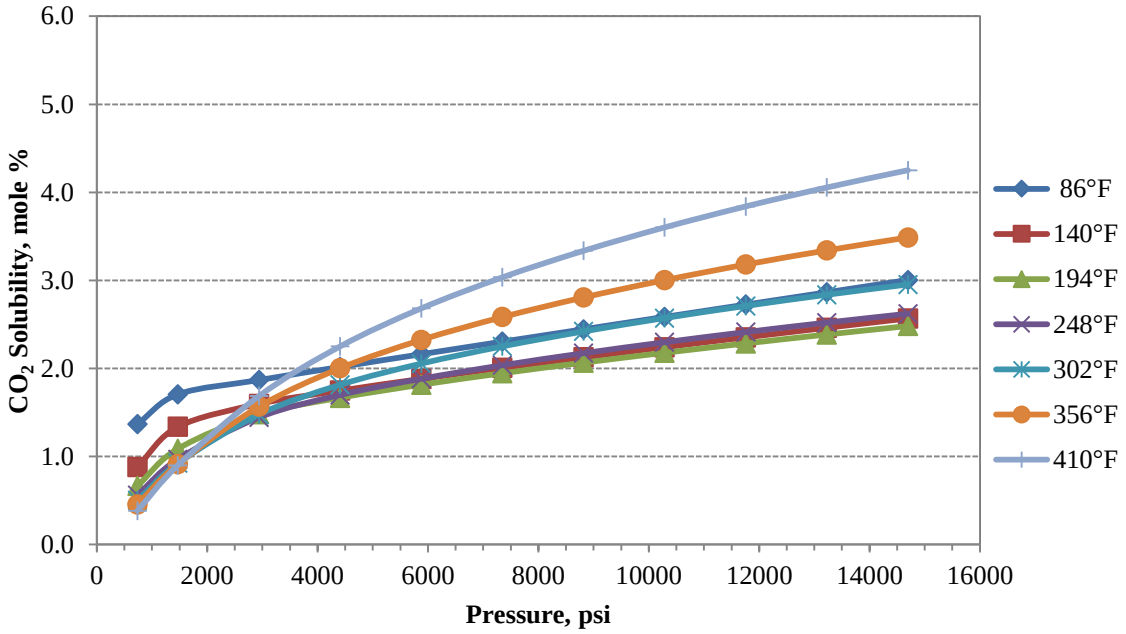

Figure 3-3: CO_2 solubility in 2 m brine (105,000 ppm).

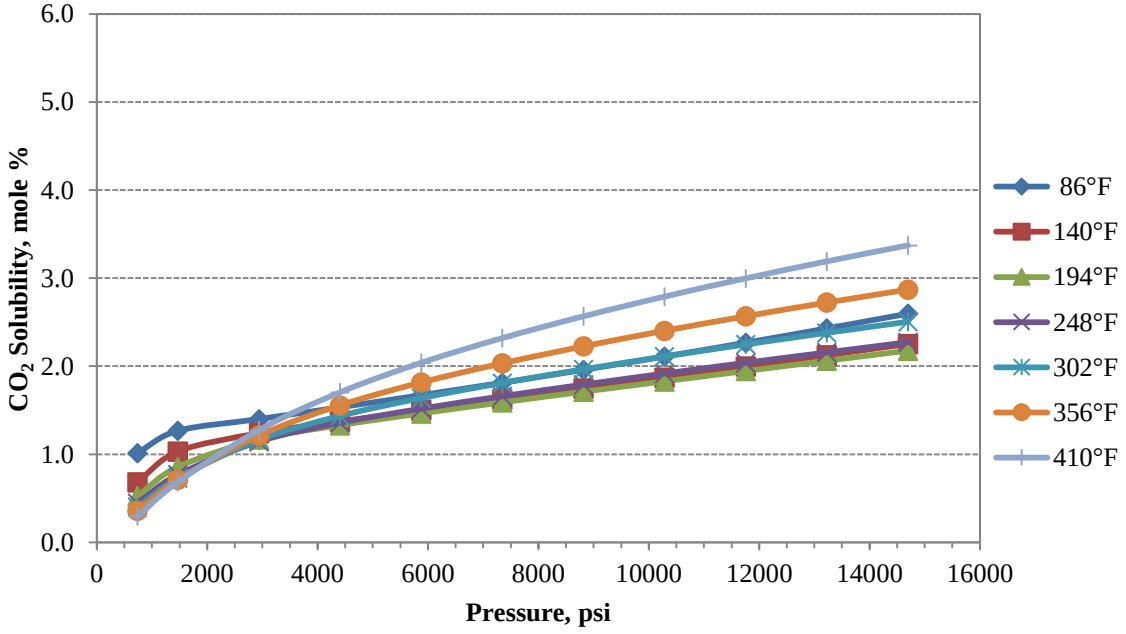

Figure 3-4: CO_2 solubility in 4 m brine (190,000 ppm).

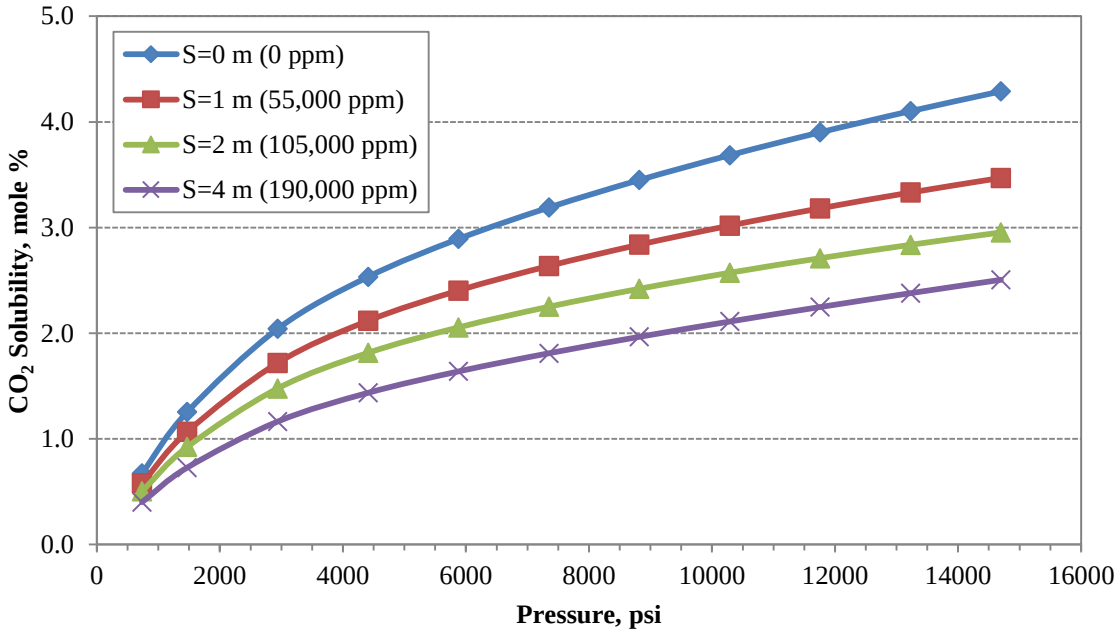

Figure 3-5: CO_2 solubility in brine at T = 302 °F.

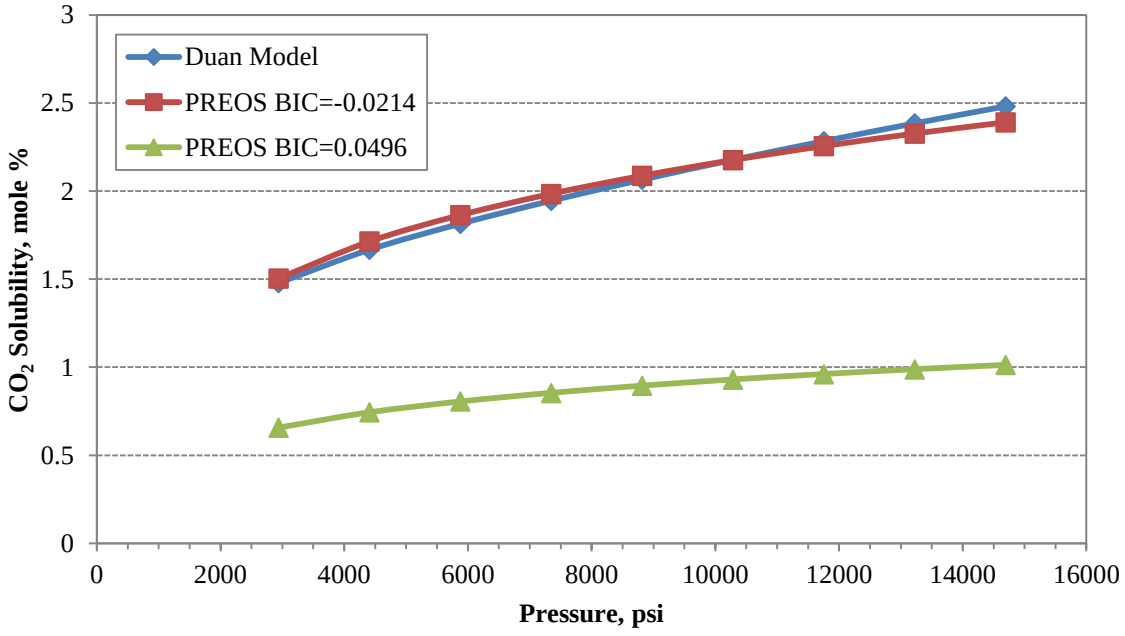

Figure 3-6: Comparison of the CO_2 solubility calculated by PREOS and by Duan model at T = 194 °F.

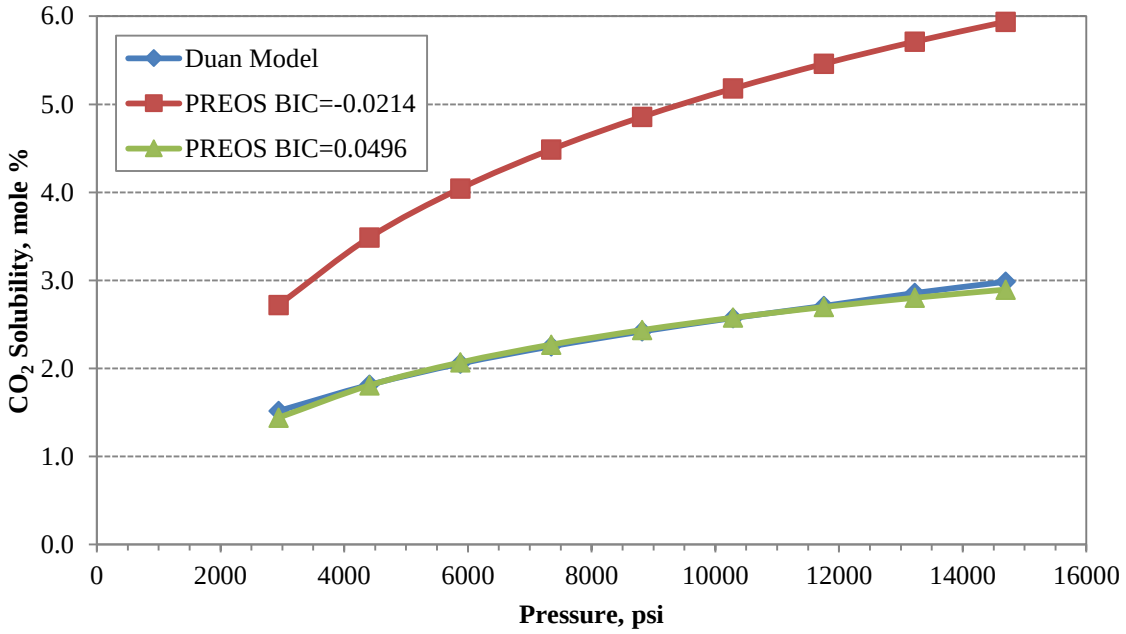

Figure 3-7: Comparison of CO_2 solubility calculated by PREOS and by Duan model at T = 302 °F.

Duan and Mao (2006) present a thermodynamic model for solubility of CH_4 in aqueous NaCl solutions over wide ranges of temperatures, pressures and salinities that are in good agreement with the experimental data. Therefore, the solubility from their model has been used to tune the interaction coefficients for PREOS. Figure 3-8 shows the solubility of CH_4 in pure water for wide ranges of pressures and temperatures. This plot shows that CH_4 solubility increases by increasing pressure. Most of this increase occurs from 0 to 3000 psi. Also, solubility always increases by increasing temperature. Figures 3-9 through 3-11 illustrate the CH_4 solubility in brine for values of salinity of 1, 2 and 4 m (molality), respectively. Also, Figure 3-12 shows that the solubility decreases by increasing the salinity at a fixed temperature. Binary interaction coefficient between H_2O and CH_4 has been tuned for PREOS at salinity of 2 m (105,000 ppm) and temperatures of

194 and 302 °F. The tuned BIC's are -0.0863 and 0.0547 for 194 and 302 °F, respectively. Figures 3-13 and 3-14 compare experimental solubility data and calculated solubility by PREOS. Solubility is calculated for both temperatures with two different BIC values. At 194 °F, PREOS is perfectly matched to experimental data using a BIC of -0.0863, while at 302 °F, a BIC of 0.0547 gives a good match. As for CO_2, comparison with experimental data shows that the results are very sensitive to temperature. It is concluded that if temperature changes in the aquifer, the previously tuned BIC cannot be used anymore.

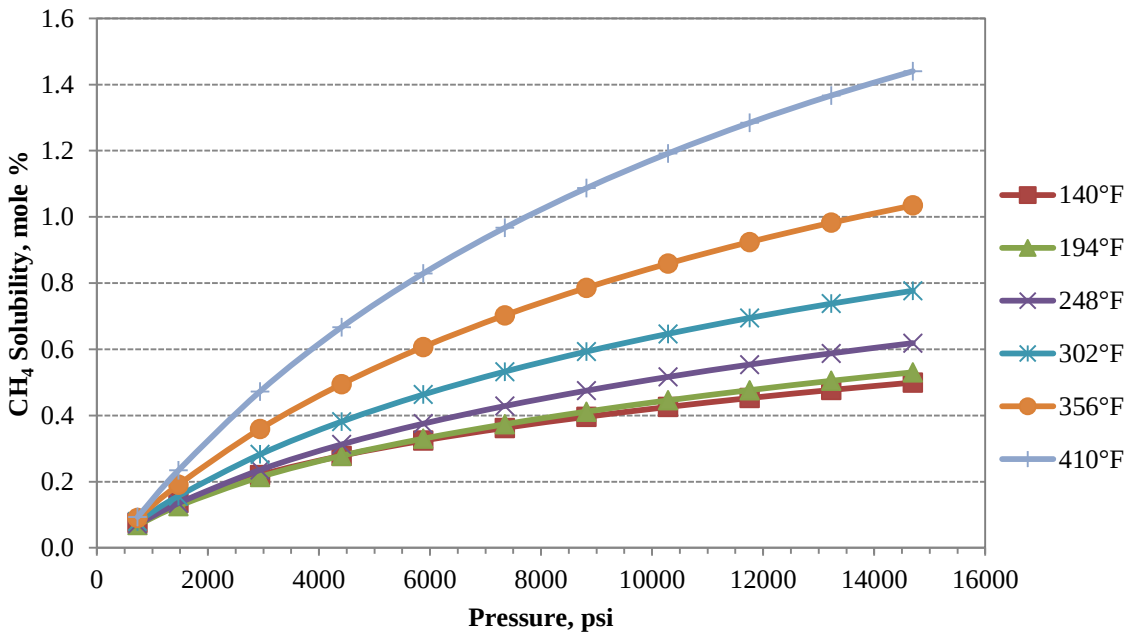

Figure 3-8: CH_4 solubility in pure water.

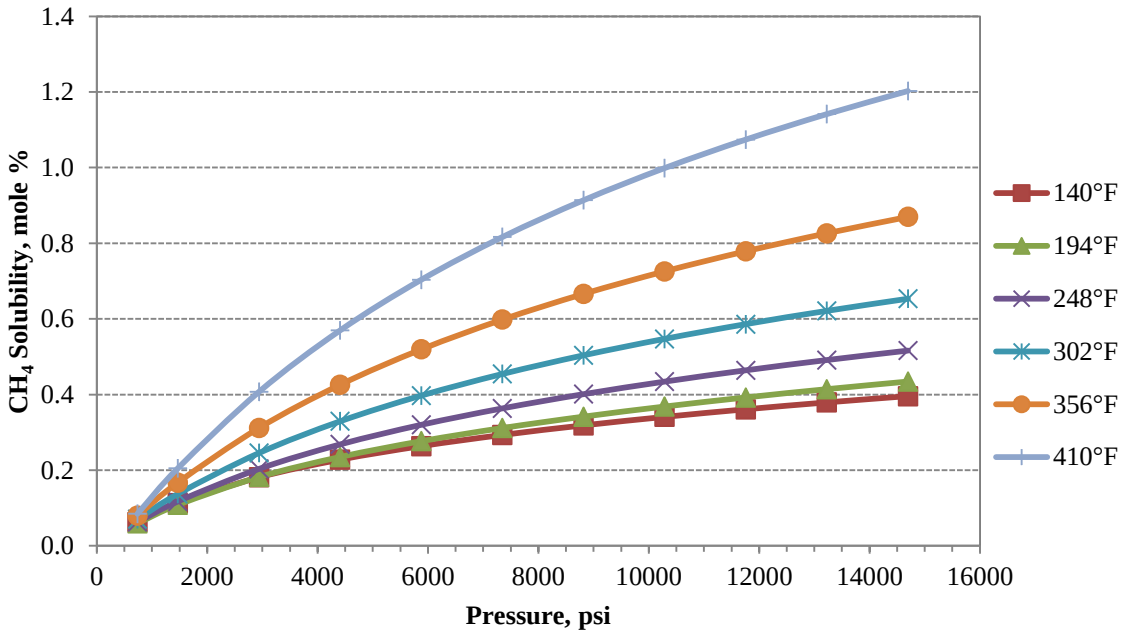

Figure 3-9: CH_4 solubility in 1 m brine (55,000 ppm).

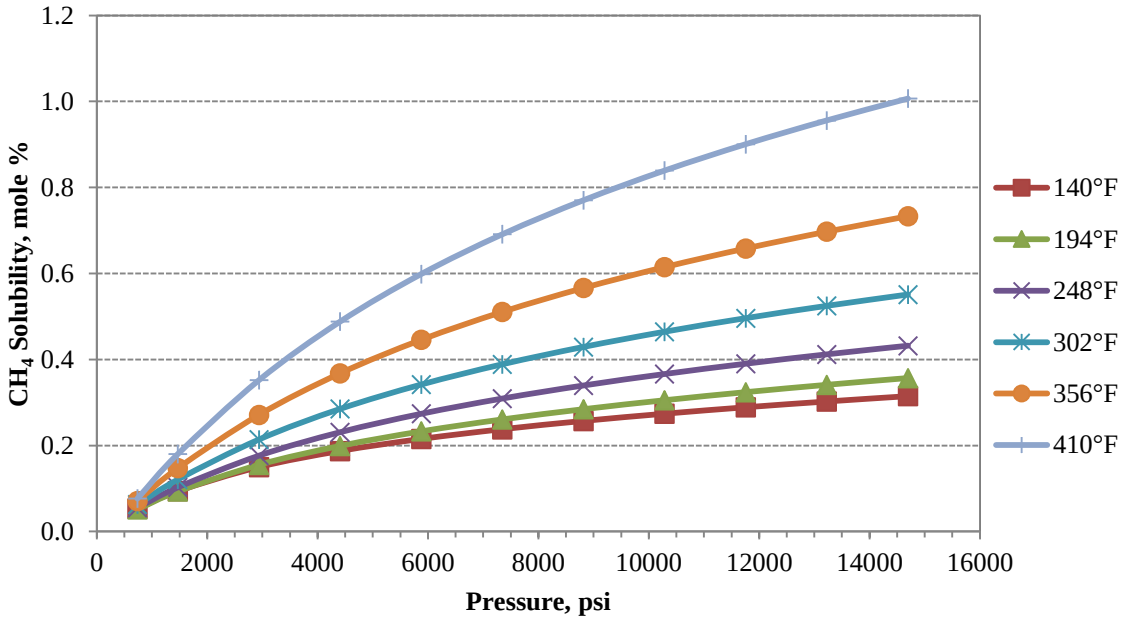

Figure 3-10: CH_4 solubility in 2 m brine (105,000 ppm).

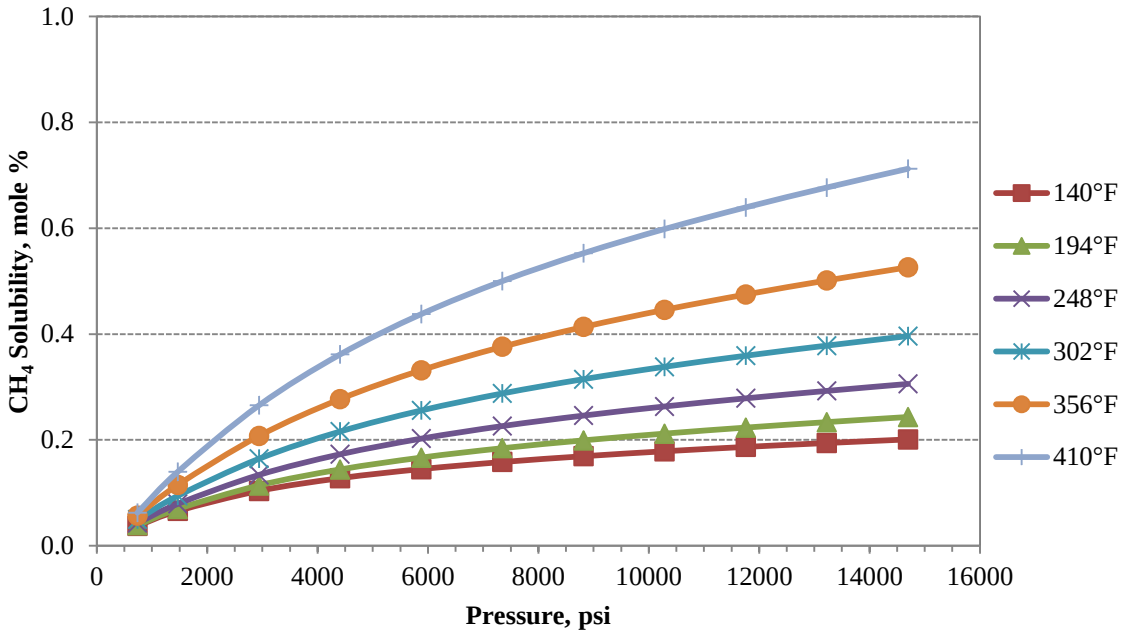

Figure 3-11: CH_4 solubility in 4 m brine (190,000 ppm).

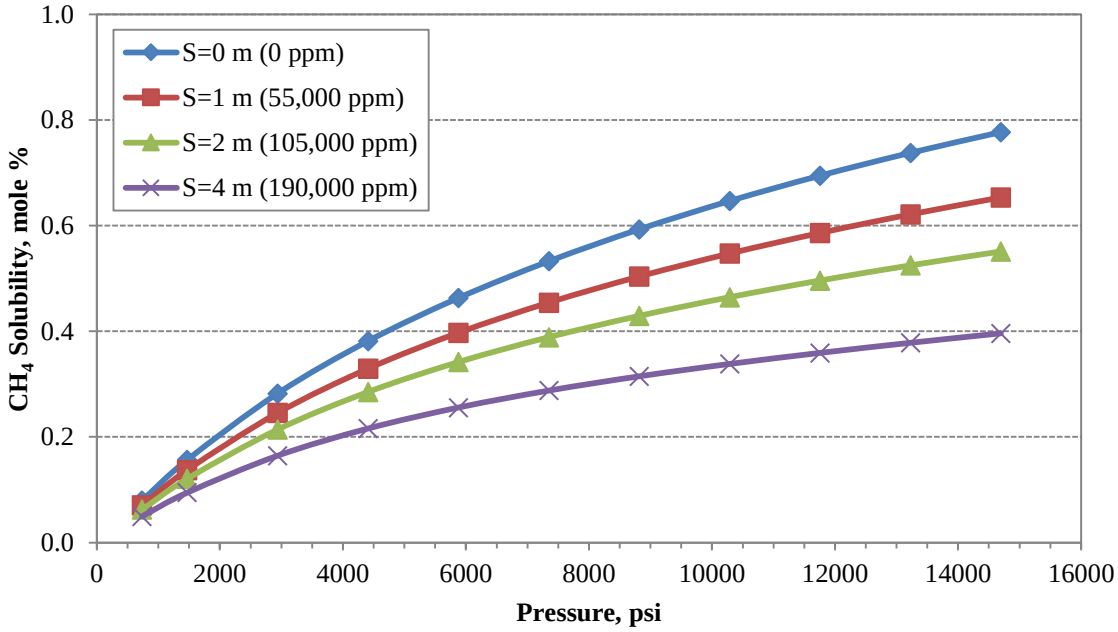

Figure 3-12: CH_4 solubility in brine at T = 302 °F.

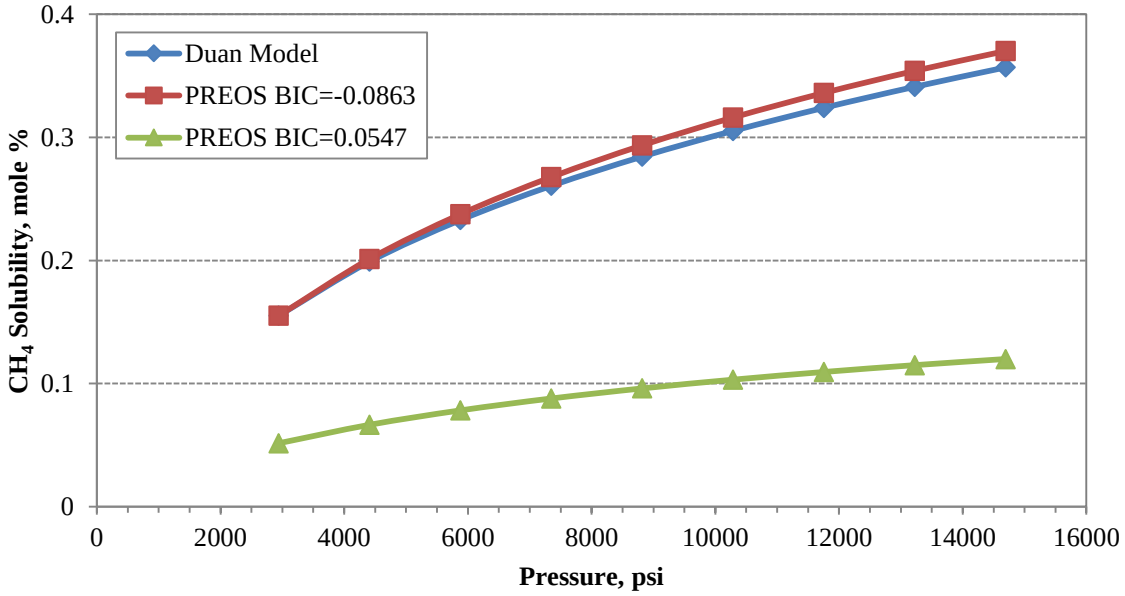

Figure 3-13: Comparison of CH_4 solubility calculated by PREOS and by Duan model at T = 194 °F.

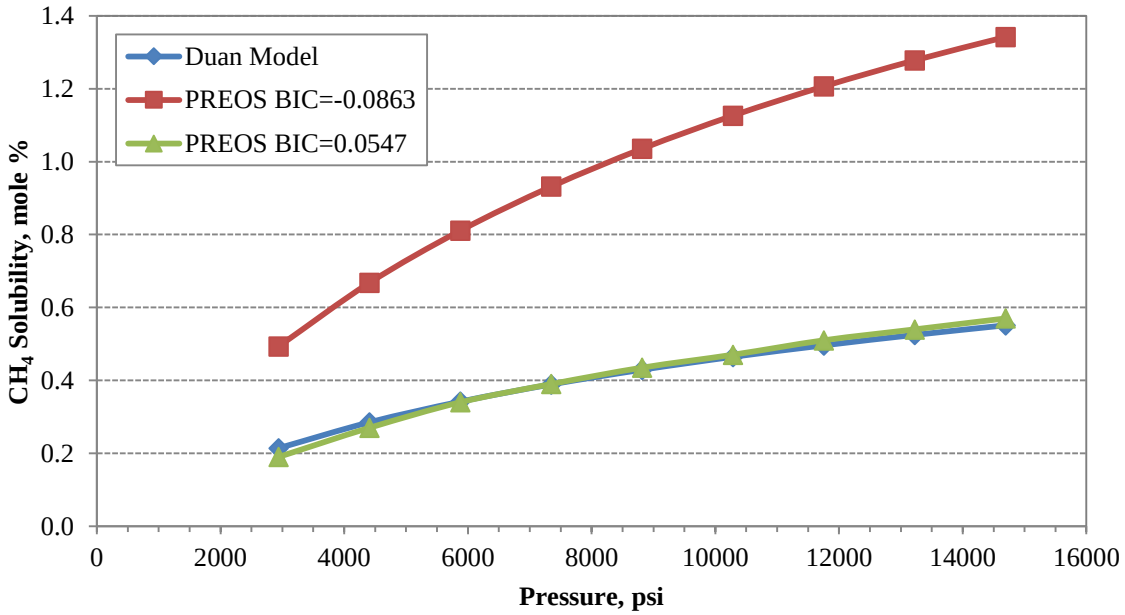

Figure 3-14: Comparison of CH_4 solubility calculated by PREOS and by Duan model at T = 302 °F.

3.3.2 Phase density

Phase densities predicted by PREOS should be improved by volume translation method of Peneloux et al. (1982). Volume shift parameters (VSP) represent the volume shifts to be applied to the molar volumes predicted by equation-of-state. Kumar (2004) suggests the only correlation for predicting the VSP's of CO_2-saturated brines for pressures up to 10,000 psi and temperatures up to 100 °C. Unfortunately, no experimental data for density of brine saturated with multiple gas components exists in the pressure and temperature range of interest. It is known that the dissolution of CO_2 in brine slightly increases the density of brine, while dissolution of CH_4 or N_2 slightly decreases the density of brine. In this study, VSP's are tuned for each component separately based on available experimental data on pure components. The predicted densities of mixtures by PREOS with the tuned VSP's show consistency with the slight effect of dissolution. Also, since the main focus of the simulations is on the injection and extraction period, the effect of post-injection buoyancy-driven flow is not of interest.

3.3.3 Phase viscosity

There are several options for calculating hydrocarbon phase viscosity in GEM. Two prominent viscosity models are the Jossi-Stiel-Thodos and Pedersen correlations. The Jossi-Stiel-Thodos correlation calculates the mixture viscosity at reservoir conditions using the following formula:

$$\left(\left(\mu_{mix} - \mu_{low,mix}\right) * \mu p_{mix} + 10^{-4}\right)^{1/4} = 0.10230 + 0.023364\rho_r + 0.058533{\rho_r}^2 - 0.040758{\rho_r}^3 + 0.0093324{\rho_r}^4, \quad (3\text{-}1)$$

where ρ_r is the reduced density of the mixture calculated using (critical molar volume)/(molar volume). Viscosity is calculated in units of centipoise.

Viscosity of the hydrocarbon mixture at low pressure is calculated using mixing rule due to Herning and Zipperer.

$$\mu_{low,mix} = \frac{\sum_{i=1}^{nc} \mu_{low,i} x_i \sqrt{M_i}}{\sum_{i=1}^{nc} x_i \sqrt{M_i}}, \quad \text{(3-2)}$$

Low-pressure viscosity of individual components is calculated using a formula suggested by Yoon and Thodos.

$$\mu_{low,i} = (4.610 T_r^{0.618} - 2.040 e^{-0.449 T_r} + 1.94 e^{-4.058 T_r} + 0.1 * 10^{-4})/\mu p, \quad \text{(3-3)}$$

where T_r is the reduced temperature of the component and μp is the viscosity parameter.

$$\mu p = (\frac{T_c}{M^3 P_c^4})^{1/6}, \quad \text{(3-4)}$$

where T_c is in K, P_c in atm, M in g/gmole and μp is calculated in centipoise.

Pedersen correlation calculates the mixture viscosity at reservoir conditions using the following formula:

$$\frac{\mu_{mix}(P,T)}{\mu_o(P_o,T_o)} = \left(\frac{T_{c,mix}}{T_{c,o}}\right)^{-1/6} \left(\frac{P_{c,mix}}{P_{c,o}}\right)^{2/3} \left(\frac{MW_{mix}}{MW_o}\right)^{1/2} \left(\frac{\alpha_{mix}}{\alpha_o}\right), \quad \text{(3-5)}$$

where α is the rotational coupling coefficient. The subscript 'mix' refers to the mixture property at reservoir condition, while the subscript 'o' refers to the reference substance property. The reference substance for this model is methane.

The critical temperature and pressure of the mixture is calculated using mixing rule and the temperature, pressure and mole fractions of the components. The molecular weight of the mixture is calculated from:

$$MW_{mix} = coef(1) \times \left(MW_w^{coef(2)} - MW_n^{coef(2)}\right) + MW_n, \quad \text{(3-6)}$$

where MW_w is the weight fraction averaged molecular weight, and MW_n is the mole fraction averaged molecular weight. The rotational coupling coefficient is calculated using the following formula.

$$\alpha = 1 + coef(3) \times \rho_r^{coef(4)} MW^{coef(5)}, \quad \text{(3-7)}$$

where ρ_r is the reduced density of the reference substance.

Unfortunately, experimental data for mixtures of CO_2 and brine under the desired reservoir temperature and pressure conditions do not exist in the literature. Therefore, it is suggested that special component critical volumes can be tuned to match the correlation results to experimental data for each pure component. These critical volumes are used in the mixing rule formula to calculate the mixture critical volume used in the Jossi-Stiel-Thodos formula. It is anticipated that the correlation would predict the mixture viscosity with high accuracy. On the other hand, GEM only allows the user to tune the five coefficients of the Pedersen correlation for mixture viscosity. Since experimental data for mixtures are not available, there is not a clear way to tune the Pedersen correlation for viscosity of mixtures. Therefore, it was concluded that the results from tuned Jossi-Stiel-Thodos correlations are more reliable than the state-of-the-art Pedersen correlation.

3.3.4 Phase identity

Phase identity is important in reservoir simulation because oil and gas phases use different relative permeability and capillary pressure data. When the EOS model predicts that only one phase exists in the reservoir, the simulator is not able to identify whether this phase is oil or gas without calculating the critical point. GEM has five different approaches for phase identification when only one phase forms in the reservoir. The approach used in this study determines whether the phase mass density is closer to a reference oil density or a reference gas density. These reference densities need not to be entered by the user. These densities may be calculated using the unstable phases found in the stability tests where it is necessary.

3.4 THERMAL MODELING

Calculation of reservoir temperature is necessary since the production of geothermal energy is one of the objectives of this study. GEM (2011) provides a thermal option wherein the energy balance equation is solved along with the other equations. The model includes an energy balance with convection, conduction and heat loss terms. The convection terms include phase enthalpies. Oil and gas phase enthalpies are determined from the equation of state, while aqueous phase enthalpy is determined from a steam table look-up. This allows modeling of non-ideal fluid effects and heating or cooling due to fluid expansion or compression, including the Joule-Thomson effect. Conduction is modeled with a term for thermal conductivity of the rock and fluids, and heat losses to overburden, underburden and edge boundaries are calculated with an analytical solution to the heat conduction equation.

Ideal gas enthalpies are determined from a polynomial correlation for the all components in the oil and gas phases. The coefficients in this polynomial for CO_2, CH_4, and H_2O are provided in Table 3-1. Final oil and gas phase enthalpies are calculated by adding the enthalpy departure term from the EOS to the ideal gas enthalpy.

Table 3-1: Enthalpy coefficients for CO_2, CH_4, and H_2O for ideal gas enthalpies from a polynomial equation.

CO_2	4.778E+0	1.144E-1	1.011E-4	-2.649E-8	3.471E-2	-1.314E-16
CH_4	-5.581E+0	5.648E-1	-2.830E-4	4.174E-7	-1.526E-0	1.959E-14
H_2O	-2.463E+0	4.574E-1	-5.251E-5	6.455E-8	-2.028E-1	2.363E-15

The rock heat capacity and thermal conductivity are 0.25 BTU/lb.°F and 2.0 BTU/hr.lb.°F, respectively. Input of rock-density is required for calculation of the

accumulation term using rock heat capacity and temperature difference. In this study, rock density is 165.434 lb/ft^3.

3.5 PETROPHYSICAL PROPERTIES

Many studies use probabilistic approaches to generate heterogeneous permeability fields. Since, the objective of this study is to assess the feasibility of a novel idea, heterogeneity is not considered as a primary factor in the preliminary studies. Thus, most of the models used in this study are homogeneous. However, the effect of heterogeneity has been studied briefly later in chapter 5 to understand the practicality of the processes in heterogeneous formations.

The permeability field for heterogeneous cases is generated for all the gridblocks using a probabilistic approach. This approach generates the permeability by means of a spatial random function. The random function is presented by the mean permeability value, the variance, and the semivariogram. The variance quantifies the heterogeneity of the model. The semivariogram characterizes the spatial arrangement and correlation of the permeability values. The distribution of the permeability values is lognormal.

The semivariogram function measures the mean-squared difference between pairs of data points separated by a specific lag distance and direction. This function is defined as

$$\gamma(\vec{h}) = \frac{1}{2} Var\left[k(\vec{x_i}) - k(\vec{x_i} + \vec{h})\right] = \frac{1}{2n} \sum_{i=1}^{n} \left[k(\vec{x_i}) - k(\vec{x_i} + \vec{h})\right]^2 . \quad \text{(3-8)}$$

In the semivariogram function, γ is the estimated semivariance of the permeability data for a separation distance and direction identified by the lag vector, n is the number of data pairs used for the calculation, and $\vec{x}$ represents the data locations.

A well-behaved theoretical model for the variogram function is given by the semivariogram

$$\gamma(h) = s\left[1 - exp\left(-\left(\frac{h}{a}\right)^{p}\right)\right]. \quad \text{(3-9)}$$

In this function, s is the variance or sill parameter, a is the range or correlation length parameter, and p is the power-law exponent. In this study, p = 1 was used to produce the common exponential model. The semivariance increases with increasing the lag distance until a certain distance at which it becomes constant at its maximum value. The lag distance at which it becomes constant is called range or correlation length. It represents the separation distance beyond which the pairs of data points are not correlated. The value of the variogram at this point is called the sill which indicates the semivariance of the entire data set. In case where the semivariogram reaches the sill asymptotically, the correlation length is selected to be the lag distance at which 95 percent of the sill is reached. The correlation lengths in the horizontal direction are usually larger than those in the vertical direction.

In reservoir simulation studies, it is common to use correlations that relate porosity, permeability, irreducible (i.e. residual) water saturation and maximum residual gas saturation in sandstone reservoirs. Cross-property correlations from literature used in this study are presented.

Holtz (2002) describes how the petrophysical properties are interrelated. This interrelationship is a function of the pore network geometry of the rock. In his proposed methodology: (1) a porosity-permeability relationship is developed; (2) a correlation for irreducible water saturation is developed from capillary pressure data; (3) and a correlation for maximum residual gas saturation as a function of porosity is introduced. This methodology has been applied to data from Miocene section of the Louisiana Gulf Coast.

From available data, Holtz (2002) correlates porosity and permeability with a power law equation. In this equation, permeability ranges from a low end of 1 md at a porosity of 0.14 and a high end of 1 D at a porosity of 0.3. Permeability can be estimated from

$$k = 7 \times 10^7(\varphi^{9.606}). \quad \text{(3-10)}$$

In this and the following equations, k is in md and φ and S are fractions. Since the petrophysical properties are functions of pore geometry, the ratio of $\log(k)/\varphi$ gives a good measure of the pore geometry as well. This ratio corresponds to variations in capillary characteristics. For instance, capillary pressure curves with low irreducible water saturations correspond to larger $\log(k)/\varphi$ ratios. Holtz (2002) uses this relationship to develop an equation for calculating the irreducible water saturation.

$$S_{wirr} = 5.159\left(\frac{log(k)}{\varphi}\right)^{-1.559}, \quad \text{(3-11)}$$

Holtz (2002) develops a model for residual gas saturation from field and published data. It is documented that a strong relationship exists between decreasing residual gas saturation and increasing porosity. This relationship has a linear trend that predicts and S_{gr}^{max} upper bound of 0.5 for a porosity of 0.05 and a lower bound of 0.125 for unconsolidated sandstones.

$$S_{gr}^{max} = -0.9696\varphi + 0.5473, \quad \text{(3-12)}$$

The data used by Holtz (2002) are from typical tertiary formations of Gulf Coast. Thus, the cross-property correlation for porosity, permeability, irreducible water saturation and maximum residual gas saturation are appropriate for this study of Gulf Coast formations. Hence, for generating layered heterogeneous aquifers, several permeability quantities are selected to represent different rock types. Then, porosity is calculated for each rock type from equation (3-10). Also, equation (3-11) is used to

calculate irreducible water saturation for each rock type. Equation (3-12) was used to estimate the maximum residual gas saturation for each rock type to include the effect of hysteresis in relative permeability.

3.6 ROCK-FLUID PROPERTIES

The main rock-fluid properties consist of relative permeability and capillary pressure. Also, hysteresis was included in the relative permeability to study the effect of trapped gas saturation.

3.6.1 Relative permeability

Bennion and Bachu (2008) implemented a series of relative permeability experiments at reservoir conditions. They used supercritical CO_2 and water on samples of sandstone, shale, carbonate, and anhydrite rock. They observed that the maximum CO_2 saturation varied from 18% to more than 80% in various samples. They also reported a wide range of residual gas saturations from 10% to more than 34%.

In reservoir simulations studies, it is common to use relative permeability models instead of experimental data. The relative permeability curve is fit to experimental data. The model used here is:

$$k_{rg} = \begin{cases} 0, & S_g < S_{gcr} \\ k_{rg}^0 \left(\frac{S_g - S_{gcr}}{1 - S_{wir} - S_{gcr}} \right)^{N_g}, & S_g > S_{gcr} \end{cases}, \quad \text{(3-13)}$$

and

$$k_{rw} = \begin{cases} 0, & S_g < S_{gcr} \\ k_{rw}^0 \left(\frac{S_w - S_{wr}}{1 - S_{gcon} - S_{wr}} \right)^{N_w}, & S_g > S_{gcr} \end{cases}, \quad \text{(3-14)}$$

where

k_{rg}^{0} = Gas end point relative permeability (at irreducible water saturation),

S_g = Gas saturation,

S_{gcr} = Critical gas saturation,

S_{gcon} = Connate gas saturation,

k_{rw}^{0} = Water end point relative permeability (at connate gas saturation),

S_w = Water saturation,

S_{wr} = Residual water saturation,

S_{wir} = Irreducible water saturation,

N_g = Gas relative permeability Corey exponent,

N_w = Water relative permeability Corey exponent.

Bennion and Bachu (2008) concluded that Corey exponents are generally larger for the non-wetting than the wetting phase. Drainage relative permeability curves were generated by equations (3-13) and (3-14) and then entered by table in GEM.

3.6.2 Hysteresis effect

Previous CO_2 sequestration studies (Kumar et al., 2005; Ghomian et al., 2008) indicated that gas saturation increases and then decreases in some regions of the aquifer which were initially saturated with water. If hysteresis is not modeled in the simulations, the drainage gas relative permeability will be used in both drainage and imbibition processes. In this situation, the effect of trapped gas will not be taken into account. Trapped gas saturation has been found to be important in CO_2 sequestration studies. Hence, a hysteresis model was used in this study to determine the effect of residual gas saturation on storage and production.

In GEM, hysteresis is modeled using a method similar to Killough (1976). Hysteresis is modeled for both the oil and gas relative permeability. In this method, shifted gas saturation is used to calculate relative permeability for the imbibition process.

$$k_{rg} = k_{rg}^{0}\left(\frac{S_g(shifted)-S_{gr}}{1-S_{wir}-S_{gr}}\right)^{n_g}, \quad \text{(3-15)}$$

where

$$S_g(shifted) = S_{gr} + \frac{(S_g-S_{grh})(S_{gh}-S_{gr})}{(S_{gh}-S_{grh})}, \quad \text{(3-16)}$$

where S_{gh} is the value of S_g when the shift to imbibition (flow reversal) occurs. Also, S_{grh} is the residual gas saturation corresponding to S_{gh} that can be calculated using the modified Land's (1971) equation:

$$\frac{1}{S_{gr}^{max}-S_{gr}} - \frac{1}{S_g^{max}-S_{gr}} = \frac{1}{S_{grh}-S_{gr}} - \frac{1}{S_{gh}-S_{gr}}, \quad \text{(3-17)}$$

where S_{gr}^{max} is the maximum residual gas saturation and S_g^{max} is the maximum gas saturation, which was set to one in this study. The maximum residual gas saturation is the adjustable parameter which determines the imbibition curve from the given drainage curve. The quantity of this parameter must be between zero and $1 - S_{wir}$ that can be calculated from Eq. (3-12) developed by Holtz (2002). For instance, the maximum residual gas saturation would be 0.35 for average porosity of 0.2.

3.6.3 Capillary pressure

In reservoir simulation studies, it is common to fit analytical models to capillary pressure experimental data. The most prominent empirical model is Brooks-Corey (Brooks and Corey, 1966). Their model for drainage capillary pressure is

$$P_c = P_e.(S_w^*)^{-\frac{1}{\lambda}}, \quad \text{(3-18)}$$

where P_e is the capillary pressure at $S_w = 1$ (capillary entry pressure), λ is pore size distribution index, and S_w^* is reduced wetting phase saturation which is defined as

$$S_w^* = \frac{S_w - S_{wir}}{1 - S_{wir}}. \quad \text{(3-19)}$$

The index λ determines the slope of the capillary pressure curve. A small λ gives a large slope which corresponds to a wide pore size distribution, while a large λ gives a small slope which corresponds to a narrow pore size distribution. A $\lambda = \infty$ corresponds to a uniform pore size.

The Brooks-Corey model gives good matches for capillary pressure curves with hyperbolic shape, but it does fit well to the S-shaped capillary pressure curves with inflection points.

In this study, hysteresis in the capillary pressure has been neglected.

3.7 WELLBORE MODEL

In this study, the energy required to inject fluids into the aquifer should be calculated. Thus, wellhead pressure of the fluids needed to be computed. The surface pressure needed to inject or produce the fluids at the desired flow rate for a given aquifer pressure depends on both the pressure change in the well and the pressure drop in the aquifer. The best way to inject the brine and CO_2 will depend in part on how much compression is needed. Thus, there is a strong coupling between the surface facility, the wellbore, and the aquifer, so a simulator that couples the wellbore and the aquifer was needed. The CMG's wellbore model is a modification of the method of Aziz et al. (1972). This modification takes into account the hydrostatic pressure over the length of the well, pressure drop due to friction and pressure drop due to kinetic energy:

$$\Delta P = \Delta P_H - \Delta P_F - \Delta P_{KE}, \quad \text{(3-20)}$$

where $\Delta P_H = \rho g \Delta z$ is hydrostatic head over Δz, $\Delta P_F = \frac{2f\rho v^2}{D}\Delta z$ is friction over Δz, and $\Delta P_{KE} = -\rho v^2 ln\left(\frac{P_2}{P_1}\right)$ kinetic energy.

Here

ΔP = Pressure drop over Δz,

ρ = density of the in-situ mixture,

g = gravity acceleration,

f = fanning friction factor,

v = average velocity of mixture,

D = inside pipe diameter.

The modification includes an equation-of-state to compute the phase behavior and fluid properties of the fluid.

3.8 NUMERICAL MODEL

In general, most of the grid blocks can be solved using an IMPES approach and only a few of the grid blocks need to be solved implicitly. GEM has the options to be run in fully implicit, IMPES, and adaptive implicit modes. In the adaptive implicit mode, GEM selects the implicitness of the grid block dynamically during the computation at each time step. This feature is useful in coning problems where the fluid rate is high near the wellbore or in stratified formations where the layers are very thin. GEM provides several options for implicit treatment.

GEM has the option of Total Variation Limiting (TVD) flux limiter for numerical dispersion control. The TVD limiter guarantees that the overall numerical solution maintains numerical stability and eliminates overshoot and undershoot in the calculations. The limiter allows the higher-order flux calculation scheme to dominate in regions away from the edges of saturation fronts and fluid banks, and switches to the

more stable upstream scheme near these frontal regions where saturations and compositions are changing rapidly. This method results in higher resolution over fronts.

Chapter 4: Energy Production from Geopressured-Geothermal Aquifers

In this chapter, a systematic study has been performed to determine the feasibility of energy production from saline aquifers. This study has focused on geopressured-geothermal aquifers as well-established sources of methane and geothermal energy.

4.1 INTRODUCTION

Formations of abnormally high pressure and temperature lie along the Gulf Coast of the United States at depths exceeding 10,000 feet. The water of these formations is often saturated with methane. During the 1970s, DOE funded several studies related to the development of these geopressured-geothermal reservoirs as an energy resource, both from the standpoint of heat recovery and as a source of natural gas (Ganjdanesh et al., 2012). The goal of the project was to provide the information necessary to assess the production characteristics of geopressured-geothermal reservoirs and their economic potential.

In this study, the findings of the DOE project were utilized to estimate the amount of producible energy from geopressured-geothermal aquifers. First, a simulation model of the aquifer was developed based on the typical geopressured-geothermal aquifers of Gulf

Coast. Then, a systematic investigation over a range of conditions was conducted to determine the range of favorable conditions and also to explore the best strategy for the coupled production of natural gas and geothermal energy.

During 70's and 80's DOE began an organized program to evaluate the production of energy from geopressured wells (Griggs, 2005). The program had two aspects: the wells of opportunity program and design wells. In the wells of opportunity program, the deep abandoned exploration wells in geopressured zone were recompleted and tested. While in the design wells program, several wells were designed and drilled specifically as geopressured wells. Tables 4-1 and 4-2 summarize the results of well tests from wells of opportunity and design wells programs, respectively. The models in our study were built based on the results from DOE study.

Geopressure is the pressure exceeding the hydrostatic pressure gradient of a water column with a salinity of 80,000 ppm, which is about 0.465 psi/ft. Figure 4-1 shows the average bottomhole shut-in pressure versus depth for several wells in Lavaca County, Texas. The red line with a gradient of 0.465 psi/ft distinguishes the geopressured region from normally pressured regions. It is observed that the average bottomhole pressure of the wells is normal above the depth of 10,000 ft. Below the depth of 10,000 ft, the average bottomhole pressure of the wells falls into the category of geopressured. Also, Figure 4-2 shows the average bottomhole temperature for the same wells. It is observed that the temperature gradient below the depth of 10,000 ft is twice as much as one above the depth of 10,000 ft.

Table 4-1: Well test results of 'wells of opportunity' program.

	Girouard No.1	**Koelemay No. 1**	**Saldana No. 2**	**Prairie Canal No.2**	**Crown Zellerbach No.1**	**Fairfax Sutter No. 2**
County	Lafayette, LA	Jefferson, TX	Zapata, TX	Calcasieu, LA	Livingston, LA	St. Mary, LA
Max Flow Rate (STB/Day)	15,000	3,200	1,950	7,100	2,832	7,700
Max Gas Rate (MCF/Day)	600	1,017	105	390	93	
Produced Gas-Water Ratio (SCF/STB)	40	30	47-54	43-55	33	22.5-30
Water Salinity-TDS (ppm)	23,500	15,000	12,800	42,600	32,000	7.8
Formation	Frio-Marg. Tex No.1	Yegua – Leger	Hackberry, Upper Frio	Hackberry, Upper Frio	Tuscaloosa	-
Perforations (ft)	14,774-14,819	11,639 – 11,780	14,782 – 14,820	14,782-14,820	16,720-16,750	15,781-15,878
Net Interval (ft)	91	77	79	14	35	58
Original Reservoir Pressure (psi)	13,203	9,450	6,627	12,942	10,075	12,203
Original Reservoir Temperature (F)	274	260	300	294	327	270
Porosity-Log (%)	26	20	16	28	17	19.3
Permeability-Test (md)	200 - 240	100 - 200	16.7	95	16.6	14.5

Table 4-2: Well test results of 'design wells'.

	Pleasant Bayou No.2	**Glaydis - McCall No.1**	**Amoco Fee No.1**	**L.R. Sweezy No. 1**
County	Brazoria, TX	Cameron, LA	Cameron, LA	Vermillion, LA
Max Flow Rate (STB/Day)	28,900	36,500	36,500	10,700
Produced Gas-Water Ratio (SCF/STB)	23	23	27-29.8	20.2
Water Salinity-TDS (ppm)	131,320	165,000	97,800	99,700
Formation	Lower Miocene Oligocene	Frio Oligocene	Upper Oligocene	Upper Frio Oligocene
Perforations (ft)	14,644-14,704	15,390-15,470	15,160-15,470	15,511-15,627
Net Interval (ft)	53	27	333	57
Original Reservoir Pressure (Psi)	11,168	12,082	12,799	11,410
Original Reservoir Temperature (°F)	305	298	291	237
Porosity-Log (%)	18	22	16	27
Permeability-Test (md)	192	12-162	160	126

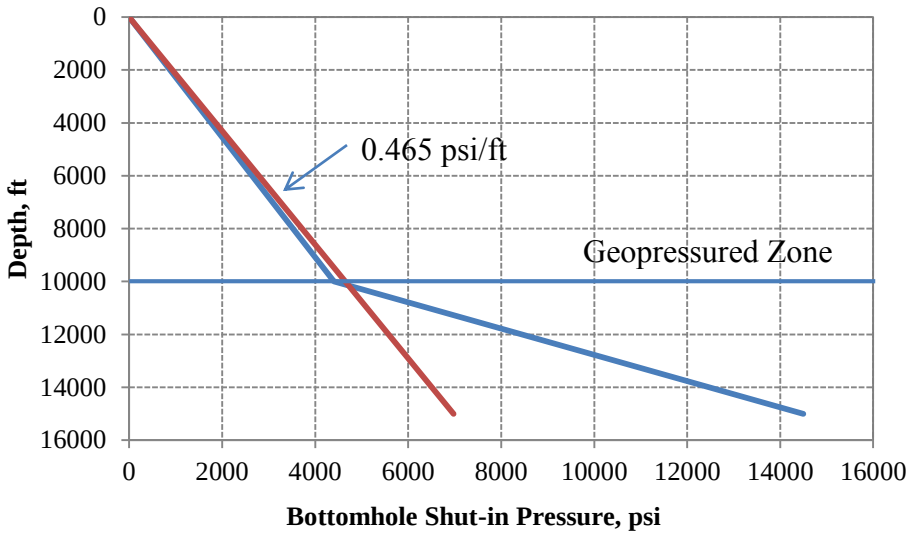

Figure 4-1: Average bottomhole shut-in pressure of several wells in Lavaca County, Texas.

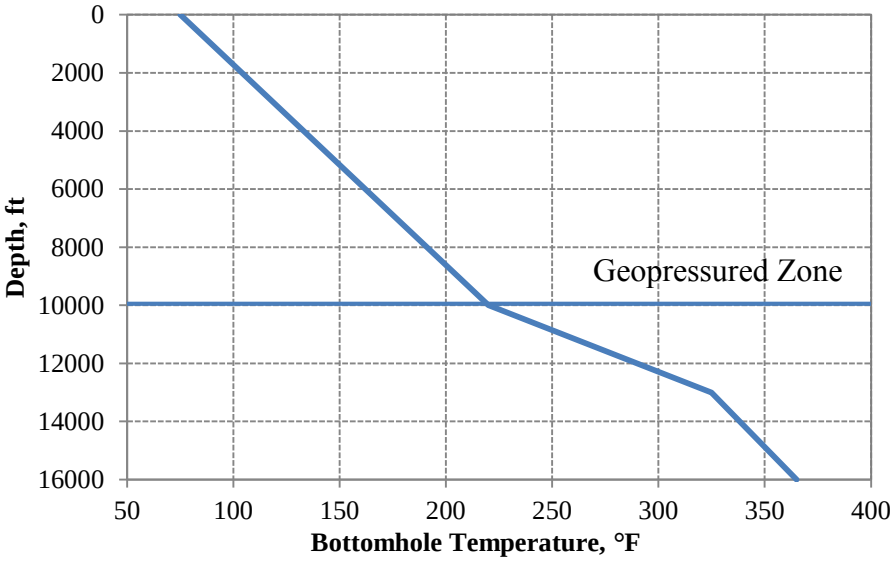

Figure 4-2: Average bottomhole temperature of several wells in Lavaca County, Texas.

4.2 ANALYSIS OF UNCERTAINTIES

The first step of this study was to analyze the uncertainty of the variables involved in the modeling of energy production from geopressured-geothermal aquifers. Parameters related to reservoir size and quality, fluid properties, well productivity and development scenarios were investigated to find out the effect of these parameters on the energy production and also the range of variation of these parameters. For this study, available data from DOE program was used to assess the importance of different variables.

4.2.1 Reservoir size

Figures 4-3 and 4-4 show the cumulative chance for the areal size of fault blocks in Frio and Wilcox formations. These plots were achieved from the data of hundreds of compartments in geopressured aquifers of Texas (Ewing, 1986). These plots show that the majority of the fault blocks are smaller than 10 square miles and fault blocks larger than 30 square miles rarely can be found. It is assumed that faults are sealing. Thus, fault blocks are not connected to each other and reservoir sizes and fault block sizes are the same.

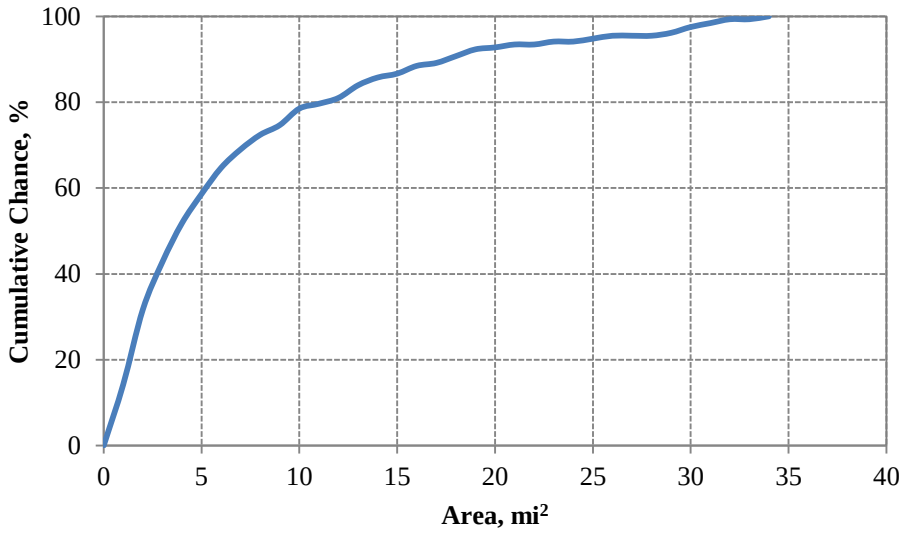

Figure 4-3: Cumulative chance of the areal size of the fault blocks in Frio formation.

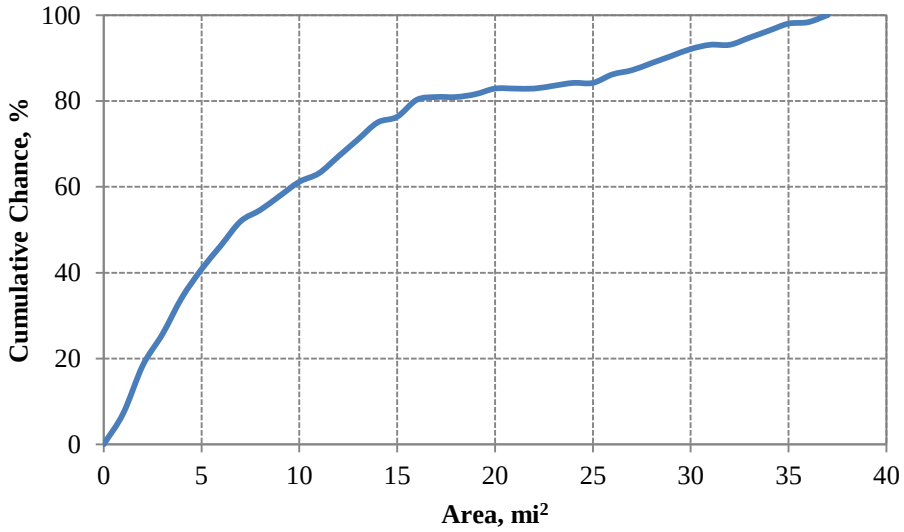

Figure 4-4: Cumulative chance of the areal size of the fault blocks in Wilcox formation.

Esposito et al. (2012) investigated the geopressured-geothermal resource of the Gulf Coast for combined production of methane and geothermal energy. They estimated (1) the total natural gas that could be recovered with geothermal fluid (2) the total heat in place and recoverable geothermal energy and (3) the total geothermal electricity generation potential. They provide the areal size and average sand thickness for geopressured zones of four different formations in Texas Gulf Coast. These formations are lower Wilcox, lower and upper Claiborne, Vicksburg-Jackson, and lower Frio. Figure 4-5 shows the location of these formations on a map of the Texas Gulf Coast. Some of these formations are present at the same location but at different depths. Table 4-3 shows the area and average sand thickness of geopressured zone of these formations.

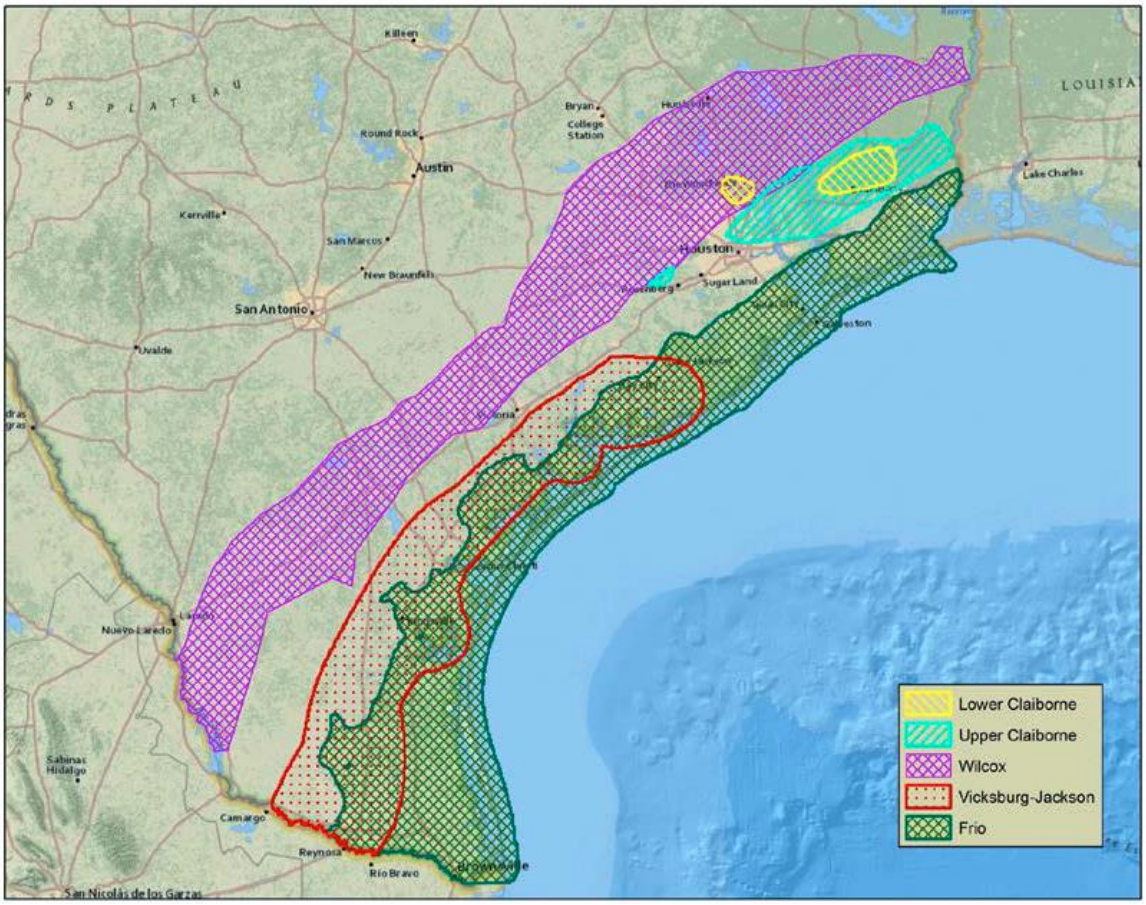

Figure 4-5: Location of geopressured formations in Texas Gulf Coast (Source: Esposito et al., 2012).

Table 4-3: Area and average sand thickness in geopressured zones.

Formation	Lower Wilcox	Claiborne	Vicksburg Jackson	Lower Frio
Area, mi^2	16,429	2,790	10,360	16,351
Average sand thickness, ft	607	184	374	404

The area and average sand thickness of these formations indicate that the lower Wilcox, lower Frio, and Vicksburg-Jackson formations have much higher potential for energy production than Claiborne formation.

4.2.2 Reservoir quality

The most important parameter about the reservoir quality is permeability. Permeability of the reservoir rocks in geopressured zone varies between 1 md for very low quality shaly sands to several hundred md for high quality sands. Many regions of geopressured aquifers contain low permeability sands as a result of diagenesis caused by high temperatures. Rocks with permeability on the order of 10 to 20 md are considered as marginal quality. Rocks with permeability higher than 20 md are considered as good quality. This sand quality exists only at some regions of Frio and Wilcox formations. Figure 4-6 illustrates the reservoir quality for onshore Frio and Wilcox formations in Texas (Loucks et al., 1986). The quality of sand at Vicksburg-Jackson formation is low because of very high depths and temperatures. High depths and temperatures at this formation result in diagenesis and loss of permeability.

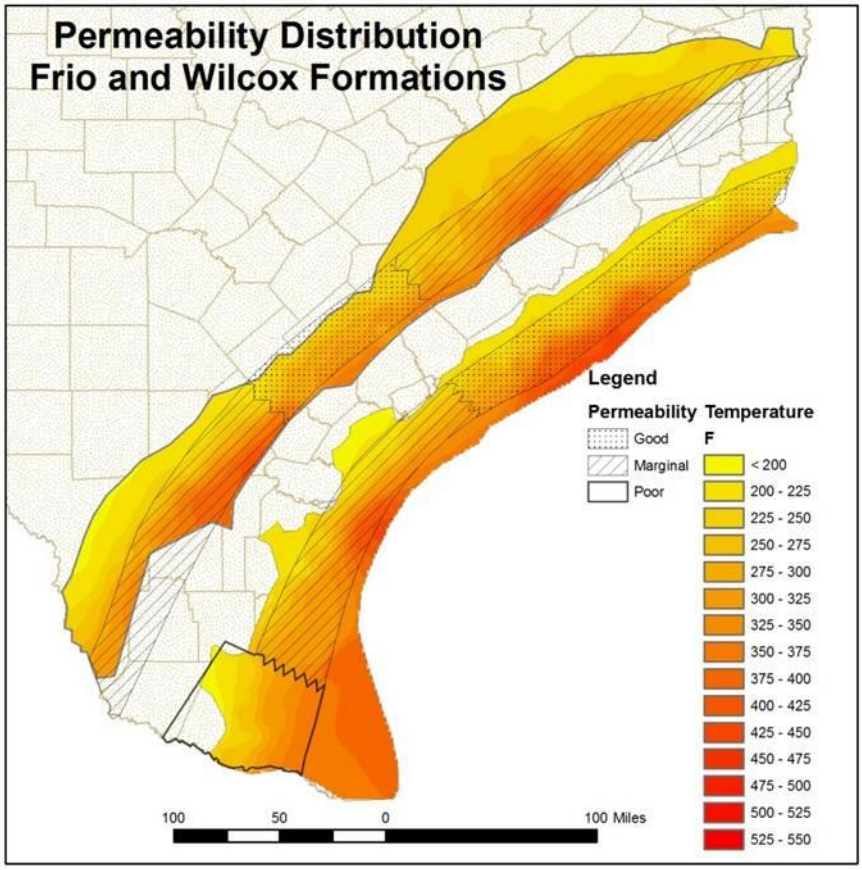

Figure 4-6: Sand quality of Frio and Wilcox formations in geopressured regions.

4.2.3 Fluid properties

Methane content of brine depends on the initial pressure, temperature and salinity of the brine. The range of temperatures in the geopressured zones varies between 250 to 350 °F. Figures 4-7 illustrate the temperature of geopressured formations of Texas Gulf Coast. The temperature in all formations increases towards the coast due to the large dip of each formation. This figure shows that Vicksburg-Jackson in South Texas has the highest temperature among all the geopressured formations in Texas Gulf Coast. The highest measured temperature in this formation is about 523 °F.

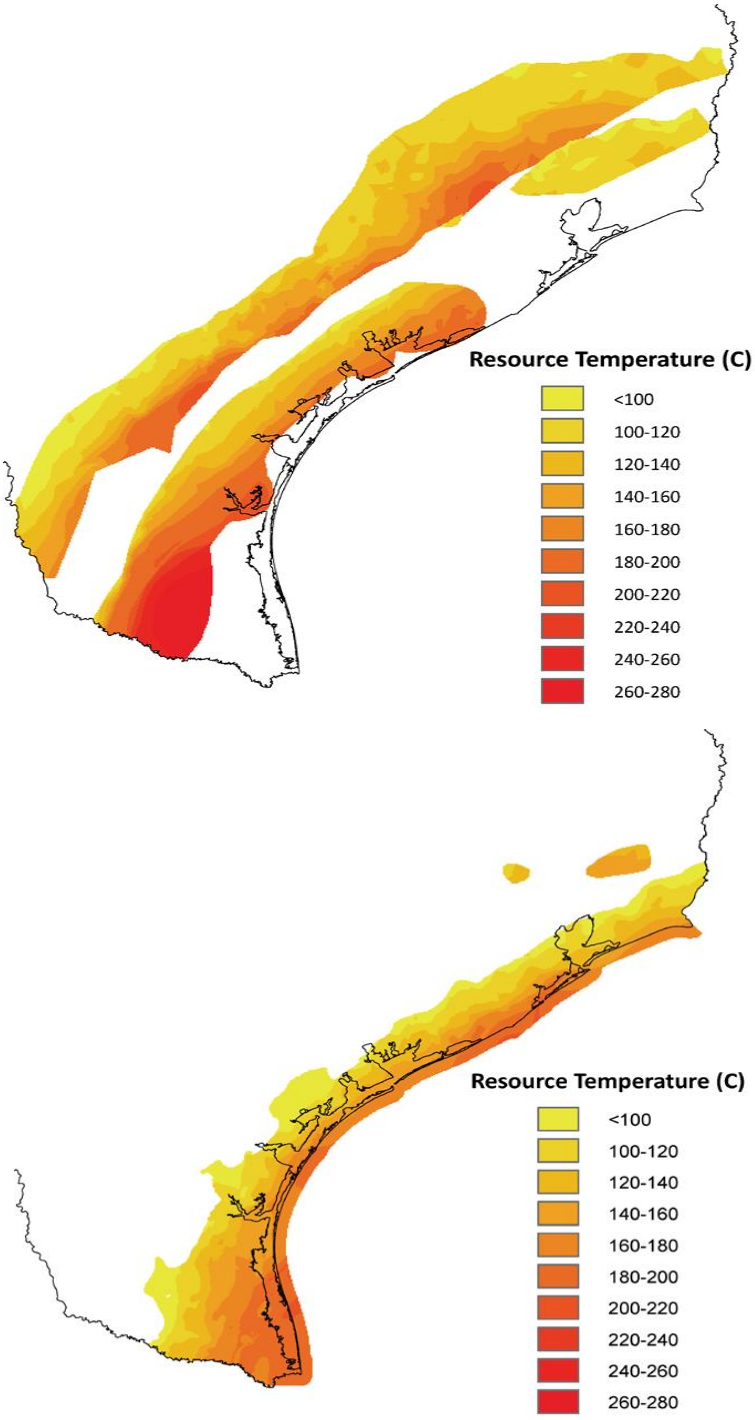

Figure 4-7: Temperature of geopressured formations, Texas Gulf Coast (a) lower Wilcox, Vicksburg-Jackson, upper Claiborne (b) lower Frio, lower Claiborne (Source: Esposito et al., 2012).

Initial pressures in geopressured aquifers are usually more than 10,000 psi. Salinity varies between 10,000 ppm to 200,000 ppm. The solubility of methane in brine varies between 25 to 50 standard cubic feet per barrel of brine for geopressured-geothermal conditions. Figure 4-8 shows the solubility of methane over wide ranges of pressure and temperature at the salinity of 105,000 ppm (Duan and Mao 2006). Also, Figure 4-9 shows the solubility of methane over wide ranges of pressure and salinity at 302 °F. The solubility increases by increasing the pressure and temperature and decreases by increasing the salinity.

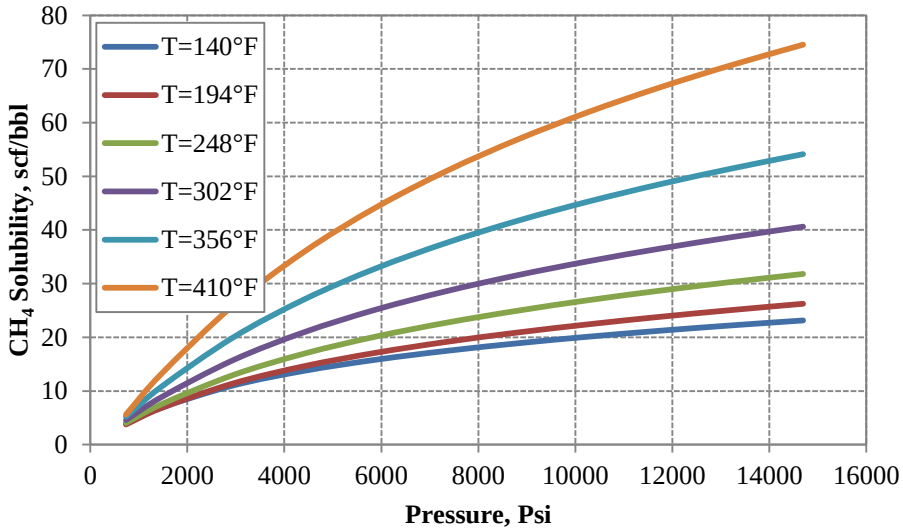

Figure 4-8: Solubility of methane in brine at 105,000 ppm.

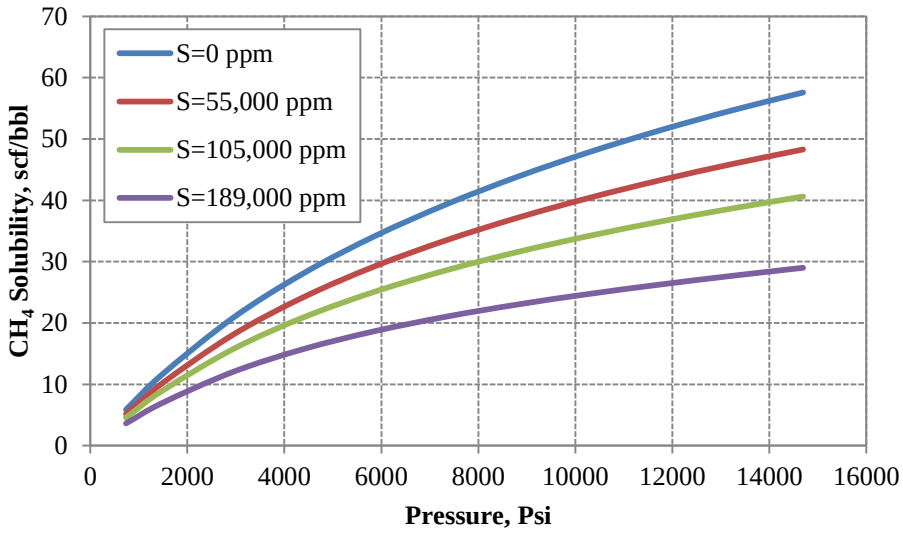

Figure 4-9: Solubility of methane in brine at 302 °F.

The initial condition of the reservoir fluid can be undersaturated, saturated or oversaturated. Table 4-4 summarizes the initial composition and gas-water ratio for five different conditions at initial temperature, pressure and salinity of 302 °F, 11,000 psi and 105,000 ppm.

Table 4-4: Initial conditions of fluid at 302 °F, 11,000 psi, and 105,000 ppm.

Initial condition	Methane mole %	Brine mole %	GWR (SCF/STB)
Bubble point 4795 psi	0.3	99.7	22.0
Bubble point 8058 psi	0.41	99.59	30.2
Saturated	0.48	99.52	35.4
Gas saturation 2.5%	1.21	98.79	89.8
Gas saturation 5.0%	1.96	98.04	146.5

Modeling the initial condition of the aquifer requires a phase behavior model. The Peng-Robinson equation-of-state (PREOS) was used to model the interaction between methane and brine. The phase behavior model should be tuned to the experimental data corresponding to similar pressure, temperature and salinity conditions. Solubility of methane in brine, density and the viscosity of gas and brine are the properties that must be modeled. Binary interaction coefficients, volume shift parameters, and viscosity correlation parameters correspond to these properties. In this study, Jossi-Stiel-Thodos correlation was used to model the viscosity. This correlation could be tuned by tuning the critical volume for each component. One fluid sample at the condition of 11,000 psi, 302 °F, and 105,000 ppm was used to build a phase behavior model. The values of the parameters for this model are shown in Table 4-5. This EOS model matches the fluid properties accurately at high pressures. An EOS model is also needed for surface pressure and temperature conditions. The solubility of methane in brine at surface conditions is negligible. The PVT properties of gas at surface conditions are predicted accurately by ideal gas law. Volume shift is the only parameter that needs to be tuned at surface condition. The density of the mentioned brine at aquifer condition is 1022.7 kg/m^3, while its density at surface condition (14.7 psi and 60 °F) is 1072.3 kg/m^3. This 5 percent difference in density emphasizes the importance of separate phase behavior model for surface condition. Also, molecular weight of H_2O was adjusted to account for the effect of salinity on brine density. For example, molecular weight was increased from 18.01 g/g-mole to 19.42 g/g-mole for salinity of 105,000 ppm.

Table 4-5: Component properties tuned for 11,000 psi, 302 °F, and 105,000 ppm.

Component name	CH_4	H_2O
Critical pressure, atm	45.4	217.6
Critical temperature, °K	190.6	647.3
Critical volume, m^3/k-mole	0.099	0.056
Molecular wt., g/g-mole	16.043	19.421
Acentric factor	0.008	0.344
Parachor	77	52
Omega A	0.4572	0.4572
Omega B	0.077796	0.077796
Volume shift (at reservoir condition)	-0.15400	0.21591
Volume shift (at surface condition)	0.0	0.15859
Critical volume (viscosity), m^3/k-mole	0.092217	0.04941
Binary Interaction Coefficient corresponding to H_2O	0.0565	0

4.2.4 Rock-fluid properties

Flow behavior of gas at low saturation in Gulf Coast geopressured brine is a critical question. Free gas is released from the brine inside the aquifer by decreasing the pressure below the bubble point pressure as a result of brine production. As the gas bubbles continue to grow, they will eventually link up throughout the pore structure of the reservoir rock. The saturation at which this link up occurs depends on the pore size distribution and is called critical gas saturation. If the gas saturation builds up to a level higher than that at which a continuous gas phase is formed, gas will begin to flow. Critical gas saturation is always equal or larger than initial gas saturation except in gas caps.

Some geopressured aquifers may initially contain a free gas saturation which is below the critical gas saturation. The critical gas saturation is an important parameter in relative permeability data for production of mobile gas. It is generally assumed that the critical gas saturation is about 2 to 5% and depends on the quality of the reservoir rock (Matthews, 1981). In this study, existence of gas layers and gas caps has been neglected and only dissolved gas or initial immobile gas is studied.

The flow behavior of gas at low saturation in the presence of brine should be carefully modeled via relative permeability curves. Equations 3-13 and 3-14 have been used to build relative permeability curves for two phase flow of gas and brine. Table 4-6 summarizes the parameters used in these equations. Also, Figure 4-10 illustrates the relative permeability curves of phases with zero critical gas saturation. This example has been built for a rock with average permeability of 20 md. Equations 3-10 to 3-12 have been used to correlate porosity, irreducible water saturation and maximum residual gas saturation. The corresponding porosity is 0.208.

Table 4-6: Relative permeability parameters.

Gas end-point relative permeability	0.6
Water end point relative permeability	1.0
Critical gas saturation	0.0
Connate gas saturation	0.0
Maximum trapped gas saturation	0.345
Irreducible water saturation	0.297
Gas relative permeability exponent	2.5
Water relative permeability exponent	3.0

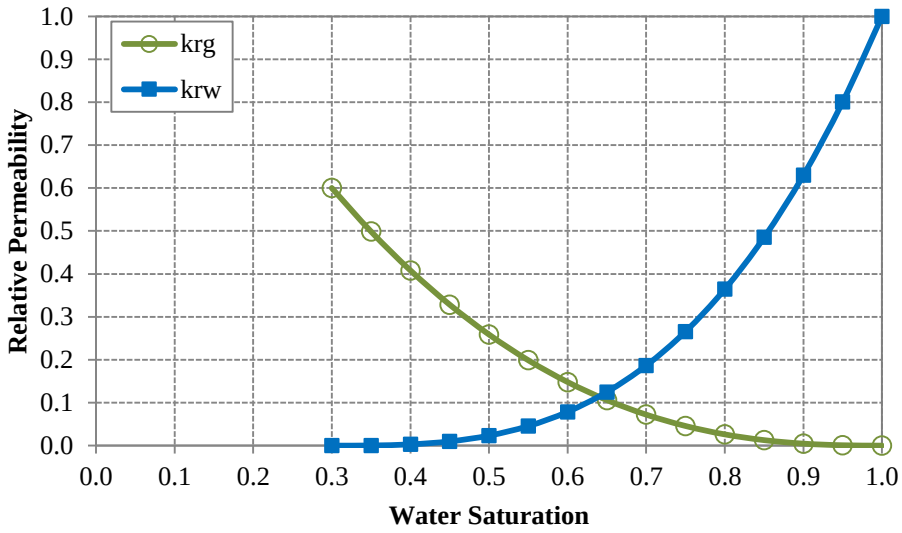

Figure 4-10: Two-phase drainage relative permeability curves.

Table 4-7 shows the Brooks-Corey parameters for capillary pressure curve in equation 3-18 used along with relative permeability curves. Also, Figure 4-11 shows the capillary pressure curves from those parameters. Also, since methane exsolution occurs as a result of pressure drop, counter-current flow of gas and brine might happen in the vertical direction. Hence, hysteresis modeling for imbibition is necessary. Equation 3-12 predicts that maximum trapped gas saturation is 0.345. Figure 4-12 shows several imbibition gas relative permeability curves.

Table 4-7: Parameters of Brooks-Corey for capillary pressure curve.

P_e	2.0
λ	8.0
Irreducible water saturation, S_{wir}	0.297

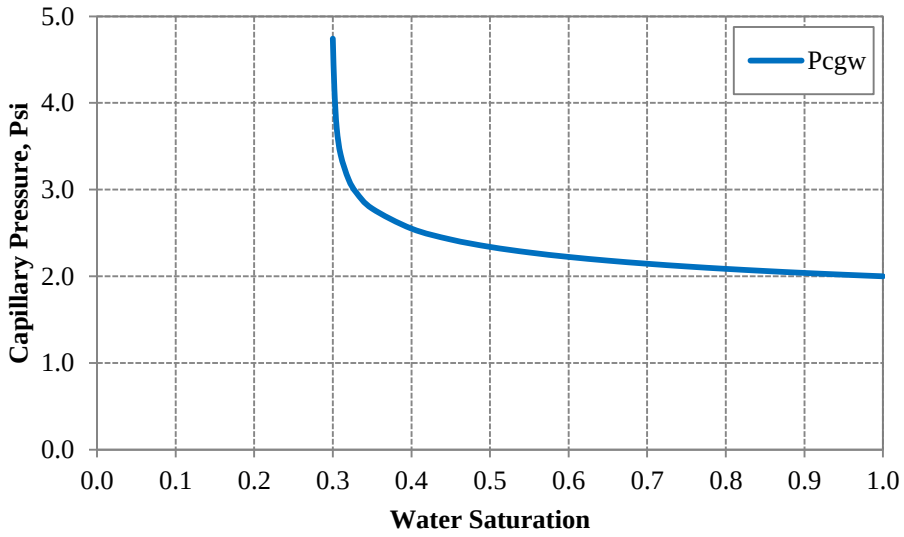

Figure 4-11: Capillary pressure curve for drainage.

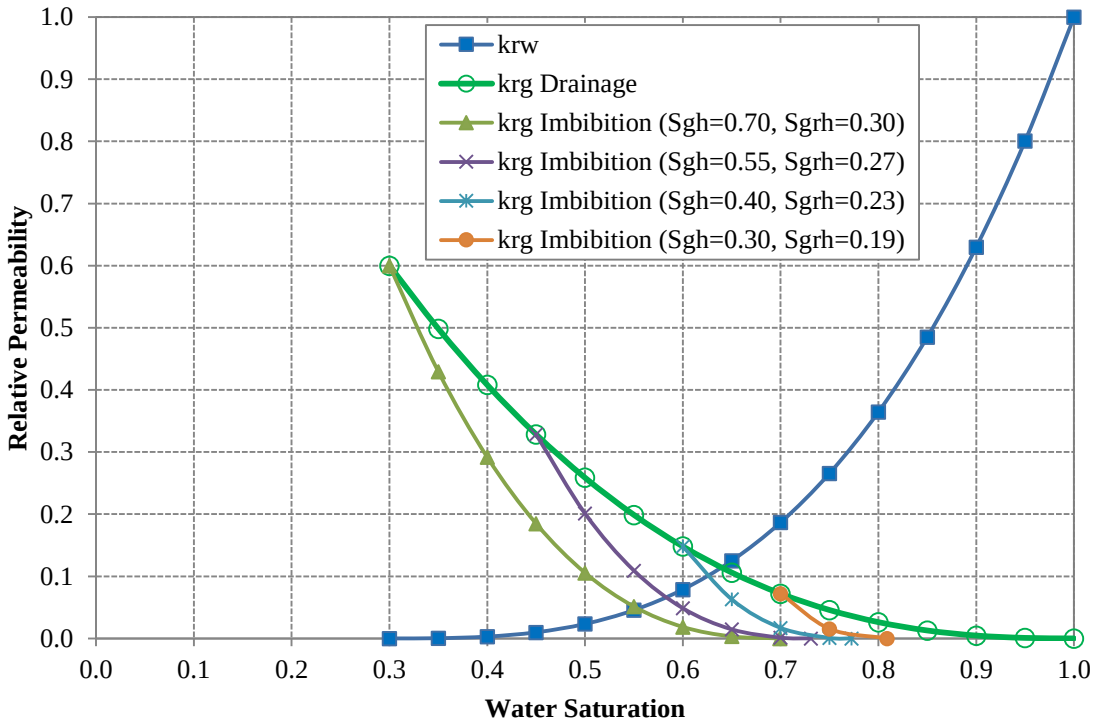

Figure 4-12: Relative permeability curves with hysteresis.

The effect of critical gas saturation on the flow of small gas saturations should be studied carefully. Figures 4-13 and 4-14 show the relative permeability models with critical gas saturation of 2.5% and 5.0%, respectively.

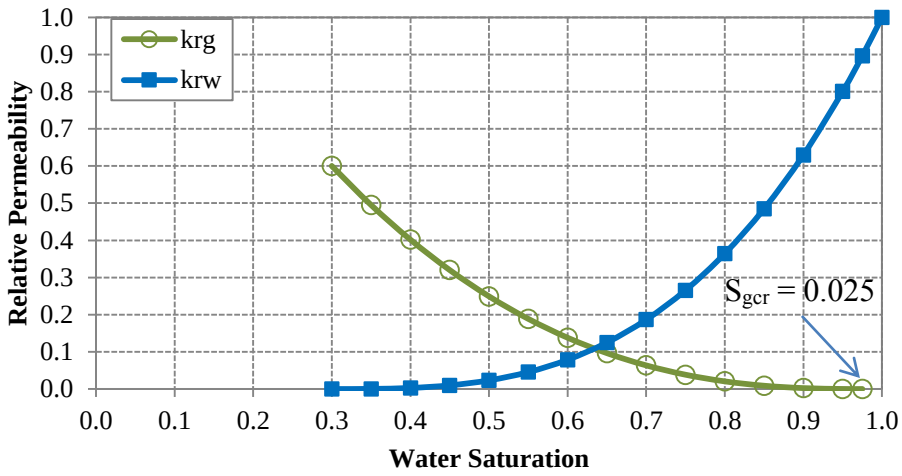

Figure 4-13: Relative permeability curves with critical gas saturation of 0.025.

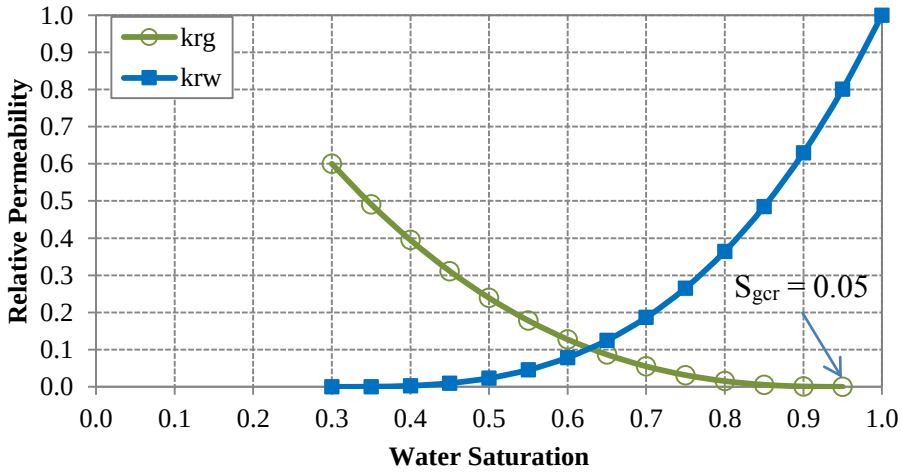

Figure 4-14: Relative permeability curves with critical gas saturation of 0.05.

4.2.5 Development Scenario

The process of gas evolution from high pressure brine as the pressure declines was studied. Questions asked about development scenarios examined in this study include: (1) could the evolved gas migrate upward and form a gas cap? If it is possible, wells can be drilled into the gas cap to produce the mobile gas similar to conventional reservoirs. (2) Is it possible to drop the reservoir pressure to a very low value so that huge volumes of gas evolve from the brine and flow toward the well? (3) Is it practical to perform pressure maintenance similar to conventional oil and gas reservoirs by re-injection of the produced brine?

The most important question in production of energy from aquifers is the necessity of reinjection of produced brine into the same aquifer. The reinjection of brine into the same aquifer provides pressure maintenance, which leads to a much higher energy recovery. Also, the issue of disposing the produced brine will be resolved. The disadvantage of reinjection is the amount of required energy which is comparable to the amount of produced energy. Two important questions about the reinjection strategy are the rate of injection and the start time of injection.

4.2.6 Well productivity

Migration of silt and clay, sand production as a result of high production rates, precipitation of salts from solution and evolution of free gas near the wellbore can reduce the permeability near the wellbore. These effects may be estimated by including the skin factor in the models. Another important factor in well productivity is the wellbore radius. Friction loss in wellbore is highly dependent on wellbore radius. Therefore, high production rates would be controlled by high friction loss in wellbore. A list of tubing diameters that are used in petroleum industry is presented in Table 4-8.

Table 4-8: Tubing inner and outer diameter and wellbore radius.

Tubing OD (in)	Tubing ID (in)	Wellbore Radius (ft)
3.5	2.992	0.1247
4.5	3.826	0.1594
5.5	4.778	0.1991
7	6.04	0.2517
8.5	7.2	0.3

4.2.7 Second order parameters

There are several other parameters related to the production of energy from geopressured-geothermal aquifers. Heterogeneity, fault block shape, wellbore flow, salts other than NaCl and gases other than methane are assumed to be second order effects with respect to the production of energy from aquifers.

4.3 SIMULATION MODEL

The first step in the study was to build a base case simulation model. The base case model was built using typical data for geopressured-geothermal aquifers presented in previous section. The dimensions are 2 miles × 2 miles × 400 ft. A five-spot well pattern is used for injection and production wells. Therefore, only a quarter of the model is used in simulation as a result of symmetry. Figure 4-15 is a schematic of the base case reservoir model.

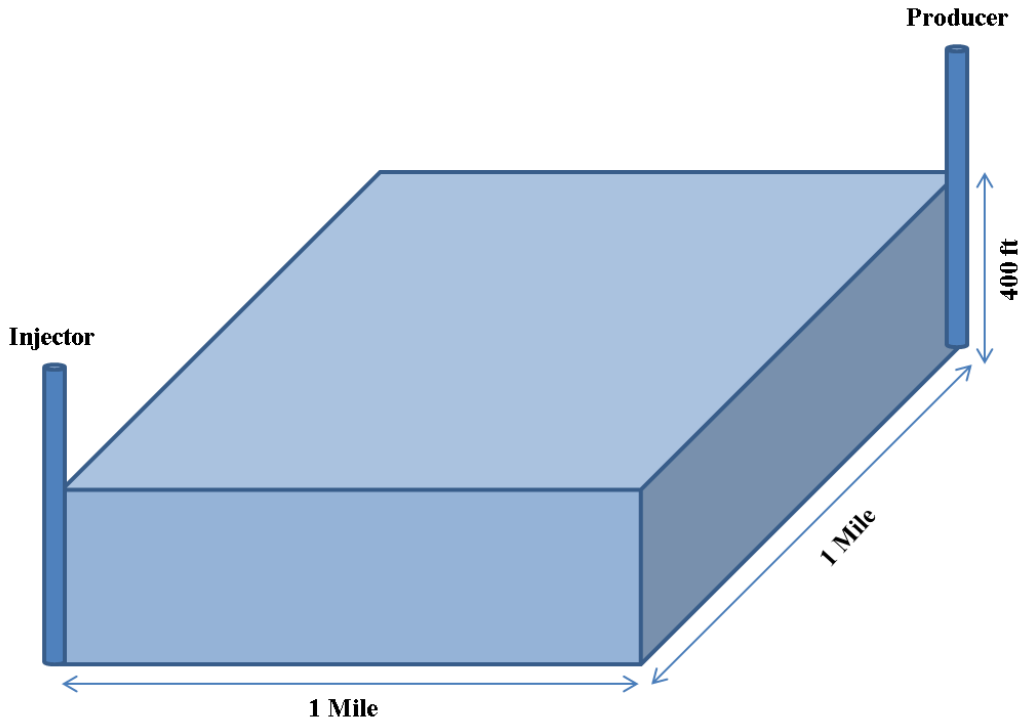

Figure 4-15: Schematic of the base case aquifer model.

The whole pattern is divided into 100 × 100 × 10 gridblocks. The dimension of each gridblock is 105.6 ft × 105.6 ft × 40 ft. The largest pressure drop occurs within 100 ft of the producer causing the most gas evolution in this area. Thus, the gridblocks where the producer is located has been refined into 10 × 10 × 10 smaller gridblocks. Figure 4-16 illustrates a 3-D view of the gridblocks. The depth at top of the formation is 15,000 feet. The fluid initial conditions are 11,000 psi, 302 °F, and 105,000 ppm similar to the sample described in Table 4-5. The initial pressure gradient is 0.733 psi/ft corresponding to geopressured condition. The brine is initially saturated with methane. Table 4-9 summarizes the most important properties of the aquifer model.

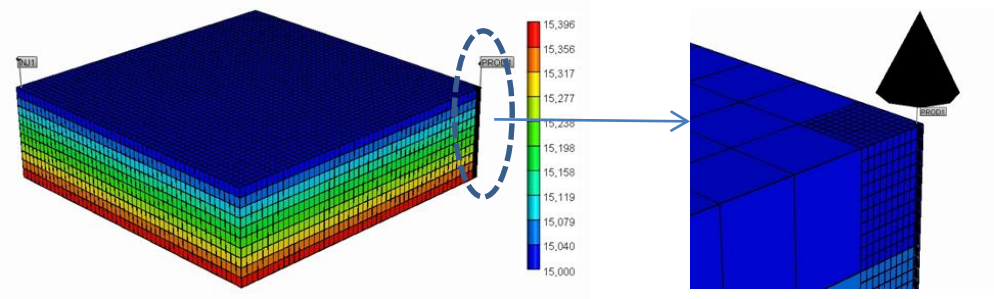

Figure 4-16: 3-D view of the grid structure and the model zoomed around the producer.

Table 4-9: Properties of base case aquifer model.

Length and width, mile	2
Thickness, ft	400
Number of gridblocks	100×100×10
Gridblock size, ft	105.6×105.6×40
Depth at top of the formation, ft	15000
Temperature, °F	302
Initial Pressure, psi	11,000
Salinity, ppm	105,000
Initial CH_4 concentration, mole %	0.48063
Initial brine concentration, mole %	99.51937
Porosity	0.2084
Permeability, md	20
K_V / k_h	0.1
Initial CH_4 in place, Billion SCF	57.68
Initial brine in place, Billion STB	1.607
Solution gas-water-ratio, SCF/STB	35.90
Total pore volume, Billion RB	1.705

The rock-fluid model is described in Tables 4-6 and 4-7. Also, hysteresis model is included in this study. Relative permeability curves, capillary pressure curve and hysteresis model are shown in Figures 4-10 through 4-12.

The GEM wellbore model was used to relate the wellhead pressures and bottomhole pressures. The wellbore radius is 0.2517 ft. The maximum liquid production rate is 25,000 stock tank barrels per day. It was assumed that the wellhead pressure of producer should not drop below 250 psi to have a high enough pressure to cause the fluid to flow to the surface. After a period of time, the wellhead pressure will drop to 250 psi. At this time, the constraint of maximum liquid production rate will be automatically switched to minimum wellhead pressure and the production rate will begin to drop until the production ceases.

4.4 SIMULATION RESULTS

In this section, simulation results are presented for three development scenarios. These scenarios are (1) drop the reservoir pressure to a very low value so that huge volumes of gas evolve from the brine and flow toward the well; (2) drop the reservoir pressure for a period of production and let the evolved gas migrate upward and form a gas cap; (3) perform pressure maintenance similar to conventional oil and gas reservoirs by re-injection of the produced brine.

4.4.1 Depletion to low pressure

The first production scenario is to produce the in-situ fluid until the pressure declines and production ceases. It is speculated that by decreasing the reservoir pressure, the evolved gas would form noticeable gas saturation and would flow as a bulk phase

toward wellbore. The critical gas saturation is selected to be zero for this part of the study to examine the best case scenario for the onset of the free gas flow. It is important for economic reasons to attain high production rate from geopressured aquifers. On the other hand, very high flow rates lead to production of small solid particles causing erosion in tubing. Maximum brine production rate is 25,000 STB per day. Table 4-10 shows the results of production for a 20-year period. Also, Figure 4-17 shows the brine production rate and cumulative produced brine versus time.

Table 4-10: Simulation results for depletion to low pressure.

Maximum brine production rate, STB/day	25,000
Minimum wellhead pressure of producer, psi	250
Tubing ID, inch	6.04
Production period, year	20
Injection period, year	0
Cumulative produced brine, Million STB	52.85
Cumulative produced gas, Billion SCF	1.624
Average produced gas-water ratio, SCF/STB	30.72
CH_4 recovery, %	2.82
Brine recovery, %	3.29

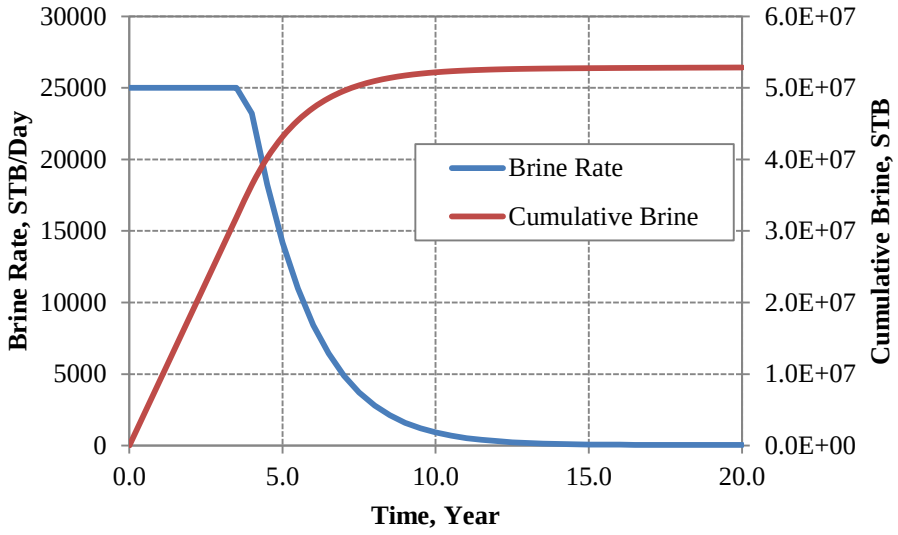

Figure 4-17: Brine production rate and cumulative brine at standard condition.

Figure 4-17 shows that the reservoir could only hold the maximum production rate for less than four years. At this time, the producer wellhead pressure drops to 250 psi. The well constraint is switched to constant wellhead pressure and the flow rate begins to drop gradually. At the end of 20-year period, the flow rate is less than 10 STB per day.

Figure 4-18 shows the gas production rate and gas-brine ratio at standard conditions. It was speculated that by pressure decline in the formation, gas would evolve from brine and would be produced at a higher rate, while it is observed that gas production rate decreases with time. Also, gas-brine ratio decreases gradually from initial ratio of 35.0 SCF/STB to 26.5 SCF/STB. The preliminary results show that a fraction of the in-situ gas could not be produced even by decreasing the pressure close to hydrostatic pressure.

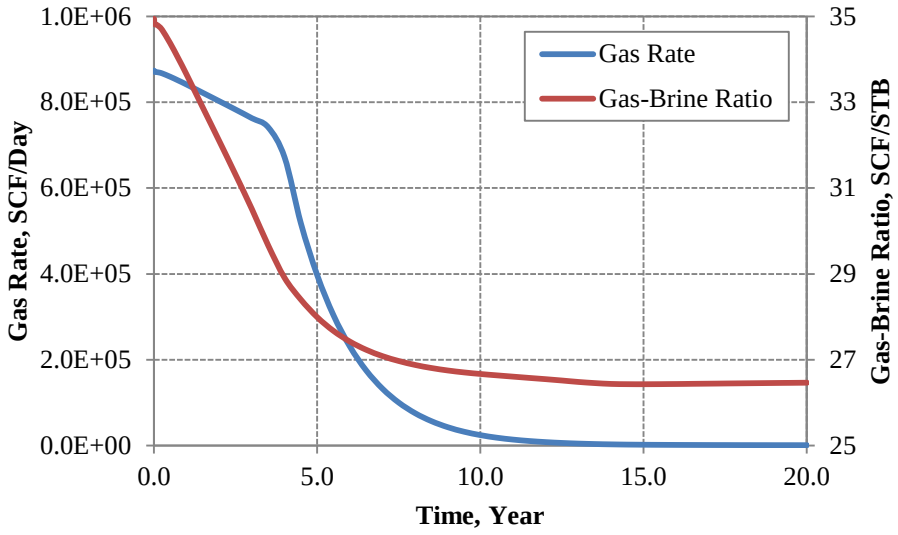

Figure 4-18: Gas production rate and gas-brine ratio at standard condition.

Figure 4-19 shows the pressure profile in the top layer of gridblocks on a straight line between injector and producer for six different times. Injector is shut throughout the whole 20 years of production. The pressure drawdown inside the aquifer is about 550 psi as long as the wellhead pressure of producer is above the minimum constraint. At the end of the production period, the pressure drawdown tends to zero and the reservoir pressure to hydrostatic pressure. The hydrostatic pressure is the minimum pressure that can be achieved without using artificial lift. The minimum attainable pressure near the producer is about 6,250 psi. Figure 4-9 shows that by dropping the pressure from 11,000 psi to 6,250 psi in the aquifer, about 9 SCF of methane would be released from each barrel of brine. This is equivalent to about 0.6 percent gas saturation which is very low to trigger significant flow of gas phase.

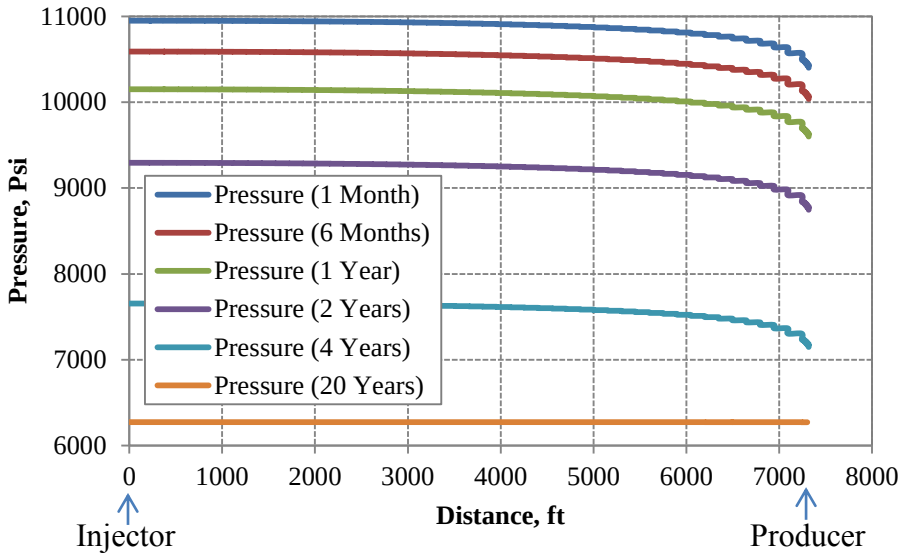

Figure 4-19: Pressure profile in the top layer of gridblocks between injector and producer at several times. Injector is shut in.

Figure 4-20 illustrates the gas saturation profile on a vertical cut between injector and producer at 20 years. It is observed that the evolved gas saturation far from the producer is less than one percent. The gas saturation is about 3 percent near wellbore. The relative permeability curve in Figure 4-10 shows that the flow of gas at 3 percent saturation is negligible even when assuming zero critical gas saturation. The results illuminate that the production of gas evolved by depletion of the formation is not practical without using artificial lift. The artificial lift for production of huge rates at high depths is very expensive if it is technically possible. It is concluded that only the fraction of methane which is still dissolved at bottomhole conditions can be produced along with the brine.

Figure 4-20: Gas saturation profile on a vertical cut between injector and producer at 20 years. Injector is shut in.

4.4.2 Formation of a gas cap

The second development scenario is to attempt to drop the reservoir pressure by a period of production and let the evolved gas migrate upward and form a gas cap. If this could be accomplished, subsequent wells could be drilled into the gas cap and produce the gas alone. The strategy for this part of study consists of reservoir depletion over 20 years to let the gas evolve from brine. After shutting in the producer, simulations would continue for 50 years to see if a gas cap forms. The base case simulation model in section 4.4.1 is used in this study. Since the vertical migration of gas is of interest, the thickness of gridblocks is refined from 40 ft to 10 ft. Also, the ratio of vertical to horizontal permeability is the main factor in the vertical migration of gas. Therefore, this scenario has been examined with three ratios. These ratios are 0.01, 0.1, and 1.0. Figures 4-21 through 4-23 show the pressure profile on a vertical cut between injector and producer after 20 years of depletion and 50 years of upward migration.

Figure 4-21: Gas saturation after 70 years for $k_v/k_h = 0.01$.

Figure 4-22: Gas saturation after 70 years for $k_v/k_h = 0.1$.

Figure 4-23: Gas saturation after 70 years for $k_v/k_h = 1.0$.

Figure 4-21 shows that gas saturation in the top layer barely exceeds 1 percent at a small permeability ratio of 0.01. Figure 4-22 shows that gas saturation in the top layer is less than 2 percent at moderate permeability ratio of 0.1. Figure 4-23 shows highest gas accumulation at top layer for very favorable permeability ratio of 1.0. The highest gas saturation for the best scenario is less than 5 percent. Very low gas saturation in the top layers might be a result of hysteresis effect. During the upward migration of evolved gas, aqueous phase flows downward. The counter-current flow of two phases leads to trapping of a fraction of the gas. Also, at the end of the production period, saturation of evolved gas in each gridblock is very small resulting in very small relative permeability. Thus, the gas velocity would be very small. It is concluded that formation of gas cap after reservoir depletion is not achievable even after 50 years from termination of depletion.

4.4.3 Pressure maintenance

Another scenario for enhancing gas production from geopressured aquifers is to perform pressure maintenance similar to conventional oil and gas reservoirs by re-injection of the produced brine into the same aquifer from which it was produced. In this strategy, first the aquifer would be depleted as long as the wellhead pressure of the producer is above minimum constraint and the producer maintains its maximum flow rate. As soon as the wellhead pressure of the producer reaches the minimum constraint, re-injection would commence at the same rate of production. The principal advantage of pressure maintenance is significant recovery of in-situ energy compared to sole depletion. Another advantage of this strategy is the disposal of extracted brine into the same formation preventing environmental issues and land subsidence. Furthermore, it could make possible the exploitation of much smaller geopressured aquifers than those required

for deletion alone. Table 4-11 shows the results of injection and production for a 20-year period. The base case simulation model in section 4.4.1 is used in this study. All the gridblocks in which the injector and producer are perforated are refined into 10 × 10 × 10 smaller gridblocks.

Table 4-11: Injection and production summary for pressure maintenance strategy.

Maximum brine production rate, STB/day	25,000
Minimum wellhead pressure of producer, psi	250
Minimum wellhead pressure of producer at start of reinjection, psi	400
Maximum brine injection rate, STB/day	25,000
Maximum wellhead pressure of injector, psi	4500
Tubing ID, inch	6.04
Production period, year	20
Injection period, year	16.4
Cumulative produced brine, Million STB	181.03
Cumulative produced gas, Billion SCF	5.399
Average produced gas-water ratio, SCF/STB	29.82
Cumulative injected brine, Million STB	149.71
CH_4 recovery, %	9.36
Brine recovery, %	11.27

Figure 4-24 shows the wellhead pressure of injector and producer versus time. As soon as the wellhead pressure of producer drops below 400 psi, re-injection of the produced brine begins. After about 10 years, the wellhead pressure of injector and producer tend to about 3,000 and 250 psi, respectively.

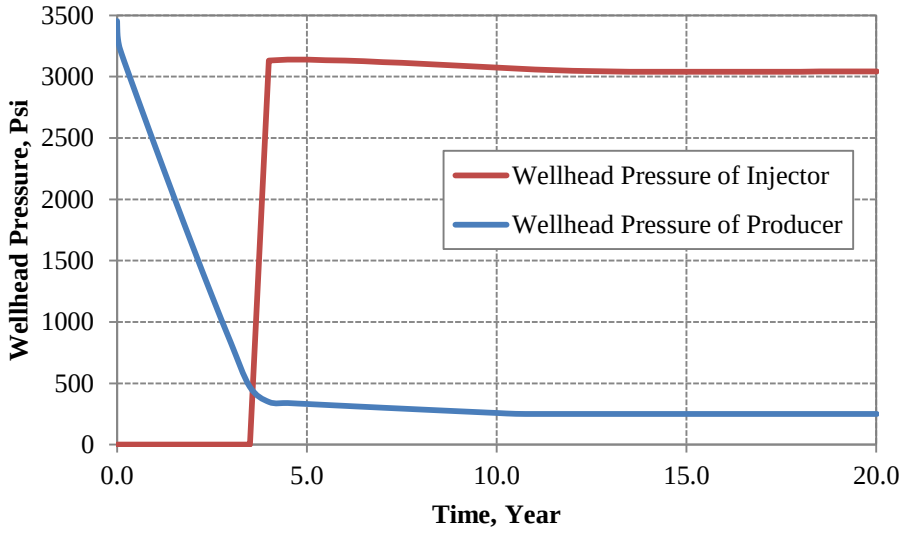

Figure 4-24: Wellhead pressure of producer and injector for pressure maintenance strategy.

Figure 4-25 shows the cumulative produced and injected brine over 20 years. After about 3.6 years, re-injection of the produced brine begins. The rate of production and reinjection are almost equal. There is always a difference between the cumulative produced brine and injected brine. The difference represents the amount of produced brine before the start of re-injection. Figure 4-26 shows the gas production rate and produced gas-brine ratio over 20 years. The gas production rate decreases until the start of re-injection. After beginning of re-injection, the gas production almost remains constant. The reason is that the pressure becomes steady by pressure maintenance. Thus, the amount of dissolved gas in brine remains constant near wellbore.

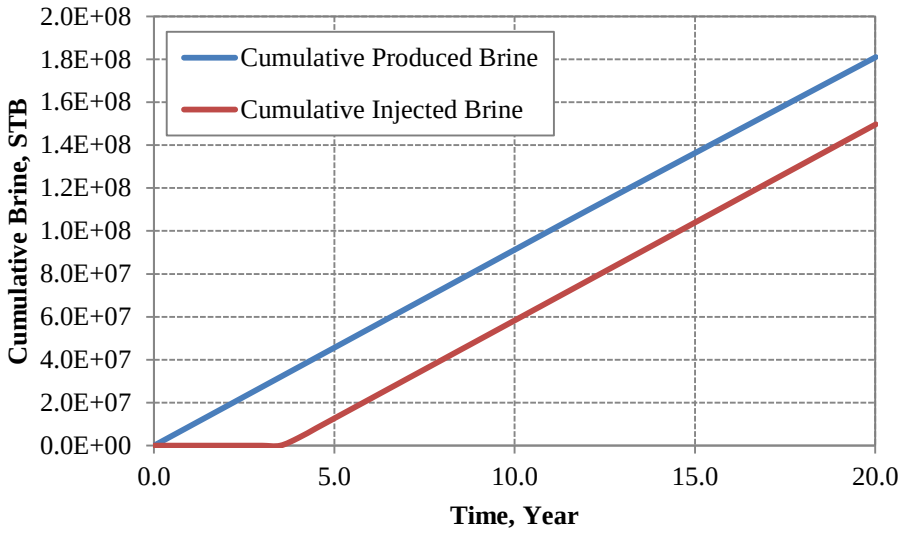

Figure 4-25: Cumulative produced and injected brine for pressure maintenance strategy.

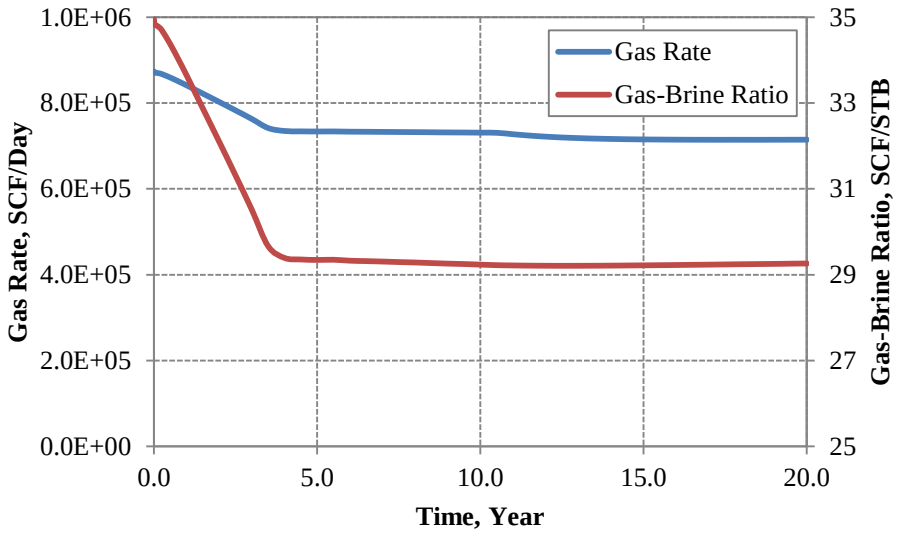

Figure 4-26: Produced gas rate and gas-brine ratio for pressure maintenance strategy.

Figure 4-27 shows the pressure profile in the top layer of gridblocks on a straight line between the injector and producer for six different times. The pressure drawdown inside the aquifer is about 850 psi before the start of re-injection. The pressure profile becomes steady state after start of re-injection. The pressure drawdown inside the aquifer is about 1,800 psi during this period. Also, the released gas saturation would not go beyond 2 percent even close to the wellbore of the producer.

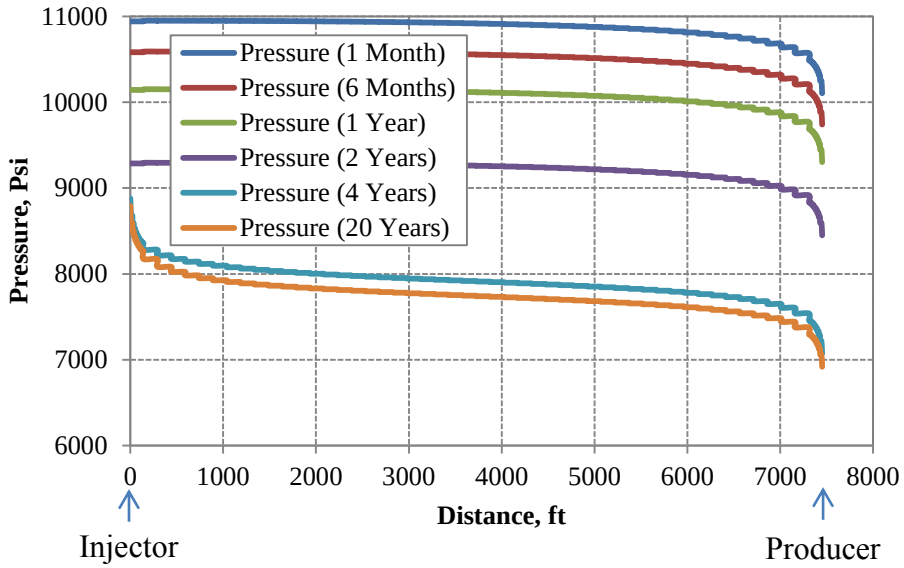

Figure 4-27: Pressure profile at top layer gridblocks between injector and producer at several times for pressure maintenance strategy.

Figures 4-28 and 4-29 illustrate the CH_4 mole fraction distribution and temperature distribution on a vertical cut between injector and producer after 20 years. The zero CH_4 concentration in Figure 4-28 corresponds to the region where has been swept by injected brine. Comparing the front of injected brine in Figure 4-28 and front of

temperature in Figure 4-29 specifies that the temperature front falls behind the mass front. Thus, all the methane can be swept before the breakthrough of cold brine.

Figure 4-28: Distribution of CH_4 concentration between injector and producer.

Figure 4-29: Distribution of temperature between injector and producer.

The results show that pressure maintenance has the advantage of keeping the brine and gas production rates constant during the 20-year period. Hence, the energy recovery factor is much higher compared to depletion case. Also, the recovery factor is almost 10 percent indicating the presence of significant amounts of energy still in place at

the end of 20-year period. It is concluded that pressure maintenance scenario requires much smaller aquifer size compared to aquifer depletion case.

4.4.4 Effect of critical gas saturation on gas recovery

The possibility of production of an initial immobile free gas should be investigated. Some aquifers might have an initial immobile gas saturation which is smaller than the critical gas saturation. The question is whether it is practical to mobilize the gas by depleting the aquifer. Reservoir simulation study was performed for three initial gas saturations of 0.0, 0.025 and 0.05. Relative permeability models shown in Figures 4-10, 4-13, and 4-14 were used for the three initial gas saturations, respectively. Table 4-12 summarizes the initial conditions for the three models.

Table 4-12: Initial condition for three critical gas saturations of 0.0, 0.025, and 0.05.

Initial gas saturation	Initial gas mole fraction	Initial gas-brine ratio (SCF/STB)	Critical gas saturation
0.0	0.0048	35.90	0.0
0.025	0.0121	91.06	0.025
0.05	0.0196	148.65	0.05

Table 4-13 shows the cumulative produced gas and water and also the average produced gas-brine ratio after 20 years. The results show that increasing the initial immobile gas saturation increases the cumulative produced gas and brine, whereas it has very small effect on average produced gas-brine ratio. It is concluded that a very slight percentage of immobile gas can be produced by reservoir depletion.

Table 4-13: Production summary for three critical gas saturations of 0.0, 0.025, and 0.05.

Initial gas saturation	Cumulative produced gas (SCF)	Cumulative produced brine (STB)	Produced gas-brine ratio (SCF/STB)
0.0	1.62E+09	52.85E+06	30.72
0.025	2.11E+09	67.98E+06	30.99
0.05	2.33E+09	83.12E+06	32.63

Figure 4-30 shows the brine production rate for three initial gas saturations. It is observed that aquifer with higher initial immobile gas saturation maintains the liquid production rate for a longer period of time. The expansion of in-situ gas maintains the reservoir pressure during the depletion process. Thus, production decline occurs later resulting in higher cumulative production.

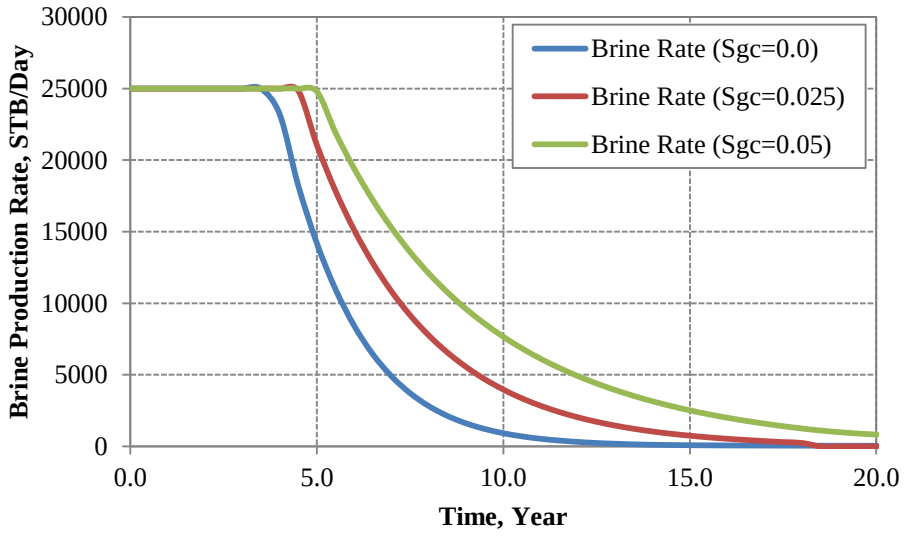

Figure 4-30: Brine production rate for three initial and corresponding critical gas saturations of 0.0, 0.025, and 0.05.

4.5 SENSITIVITY ANALYSIS

Parameter space sampling is the most important step in Sensitivity Analysis and Uncertainty Assessment. The outcome of parameter space sampling is a Design for laying out a detailed simulation plan in advance of doing simulations. A well selected design maximizes the amount of "information" that can be obtained for a given amount of simulation effort. Figure 4-31 shows an uncertainty prioritization matrix. The parameters are prioritized based on their expected impact on the results and the ability to include them in the study based on the computational cost.

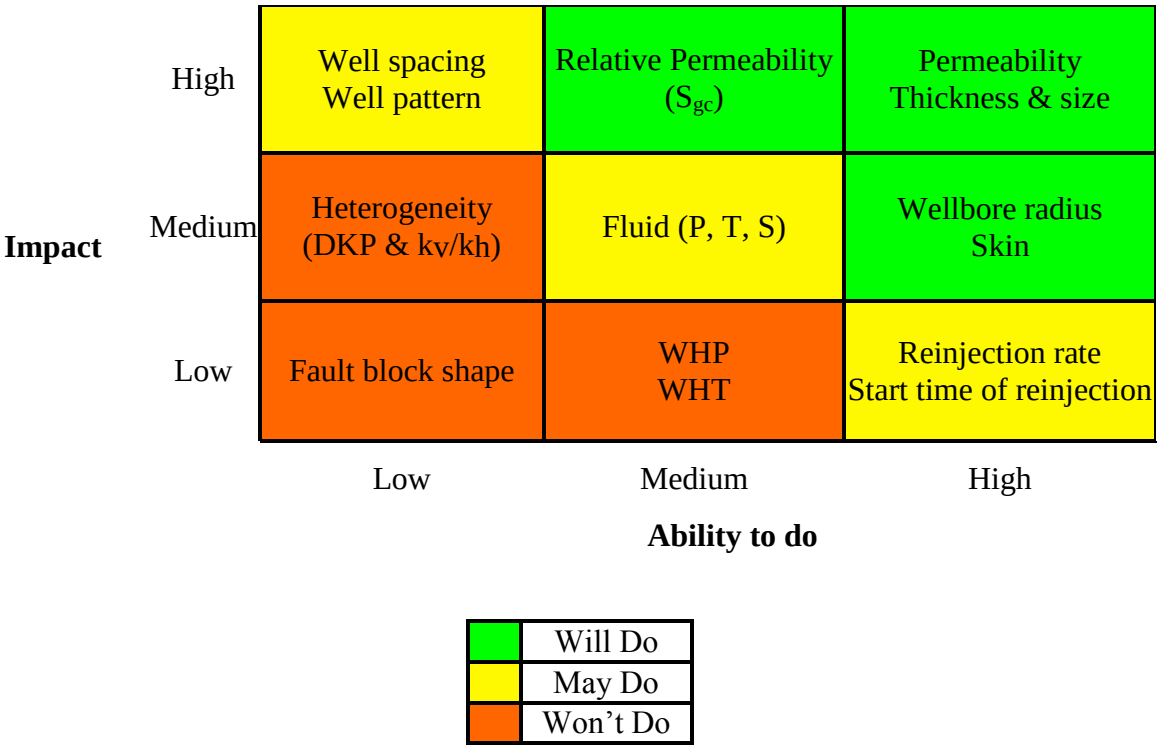

Figure 4-31: Uncertainty prioritization matrix.

Six parameters are involved in sensitivity analysis. Five samples are selected for each parameters based on the information from the analysis of uncertainty. Therefore, the

parameter space, which is the number of all possible job patterns, is 15,625. Table 4-14 summarizes all the samples for the selected parameters.

Table 4-14: Samples of parameters in sensitivity analysis.

Parameters	Samples				
Size, mi^2	1	4	9	16	25
Thickness, ft	180	300	400	500	600
Permeability, md	2	10	20	50	100
Reinjection ratio, %	0	25	50	75	100
Skin	-4	-2	0	10	20
Tubing ID, in	2.992	3.826	4.778	6.04	7.2

It is not feasible to perform simulations over the whole parameter space. Therefore, a sampling method is used to select a set of job patterns from all possible job patterns. A set of job patterns generated by sampling method is called a design. A good design with favorable characteristics can be used to fit an accurate proxy model and draw reliable conclusions regarding parameter effects. In order to efficiently explore the parameter space, the design selected should possess two desirable characteristics: (1) approximate orthogonality of the input parameters. (2) space-filling, that is, the sampling points (job patterns) should be evenly distributed in the parameter space. In other words, the collection of job patterns (computational experiments) should be a representative subset of all possible job patterns.

4.5.1 One-Parameter-at-a-Time method

In this study, first the method of One-Parameter-at-a-Time is used to draw preliminary conclusions. These conclusions help to shrink the parameter space significantly. In this method, one of the parameters is varied over the range of the samples and all other parameters are fixed at a base case condition. This procedure was performed for all the parameters. The strategy of brine reinjection for pressure maintenance was selected for the base case model. It is assumed that the maximum brine production rate is 25,000 STB/Day and the wellhead pressure of the injector is limited to 4,500 psi. Cumulative produced brine and cumulative produced gas were chosen as objective functions. The job patterns and the results of objective functions are presented in Appendix A.1.

Tornado plots are a visual display of the effect of variation of parameters on objective functions. There is one tornado plot for each objective function. Parameters (terms) are ordered from having the greatest effect on the objective function to having the least effect. Each parameter is given its own color for all plots. The maximum bar represents the maximum objective function value among all the training jobs. The minimum bar represents the minimum objective function value among all the training jobs. Figures 4-32 and 4-33 show the tornado charts for cumulative produced water and gas, respectively. Based on the results of One-Parameter-at-a-Time method, the following preliminary conclusions are drawn:

- Most of the increase in production occurs from 0% to 75% reinjection. There is less increase from 75% to 100% reinjection.
- The majority of the increase in production happens from 2 md to 10 md. The production is not sensitive to permeability above 20 md.

- The relationship between the change in skin and the change in production is almost linear.
- By decreasing the tubing ID below the 4.778 in, a significant drop in production rate occurred.

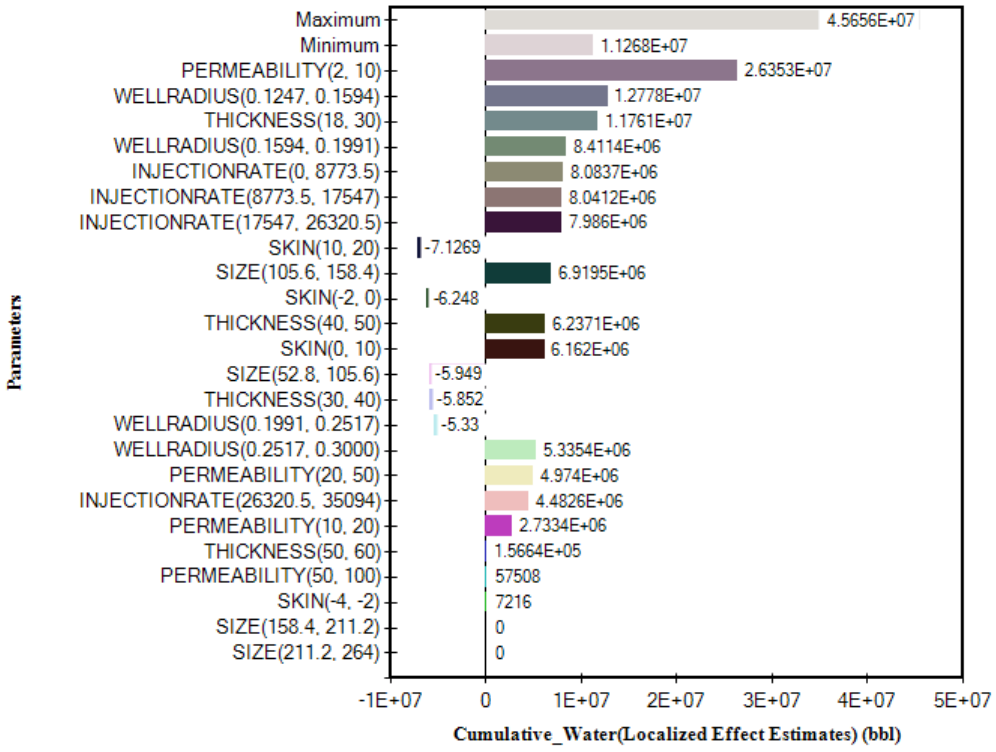

Figure 4-32: Tornado chart for cumulative produced brine for One-parameter-at-a-Time.

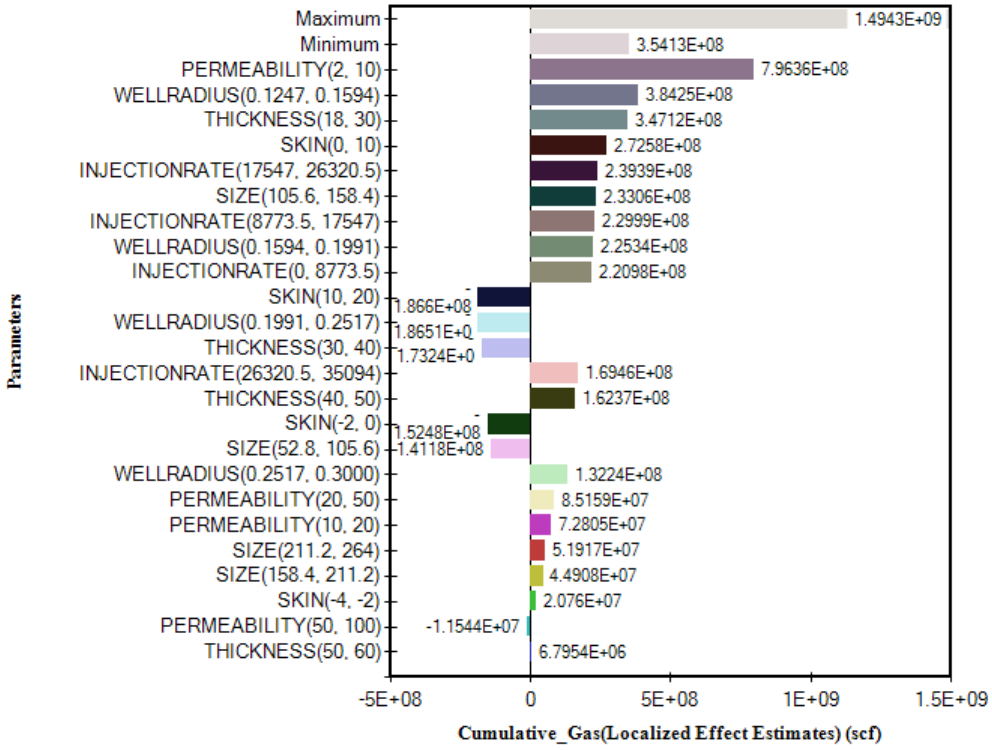

Figure 4-33: Tornado chart for cumulative produced gas for One-parameter-at-a-Time.

4.5.2 Latin Hypercube method

Based on the preliminary results from the One-Parameter-at-a-Time method, the parameter space was reduced to 972 job patterns. Table 4-15 shows the parameters selected based on the conclusions from One-Parameter-at-a-Time method.

Table 4-15: Samples of parameters used for Latin Hypercube sampling method.

Parameters	Samples				
Size, mi^2	1	4	9	-	-
Thickness, ft	-	300	400	-	600
Permeability, md	-	10	20	50	100
Reinjection ratio, %	0	-	50	-	100
Skin	-4	-	0	10	-
Tubing ID, in	-	-	4.778	6.04	7.2

Latin Hypercube is a state-of-the-art sampling method. Using Latin Hypercube, 120 job patterns are selected for a specific design. The job patterns and the results of objective functions are presented in Appendix A.2. The results of these simulations are used in response surface methodology. Response surface methodology is the relationship between input variables (parameters) and responses (objective functions). Quadratic polynomial functions are used as proxy models. Also, cumulative produced water and cumulative produced gas are selected as objective functions. The following two equations are the proxy models:

$$
\begin{aligned}
&\textit{Cumulative produced water} = -(1.24583E+7) \\
&+(16982.5)L+(364702)H+(180905)K+(1386.01)I-(446036)S-(2.25384E+7)R \\
&+(538.882)L^2+(3149.99)LH+(280.43)LK-(6.90341)LI+(694.635)LS-(73551.2)LR \\
&-(2203.27)H^2-(1354.2)HK-(3.37834)HI+(5285.72)HS-(504619)HR \\
&-(1067.41)K^2+(1.72197)KI+(5166.33)KS-(98739.8)KR \\
&-(0.00399153)I^2-(4.07154)IS+(1127.78)IR \\
&+(12906.4)S^2-(890237)SR \\
&+(7.70403E+7)R^2
\end{aligned}
$$

$$\text{Cumulative produced gas} = -(2.8977E+8)$$
$$-(452782)L+(1.03333E+7)H+(4.69088E+6)K+(42038.4)I-(1.06919E+7)S-(9.75814E+8)R$$
$$+(19407.7)L^2+(108138)LH+(9676.98)LK-(193.8)LI+(19799.9)LS-(2.36564E+6)LR$$
$$-(74800.3)H^2-(34091.6)HK-(106.776)HI+(154199)HS-(1.34786E+7)HR$$
$$-(26909.5)K^2+(30.6256)KI+(113269)KS-(3.76321E+6)KR$$
$$-(0.0608992)I^2+(10.4601)IS+(19657.9)IR$$
$$+(323000)S^2-(2.62885E+7)SR$$
$$+(2.97916E+9)R^2$$

Table 4-16 summarizes the parameters and their range in proxy models. Simulations were performed for a quarter of a five-spot well pattern. Thus, the injection rate represents a quarter of the total rate for each injector.

Table 4-16: Parameters and their range in proxy models for Latin Hypercube sampling method.

Parameter	Description	Range
L, ft	1/100 of fault block length	52.8 – 264
H, ft	1/10 of formation thickness	18 – 60
K, md	Permeability	2 – 100
I, ft3/day	¼ of Injection rate	0.0 – 35094
S	Skin factor	-4 – 10
R, ft	Wellbore radius	0.1991 – 0.3

4.6 ECONOMIC CRITERIA

A sensitivity analysis on important formation properties was performed to determine the economic criteria for both 100% re-injection and no re-injection cases. These two cases are identical to depletion to low pressure and pressure maintenance

cases, respectively. Since the behavior of the results are very different for 100% re-injection and no-reinjection cases, it is necessary to do the sensitivity analysis separately for these cases. Size, thickness and permeability are chosen as formation parameters and five samples are chosen for each parameter. So, the parameter space is 125 and 50 samples are selected by Latin Hypercube method. The same samples are used for both 100% re-injection and no re-injection cases. Figures 4-34 and 4-35 show the tornado charts for the case of no re-injection for cumulative produced water and gas, respectively. It can be concluded from the tornado charts that size and thickness have the dominant effects on production and effect of permeability is much smaller. Figure 4-37 shows the water production rate after 20 years for all 50 cases versus the volume of the aquifer. The volume of the aquifer can be calculated by multiplying the areal size and thickness. Considering a maximum 6% decline in production rate per year as a criterion for the case of no reinjection, the economic criterion after 20 years would be a production rate of 7,500 STB/Day. Figure 4-36 shows that the volume of the aquifer should be at least 1.0 cubic mile to have this minimum production rate after 20 years. Also, permeability has minor effect on the production rate. The data points which are larger than 1.0 cubic mile in Figure 4-37 are used to define the reservoir quality for the case of no re-injection.

- Permeabilities less than 10 md are considered as poor quality.
- Permeabilities between 10 md and 20 md are considered as marginal quality.
- Permeabilities higher than 20 md are considered as good quality.

Finally, it should be mentioned that the overall productivity of a well is determined from the combination of reservoir size and quality.

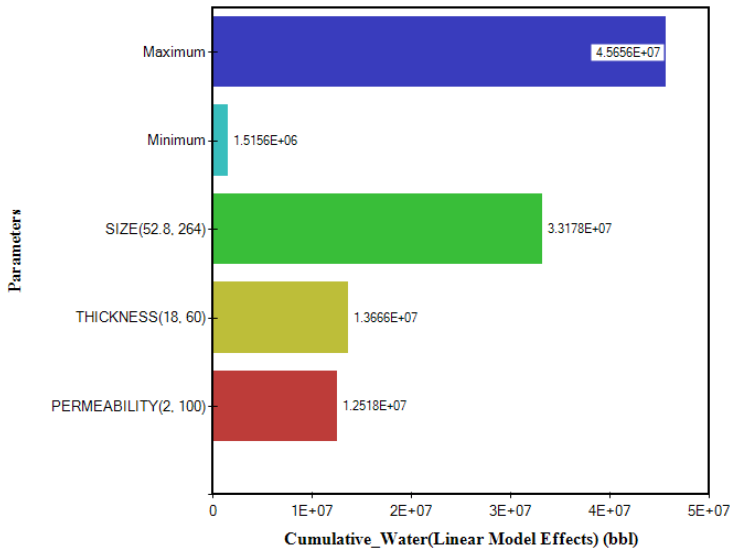

Figure 4-34: Tornado chart for cumulative water (no reinjection).

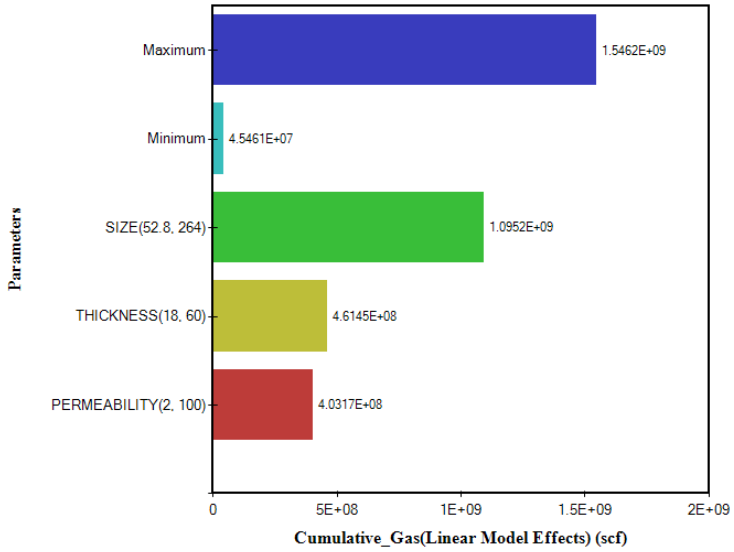

Figure 4-35: Tornado chart for cumulative gas (no reinjection).

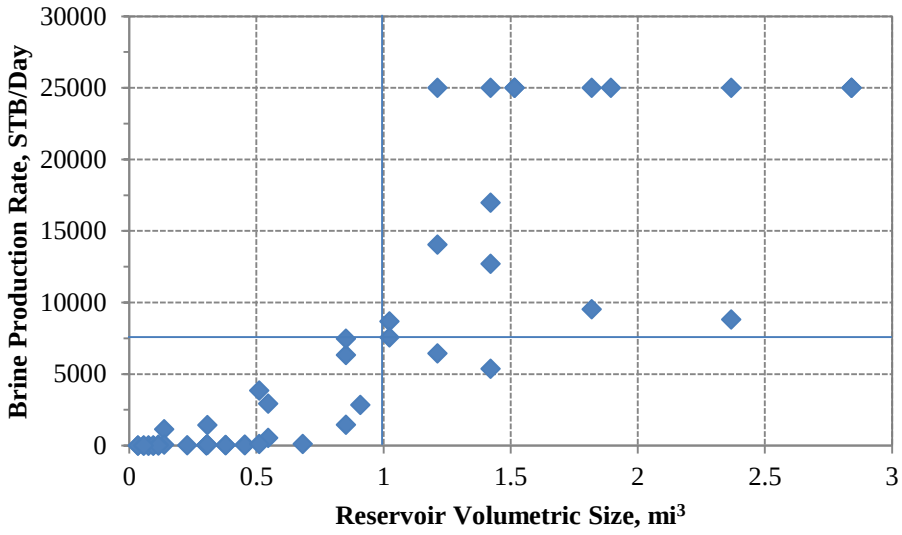

Figure 4-36: Water production rates after 20 years versus aquifer volume for 50 job patterns for areal size, thickness, and permeability (no reinjection).

Figures 4-37 and 4-38 show the tornado charts for the case of 100% re-injection for cumulative produced water and gas, respectively. It can be seen from the tornado charts that permeability and thickness have the dominant effects on production and effect of size is negligible. Figure 4-40 shows the water production rate after 20 years for all 50 cases versus the kh of the aquifer. The kh of the aquifer is calculated by multiplying the permeability and thickness. Considering a maximum 10% decline in production rate over the whole 20 years for the case of 100% re-injection, the economic criterion after 20 years would be a production rate of 22,500 STB/Day. Figure 4-39 shows that the kh of the aquifer should be at least 5000 md ft to have this minimum production rate after 20 years.

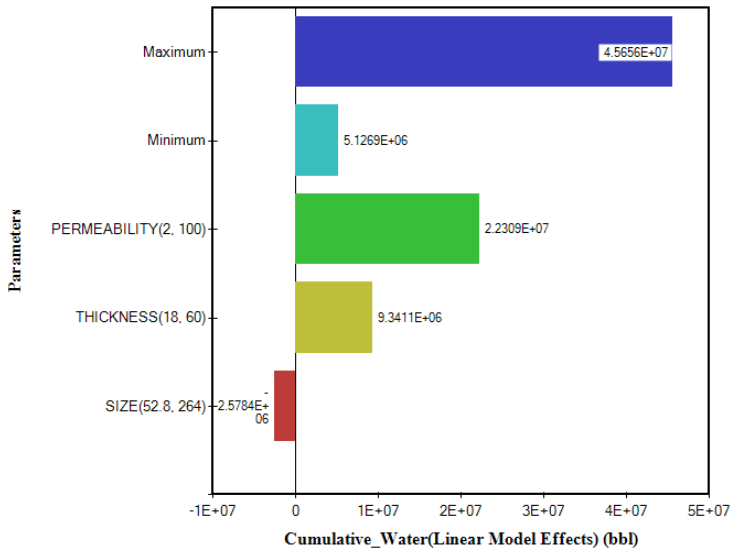

Figure 4-37: Tornado chart for cumulative water (100% reinjection).

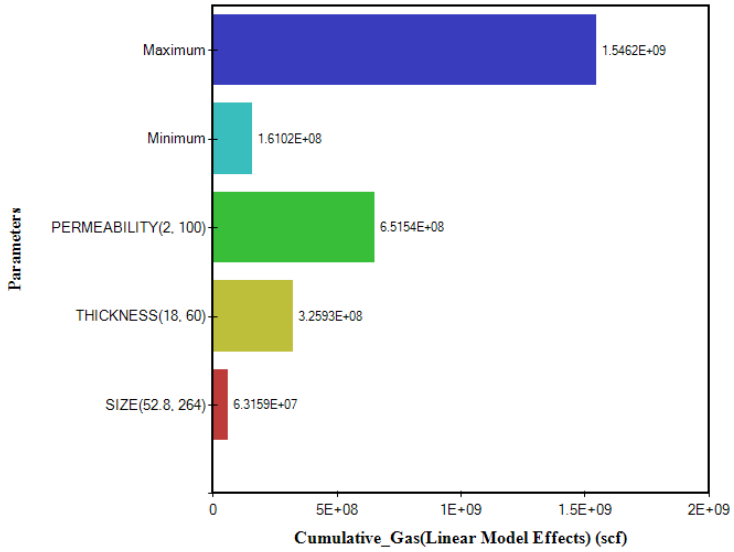

Figure 4-38: Tornado chart for cumulative gas (100% reinjection).

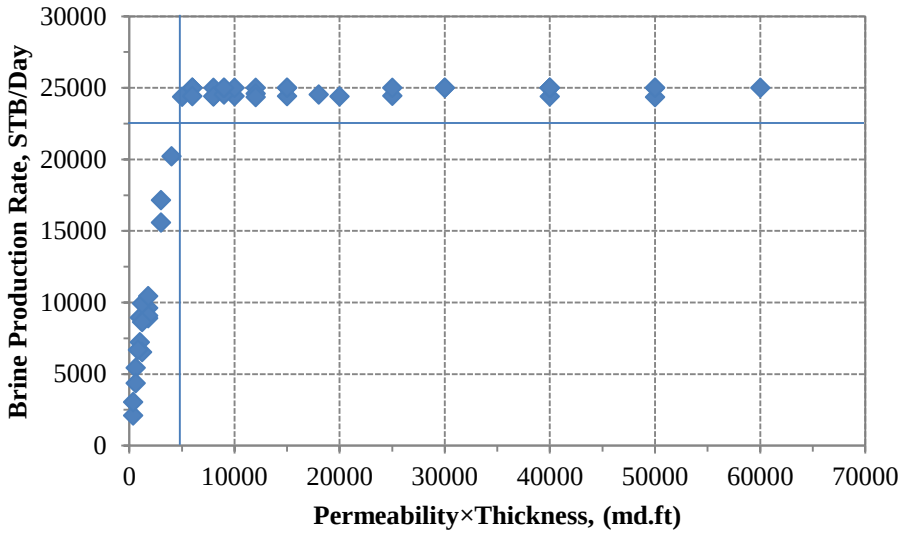

Figure 4-39: Water production rates after 20 years for 50 job patterns for areal size, thickness, and permeability (100% reinjection).

4.7 SUMMARY

In this chapter, the feasibility of energy production from geopressured-geothermal aquifers of Gulf Coast was examined. Uncertainty of parameters was studied from available data. The results of reservoir simulations were presented for various production scenarios. Finally, sensitivity analysis were performed to determine the effect of aquifer properties on produced energy and to define economic criteria.

- Methane dissolved in the brine at bottomhole conditions can be produced along with the brine.
- Production of gas evolved by depletion of the formation is not practical without using artificial lift. The artificial lift for production of huge rates at high depths would be very expensive if it were technically possible.

- Formation of gas cap after reservoir depletion is not achievable even after 50 years from termination of depletion.
- Pressure maintenance has the advantage of keeping the brine and gas production rates constant during the 20-year period.
- The energy recovery factor for pressure maintenance case is much higher compared to depletion case.
- Pressure maintenance scenario requires much smaller aquifer size compared to aquifer depletion case.
- A very small percentage of immobile gas can be produced by reservoir depletion. The gas saturation is increased by less than one percent when a fraction of dissolved gas is released.
- Aquifers with higher initial immobile gas saturation maintain the liquid production rate for longer period as a result of the expansion of in-situ gas phase. Thus, production decline occurs later resulting in higher cumulative production.
- Size, thickness and permeability are the most important formation parameters in production.
- Reservoir volume is the governing factor in production by depletion.
- The product of thickness and permeability (kh) is the governing factor in production by reinjection.
- Reinjection has several advantages such as increasing the sustainability of production, reducing reservoir connectivity risk, and disposal of produced brine in the same formation.

Chapter 5: Coupled Carbon Dioxide Sequestration and Energy Production from Geopressured-Geothermal Aquifers

In this chapter, a feasibility study of coupling the CO_2 storage and energy production from aquifers was investigated. This study was focused on geopressured-geothermal aquifers as well-established sources of methane and geothermal energy.

5.1 INTRODUCTION

The sequestration of carbon dioxide and other greenhouse gases in deep saline aquifers as well as the extraction of methane and geothermal energy (heat) from deep geopressured-geothermal aquifers have been studied independently in the past. However, capturing and storing CO_2 in aquifers is an expensive process without any monetary return on investment. On the other hand, energy extraction from deep geopressured aquifers was abandoned as a result of low natural gas prices in the 70s and 80s (Griggs, 2005), which prevented this process from becoming economically feasible. In addition the strategies used at the time were not the best strategies for maximizing energy extraction. In this study, we present a new strategy in which the CO_2 sequestration and methane/geothermal energy extraction are combined. In fact, we suggest that the cost of the former can be offset by the profits from the latter.

Geologic formations are capable of storing huge amounts of CO_2. Specifically, deep saline aquifers are the best candidates for the storage of significant amounts of CO_2 emitted by pulverized coal-fired power plants. However, the storage technology faces several constraints. The most important constraint is the cost of the storage process which includes capturing, purifying, pressurizing, and injecting CO_2 (Rochelle, 2009). In addition to the storage cost, other possible constraints exist such as the injection capacity of the aquifer and environmental risks.

Formations of abnormally high pressure and temperature lie along the Gulf Coast of the United States at depths exceeding 10,000 feet. The brine in these formations is saturated with methane. The methane content of this brine is on the order of 30-45 SCF of methane per barrel and the total amount is estimated to be between 3,000 to 46,000 TCF (Griggs, 2005). For example, at 34 SCF per barrel, a small geopressured aquifer with a pore volume of 1 billion barrels would hold a volume of dissolved methane of 34 BCF with an energy content of 35 trillion Btu. When CO_2 is dissolved in brine saturated with methane, almost all of the methane comes out of the solution and forms a gas phase of almost pure methane (Taggart, 2010). The production of this methane could help offset the cost of CO_2 storage. Moreover, the production of methane gas and/or brine saturated with methane while CO_2 is being injected will reduce or eliminate concerns about pressure build-up accompanying CO_2 injection. This pressure build-up is a key constraint on large-scale sequestration, because it significantly reduces achievable rates of CO_2 injection.

The geothermal energy content of the hot brine is also significant. The temperature of Gulf Coast geothermal aquifers is about 300°F. Therefore, the energy that can be extracted from produced brine is of the same order of magnitude as the energy from the produced methane. For example, 35,000 Btu (10.25 kWh) of heat can be

extracted by reducing the temperature of one barrel of hot water from 300 °F to 200 °F. Thus, a 1 billion barrel aquifer at 300 °F contains 35 trillion Btu (10.25 Billion kWh) of geothermal energy.

Injection into the aquifer as a supercritical fluid is the most common method to inject the CO_2. When the CO_2 mixes with the brine in the aquifer, the methane will come out of the solution and flow upward where it can be captured and produced from a production well at a higher elevation in the aquifer. However, our preliminary calculations indicate a superior approach: inject CO_2 and brine simultaneously deep in the aquifer and allow the brine with dissolved CO_2 to displace the brine with dissolved methane upward to production wells. This approach is more efficient because the cold brine saturated with CO_2 is more viscous and heavier than the warm brine saturated with methane. This process results in higher recovery of the methane as well as other significant advantages that will be discussed later.

Issues that need further consideration to optimize and predict the potential for production of dissolved methane and geothermal energy by CO_2 injection are the following: The locations of suitable aquifers; the volume and concentration of methane in brine; the most favorable aquifer conditions; the fraction of dissolved methane that can be produced; the best strategies for injecting CO_2 and producing methane and geothermal energy; and the best strategy for well types, locations, and the operating conditions.

In this study, first, the feasibility of striping out the methane by injecting CO_2 is studied using a 1-D simulation model. Then, injection strategies were investigated and compared using 3-D numerical simulation models.

5.2 1-D SIMULATION OF INJECTING CO_2 INTO CH_4-SATURATED AQUIFER

CO_2 is an extractive component that is capable of removing lighter components from host fluids such as brine. In this study, it will be demonstrated that CO_2 is capable of stripping out methane from brine. In a two-phase system consisting of a CO_2-rich phase and a CH_4-saturated aqueous phase, methane is extracted from brine and appears in a gas phase. Also, CO_2 replaces the methane in aqueous phase in dissolved form. This research investigated whether a significant proportion of methane can be produced while CO_2 is stored permanently. The phase behavior of a three component mixture consisting of CO_2, CH_4, and brine was studied at subsurface conditions. Then 1-D simulations were performed to evaluate the process of methane extraction in the presence of CO_2.

5.2.1 Phase behavior of CO_2-CH_4-brine mixtures

Figure 5-1 shows the solubility of CO_2 and methane over wide ranges of pressure and temperature at the salinity of 55,000 ppm (Duan and Mao, 2006 and Duan and Sun, 2003). The solubility increases by increasing the pressure and temperature. It is observed that the solubility of CO_2 in brine is about an order of magnitude higher than the solubility of methane. Figure 5-2 shows the ratio of solubility of CO_2 to solubility of methane at 55,000 ppm. The solubility ratio decreases by increasing the pressure and temperature. This ratio is about 5 to 7 at pressures and temperatures identical to geopressured-geothermal aquifers of Gulf Coast. It means that each mole of methane could be substituted by 5 to 7 moles of CO_2. The polar CO_2 molecule has the upper hand in competition for dissolution in brine compared to the non-polar CH_4 molecule. Thus, CH_4 is replaced by CO_2 when CO_2 is injected into CH_4-saturated brine.

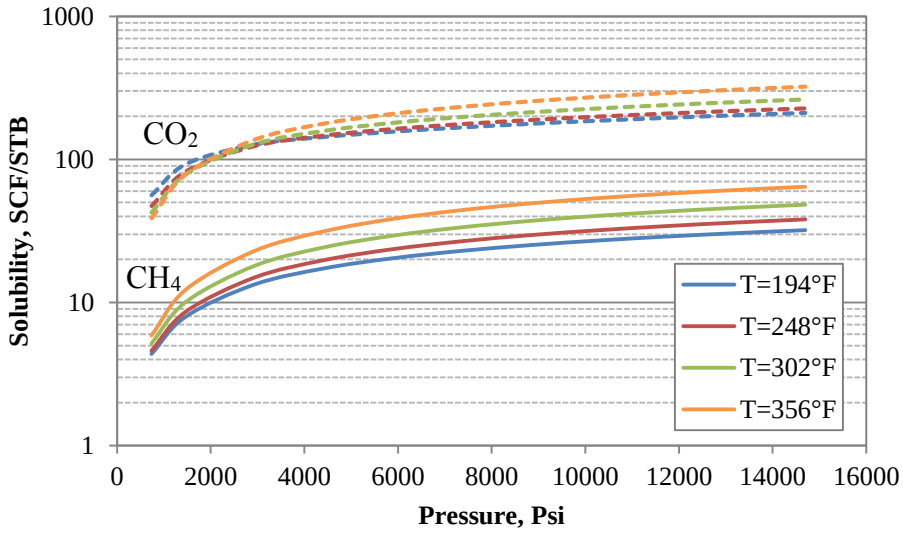

Figure 5-1: Solubility of CO_2 and CH_4 in brine at 55,000 ppm salinity.

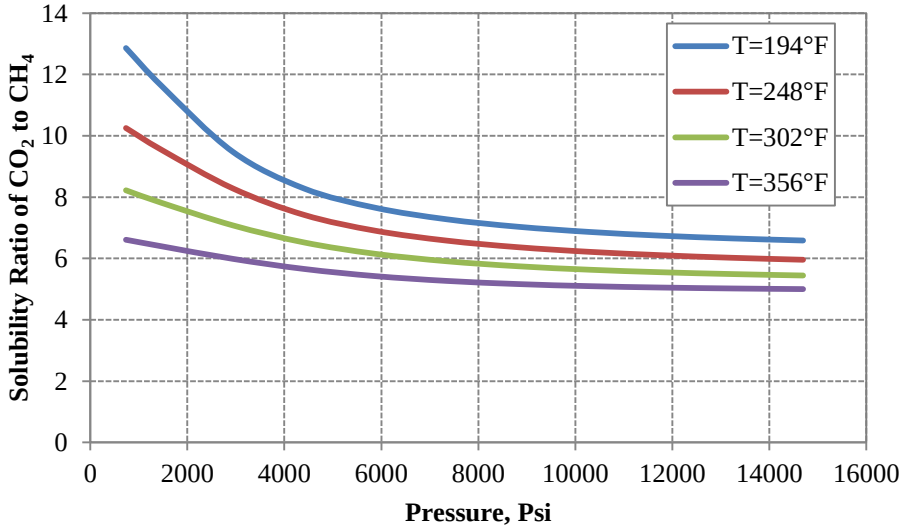

Figure 5-2: Ratio of solubility of CO_2 in brine to solubility of CH_4 at 55,000 ppm.

5.2.2 1-D simulation model

A one-dimensional reservoir model was prepared to examine the hypothesis of methane stripping by CO_2 injection. The model is of a high poro-perm aquifer with good quality homogeneous sand. The aquifer brine is initially saturated with methane at 11,000 psi. Table 5-1 summarizes the properties of the 1-D model.

Table 5-1: Properties of one-dimensional aquifer model.

Dimensions, ft	1000×1×1
Number of gridblocks	1000×1×1
Gridblock size, ft	1000×1×1
Depth at top of the formation, ft	15000
Temperature, °F	302
Initial Pressure, psi	11,000
Salinity, ppm	55,000
Initial CH_4 concentration, mole %	0.573
Initial brine concentration, mole %	99.427
Porosity	0.2463
Permeability, md	100
k_V / k_h	0.1
Solution gas-water-ratio, SCF/STB	42.91

Peng-Robinson equation-of-state (PREOS) was used to model the interaction between CO_2, CH_4, and brine. The phase behavior model was tuned to the experimental data for solubility, density, and viscosity. One fluid sample at the condition of 11,000 psi, 302 °F, and 55,000 ppm was to build a phase behavior model. The data of this model are

gathered in Table 5-2. To predict the fluid rates at surface condition, a separate phase behavior model was prepared at surface pressure and temperature. The solubility of CO_2 and methane in brine at surface condition are negligible. The properties of gas at surface condition are predicted accurately by ideal gas law. Volume shift is the only parameter that was tuned at surface condition. The density of the brine sample at aquifer condition is 989.5 kg/m3, while its density at surface condition (14.7 psi and 60 °F) is 1036.0 kg/m3. Also, molecular weight of H_2O is corrected to consider the effect of salinity on density. The molecular weight is increased from 18.01 g/g-mole to 19.42 g/g-mole for salinity of 55,000 ppm.

Table 5-2: Component properties tuned for 11,000 psi, 302 °F, and 55,000 ppm.

Component name	CO_2	CH_4	H_2O
Critical pressure, atm	72.8	45.4	217.6
Critical temperature, °K	304.2	190.6	647.3
Critical volume, m^3/k-mole	0.094	0.099	0.056
Molecular wt., g/g-mole	44.01	16.043	18.73
Acentric factor	0.225	0.008	0.344
Parachor	78	77	52
Omega A	0.4572	0.4572	0.4572
Omega B	0.077796	0.077796	0.077796
Volume shift (at reservoir condition)	-0.075904	-0.17121	0.22001
Volume shift (at surface condition)	0.0	0.0	0.16025
Critical volume (viscosity), m^3/k-mole	0.095190	0.092283	0.047835
BIC corresponding to H_2O	0.0326	0.0277	0

The behavior of two phase flow of gas and aqueous phases is carefully modeled via relative permeability curves. Equations 3-13 and 3-14 have been used to build relative permeability curves for two phases. Table 5-3 summarizes the parameters used in these equations. Also, Figure 5-3 illustrates the relative permeability curves of phases with zero critical gas saturation including the curves corresponding to hysteresis effect during gas imbibition. This example has been built for a rock with average permeability of 100 md. Equations 3-10 to 3-12 have been used to predict porosity, irreducible water saturation and maximum residual gas saturation. The corresponding porosity is 0.2463.

Table 5-3: Relative permeability parameters.

Gas end-point relative permeability	0.7
Water end point relative permeability	1.0
Critical gas saturation	0.0
Connate gas saturation	0.0
Maximum trapped gas saturation	0.3085
Irreducible water saturation	0.1970
Gas relative permeability exponent	2.5
Water relative permeability exponent	3.0

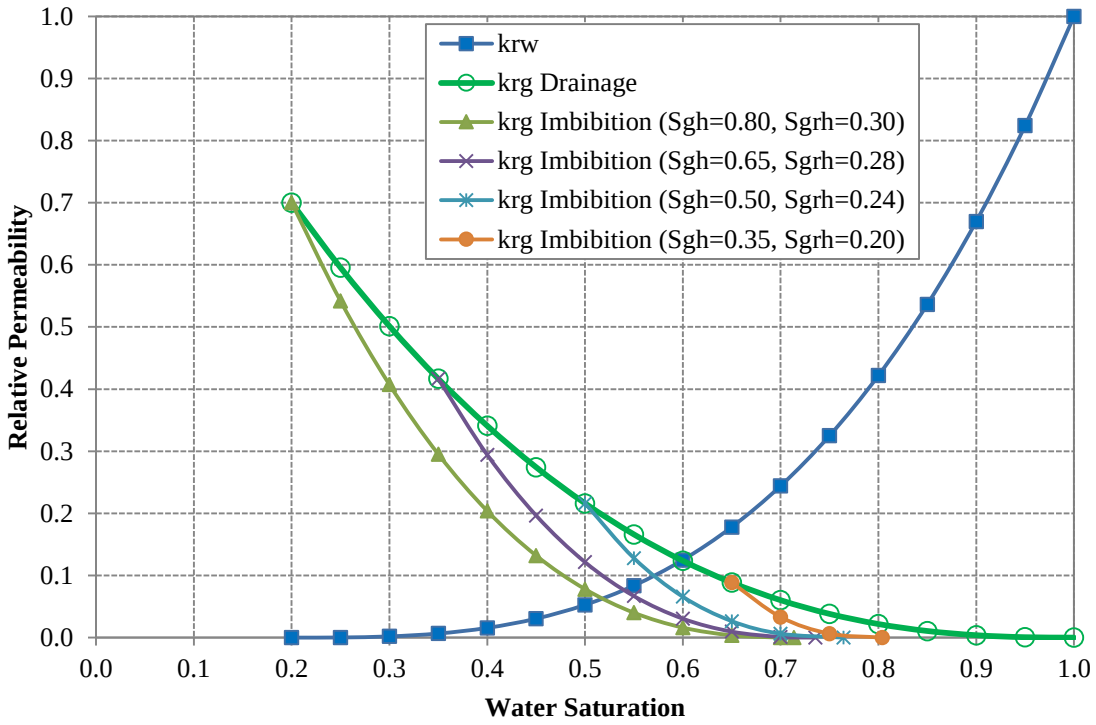

Figure 5-3: Relative permeability curves with hysteresis.

Table 5-4 shows the Brooks-Corey parameters for capillary pressure curve in equation 3-18 used along with relative permeability curves. Also, Figure 5-4 shows the capillary pressure curves from those parameters.

Table 5-4: Parameters of Brooks-Corey for capillary pressure curve.

P_e	1.5
λ	8.0
Irreducible water saturation, S_{wir}	0.1970

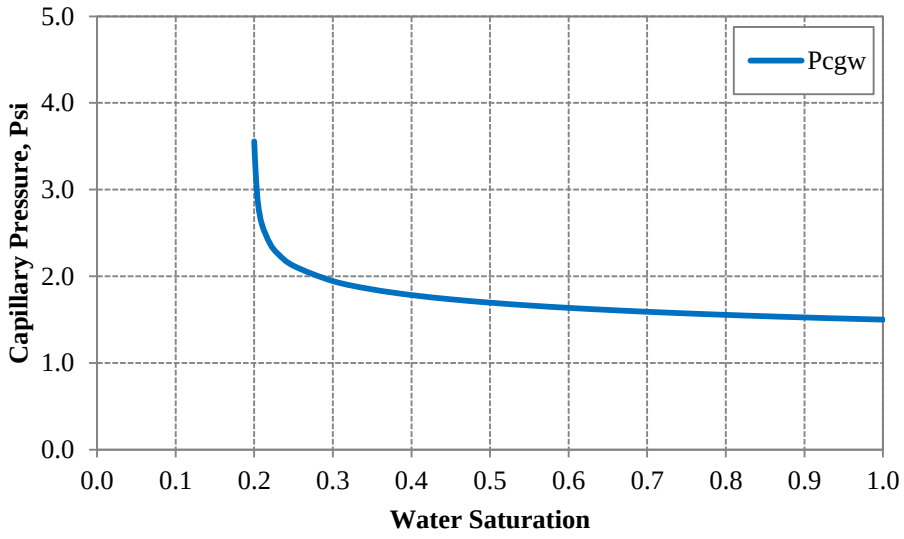

Figure 5-4: Capillary pressure curve for drainage.

5.2.3 1-D simulation results

A left-to-right displacement of methane-saturated brine by injecting CO_2 in a 1000 ft linear segment was simulated using GEM (2011). One thousand gridblocks were chosen in the direction of segment to mitigate the numerical dispersion and allow the simulator to capture sharp fronts. The bottomhole pressures of injector and producer were 12,000 and 11,000 psi, respectively.

Figure 5-5 shows the composition profiles of CH_4 and CO_2 throughout the segment from injector to producer after 20, 40, and 60 days. It is observed that the injected CO_2 bank is preceded by a CH_4 bank and there is no methane left behind the methane bank. Also, it is revealed that the methane bank becomes more separated from injected CO_2 by time. Nevertheless, there is always a mixing zone between injected CO_2 and back end of the methane bank.

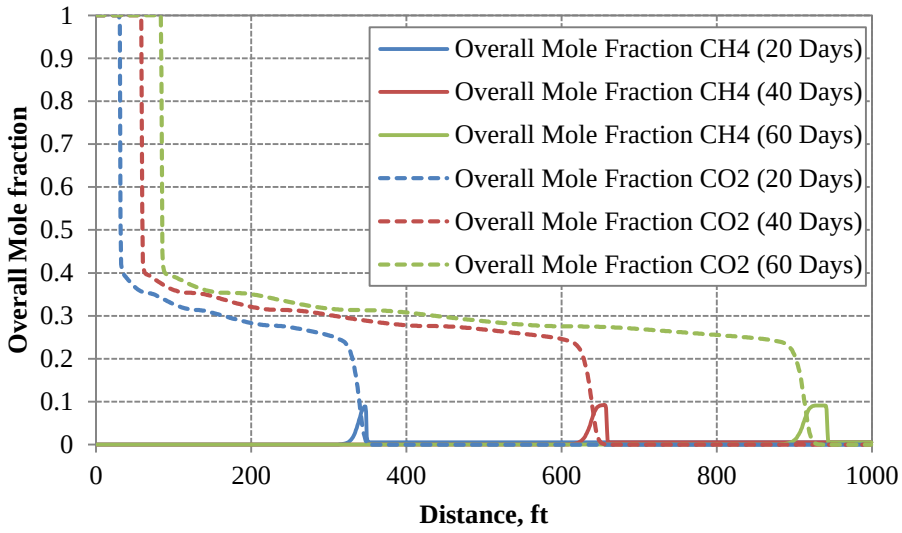

Figure 5-5: Composition profile of CH_4 and CO_2 between injector to producer after 20, 40, and 60 days.

Figure 5-6 illustrates the overall mole fraction of CO_2 and CH_4 for the effluent composition. The breakthrough of methane bank occurs after 64 days. Before the breakthrough, only methane-saturated brine is produced. After 70 days, no methane exists in the effluent. Also, drying occurs close to injector where the irreducible water is totally evaporated. The simulation results provide a very good understanding of the chromatographic separation.

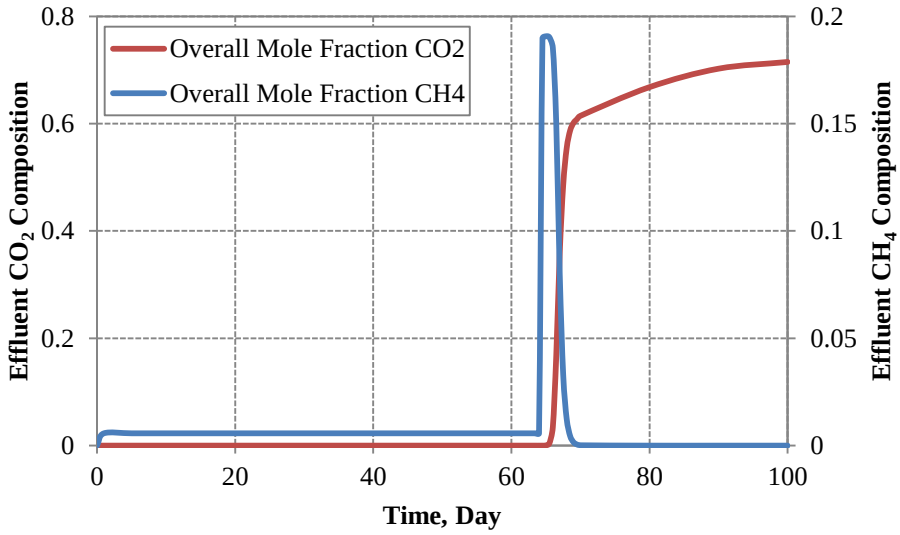

Figure 5-6: Overall mole fraction of CH_4 and CO_2 in the effluent.

5.3 3-D SIMULATION OF INJECTING CO_2 INTO CH_4-SATURATED AQUIFER

The 1-D simulation study verified that injected CO_2 extracts methane from brine. The next step was to investigate the potential of producing methane and hot brine by injecting CO_2 in more realistic 3-D aquifers, while the ultimate objective was to assess the feasibility of energy production by permanent CO_2 storage. The same methane extraction mechanism may be capable of improving the methane recovery in 3-D simulations. However, sweep efficiency drawbacks such as unfavorable mobility ratio and gravity override of bulk CO_2 are involved in 3-D cases.

Three main strategies may be considered to inject CO_2 and produce methane and/or hot brine: (1) To inject CO_2 at high depth and let the methane come out and form a gas cap; (2) To inject supercritical CO_2 and produce methane and brine simultaneously; (3) To dissolve CO_2 into the produced brine and inject the CO_2-saturated brine to

improve the recovery of methane and hot brine. These injection strategies will be examined after presenting the 3-D simulation model.

5.3.1 3-D simulation model

A 5280 ft by 5280 ft by 300 ft segment was selected as base case for three-dimensional simulation study. The depth at top of the formation is 15,000 ft. The brine is initially saturated with methane at 11,000 psi, 302 °F, and 55,000 ppm. The initial pressure gradient is 0.733 psi/ft corresponding to geopressured condition. A parallel horizontal well pattern is used for injection and production wells. It is supposed that half of the wells are placed at the edge of the gridblocks to maintain the symmetry. Larger aquifer models may be built by placing several of these patterns next to each other. Figure 5-7 illustrates a simple schematic of the base case segment model. Table 5-5 summarizes the most important properties of the segment model.

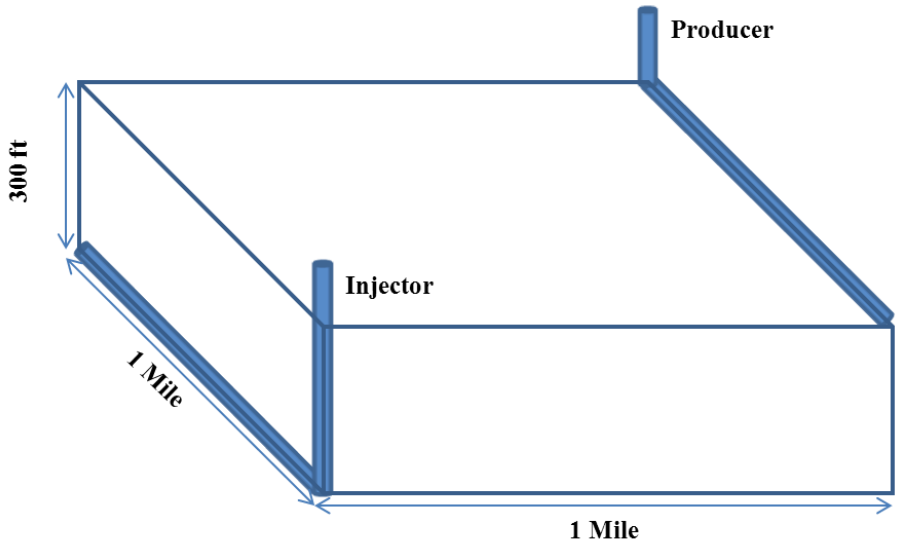

Figure 5-7: Schematic of the half of the base case aquifer model with half a horizontal injector and half a horizontal producer.

Table 5-5: Properties of base case aquifer model.

Length and width, mile	1
Thickness, ft	300
Number of gridblocks	80×80×30
Gridblock size, ft	66×66×10
Depth at top of the formation, ft	15000
Temperature, °F	302
Initial Pressure, psi	11,000
Salinity, ppm	55,000
Initial CH_4 concentration, mole %	0.573
Initial brine concentration, mole %	99.427
Porosity	0.2463
Permeability, md	100
k_V / k_h	0.1
Initial CH_4 in place, Billion SCF	15.28
Initial brine in place, Billion STB	0.356
Solution gas-water-ratio, SCF/STB	42.91
Total pore volume, Billion RB	0.378

The initial conditions are similar to the 1-D case. Thus, the phase behavior dataset in Table 5-2 is used here. Also, relative permeability and capillary pressure models are the same as the ones used for 1-D simulation. Next, simulation results will be presented for three injection and extraction strategies.

5.3.2 Formation of gas cap by CO_2 injection

The first investigated strategy was to inject supercritical CO_2 deep into the aquifer and let the CO_2 migrate upward. It is speculated that the rising CO_2 would contact the methane-saturated brine and the methane would be stripped out of the brine. Finally, the free methane would form a gas cap under the top seal that can be produced later.

Supercritical CO_2 was injected for the first six months while the producer was shut. A maximum bottomhole pressure of 12,000 psi was set for the injector to avoid fracturing the formation that may cause the CO_2 leakage. Thus, the production tended to zero after six months because of the increase in formation pressure. Figure 5-8 shows the CO_2 injection rate for the six-month period. During this period, about 300,000 metric tons of supercritical CO_2 was injected into the aquifer.

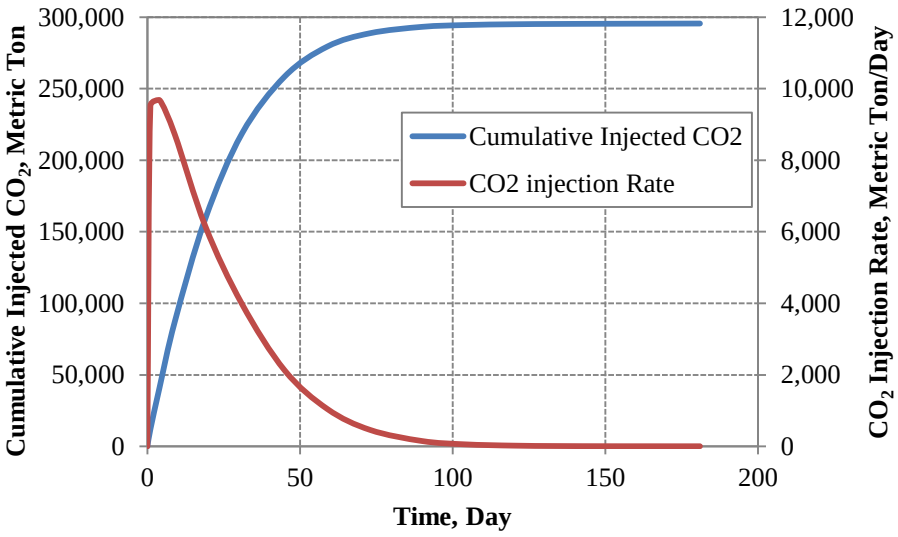

Figure 5-8: Cumulative injected CO_2 and injection rate for six months for the case of injection without production.

After the end of injection, simulation was continued for 50 years to investigate the movement of the methane bank and CO_2 plume. Figure 5-9 shows the overall mole fraction of methane after 50 years. It is observed that the methane bank has not reached the top of the formation even after 50 years. Also, the concentration of methane barely reaches the 4 percent in the methane bank. Figure 5-10 shows the gas saturation throughout the segment after 50 years. It is noted that no gas cap has been formed after 50 years. The reason is that a vast percentage of gas would be trapped during the counter-current flow of gas and aqueous phases. Additional injection of CO_2 is required which is not viable due to the limited capacity of the aquifer. Hence, it is concluded that the formation of methane-rich gas cap by injecting CO_2 is not practical.

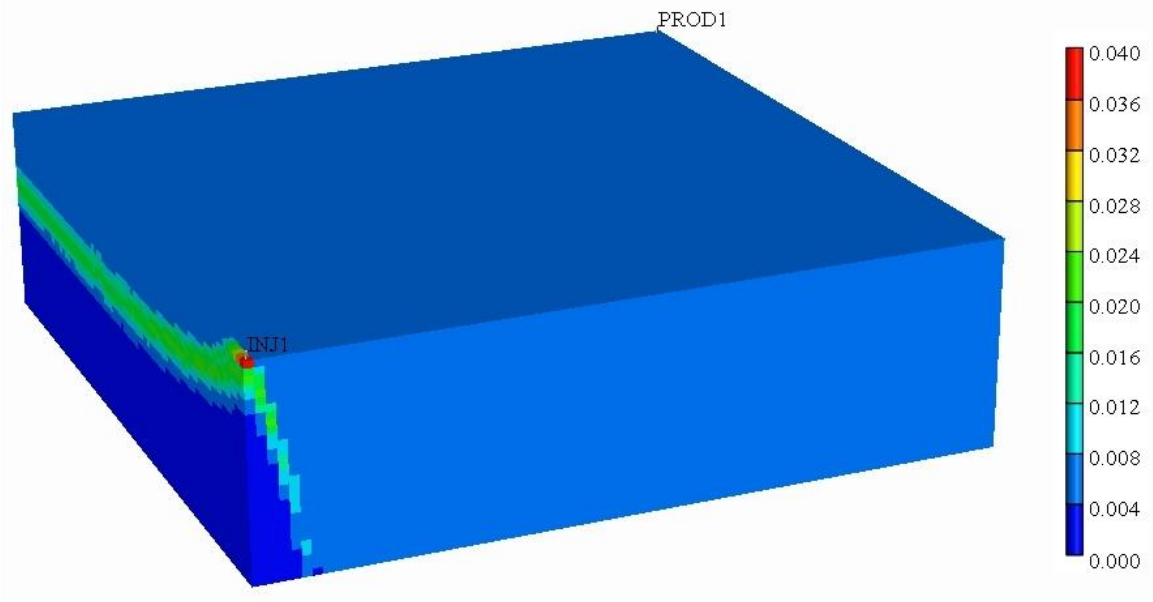

Figure 5-9: Overall molar concentration of methane after 50 years for the case of formation of gas cap by CO_2 injection.

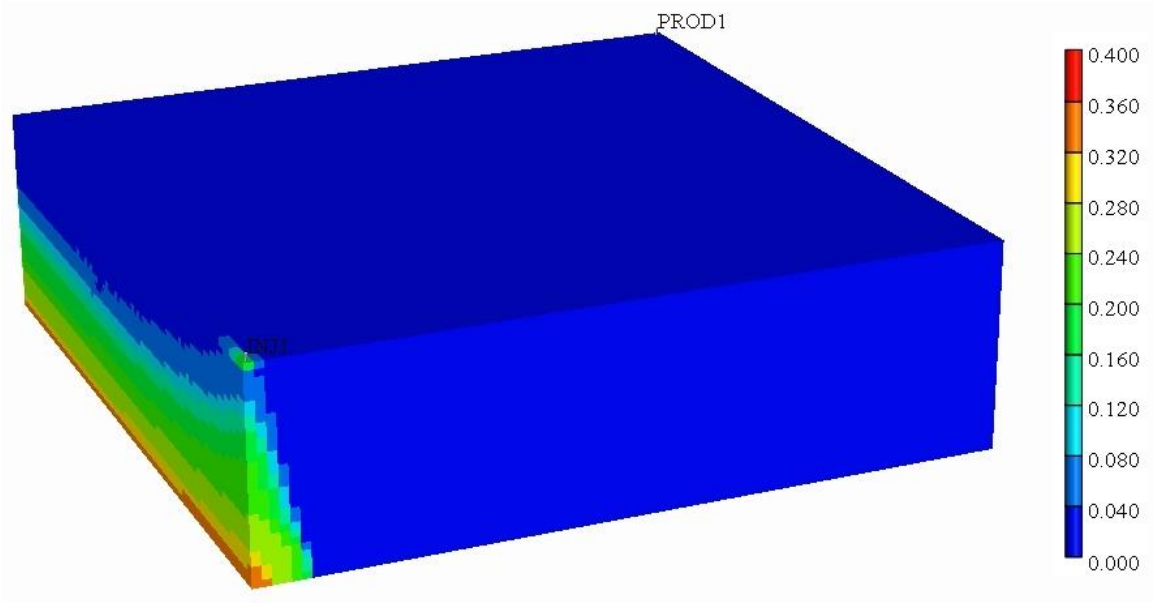

Figure 5-10: Gas saturation after 50 years for the case of formation of gas cap by CO_2 injection.

5.3.3 Injection of supercritical CO_2 and production of CH_4 and brine

The second investigated strategy was to inject supercritical CO_2 while methane and brine are produced. The injected bulk CO_2 would push the methane-saturated brine toward the producer. Also, it is expected that the injected CO_2 strips out the dissolved methane which leads to higher recovery of methane.

First, supercritical CO_2 was injected at constant bottomhole pressure of 12,000 psi for 15 years. The producer was open to flow from the first day at constant bottomhole pressure of 11,000 psi. Figure 5-11 shows the overall molar concentration of CH_4 and CO_2 in the production stream.

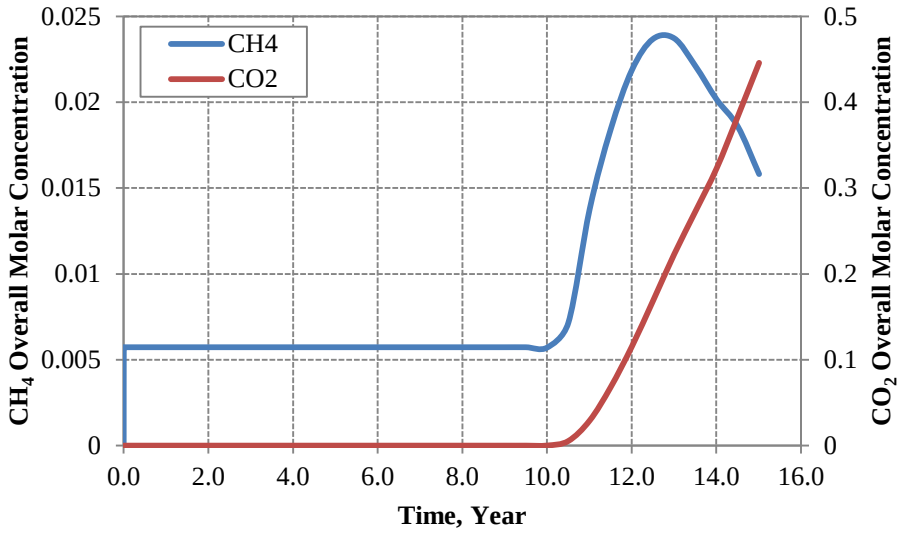

Figure 5-11: Overall molar concentration of CH_4 and CO_2 in production stream for injection of supercritical CO_2.

It is noticed from Figure 5-11 that the molar concentration of methane in the first 10 years is 0.00573, which is identical to the concentration in methane-saturated brine at 11,000 psi. After 10 years, the methane bank arrives at the producer. However, CO_2 concentration in production stream exceeds the methane concentration in a few months before the majority of methane bank is produced. This observation is in contrast to the 1-D simulation result where the majority of methane bank had been produced as pure methane before CO_2 breakthrough occurred in the producer. The cause of this behavior is that the methane bank spreads in 3-D space in front of CO_2 plume whereas the methane bank is accumulated in one spot in the 1-D case. Hence, the methane bank in 3-D case is produced along with a huge amount of CO_2. It is necessary to define a threshold for the percentage of CO_2 in production stream since separation of CO_2 and CH_4 is costly. In this study, 15% CO_2 in produced gas is specified as cut-off for production. This concentration is detected after 3734 days.

Table 5-6 summarizes the results of injection of supercritical CO_2 and production of methane and brine after 10 years and 3 months. In this period, about 23 million metric tons of CO_2 is stored while 44.1 percent of in-situ methane and brine are produced.

Table 5-6: Injection and production summary for injection of supercritical CO_2.

Minimum bottomhole pressure of producer, psi	11,000
Maximum bottomhole pressure of injector, psi	12,000
Wellhead pressure of producer, psi	2,798
Wellhead pressure of injector, psi	7,895
Tubing ID, inch	6.0
Production period, year	10.23
Injection period, year	10.23
Cumulative produced gas, Billion SCF	6.753
Cumulative produced brine, Million STB	157.07
Average produced gas-water ratio, SCF/STB	42.99
Cumulative injected CO_2, Billion SCF (Million metric ton)	431.88 (22.86)
CH_4 recovery, %	44.1
Brine recovery, %	44.1

Figure 5-12 shows the overall molar concentration of CH_4 at breakthrough time. This figure illustrates the 3-D characteristic of methane bank. Also, Figure 5-13 shows the overall molar concentration of CO_2 at breakthrough time. The pressure drop along the horizontal part of the wellbores causes the asymmetric fronts of CH_4 and CO_2 resulting in early breakthrough at the toe of the producer. The comparison of these two figures shows why the methane bank is produced with huge percentage of CO_2.

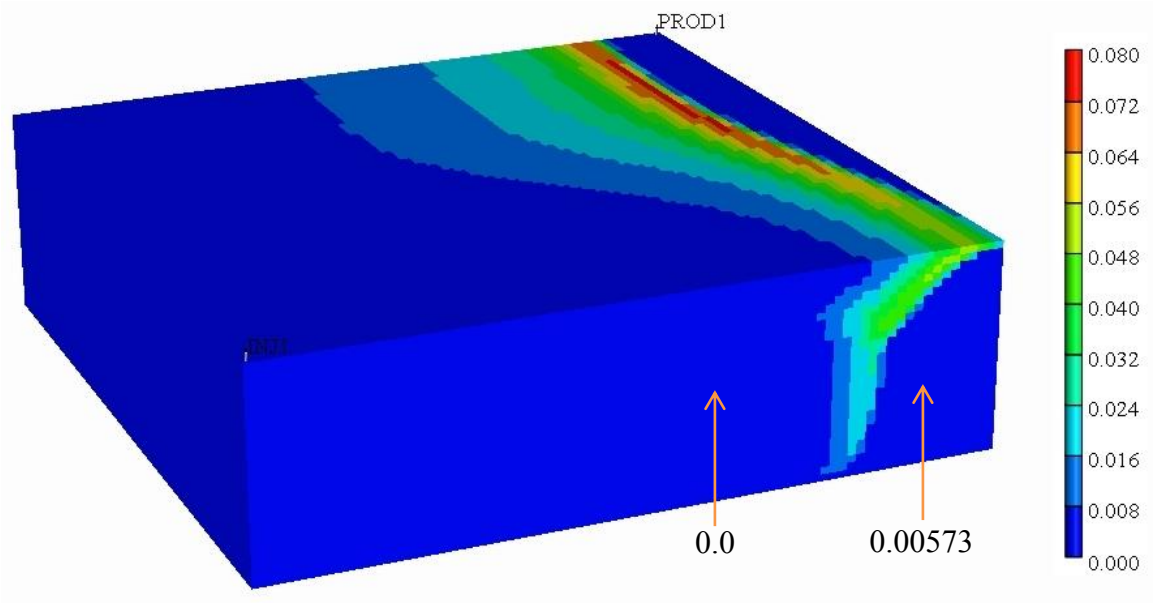

Figure 5-12: Overall molar concentration of CH_4 at breakthrough of CO_2 for the strategy of injection of supercritical CO_2.

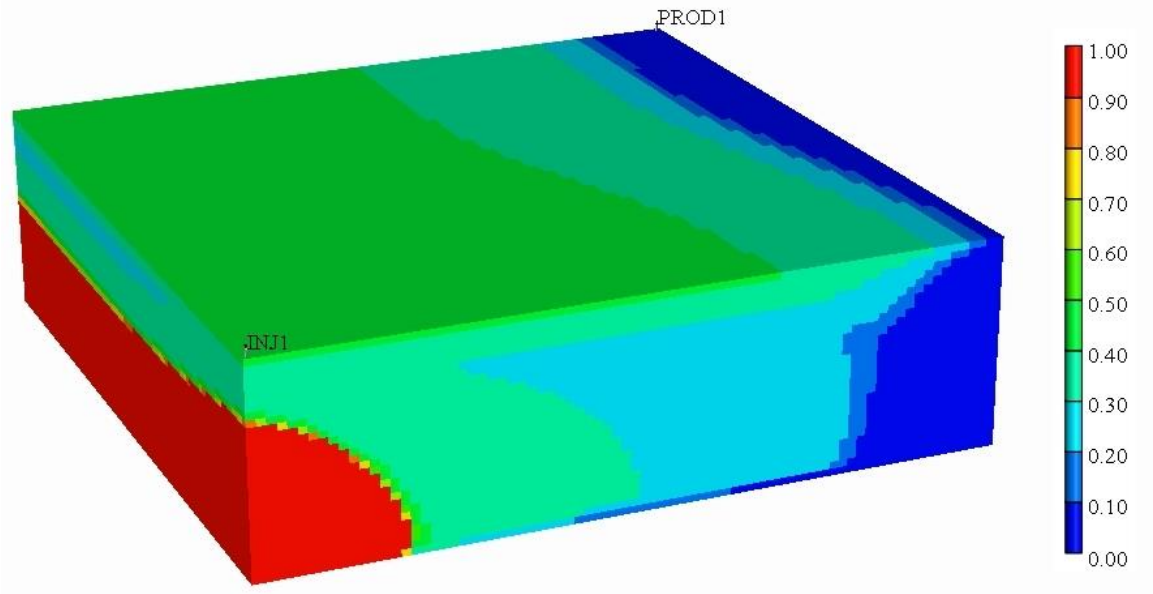

Figure 5-13: Overall molar concentration of CO_2 at breakthrough of CO_2 for the strategy of injection of supercritical CO_2.

Figure 5-14 shows the gas saturation profile at CO_2 breakthrough time. The gravity override results in imperfect volumetric sweep efficiency. Also, unfavorable mobility ratio leaves behind a large fraction of in-situ hot brine. These effects justify the low recovery of methane and brine in homogeneous aquifer. It is expected that adding heterogeneity would worsen the recovery issue for injection of supercritical CO_2.

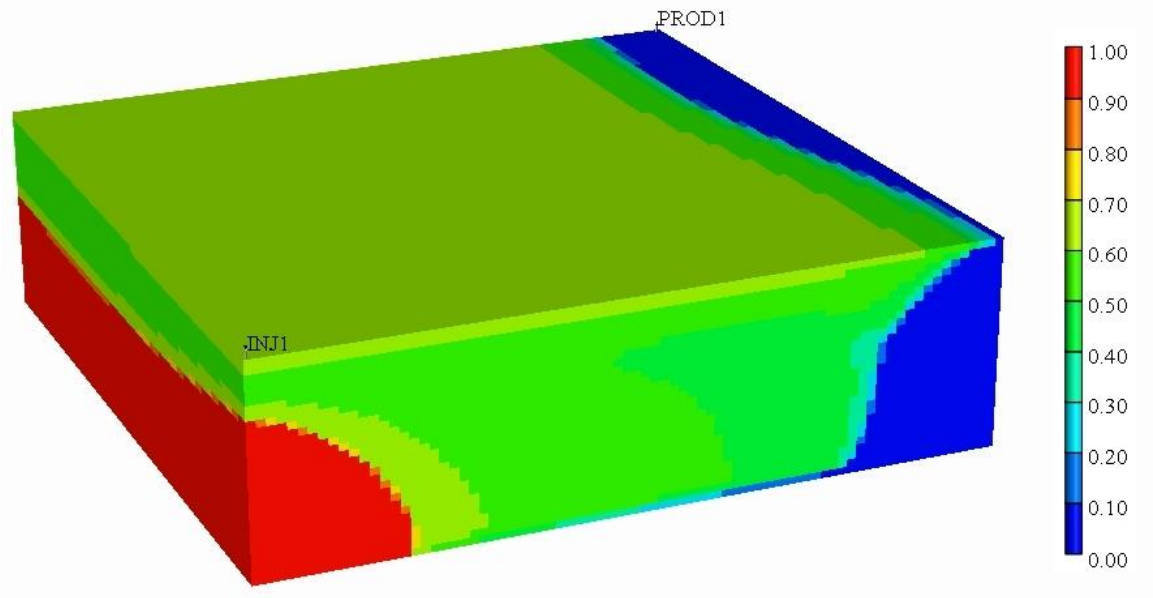

Figure 5-14: Gas saturation profile at CO_2 breakthrough time for the strategy of injection of supercritical CO_2.

5.3.4 Injection of CO_2-saturated brine and production of CH_4 and brine

The third investigated strategy was to dissolve the CO_2 into the produced brine and to inject the CO_2-saturated brine into the same aquifer to push the methane-saturated brine toward the producer.

In this strategy, the producer is open to flow from the first day at constant bottomhole pressure of 11,000 psi. The temperature of the produced brine is reduced to

200 °F to extract the geothermal energy. After extracting the methane and geothermal energy, the produced brine is co-injected with CO_2 at constant bottomhole pressure of 12,000 psi for 30 years. The concentration of CO_2 in the injected fluid is in a way that the CO_2 remains dissolved in brine at bottomhole pressure. This molar concentration is equivalent to 0.025. Figure 5-15 shows the overall molar concentration of CH_4 and CO_2 in the production stream.

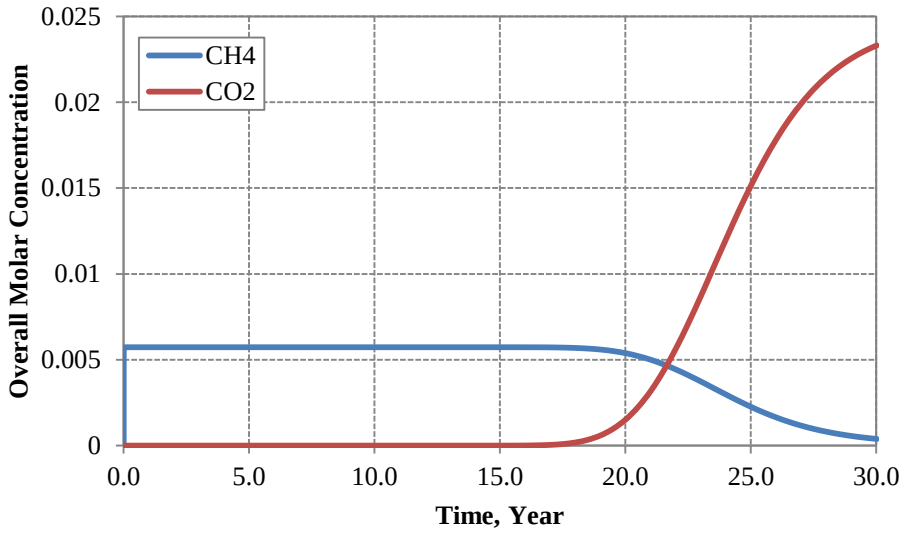

Figure 5-15: Overall molar concentration of CH_4 and CO_2 in production stream for injection of CO_2-saturated brine.

It can be seen in Figure 5-15 that the molar concentration of methane in the first 18 years is 0.00573 which is identical to the concentration in methane-saturated brine at 11,000 psi. After 18 years, the methane concentration in produced fluid decreases gradually, whereas CO_2 concentration exhibits reverse behavior. In this strategy, CO_2-saturated brine sweeps the CH_4-saturated brine toward the producer. Therefore, there is

no gas in the aquifer resulting in one-phase flow. It is necessary to define a threshold for the percentage of CO_2 in production stream since separation of CO_2 and CH_4 is costly. In this study, 15% CO_2 in produced gas is specified as cut-off for production. This concentration is detected after 7131 days.

Table 5-7 summarizes the results of injection of CO_2-saturated brine and production of methane and brine after 19 years and 6 months. In this period, about 2.7 million metric tons of CO_2 is stored while about 80 percent of in-situ methane and brine are produced.

Table 5-7: Injection and production summary for injection of CO_2-saturated brine.

Minimum bottomhole pressure of producer, psi	11,000
Maximum bottomhole pressure of injector, psi	12,000
Wellhead pressure of producer, psi	2,929
Wellhead pressure of injector, psi	7,675
Tubing ID, inch	6.0
Production period, year	19.54
Injection period, year	19.54
Cumulative produced gas, Billion SCF	12.143
Cumulative produced brine, Million STB	283.52
Average produced gas-water ratio, SCF/STB	42.83
Cumulative injected CO_2, Billion SCF (Million metric ton)	51.44 (2.71)
Cumulative injected brine, Million STB	273.28
CH_4 recovery, %	79.5
Brine recovery, %	79.6

Figure 5-16 shows the overall molar concentration of CH_4 at breakthrough time. This figure illustrates that no methane bank forms in the aquifer. Also, Figure 5-17 shows the overall molar concentration of CO_2 at breakthrough time. The pressure drop along the horizontal part of the wellbores causes the asymmetric front of CO_2 resulting in early breakthrough at the toe of the producer. The comparison of these two figures shows that there is a mixing zone between CO_2 and CH_4 made by dispersion. The methane-saturated region represents the in-situ brine, while the CO_2-saturated region represents the injected brine. No mobility ratio or gravity override issues have been detected, since the cold injected brine is denser and more viscous than the in-situ brine.

Figure 5-18 illustrates the temperature profile at CO_2 breakthrough time. The temperature profile falls behind the mass profile. Thus, the temperature of the produced brine remains constant at 302 °F during the production period.

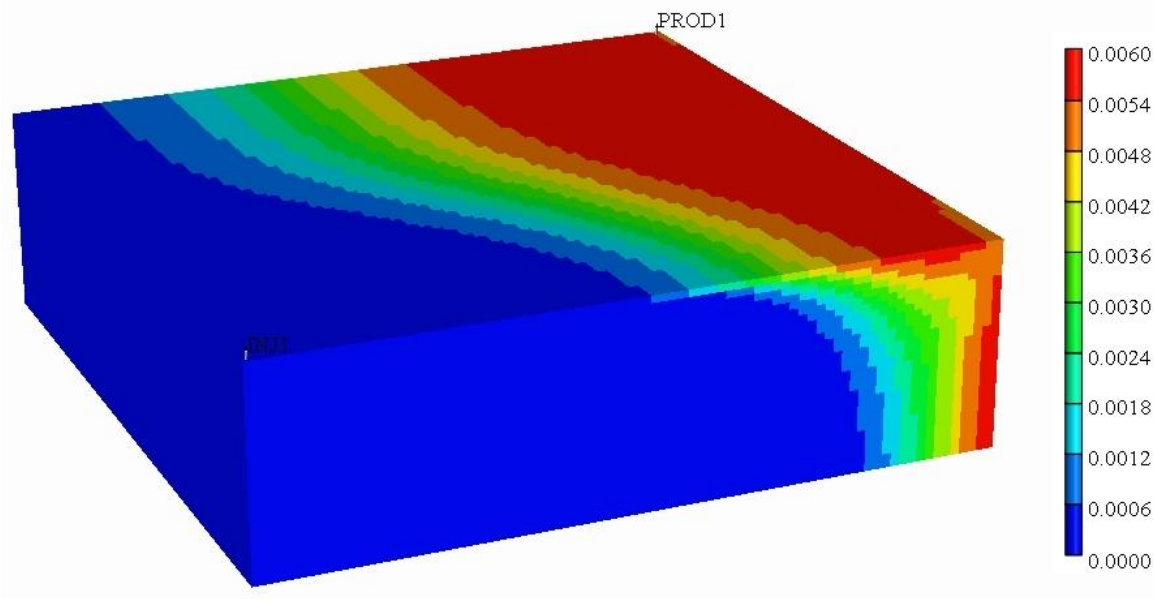

Figure 5-16: Overall molar concentration of CH_4 at breakthrough of CO_2 for the strategy of injection of CO_2-saturated brine.

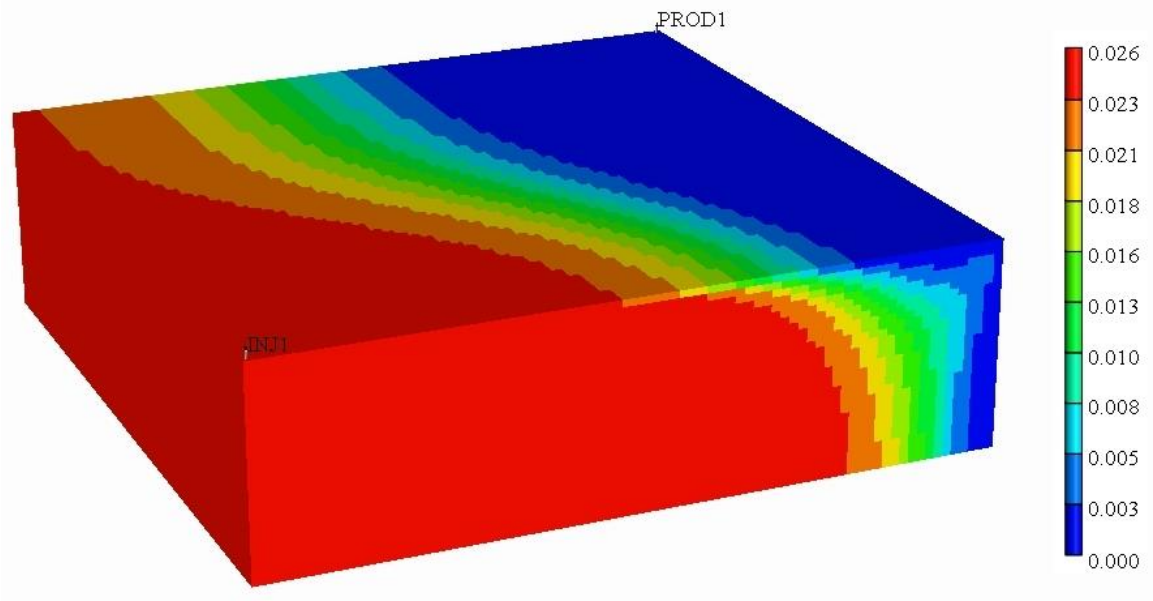

Figure 5-17: Overall molar concentration of CO_2 at breakthrough of CO_2 for the strategy of injection of CO_2-saturated brine.

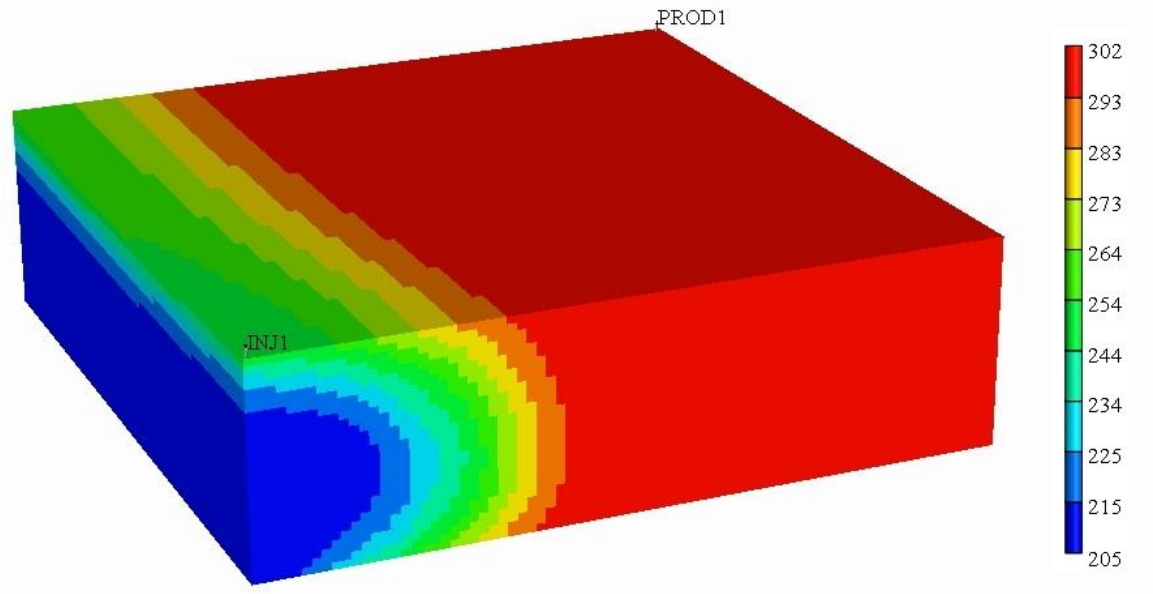

Figure 5-18: Temperature profile at breakthrough of CO_2 for the strategy of injection of CO_2-saturated brine.

5.4 SENSITIVITY ANALYSIS

In previous section, three strategies for coupled CO_2 storage and energy production from geopressured-geothermal aquifers were investigated. It was concluded that formation of a gas cap by CO_2 injection is not practical. However, the strategies of injecting supercritical CO_2 and CO_2-saturated brine seem technically feasible. In this section, based on the initial observations from the base case study, several simulations will carried out to quantify the effect of variation of different parameters such as well types, well spacing and permeability on storage and production for both injection strategies.

5.4.1 Injection of supercritical CO_2

In this section, the method of One-Parameter-at-a-Time is used to study the effect of variation of the parameters. In this method, one of the parameters is varied over the range of the samples and all other parameters are fixed at a base case condition. The base case model was introduced in section 5.3.1. Well type, well spacing, permeability, and permeability ratio are the parameters involved in sensitivity analysis for injection of supercritical CO_2.

5.4.1.1 Effect of well type and well spacing

Horizontal wells are capable of producing at higher rates with better recovery efficiency compared to vertical wells whereas the cost of horizontal drilling is higher. In this study, the effect of well type on the strategy of injection of supercritical CO_2 is investigated. Figure 5-19 shows the parallel and five spot well configurations for well types used in this study.

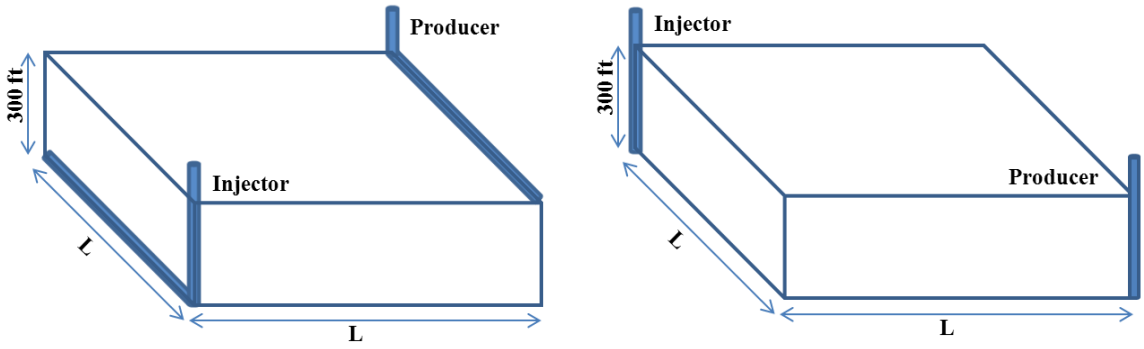

Figure 5-19: Parallel and five-spot well patterns for horizontal and vertical wells.

Both the well type and well spacing effect the time of CO_2 breakthrough and the fraction of the initial fluid in place that can be recovered before CO_2 breakthrough. The well spacing parameter is identified by L in Figure 5-19. Table 5-8 summarizes the simulation results of horizontal wells for five well spacing. The energy recovery represents the recovery of methane and brine which are similar in this case since only CH_4-saturated brine is produced. The favorable process is designed in a way that the CO_2 breakthrough occurs after about 20 years. Hence, the optimum well spacing is between 6600 ft to 7920 ft. Furthermore, increasing the horizontal section of wells decreases the energy recovery because of higher pressure drop in longer wells that makes the CO_2 front more asymmetric. Higher wellhead pressure of injectors and lower wellhead pressure of producers are the results of higher pressure drop in longer wells.

Table 5-8: Effect of well spacing for injection of supercritical CO_2 using horizontal wells.

L (ft)	Injected CO_2 (BCF)	Produced CH_4 (BCF)	Produced Brine (MMSTB)	Energy Recovery %	Time (year)	Injector WHP (psi)	Producer WHP (psi)
2640	117.3	1.83	42.6	47.9	3.16	7499	3396
3960	249.2	3.90	90.6	45.2	6.07	7772	2980
5280	431.9	6.75	157.1	44.1	10.23	7895	2798
6600	667.0	10.44	242.7	43.6	15.67	7961	2686
7920	951.3	14.89	346.3	43.2	22.40	7971	2611

Table 5-9 shows the simulation results of vertical wells for four well spacing. In order to have a 20-year process, the well spacing should be between 3960 ft to 5280 ft. Moreover, it is concluded that larger distance between injector and producer intensifies the gravity override and dispersion effects leading to lower recovery efficiency.

Table 5-9: Effect of well spacing for injection of supercritical CO_2 using vertical wells.

L (ft)	Injected CO_2 (BCF)	Produced CH_4 (BCF)	Produced Brine (MMSTB)	Energy Recovery %	Time (year)	Injector WHP (psi)	Producer WHP (psi)
2640	97.7	1.52	35.4	39.7	6.93	7183	3957
3960	205.5	3.20	74.4	37.2	15.13	7144	4013
5280	347.3	5.40	125.7	35.3	26.16	7119	4047
6600	522.5	8.12	189.2	34.0	40.00	7102	4073

Comparison of the results of horizontal and vertical wells reveals that the recovery factor using horizontal wells is about 10 percent higher than using vertical wells because of higher sweep efficiency. The average production rate from a half of a horizontal well is about 40,000 STB/day, whereas the average production rate from a quarter of a vertical well is about 13,000 STB/day. Hence, the average production rate from full horizontal and vertical wells are 80,000 and 52,000 STB/day, respectively. Horizontal wells are obviously capable of producing at much higher rates compared to vertical wells.

5.4.1.2 Effect of permeability

In order to estimate the effect of permeability on storage and production, five simulations were conducted using horizontal permeabilities of 500 md, 200 md, 100 md, 50 md, and 20 md. All the aquifer parameters, well constraints, well types, and spacing are the same as the base case. A pressure drawdown of 1,000 psi is applied between the injector and the producer. As expected, the cases with higher permeability have higher production rates leading to earlier CO_2 breakthrough. Moreover, higher production rates causes more pressure drop in the wellbore. Consequently, the pressure drop in the horizontal section of the wellbore brings about asymmetry in CO_2 front and earlier breakthrough at the toe of the producer. Figure 5-20 shows the CO_2 breakthrough time and recovery factor versus permeability. It is observed that higher permeability leads to lower recovery.

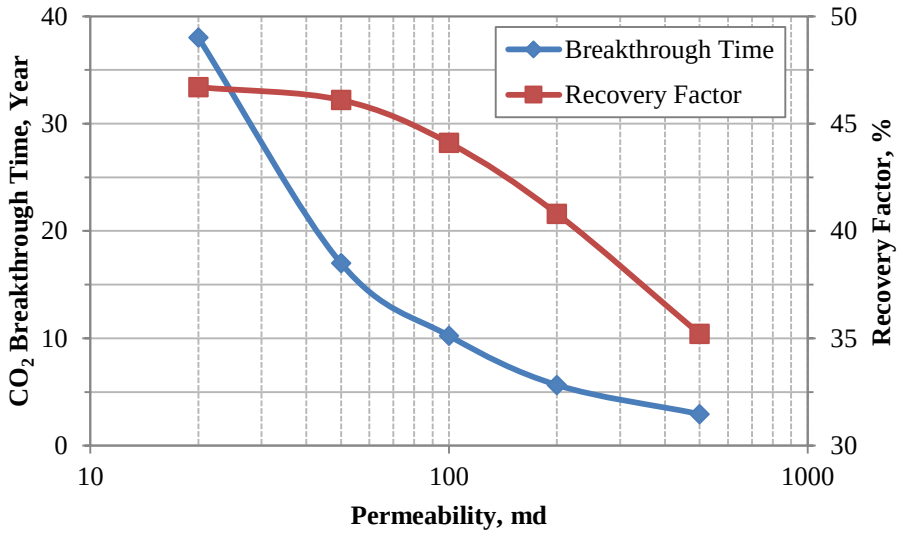

Figure 5-20: Breakthrough time and recovery factor versus permeability for injection of supercritical CO_2 using horizontal wells.

5.4.1.3 Effect of ratio of vertical permeability to horizontal permeability

Seven simulations were performed with k_v/k_h values of 0.001, 0.005, 0.01, 0.05, 0.1, 0.5, and 1.0 to study the effect of the ratio of vertical permeability to horizontal permeability on storage and production. The permeability ratio controls the communication between different layers. High permeability ratio means high vertical permeability for a constant horizontal permeability value. Therefore, higher permeability ratio causes faster migration of CO_2 toward the producer and earlier breakthrough. Furthermore, high permeability ratio induces override, while low permeability ratio generates underride. Thus, depending on the aspect ratio of the reservoir, each case has an optimum permeability ratio in which the CO_2 front sweeps the reservoir both horizontally and vertically. Figure 5-21 shows the CO_2 breakthrough time and the energy recovery versus permeability ratio. It is noted that the recovery is maximum at a

permeability ratio of 0.01. CO_2 migrates upward and flows toward producer through upper layers at mobility ratios higher than 0.01 while it flows through lower layers at ratios lower than 0.01 leaving behind in-situ methane and hot brine at upper layers.

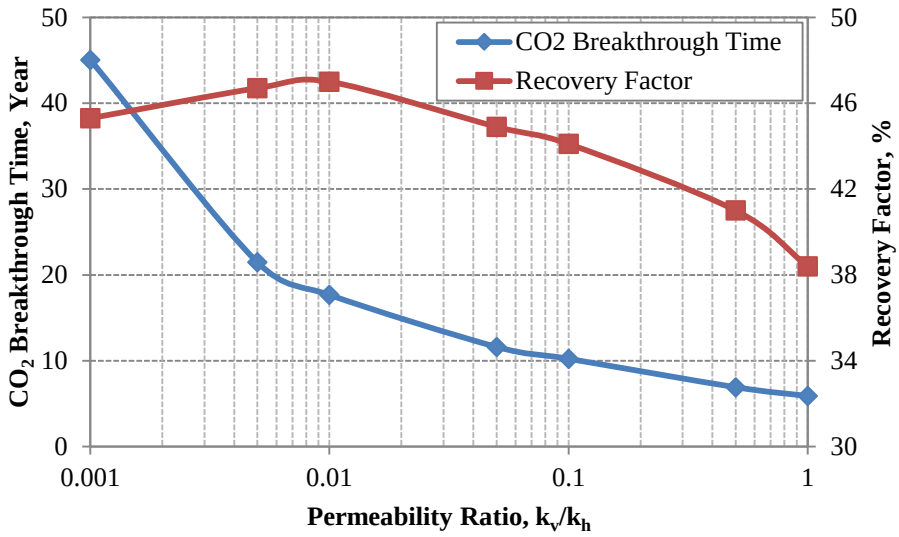

Figure 5-21: Breakthrough time and recovery factor versus permeability ratio for injection of supercritical CO_2 using horizontal wells.

5.4.2 Injection of CO_2-saturated brine

In this section, a sensitivity analysis similar to section 5.4.1 is performed for strategy of injection of CO_2-saturated brine. Again, One-Parameter-at-a-Time is used as the sensitivity analysis method for the base case model which was introduced in section 5.3.1. Well type, well spacing, permeability, and permeability ratio are the parameters involved in sensitivity analysis for injection of CO_2-saturated brine.

5.4.2.1 Effect of well type and well spacing

In this study, the effect of well type and well spacing on the strategy of injection of CO_2-saturated brine was investigated. The well configurations are the same as those shown in Figure 5-19. The well spacing parameter is identified by L in Figure 5-19. Table 5-10 summarizes the simulation results of horizontal wells for five well spacing. The energy recovery represents the recovery of methane and brine which are similar in this case since only CH_4-saturated brine is produced. The favorable process is designed in a way that the CO_2 breakthrough occurs after about 20 years. Hence, the optimum well spacing is about 5280 ft. The heavier injected brine tends to slightly underride the in-situ brine. Thus, in the cases of shorter well spacing, the injected brine sweeps the reservoir faster in horizontal direction than in vertical direction resulting in lower recovery.

Table 5-10: Effect of well spacing for injection of CO_2-saturated brine using horizontal wells.

L (ft)	Injected CO_2 (BCF)	Produced CH_4 (BCF)	Produced Brine (MMSTB)	Energy Recovery %	Time (year)	Injector WHP (psi)	Producer WHP (psi)
2640	12.1	2.88	66.7	74.9	5.42	7104	3497
3960	28.28	6.73	155.9	77.8	11.18	7519	3083
5280	51.44	12.24	283.5	79.6	19.54	7675	2929
6600	80.19	19.10	442.0	79.4	30.24	7693	2902
7920	115.80	27.57	638.3	79.6	43.88	7672	2938

Table 5-11 shows the simulation results of vertical wells for three well spacing. In order to have a 20-year process, the well spacing should be between 2640 ft to 3960 ft.

Moreover, it is concluded that energy recovery for vertical wells are almost insensitive to well spacing because the injected brine is distributed vertically.

Table 5-11: Effect of well spacing for injection of supercritical CO_2 using vertical wells.

L (ft)	Injected CO_2 (BCF)	Produced CH_4 (BCF)	Produced Brine (MMSTB)	Energy Recovery %	Time (year)	Injector WHP (psi)	Producer WHP (psi)
2640	10.85	2.58	59.7	67.0	14.25	6425	4275
3960	24.16	5.74	133.0	66.4	33.16	6369	4332
5280	42.81	10.17	235.7	66.2	60.53	6333	4369

Comparison of the results of horizontal and vertical wells reveals that the recovery factor using horizontal wells is about 10 percent higher than using vertical wells because of higher sweep efficiency. The average production rate from a half of a horizontal well is about 40,000 STB/day, whereas the average production rate from a quarter of a vertical well is about 11,000 STB/day. Hence, the average production rate from full horizontal and vertical wells are 80,000 and 44,000 STB/day, respectively. Horizontal wells are obviously capable of producing at much higher rates compared to vertical wells.

5.4.2.2 Effect of permeability

In order to estimate the effect of permeability on storage and production, five simulations were conducted using horizontal permeabilities of 500 md, 200 md, 100 md, 50 md, and 20 md. All the aquifer parameters, well constraints, well types, and spacing are the same as the base case. A pressure drawdown of 1,000 psi is applied between the

injector and the producer. As expected, the cases with higher permeability have higher production rates leading to earlier CO_2 breakthrough. Moreover, higher production rates causes more pressure drop in the wellbore. Consequently, the pressure drop in the horizontal section of the wellbore brings about asymmetry in CO_2 front and earlier breakthrough at the toe of the producer. Figure 5-22 shows the CO_2 breakthrough time and recovery factor versus permeability. It is observed that very high permeability leads to lower recovery.

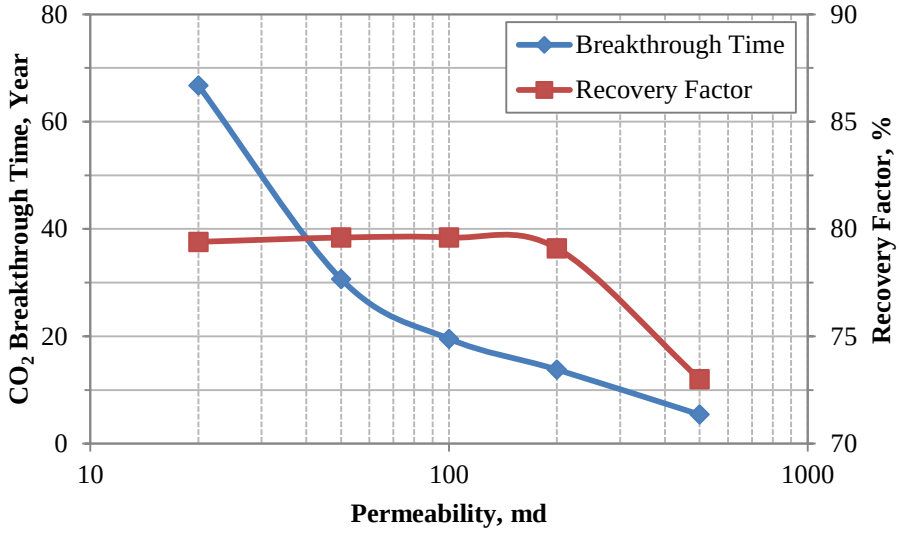

Figure 5-22: Breakthrough time and recovery factor versus permeability for injection of supercritical CO_2 using horizontal wells.

5.4.2.3 Effect of ratio of vertical permeability to horizontal permeability

Seven simulations were performed with k_v/k_h values of 0.001, 0.005, 0.01, 0.05, 0.1, 0.5, and 1.0 to study the effect of the ratio of vertical permeability to horizontal permeability on storage and production. The permeability ratio controls the communication between different layers. High permeability ratio means high vertical

permeability for a constant horizontal permeability value. Therefore, higher permeability ratio causes faster vertical migration of CO_2-saturated brine toward the producer and earlier CO_2 breakthrough. Figure 5-23 shows the CO_2 breakthrough time and the energy recovery versus permeability ratio. It is noted that the recovery is maximum at a permeability ratio of 0.5. CO_2-saturated brine migrates upward faster and flows toward the producer through upper layers at mobility ratios higher than 0.5 while it flows through lower layers at ratios lower than 0.5 leaving behind in-situ methane and hot brine at upper layers.

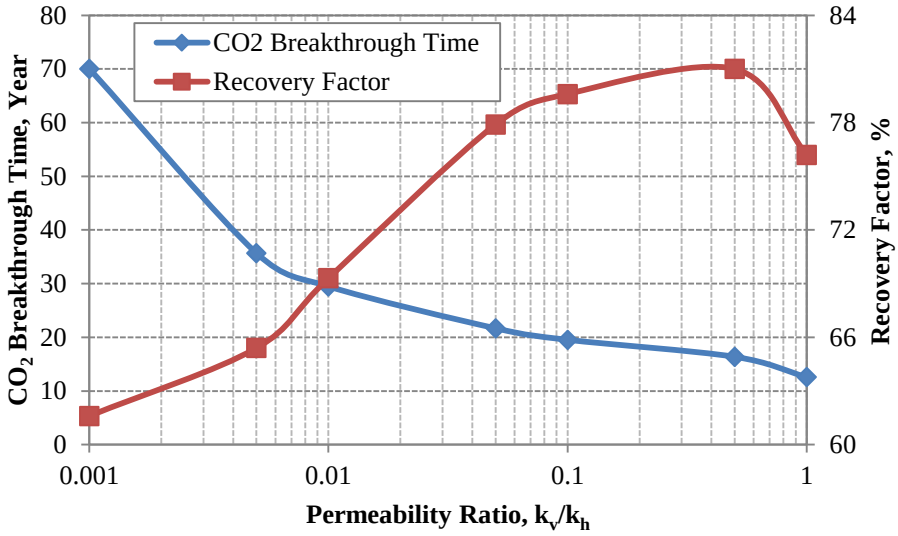

Figure 5-23: Breakthrough time and recovery factor versus permeability ratio for injection of supercritical CO_2 using horizontal wells.

5.5 EFFECT OF HETEROGENEITY

All the simulation models in the previous sections were homogeneous. Heterogeneity impacts the flow pattern and production rates and consequently the energy recovery. In this section, Petrel was used to generate stochastic permeability distributions. Permeability values were generated for all 192,000 gridblocks in aquifer model presented in section 5.3.1. Three different realizations were prepared using an exponential variogram. Stochastic parameters used to generate the permeability fields are given in Table 5-12. The aquifer is considered to be isotropic in horizontal direction. Thus, the y-direction permeability is set to be equal to the x-direction permeability. However, the vertical permeability is set to be one-tenth of the horizontal permeability. Figures 5-24 through 5-26 shows the three different realizations of the permeability fields.

Table 5-12: Stochastic parameters used for generation of permeability fields.

Parameter	Value
Correlation length in x direction, ft	1000
Correlation length in x direction, ft	1000
Correlation length in x direction, ft	50
Mean permeability, md	100
Standard deviation of Ln(k)	1.12
Dykstra-Parson's coefficient	0.7

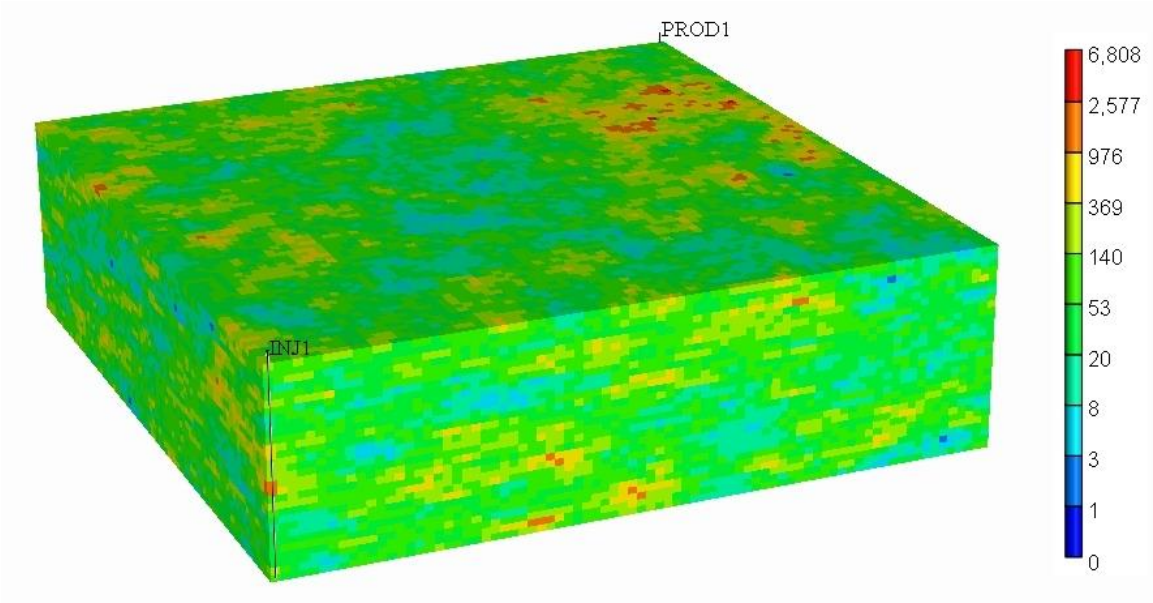

Figure 5-24: First geostatistical realization of permeability in md at a 5280 ft by 5280 ft by 300 ft. The correlation lengths are 1000 ft by 1000 ft by 50 ft.

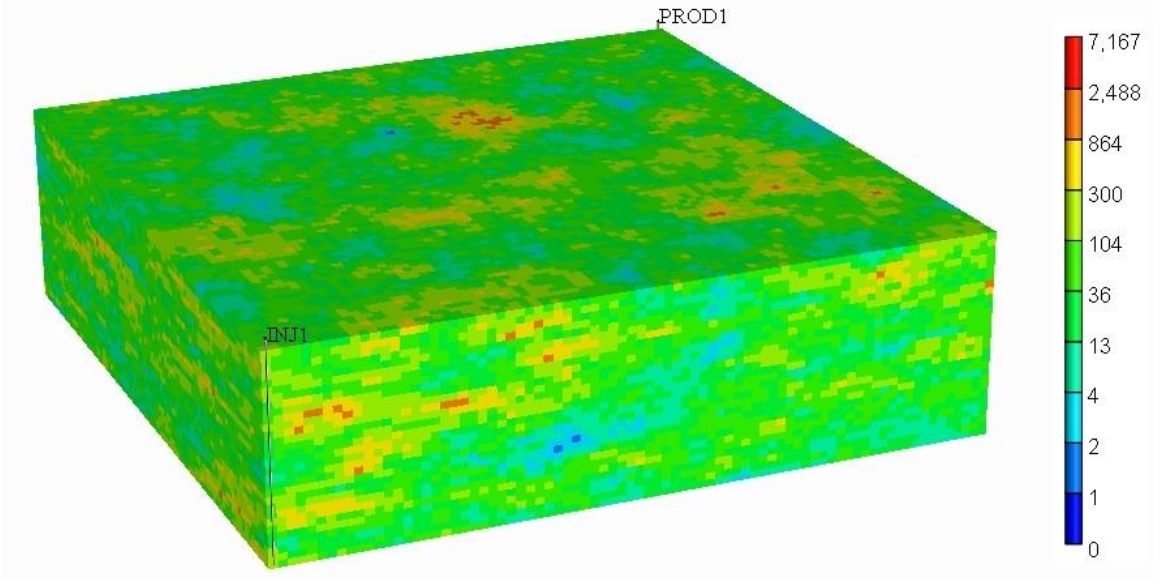

Figure 5-25: Second geostatistical realization of permeability in md at a 5280 ft by 5280 ft by 300 ft. The correlation lengths are 1000 ft by 1000 ft by 50 ft.

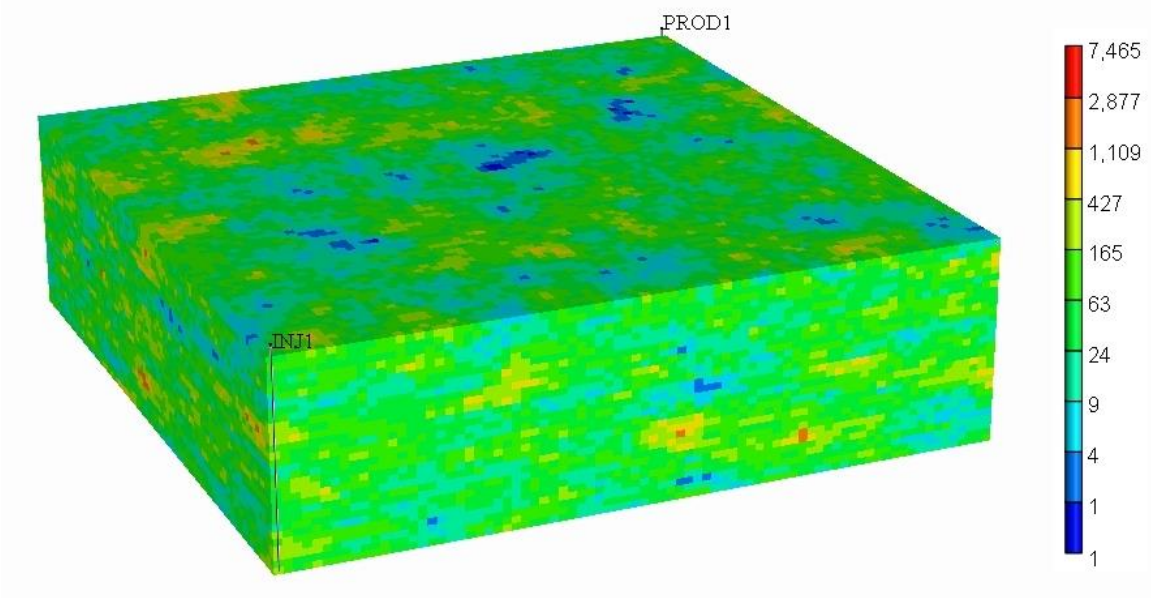

Figure 5-26: Third geostatistical realization of permeability in md at a 5280 ft by 5280 ft by 300 ft. The correlation lengths are 1000 ft by 1000 ft by 50 ft.

Simulation studies were performed on heterogeneous models for strategies of injection of supercritical CO_2 and injection of CO_2-saturated brine. Horizontal and vertical wells were used for both injection strategies. Simulation results for combinations of the three realizations, two injection strategies and two well types are summarized in Tables 5-13 through 5-16. Also, the results of corresponding homogeneous cases with identical average permeability are listed in tables for comparison. Figures 5-27 through 5-30 show the overall molar concentration of CO_2 at the time of breakthrough for case 1 for both injection strategies and well types.

Table 5-13: Results of injection of supercritical CO_2 using horizontal wells.

	Homogeneous	Case 1	Case 2	Case 3
Injected CO_2, BCF	431.88	341.0	313.3	297.8
Produced CH_4, BCF	6.75	5.34	4.86	4.67
Produced Brine, MMSTB	157.1	123.6	113.0	107.7
Energy Recovery, %	44.1	36.9	33.6	32.0
Time, year	10.23	9.91	10.56	9.42
WHP of injector , psi	7,895	7,352	7,127	7,219
WHP of producer, psi	2,798	3,562	3,905	3,754
Average brine rate, MSTB/day	42,066	34,171	29,330	31,292

Table 5-14: Results of injection of supercritical CO_2 using vertical wells.

	Homogeneous	Case 1	Case 2	Case 3
Injected CO_2, BCF	347.3	312.3	322.3	310.6
Produced CH_4, BCF	5.40	4.89	5.00	4.81
Produced Brine, MMSTB	125.7	113.2	116.0	111.7
Energy Recovery, %	35.3	33.8	34.5	33.2
Time, year	26.16	34.14	39.76	28.96
WHP of injector , psi	7119	6,773	6,703	6,882
WHP of producer, psi	4047	4,515	4,629	4,364
Average brine rate, MSTB/day	13,165	9,087	7,993	10,563

Table 5-15: Results of injection of CO_2-saturated brine using horizontal wells.

	Homogeneous	Case 1	Case 2	Case 3
Injected CO_2, BCF	51.4	31.6	33.3	27.8
Produced CH_4, BCF	12.24	7.56	7.95	6.68
Produced Brine, MMSTB	283.5	173.7	182.9	152.9
Energy Recovery, %	79.6	51.8	54.4	45.4
Time, year	19.54	14.78	17.73	14.39
WHP of injector , psi	7,675	6,979	6,673	6,737
WHP of producer, psi	2,929	3,620	3,924	3,861
Average brine rate, MSTB/day	39,759	32,189	28,262	29,105

Table 5-16: Results of injection of CO_2-saturated brine using vertical wells.

	Homogeneous	Case 1	Case 2	Case 3
Injected CO_2, BCF	42.8	29.2	29.2	28.7
Produced CH_4, BCF	10.17	6.98	6.94	6.83
Produced Brine, MMSTB	235.7	160.4	160.0	157.3
Energy Recovery, %	66.2	47.9	47.6	46.8
Time, year	60.53	64.2	64.7	47.6
WHP of injector , psi	6,333	5,984	5,979	6,170
WHP of producer, psi	4,369	4,719	4,724	4,532
Average brine rate, MSTB/day	10,666	6,846	6,775	9,064

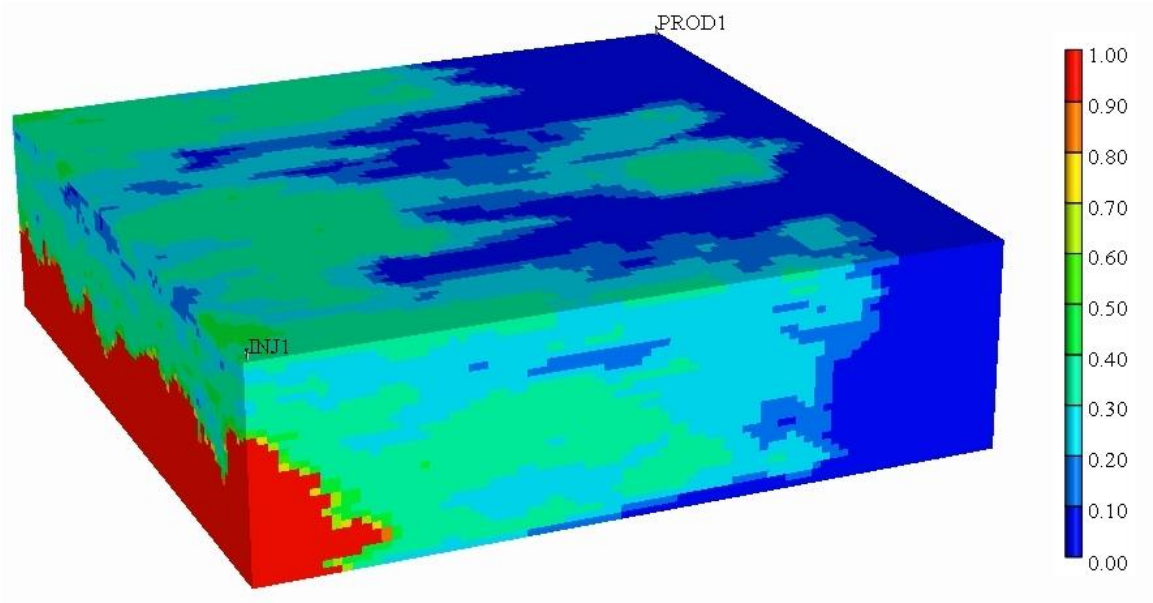

Figure 5-27: Overall molar concentration of CO_2 at breakthrough time for injection of supercritical CO_2 using horizontal wells (case 1).

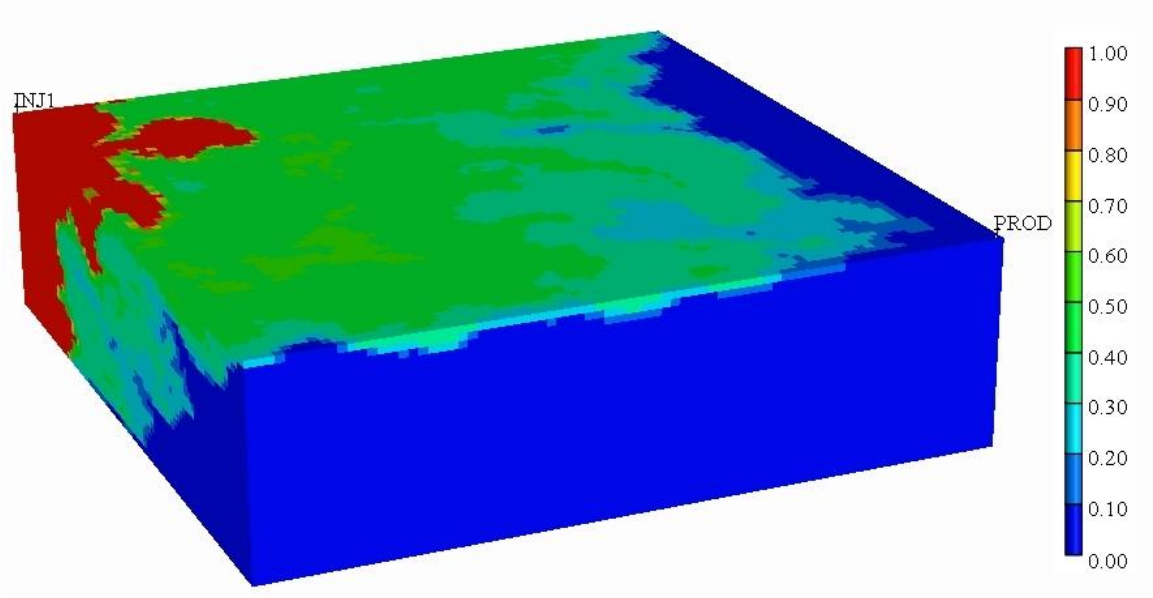

Figure 5-28: Overall molar concentration of CO_2 at breakthrough time for injection of supercritical CO_2 using vertical wells (case 1).

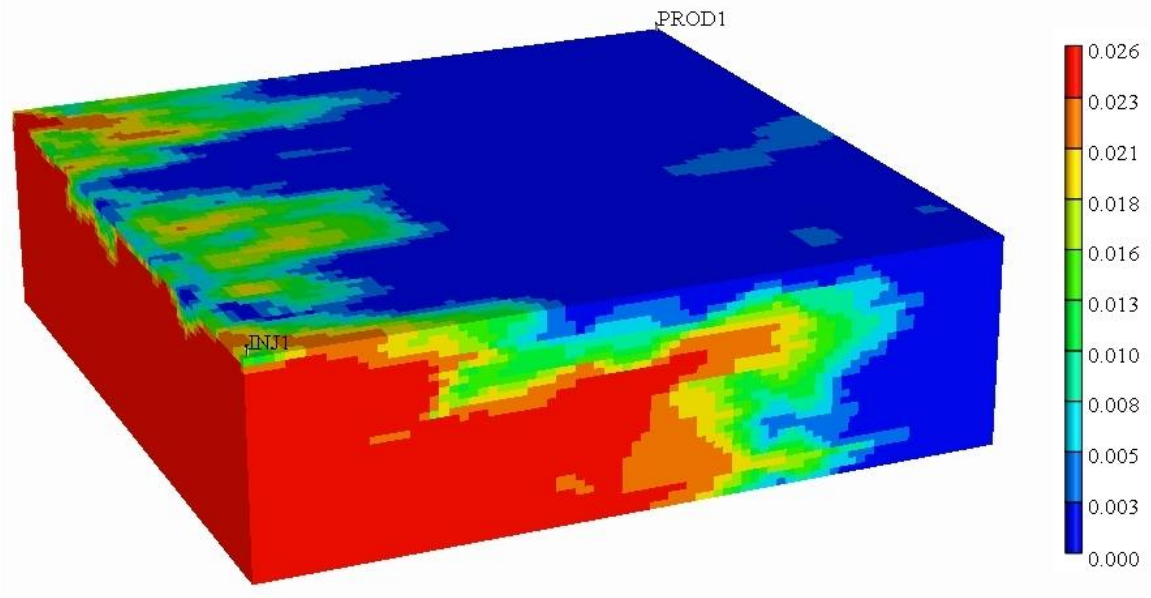

Figure 5-29: Overall molar concentration of CO_2 at breakthrough time for injection of CO_2-saturated brine using horizontal wells (case 1).

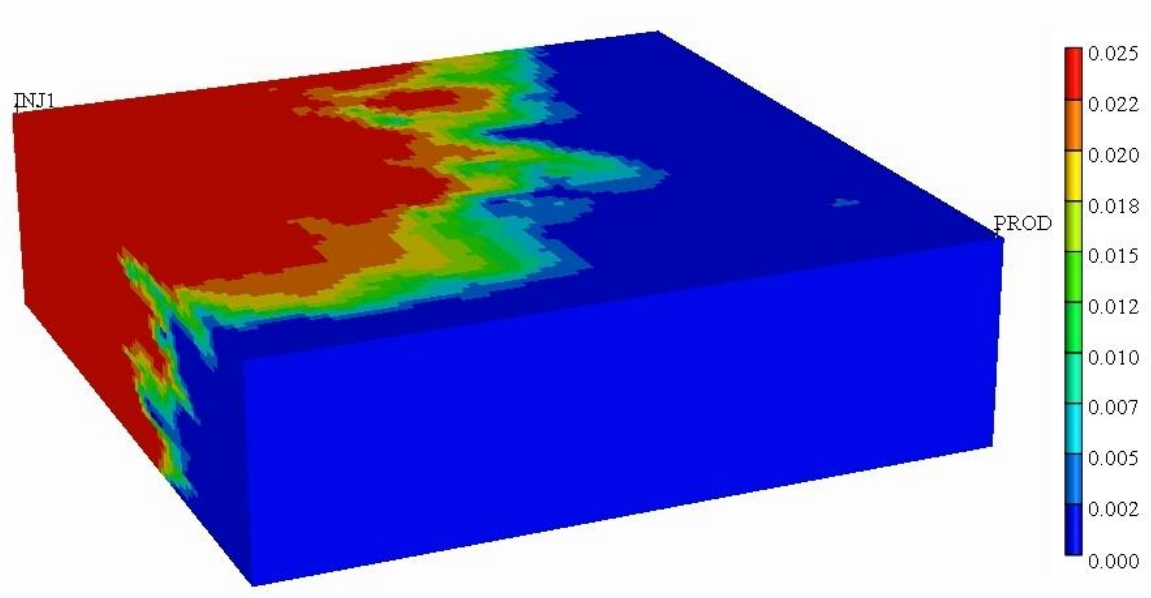

Figure 5-30: Overall molar concentration of CO_2 at breakthrough time for injection of CO_2-saturated brine using vertical wells (case 1).

The geology of the generated fields consists of patches of high permeability sand. The injected fluid tends to flow through high permeable patches toward the producer resulting in lower sweep efficiency compared to homogeneous case. Comparison between the results in Tables 5-13 and 5-14 and also between Tables 5-15 and 5-16 shows that horizontal wells are capable of producing at much higher rates compared to vertical wells. This means that in spite of higher drilling cost of horizontal wells, less number of wells is required to complete the process at a specific time period. Moreover, recovery factor using horizontal wells is slightly higher. On the other hand, comparison between the results in Tables 5-13 and 5-15 and also between Tables 5-14 and 5-16 reveals that the energy recovery by injection of CO_2-saturated brine is about 15 to 20 percent higher than by injection of supercritical CO_2.

5.6 STORAGE SECURITY

Containment security of the storage in deep saline aquifers is of significant importance. In storage project, CO_2 is injected in supercritical condition or dissolved in brine for a limited period of time. After termination of the process, the injected fluid commences to redistribute within the formation. The path of injected CO_2 and its long term distribution within the formation at post injection period is of special interest. It is believed that the supercritical CO_2 migrates upward as a result of buoyancy and accumulates below the boundary of the aquifer where the risk of leakage arises. During the upward migration of CO_2, a portion of CO_2 would be dissolved in the brine and another portion of it would be trapped as residual gas. In the case of injection of CO_2-saturated brine, it is speculated that the injected CO_2 would remain trapped in dissolved condition. Hence, the risk of leakage should be minimal if not zero.

The study of trapping mechanisms and their effect on the long term containment of injected CO_2 is out of the scope of this study. However, a brief review of the long term distribution of injected CO_2 provides a valuable insight about the reliability of different injection strategies. In order to investigate the CO_2 distribution within the aquifer, simulations were performed using base case models for 1,000 years after terminating the CO_2 injection. Figures 5-31 and 5-32 illustrate the overall molar concentration of CO_2 for the strategy of injection of supercritical CO_2 100 years and 1,000 years after shutting in the injector and the producer. Figure 5-13 in section 5.3.3 showed the CO_2 concentration at the time of terminating the process. Comparison of the Figures 5-13, 5-31, and 5-32 illuminates that a huge amount of CO_2 is mobile at the end of the injection. The mobile CO_2 migrates upward gradually and spreads horizontally as a result of advection and diffusion and finally accumulates under the upper boundary. Also, Figure 5-33 shows the gas saturation after 1,000 years. It is observed that the upper half of the aquifer has a gas saturation of 80 percent. The remaining 20 percent of the pore volume is filled with irreducible water which is saturated with CO_2. The gas saturation at the lower half of the aquifer varies between zero and about 30 percent. A portion of this gas is trapped as a result of counter-current flow of the gas and aqueous phases. Nevertheless, there is a huge cloud of mobile gas accumulated under the cap rock. Thus, the aquifer is prone to the risk of CO_2 leakage.

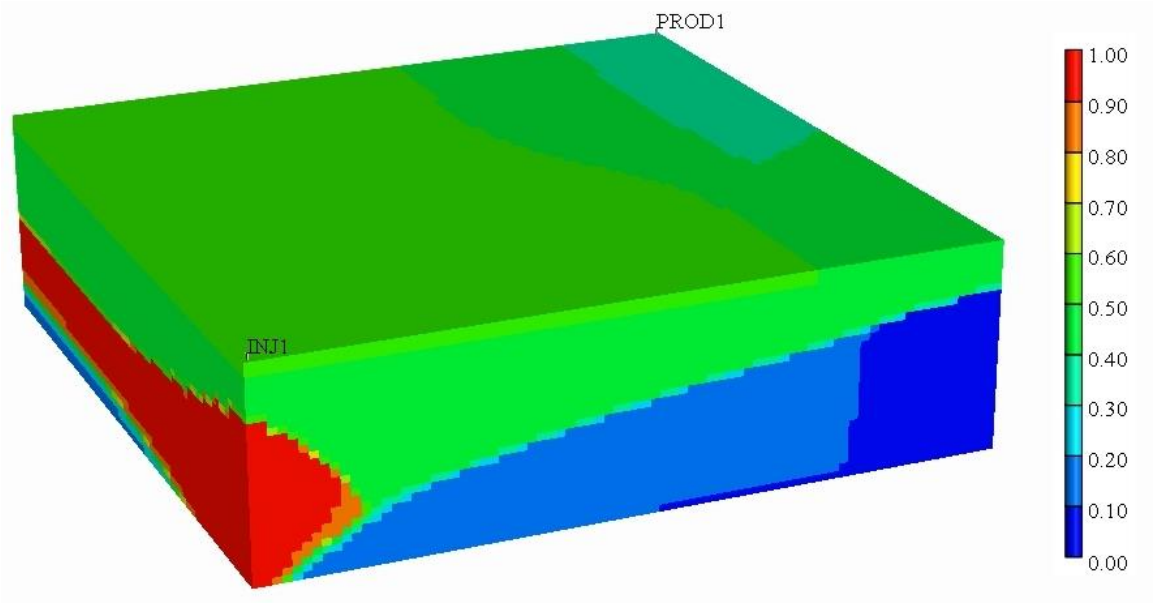

Figure 5-31: Overall molar concentration of CO_2 100 years after termination of injection of supercritical CO_2.

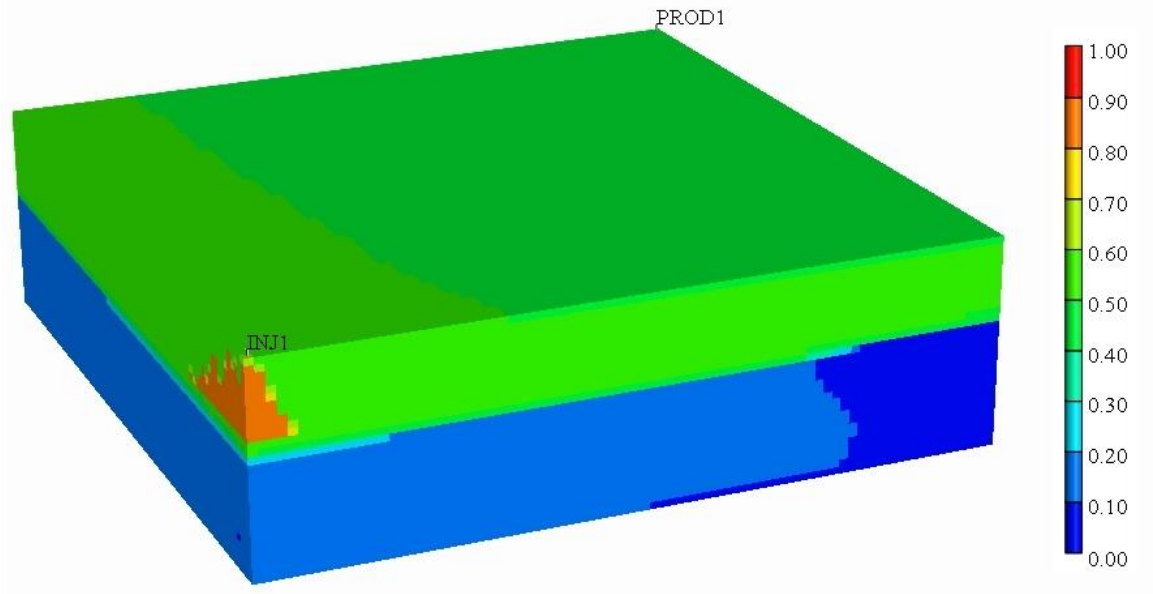

Figure 5-32: Overall molar concentration of CO_2 1,000 years after termination of injection of supercritical CO_2.

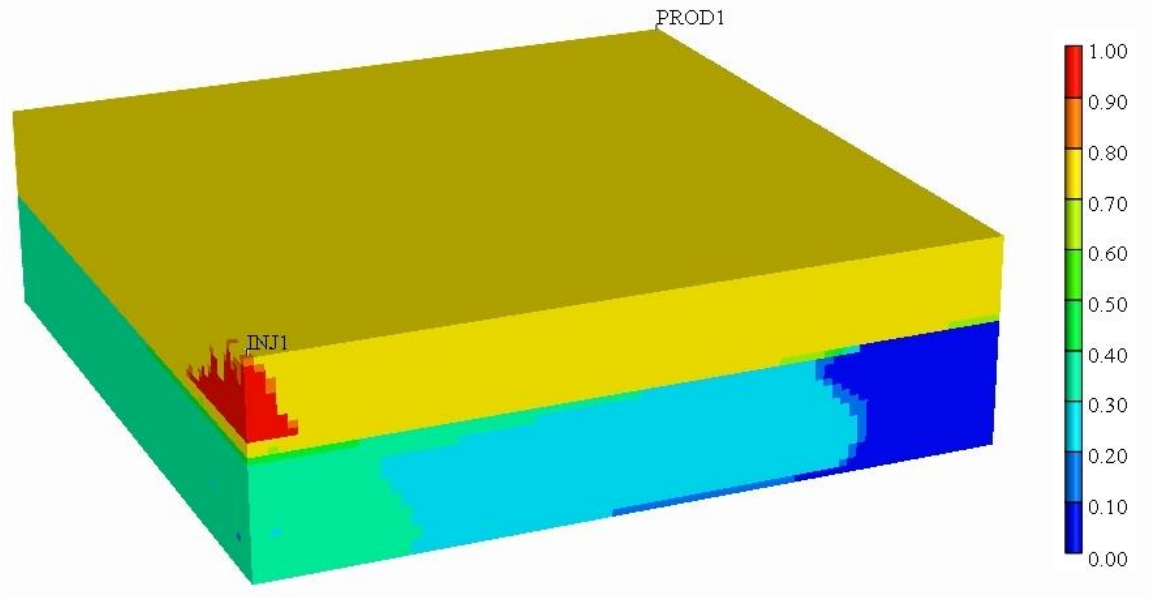

Figure 5-33: Gas saturation of CO_2 1,000 years after termination of injection of supercritical CO_2.

Figure 5-34 shows the overall molar concentration of CO_2 for the strategy of injection of CO_2-saturated brine 1000 years after the end of the process. It is observed that the molar concentration of CO_2 does not exceed the solubility of CO_2 in brine at aquifer condition throughout all the gridblocks. This means that all the CO_2 remains trapped in dissolved condition after 1000 years and the gas saturation is zero everywhere in the aquifer.

Comparison of the results of post injection simulation for two injection strategies reveals that the strategy of injection of CO_2-saturated brine shows the prospect of secure storage of CO_2 in long term compared to injection of supercritical CO_2. On the contrary, the strategy of injection of supercritical CO_2 is highly vulnerable to the risk of CO_2 leakage.

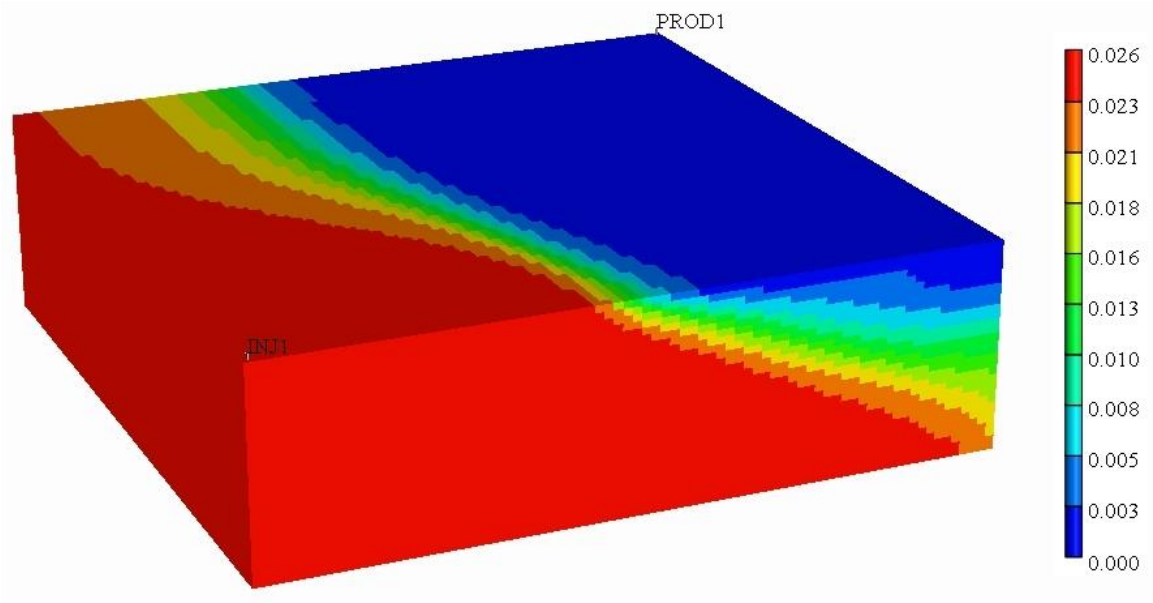

Figure 5-34: Overall molar concentration of CO_2 1,000 years after termination of injection of CO_2-saturated brine.

5.7 ENERGY REVENUE FROM PRODUCED METHANE AND GEOTHERMAL ENERGY

In this section, the energy revenue from the produced methane and geothermal energy is estimated for both injection strategies. The results of simulations of base case models presented in Tables 5-6 and 5-7 were used for revenue estimates. The produced fluid contains two sources of energy: (1) methane; and (2) geothermal energy.

The produced energy by burning methane is used for heating or power generation. Several different cycles are designed to convert the heat of combustion into power with efficiencies up to 60 percent. In this section, the gross energy by burning the produced methane is of interest. The gross heat of combustion of methane is about 1,028 BTU per cubic feet. This is identical to the lower heating value of methane.

Geothermal energy of the produced hot brine might be extracted using a heat exchanger. The temperature of the produced brine is on the order of 300 °F. In this study,

it is supposed that the temperature of the hot brine is reduced by 100 °F in a heat exchanger. The specific heat capacity of hot brine is about 1.0 BTU/lb.°F. Therefore, the recoverable geothermal energy by reducing the temperature of one barrel of brine from 300 °F to 200 °F is about 35,000 BTU. Table 5-17 summarizes the amounts of injected CO_2 and also produced methane and brine for both injection strategies. Also, this table includes the total energy revenue and revenue per ton of stored CO_2 for both injection strategies.

Table 5-17: Energy revenue for both CO_2 injection strategies.

	Supercritical CO_2	CO_2-saturated brine
Cumulative injected CO_2, Million metric ton	22.86	2.71
Cumulative injected CO_2, Billion SCF	431.88	51.44
Cumulative produced CH_4, Billion SCF	6.753	12.143
Cumulative produced brine, MMSTB	157.07	283.52
Gross energy from CH_4, Trillion BTU	6.94	12.48
Gross energy from brine, Trillion BTU	5.50	9.92
Total gross energy, trillion BTU	12.44	22.4
Energy per ton of stored CO_2, Million BTU/ton	0.455	8.266
Energy per ton of stored CO_2, kWh/ton	133	2,423

Comparison of the energy revenue of the two strategies reveals that the energy revenue by injecting CO_2-saturated brine is about twice as much as energy by injecting supercritical CO_2. Furthermore, the energy revenue per ton of stored CO_2 is 133 kWh by injecting supercritical CO_2 and 2,423 kWh by injecting CO_2-saturated brine.

5.8 CO-INJECTION OF CO_2 AND BRINE

In this section, co-injection of CO_2 and brine is presented based on the molar fraction of CO_2 in the injected fluid using the aquifer model described in section 5.3.1. Strategies of injecting CO_2-saturated brine and supercritical CO_2 are the two limiting cases of co-injecting the CO_2 and brine with CO_2 molar fraction of 2.5 percent and 100 percent, respectively. In this study, the molar fraction of CO_2 in the injection stream was varied between 2.5 and 100 percent. The results of energy recovery and stored CO_2 are presented in Figure 5-35 for different CO_2/brine ratios. Also, the results of energy offset per ton of stored CO_2 versus molar fraction of CO_2 are presented in Figure 5-36. The highest energy offset is obtained by injecting CO_2-saturated brine and this offset decreases rapidly by increasing the CO_2 fraction in the injection stream. This offset is almost insensitive to CO_2 concentration for mole fractions higher than 40 percent.

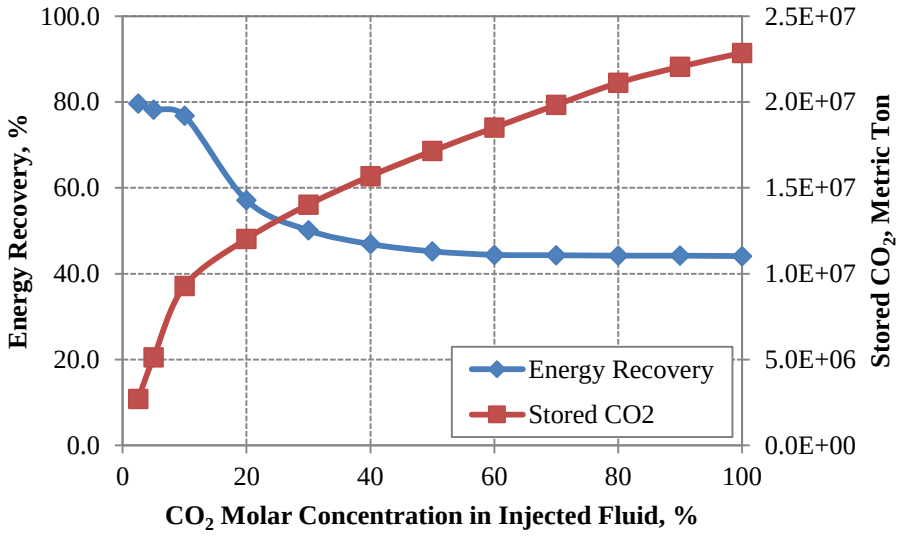

Figure 5-35: Energy recovery and stored CO_2 versus CO_2 molar concentration for co-injection of CO_2 and brine.

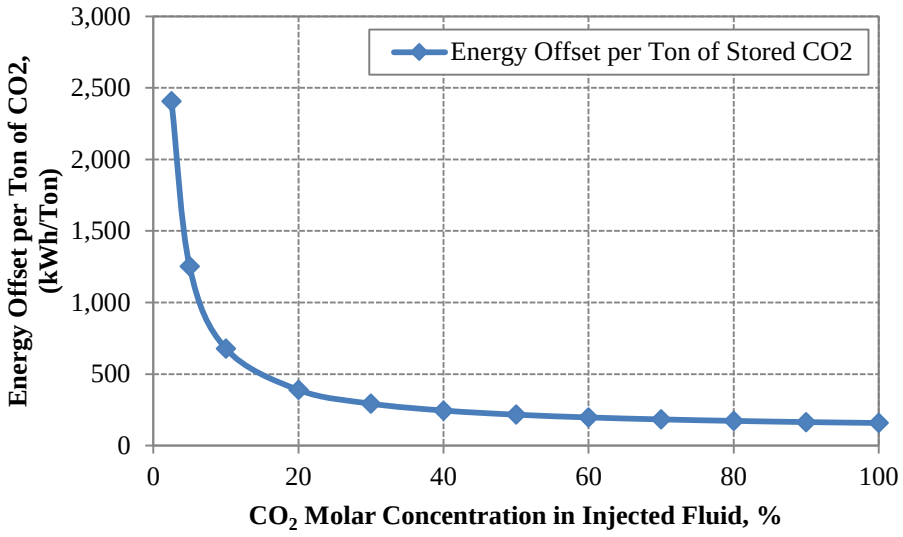

Figure 5-36: Energy offset per ton of stored CO_2 versus CO_2 molar concentration for co-injection of CO_2 and brine.

Figure 5-37 shows the volumetric ratio of re-injected brine to produced brine that gives a good estimate of the volumetric percentage of brine and CO_2 in the injection stream. Also, this figure shows the mass percentage of CO_2 versus molar concentration of CO_2 in the injected stream. Figure 5-38 shows the average brine production rate from half of the horizontal producer and the wellhead pressure of injector. Figure 5-37 shows that the volumetric percentage of brine in the injected fluid is about 60 to 40 percent for the CO_2 molar concentration of 20 to 40 percent. The dominance of the two-phase flow in this range causes higher pressure drop in the aquifer and lower injection and production rates. Also, lower injection rate causes lower wellhead pressure of the injector. For low CO_2 concentrations, liquid phase is dominant, while for high CO_2 concentrations, gas phase is dominant. The dominance of one phase flow in these two ranges causes higher flow rates and lower wellhead pressure of the injector.

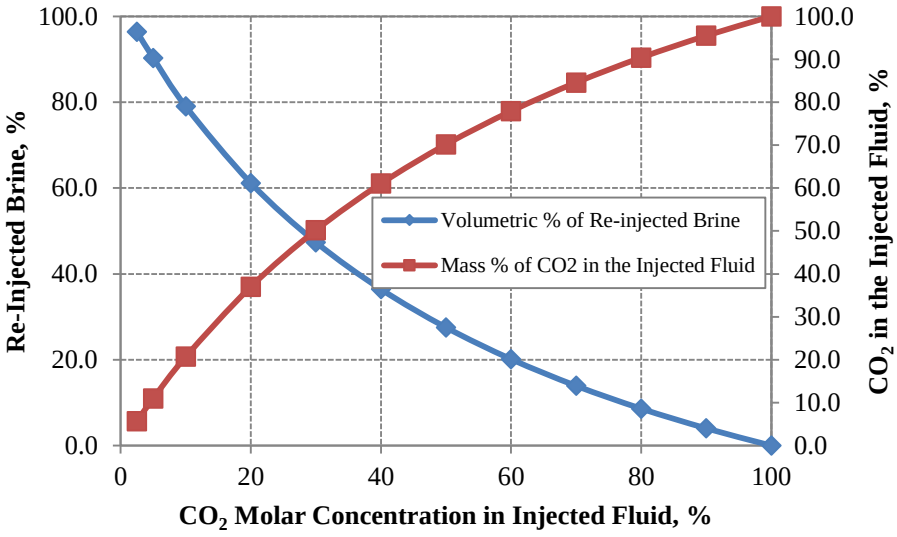

Figure 5-37: Volumetric percentage of re-injected brine and mass percentage of CO_2 versus molar concentration of CO_2 in injected fluid.

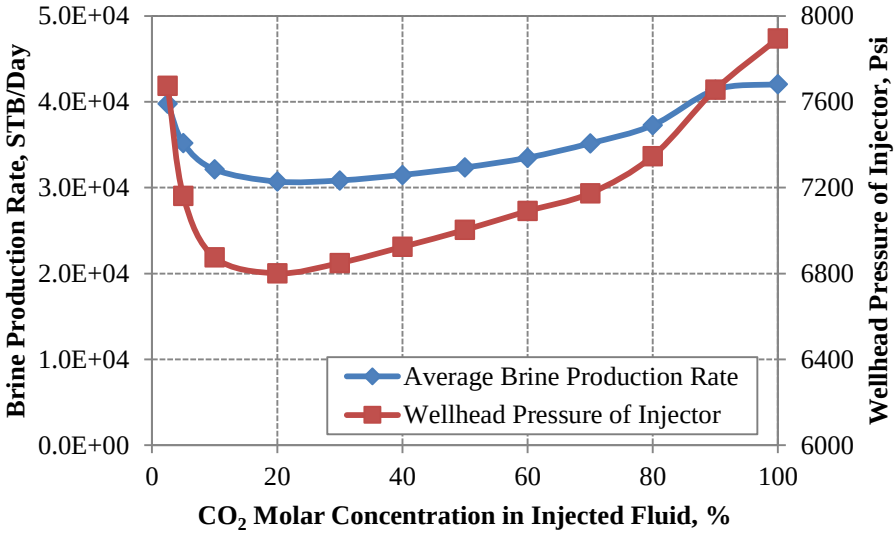

Figure 5-38: Brine production rate and wellhead pressure of injector versus molar concentration of CO_2 in injected fluid.

Figure 5-35 shows that the energy recovery is relatively insensitive to the CO_2 concentration in the injection stream for concentrations from 2.5 to 10.0 percent, while the stored CO_2 increases rapidly in the same range. Also, Figure 5-36 shows that the energy offset per ton of stored CO_2 increases significantly from 2.5 to 10.0 percent CO_2. The energy offset and amount of stored CO_2 demonstrate opposite trends while the energy recovery is almost constant in this range. The risk of escape is very low since the additional CO_2 would be trapped as residual gas. Also, the majority of the produced brine would be injected into the same aquifer. There is a compromise between the energy offset and stored CO_2 and selecting the desirable concentration depends on the objective function. For example, adding the cost of wells, possible government incentives and regulations may change the optimal CO_2 concentration. Table 5-18 summarizes the cost offset and storage results for molar CO_2 concentrations of 2.5% and 10.0%.

Table 5-18: Energy cost offset and amount of stored CO_2 for molar CO_2 concentration of 2.5 percent and 10.0 percent.

Molar concentration of CO_2 in injection stream	2.5% CO_2	10% CO_2
Cumulative injected CO_2, Million metric ton	9.29	2.71
Cumulative injected CO_2, Billion SCF	177.0	51.4
Cumulative produced CH_4, Billion SCF	11.60	12.14
Cumulative produced brine, MMSTB	273.35	283.52
Gross energy from CH_4, Trillion BTU	11.90	12.48
Gross energy from brine, Trillion BTU	9.57	9.92
Total gross energy, trillion BTU	21.47	22.4
Energy per ton of stored CO_2, Million BTU/ton	2.311	8.266

5.9 SUMMARY

The coupling of CO_2 geological storage with methane and geothermal energy production from geopressured-geothermal aquifers is a new and promising idea. The potential for offsetting the cost of CO_2 capture and storage by producing large quantities of valuable methane and geothermal energy is very significant. Based on the results of this chapter the following insights and conclusions have been obtained:

- CO_2 solubility in brine is of the order of magnitude higher than the methane solubility. This ratio is about 5 to 7 at geopressured-geothermal conditions.
- 1-D simulations demonstrate that the methane extraction follows chromatographic theory based on the method of characteristics.
- The injected CO_2 removes all of the dissolved methane and a leading methane-rich bank forms in front of the injected CO_2.
- 3-D simulations indicate that the methane bank forms in 3-D models, too. However, it is impossible to produce the entire methane bank before CO_2 breakthrough since the methane bank is spread in 3-D space. The arrival of a methane bank signals the presence of a trailing CO_2.
- Two different strategies have been introduced for injection of CO_2 and production of energy. The first strategy is to inject supercritical CO_2 and to produce methane-saturated brine. The second strategy is to inject CO_2-saturated brine. In the second strategy, methane saturated brine is produced and CO_2 is dissolved into or co-injected with produced brine.
- The strategy of injection of supercritical CO_2 is capable of storing about 8 to 10 times more CO_2 compared to strategy of injection of CO_2-saturated brine. On the other hand, about 1.5 to 2 times more energy can be produced by injecting CO_2-saturated brine.

- When CO_2-saturated brine is injected, the amount of produced energy is about 8.27 million BTU (2,423 kWh) per ton of stored CO_2.
- When supercritical CO_2 is injected, the amount of produced energy is about 0.46 million BTU (133 kWh) per ton of stored CO_2.
- Injecting dissolved CO_2 produces a greater cost offset for the capture and storage than injecting supercritical CO_2 as well as higher energy recovery.
- The strategy of injecting CO_2-saturated brine is much less vulnerable to leakage because the injected CO_2 remains dissolved for long term, while a huge CO_2 plume would be formed under the upper boundary by injecting supercritical CO_2. The large mobile gas phase is prone to escape from pathways to shallow formations.
- The strategy of injection of CO_2-saturated brine is capable of disposing the produced brine into the same aquifer, while the produced brine in the strategy of injection of supercritical CO_2 should be disposed elsewhere. Disposing in another formation is costly and may trigger environmental issues.
- There is a compromise between energy offset and amount of stored CO_2 by increasing the CO_2 concentration in the injected fluid from CO_2-saturated brine to supercritical CO_2. Adding the other costs and incentives to the objective functions varies the optimum CO_2 concentration between the two extents.

Additional investigation of the process of coupling of CO_2 geological storage with methane and geothermal energy production from geopressured-geothermal aquifers appears to be justified.

Chapter 6: Offsetting the Energy Cost of Carbon Capture and Storage by Production of Energy from Saline Aquifers

6.1 INTRODUCTION

The current approach to carbon capture and sequestration (CCS) in deep saline aquifers is not economically attractive without large subsidies or a very high price on carbon (Rochelle, 2009). Moreover, the standard approach to geologic carbon storage (GCS) of simply injecting supercritical CO_2 into deep brine-filled geological structures rises technical and environmental difficulties when scaled up to the rates needed for mitigating anthropogenic emissions. The main technical difficulties are pressure buildup (Zhou, 2008; Oruganti, 2009; Birkholzer, 2009), brine displacement (Nicot et al., 2009), and risk of buoyant escape of CO_2 (Pruess, 2004). Production of brine from the storage formations addresses many of the GCS difficulties (Burton et al., 2009). In this study, it is examined that how brine production reduces the economic challenges facing CCS.

It is often assumed that deep saline aquifers have no economic value. The key is to recognize inherent value in the energy content of brine in many parts of the world. Dissolved methane in brine is one of the sources of energy of many aquifers. For example, geopressured-geothermal aquifers lie along much of the Gulf Coast of the United States at depths exceeding 10,000 feet. The brine in these formations is saturated with methane, with concentrations on the order of 30 to 45 standard cubic feet per barrel (Griggs, 2005). Because of the sheer volume of brine, the total amount of methane held in

this form is prodigious, estimated to be between 3,000 to 46,000 TCF (Taggart, 2010). For the same reason, the capacity of these geopressured-geothermal aquifers for storage of CO_2 is remarkable. Figure 6-1 shows the average bottomhole pressure and temperature versus depth for several wells in Lavaca County, Texas. It is observed that the pressure and temperature grows abnormally below the depth of 10,000 feet.

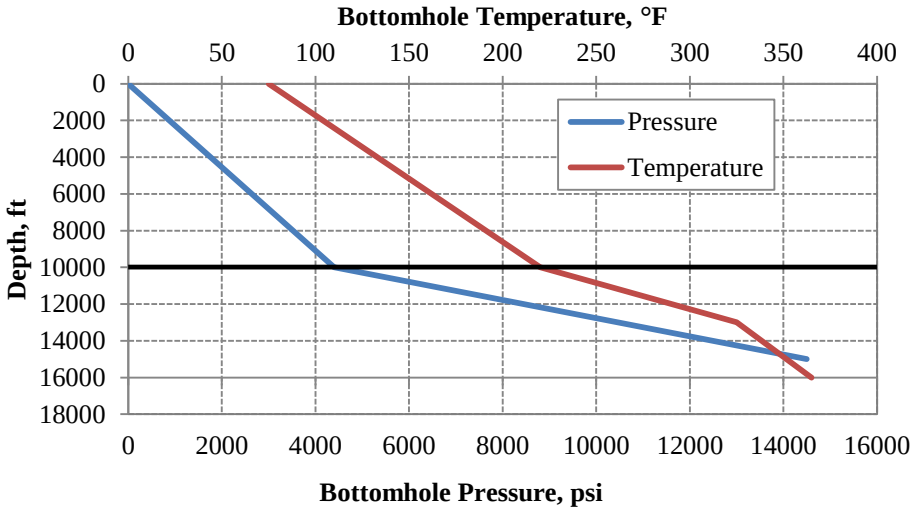

Figure 6-1: Average bottomhole pressure and temperature for several wells in Lavaca County, Texas.

Hydrostatically pressured aquifers may also contain dissolved methane as source of energy. All the aquifers which are crossed by gas during its migration toward the reservoir rock are largely saturated with methane. Figure 6-2 illustrates the solubility of methane in brine for wide ranges of pressures and temperatures. It is shown that the solubility of methane in hydrostatically pressured cases is comparable to the geopressured cases. The observations from the ongoing CO_2 storage project in Cranfield

(Hosseini et al., 2013) shows that the brine of the water leg of the reservoir is saturated with methane. This is an example of methane saturated brine in hydrostatically pressured aquifers in the United States. Also, production of methane from deep saline aquifers has been undertaken in Russia (Littke et al., 1999) and Japan (Manrique, 2000).

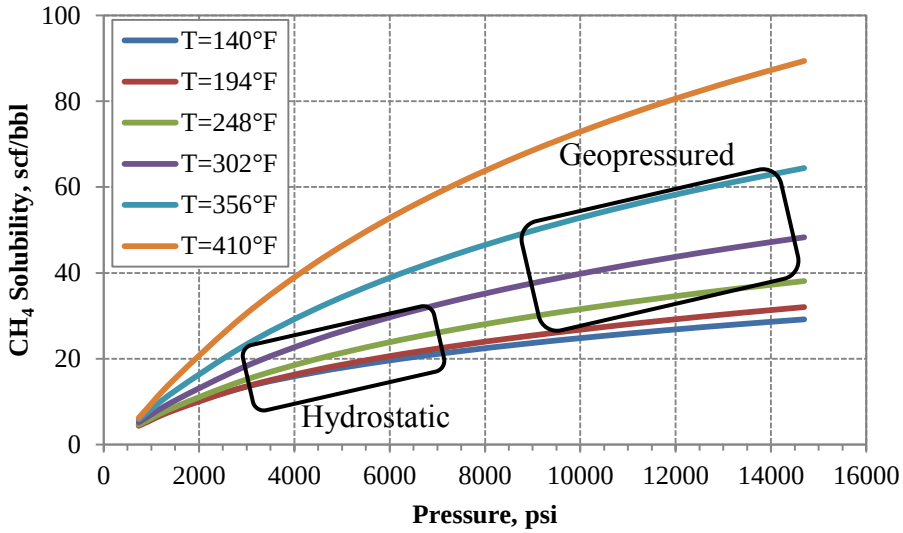

Figure 6-2: Methane solubility in brine at 55,000 ppm. Geopressured-geothermal conditions and hydrostatically-pressured conditions are distinguished by rectangular boxes.

The geothermal energy content of the hot brine is also significant. For example, the temperature of U.S. Gulf Coast aquifers is about 300 °F at depths where the geopressured condition begins (Knapp et al., 1977). Also, the reported temperature of Cranfield is about 260 °F. Hence, the geothermal potential of some of hydrostatically-pressured aquifers might be remarkable. The extractable geothermal energy from each barrel of the produced brine is of the same order of magnitude as the energy from the produced methane.

On the other hand, the majority of energy required for the CCS process is consumed by the CO_2 capture from flue gas. Two methods for capturing CO_2 from flue gas are chemical absorption and separation by membranes. Amine scrubbing has been developed as an absorption method for CO_2 capture from coal-fired power plants. Figure 6-3 illustrates the simple schematic of this process. This method is capable of removing about 90% of the CO_2 from flue gas (Plaza et al., 2010). It is estimated that amine scrubbing takes about 20% of the output of the power plant in the form of diverted low pressure steam from turbines. In this process, amine solution absorbs CO_2 in the absorber column. This CO_2 is released after the temperature of the solution is increased in the stripper column. The diverted steam provides the heat for stripper. Thermal degradation of amine determines the maximum temperature of the column. This temperature is 120 °C for monoethanolamine (Van Wagener et al., 2011a) and 155 °C for piperazine (Van Wagener et al., 2013).

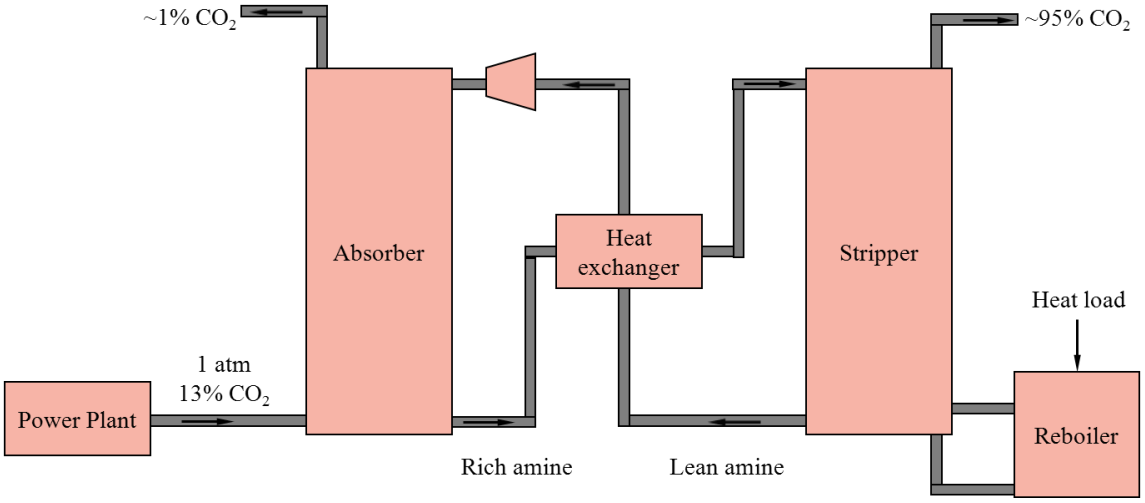

Figure 6-3: CO_2 capture by amine scrubbing process.

The driving force for membrane process is pressure difference between the feed and the permeate sides (Bounaceur et al., 2006). Membrane process operates by passing the gas mixture over a CO_2-selective membrane. The pressure on either side of the membrane is different. This pressure difference can be achieved by compressing the flue gas or by using vacuum pumps on the permeate side or a combination of both (Favre, 2007). The main advantage of membranes is their lower energy requirement for operation compared to other CO_2 capture methods (Ho et al., 2008). The flue gas containing CO_2 is fed along one side of the porous membrane. CO_2 diffuses through the pores of the membrane and is captured in the permeate side. Figure 6-4 illustrates the simple schematic of this process using blower and vacuum pump instead of compressor. Energy cost of vacuum operation is lower than compression while the capital cost of vacuum operation is higher. The enrichment of CO_2 in permeate compared to feed is related to pressure ratio of the two sides. Higher pressure ratio achieves higher concentration of CO_2 in single step membrane process while requiring more energy and larger equipment. Merkel et al. (2010) suggests a counter-flow module using vacuum pump to achieve higher enrichment and consume less energy.

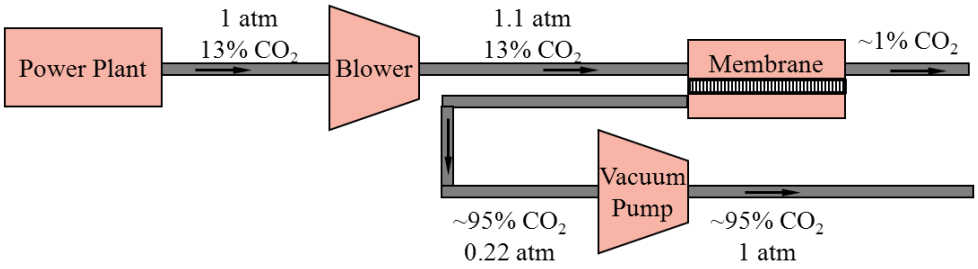

Figure 6-4: CO_2 capture by membrane process using blower and vacuum pump.

The potential for offsetting the cost of CO_2 capture and storage by producing large quantities of valuable methane and geothermal energy is clearly significant. The magnitude of this cost offset has been evaluated for two injection strategies: dissolving the CO_2 into extracted brine and then re-injecting the brine, and injecting supercritical CO_2 (Ganjdanesh et al. 2013a). Figure 6-5 illustrates the simple schematic of injection of dissolved CO_2. Geothermal energy and dissolved methane are extracted from produced high pressure hot brine. Then captured CO_2 and low temperature brine are pressurized and co-injected into the same aquifer, while in the case of injecting supercritical CO_2, only captured CO_2 is injected into the same aquifer and the extracted brine should be disposed elsewhere.

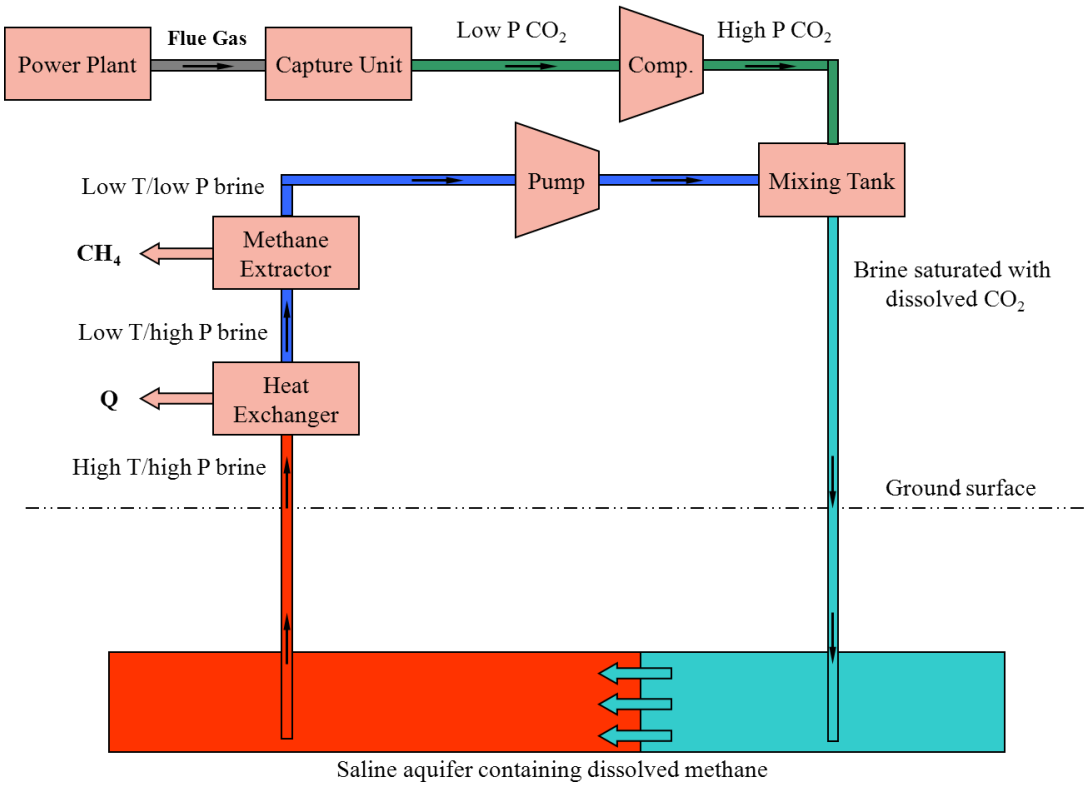

Figure 6-5: Schematic of injection of CO_2-saturated brine and extraction of energy.

Numerical simulations indicate that injecting dissolved CO_2 yields higher cost offset per metric ton of stored CO_2 compared to the offset obtained when supercritical CO_2 is injected. Injecting dissolved CO_2 conveys other significant advantages such as (1) the produced brine is injected into the same aquifer rather than requiring disposal elsewhere; (2) the stored CO_2 has negligible tendency to escape from the aquifer; (3) a higher fraction of the energy in the aquifer is recovered because single-phase flow has much larger sweep efficiency (4) the process is less sensitive to aquifer heterogeneities and other uncertain geological characteristics and (5) lower surface pressure is needed to inject CO_2 dissolved in brine due to the gravity head of brine in the wellbore.

The level of cost offset of CCS technology by producing energy from target aquifers depends on how the produced energy is used. For example, the efficiency of converting geothermal energy to electricity is on the order of 10 percent. Developing other applications of geothermal energy might be more beneficial than converting it to electricity. The temperature of the produced brine from geopressured-geothermal aquifers is higher than the temperature of amine stripper column. Ganjdanesh et al. (2013b) propose that the produced geothermal energy from geopressured-geothermal aquifers can be used for amine scrubbing process. The geothermal energy from produced brine could be used in heat exchangers that regenerate solvent for CO_2 capture. The temperature of produced brine is above the temperature required for the stripper in an amine scrubbing unit and the heat duty of the stripper can be met with the quantities of brine required for the storage process. In fact, calculations for the strategy of injecting dissolved CO_2 show that the amount of extracted thermal energy from geopressured-geothermal aquifers exceeds the amount of heat required for capturing CO_2. This means that steam would not have to be withdrawn from an existing power plant cycle.

The produced methane can be used for pressurization. In the process of injecting dissolved CO_2, compressors and pumps should run to pressurize the CO_2 and brine to be transported and achieve the required wellhead pressure. The produced methane can be used in a gas cycle or a combined gas cycle power plant to generate additional electricity. This additional electricity is used to compensate the power used for pressurization. Also, this methane can be directly used in engines to run the coupled compressors and pumps. The preliminary estimations indicate that the produced methane provides more energy than that required for pressurization.

In the regions where the temperature gradient is normal, the temperature of the produced brine may not be high enough for using in the chemical absorption processes. Separation mechanisms driven by pressure difference might be the alternatives for chemical absorption processes since the produced methane can be burned for running the compressors and pumps. Membrane process seems to be the leading technology candidate. Vast amount of studies have been performed to develop innovative membrane process designs. These studies have been mainly focused on improving the membrane CO_2/N_2 selectivity and permeance of CO_2. They also attempt to perform the separation in single stage or multi stage operations to achieve more than 95% CO_2 in permeate stream. In all the cases, the target of removing more than 90% of CO_2 is achieved. But the energy and capital cost are very high. The preliminary estimations show that the produced power by extracted methane and geothermal energy exceeds the power needed for membranes, compressors, and pumps.

Neither storage of greenhouse gases in saline aquifers nor production of methane and/or geothermal energy from these aquifers are profitable. However, designing a closed looped system by combining methods of capture, storage and production may pay off the whole process at least from the energy point of view (Bryant, 2013). This assessment

suggests that further investigation of the process of coupling of CO_2 geological storage with methane and geothermal energy production from geopressured-geothermal aquifers is warranted. Also, co-optimization of CO_2 capture and storage processes seems to be justified.

6.2 PHASE BEHAVIOR OF MIXTURES OF CO_2, CH_4, AND BRINE

Modeling the phase behavior of the mixture of gas components and brine is the primary step in modeling the CO_2 storage and production of energy from aquifers. Solubility of methane in brine determines the amount of methane reserves as dissolved gas. Aquifer brine around hydrocarbon reservoirs contain dissolved methane. In many cases, brine is saturated with methane. While, in some cases, some initial trapped gas saturation exists. Solubility of heavier hydrocarbons diminishes quickly after methane. Therefore, their presence is rarely considered in the calculations. Also, the solubility of CO_2 governs the solubility trapping mechanism. High concentrations of N_2 and other impurities such as H_2S and NO_x in the injected gas deteriorate the solubility of CO_2 in brine.

Solubility of gas components in brine depends on the temperature, pressure and salinity of the brine. Duan and Sun (2003) and Duan and Mao (2006) present thermodynamic models for solubility of CO_2 and CH_4 in aqueous NaCl solutions for wide ranges of temperatures, pressures and salinities. Comparison of predicted solubility from these models and experimental data shows high accuracy of these models. In this study, predicted solubility from these models has been used for phase behavior modeling. Figure 6-6 compares the solubility of CO_2 and CH_4 in brine versus pressure for a specific temperature and salinity. It is observed that the solubility of CO_2 is about an order of

magnitude higher than the solubility of CH_4. For example, at 10,000 psi, this ratio is about six which means that each mole of CH_4 can be substituted by six moles of CO_2 in the dissolved form.

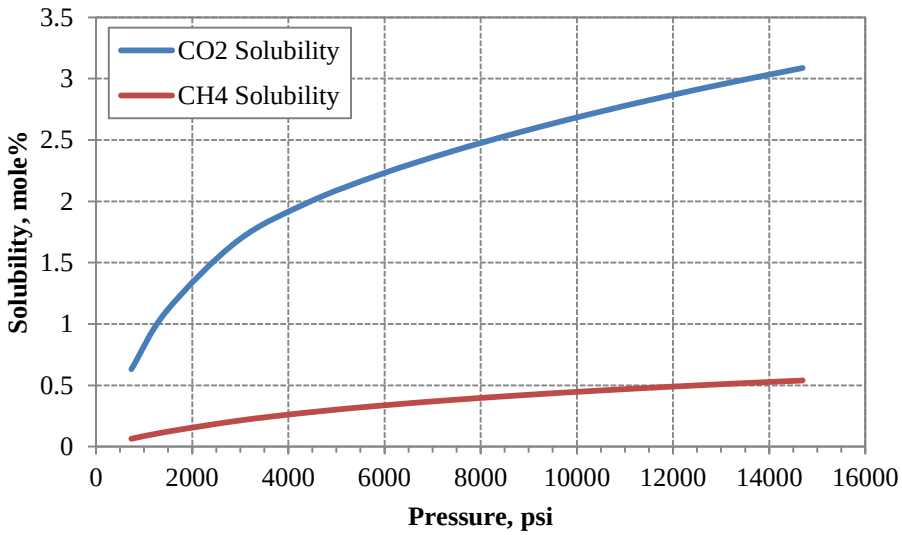

Figure 6-6: Solubility of CO_2 and CH_4 in brine at 302 °F and 55,000 ppm.

6.3 STORAGE STRATEGIES IN GEOPRESSURED-GEOTHERMAL AQUIFERS

In this section, the aquifer model that was used for numerical simulation of geopressured-geothermal aquifers is described. The results of numerical simulations are presented. Finally, an energy analysis for a 500 MW power plant is performed based on the results from simulations.

6.3.1 Simulation model

At the beginning of 1970's, Department of Energy commenced to explore the unconventional hydrocarbon resources. DOE funded several studies related to the development of the geopressured-geothermal reservoirs as prospective sources of both heat and natural gas. Several "wells of opportunity" were tested to assess the amount and quality of the natural gas associated with the geopressured-geothermal waters (Swanson et al., 1986). Production of the Pleasant Bayou No. 2 well located in Brazoria County, Texas is an example of a detailed investigation of geopressured-geothermal energy (Riney, 1991). The goal of the project was to provide the information necessary to assess the production characteristics of geopressured-geothermal reservoirs and their economic potential. The other example of the well tests in this study was Gladys McCall No. 1 which is located in Cameron Parish, Louisiana (Riney, 1988). The model in this study was built based on the data from DOE studies.

A compositional numerical reservoir simulator was used to model the fluid and geological complexities of the process. The Peng-Robinson equation-of-state (PREOS) was used to model the fluid containing carbon dioxide, methane and brine. The PREOS parameters were tuned to fit the model with experimental data under aquifer conditions. The fluid model presented in Table 5-2 is used in this study.

A numerical simulation model of the aquifer was developed. Properties such as pressure, temperature, salinity, dimensions, depth, porosity and permeability were chosen from typical conditions of geopressured-geothermal aquifers of the U.S. Gulf Coast. Relative permeability curves and capillary pressure were built using Corey model. A modified Land's equation was used to model the hysteresis including gas trapping during imbibition. The relative permeability and capillary pressure models presented in Tables 5-3 and 5-4 are used in this study.

Horizontal wells both produce at higher rates and yield higher energy recovery. Also, they are less sensitive to heterogeneity (Ganjdanesh et al., 2013a). Therefore, parallel horizontal well patterns were chosen for injector and producer. Figure 6-7 illustrates the schematic of aquifer and well placement. A unit cell of half an injector and half a producer was used for reservoir simulation. The wells were placed at the edges of the unit cell. Well types and locations affect the time of CO_2 breakthrough and the fraction of the initial methane and brine in place that can be recovered before CO_2 breakthrough. If CO_2-saturated brine is injected low in the aquifer to displace the CH_4-saturated brine upward, the displacement is gravity stable. Thus, the sweep efficiency will be high and the breakthrough late.

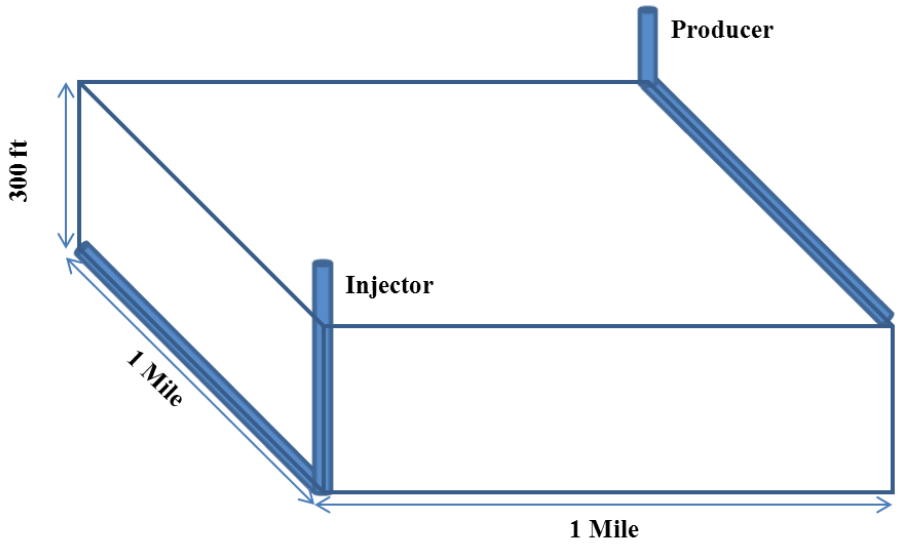

Figure 6-7: Schematic of a simulation unit cell with horizontal injector and producer. The angular fraction of the wells is 0.5 that means that the wells model a half of a circle in the numerical simulation model. The symmetry of the parallel well pattern allows modeling a half of the pattern.

Table 6-1 summarizes the specifications of the unit cell. The in-place brine was initially saturated with methane that corresponds to 0.57% CH_4 and 99.43% brine based on mole fraction. Constant wellhead pressure was used to simplify the calculation of energy required for compression. The producer and injector flow rates depend on the surface pressure, the pressure change in the wellbore and pressure drop in the aquifer. There is a strong coupling between the aquifer, the wellbore and the surface facility. CMG's compositional simulator GEM (2011) utilizes the Agarwal and Li (1988) wellbore model.

Table 6-1: Properties of geopressured-geothermal aquifer at depth of 15,000 ft.

Length and width, ft	5280
Thickness, ft	300
Number of gridblocks	80×80×30
Gridblock size, ft	66×66×10
Depth at top of the formation, ft	15000
Temperature, °F	302
Initial pressure, psi	11000
Salinity, ppm	55,000
Porosity	0.2
Horizontal permeability, md	100
Vertical permeability, md	10
Initial CH_4 in place, Billion SCF	12.407
Initial brine in place, Billion STB	0.289
Solution gas-brine-ratio, SCF/STB	42.91

6.3.2 Simulation results

The model aquifer is homogeneous and highly idealized since the purpose of this study was to explore the concept of methane and geothermal energy production by CO_2 injection. The aquifer brine was saturated with methane at the initial pressure of the reservoir of 11,000 psi. The process of injecting CO_2-saturated brine was simulated. The mole fraction of CO_2 in the injected brine was 0.025, which is equivalent to the brine saturated with CO_2 at the initial aquifer pressure of 11,000 psi. About 2.05 million metric tons (39.4 billion SCF) of CO_2 was injected in 5810 days (16 years) at a constant wellhead pressure of 4500 psi. About, 8.3 BCF of methane and 221 million barrels of brine were produced at a constant wellhead pressure of 300 psi. The amount of energy from produced methane is about 8.5 trillion BTU which is calculated from the heat of combustion of methane. Also, the amount of produced geothermal energy is about the same as energy from methane. The geothermal energy is extracted by decreasing the brine temperature from 300 to 200°F. The results are summarized in Table 6-2.

Table 6-2: Injection and production summary for a unit cell of geopressured aquifer.

Injection and production periods, Days (Year)	5810 (16)
Cumulative injected CO_2, BCF (Million ton)	39.4 (2.05)
Cumulative injected brine, MMSTB	207.0
Cumulative produced CH_4, BCF	8.27
Cumulative produced brine, MMSTB	221.2
CH_4 recovery, %	66.5
Brine recovery, %	76.5
Produced CH_4 energy, BTU (Joule)	8.50E+12 (8.98E+15)
Produced thermal energy, BTU (Joule)	7.74E+12 (8.18E+15)

The injection and production periods were chosen based on the breakthrough time of CO_2. It means that CO_2 was observed at the production stream after 16 years. After CO_2 breakthrough, producers can be converted into injectors and additional CO_2 can be injected into the aquifer since the facilities would be in place. Also, the propagation speed of thermal front was much slower than the CO_2 front. Thus, the temperature of the produced brine at CO_2 breakthrough time was still close to 300 °F.

It is assumed that the mixture of CO_2 and produced brine is injected into the same aquifer. The solubility of CO_2 in brine at 200 °F and 11,000 psi is 2.5 mole percent. Therefore, the amount of required brine to store one metric ton of CO_2 is 16.6 ton, which is equivalent to 100 STB. By dropping the temperature of one STB of hot brine from 300°F to 200 °F, about 35,000 BTU of energy can be extracted. Also, by dropping the pressure of brine to 50 psi, 37.37 SCF of methane can be extracted. During the production period, the average pressure of the aquifer decreases gradually from 11,000 psi to about 8,500 psi. A fraction of dissolved methane is released from brine forming a very small saturation of free gas. Thus, this small saturation of gas remains immobile. Maintaining the aquifer pressure above the bubble point pressure demands much higher wellhead pressure, causing much higher energy and capital cost. Therefore, operation under lower pressures seems justified.

6.3.3 Analysis of energy balance for a 500 MW power plant

The process of CO_2 capture and storage for a 500 MW power plant coupled with production of energy from geopressured-geothermal aquifers was illustrated in Figure 6-5. The energy balance for CCS combined with energy production from the aquifer is presented in the following section. The energy required for the operation of each part of

the process is analyzed separately. Also, the produced energy from methane and hot brine is estimated.

The average CO_2 emission rate from a 500 MW power plant is estimated to be 10,000 metric tons per day. It is supposed that the mixture of CO_2 and produced brine is injected into the same aquifer. The properties of the produced brine are listed in Table 6-3.

Table 6-3: Properties of the produced brine from geopressured-geothermal aquifer.

Molality (m), mole NaCl/kg water	1
Salinity, ppm	55,000
Molar mass brine, g/mole	18.73
Temperature, °F	302
Pressure, psi	11,000
Brine density at 200 °F, kg/m^3	1009.8
Brine density at standard condition, kg/m^3	1042.7

The mass of required brine to store one metric ton of CO_2 is calculated by the following equation.

$$m_{brine} = m_{CO_2} \frac{(1-x_{CO_2})M_{brine}}{x_{CO_2}M_{CO_2}}, \quad \text{(6-1)}$$

The temperature and pressure of the produced brine are reduced to 200 °F and 50 psi at surface facilities to extract the dissolved methane and geothermal energy. The solubility of CO_2 in brine at 200 °F and 11,000 psi is 2.5% on a molar basis. The amount of required brine to store one metric ton of CO_2 is estimated to be 100 STB. Therefore, about 1,000,000 STB of brine should be injected to store 10,000 metric tons of CO_2.

Table 6-4 summarizes the injection and production rates scaled up for emission rate from a 500 MW power plant.

Table 6-4: Injection and production summary for a 500 MW power plant for geopressured-geothermal aquifer.

CO_2 injection rate, Metric ton per day	10,000
Brine injection rate, STB/day	1,006,000
Brine production rate, STB/day	1,074,000
Methane production rate, MMSCF/day	40.2
Total number of injectors and producers	14

The capture process and pressurization are the major energy consumers. The pressurization process includes the compression of CO_2 and pumping the brine to the wellhead pressure of injectors. About 10,000 metric tons of CO_2 and 1,000,000 barrels of brine should be pressurized from atmospheric pressure to 4,500 psi. The methods of energy calculation for pressurization are listed in Tables 6-5 and 6-6.

Table 6-5: Properties and relationships for pumping the brine to wellhead pressure.

Property	Relationship or Value
Energy per unit mass of injected brine	$W_{brine} = \frac{P_{mixing} - P_1}{\rho_{brine}\eta_{pump}}$
Inlet pressure	$P_1 = 50$ psi
Mixing pressure	$P_{mixing} = 4{,}500$ psi
Pump efficiency	$\eta_{pump} = 80$ %

Table 6-6: Properties and relationships for compressing the CO_2 to wellhead pressure.

Property	Relationship or Value
Energy per unit mass of stored CO_2	$W_{CO_2} = \frac{SnRT_1}{(n-1)M_{CO_2}}\left(\left(\frac{P_x}{P_1}\right)^{\frac{n-1}{n}} - 1\right)$
Intermediate pressure	$P_x = P_1\left(\frac{P_{mixing}}{P_1}\right)^{\frac{1}{S}}$
Polytropic coefficient	$n = \frac{k\eta_p}{1 + k\eta_p - k}$
Compressor polytropic efficiency	$\eta_p = 80\ \%$
Number of stages	$S = 10$
Ratio of specific heats	$k = 1.3$
Inlet temperature	$T_1 = 104\ °F$
Inlet pressure	$P_1 = 14.7\ psi$
Mixing pressure	$P_{mixing} = 4500\ psi$
Gas constant	$R = 1.968\ \frac{BTU}{lbmole.°R}$

The power required for compressors and pumps are summarized in Table 6-7. In these illustrative calculations, the efficiency of compressors and pumps are assumed to be 80%. The estimated power for compressors and pumps are 43 MW and 73 MW, respectively.

Table 6-7: Power consumption by compressors and pumps for geopressured-geothermal aquifer.

CO_2 compression, MW	43
Brine pumping, MW	73

The majority of energy for capture process by amine scrubbing is taken in the form of heat by stripper. The heat load for a 500 MW power plant is about 400 MW. In the conceptual designs, this heat is provided by diverting a fraction of low pressure steam from turbines. The equivalent work of this amount of heat is about 100 MW which will be deducted from the output of the power plant.

Table 6-8 summarizes the gross energy and power produced from extracted methane and hot brine. The gross rate of produced energy based on heat of combustion of methane is about 505 MW. The rate of recoverable work from this amount of energy depends on the efficiency of the cycle which is used for power generation. Overall, this efficiency varies between 30 to 60%. In this work, it is assumed that about 235 MW of power (gas engines have efficiencies as high as 47%) can be generated from extracted methane that exceeds the amount of power required for pressurization.

Furthermore, the gross rate of extracted heat from extracted hot brine is about 449 MW. The efficiency of geothermal power plants is on the order of 10%. In this work, it is supposed that 55 MW of electricity can be produced. However, the superior application of this heat is the direct use in amine scrubbing since the amount of produced heat exceeds the heat load of the stripper and the temperature of the produced brine is sufficient for solvent regeneration.

Table 6-8: Gross and net power from methane and hot brine for geopressured-geothermal aquifer.

	Gross Power	Efficiency	Equivalent Power
Energy from CH_4, MW	505	0.47	235
Energy from Brine, MW	459	0.12	55

About 14 injectors and 14 producers are needed to maintain the required injection and production rates for a 500 MW power plant. Thus, the footprint of the project would be 28 unit cells.

6.4 STORAGE STRATEGIES IN HYDROSTATICALLY-PRESSURED AQUIFERS

In this section, the aquifer model used for numerical simulation of hydrostatically-pressured aquifers is described. The results of numerical simulations are presented. Finally, an energy analysis for a 500 MW power plant is performed based on the results from simulations.

6.4.1 Simulation model

Energy resources of hydrostatically-pressured aquifers have been assessed and documented much less than geopressured-geothermal aquifers. But, it is expected that huge reserves of energy may exist at shallower depths with normal pressure and temperature gradients.

The aquifer model for simulation of hydrostatically-pressured aquifers has the same dimensions and petrophysical properties of the ones used for simulation of geopressured-geothermal aquifers. Also, the well types and placements are the same. However, this aquifer is located at depth of 10,000 feet which is above the geopressured-geothermal zone. The initial pressure and temperature of the aquifer are 4,700 psi and 257 °F corresponding normal pressure and temperature gradients. Table 6-9 summarizes the tuned phase behavior model for PREOS at initial condition.

Table 6-9: Component properties tuned for 4,700 psi, 257 °F, and 55,000 ppm.

Component name	CO_2	CH_4	H_2O
Critical pressure, atm	72.8	45.4	217.6
Critical temperature, °K	304.2	190.6	647.3
Critical volume, m^3/k-mole	0.094	0.099	0.056
Molecular wt., g/g-mole	44.01	16.043	18.73
Acentric factor	0.225	0.008	0.344
Parachor	78	77	52
Omega A	0.4572	0.4572	0.4572
Omega B	0.077796	0.077796	0.077796
Volume shift (at reservoir condition)	0.074663	-0.12679	0.21172
Volume shift (at surface condition)	0.0	0.0	0.16037
Critical volume (viscosity), m^3/k-mole	0.090423	0.095632	0.049284
BIC corresponding to H_2O	0.0069	-0.0243	0

The gas content of the brine is about 21.64 standard cubic feet per barrel which is about the half the value in a geopressured-geothermal aquifer located at 15,000 ft. Table 6-10 shows the properties of the aquifer used in this study. The initial composition of the in situ fluid is 0.29 mole percent methane and 99.71 mole percent brine.

Table 6-10: Properties of hydrostatically-pressured aquifer at depth of 10,000 ft.

Length and width, ft	5280
Thickness, ft	300
Number of gridblocks	80×80×30
Gridblock size, ft	66×66×10
Depth at top of the formation, ft	10000
Temperature, °F	257
Initial pressure, psi	4700
Salinity, ppm	55,000
Porosity	0.2
Horizontal permeability, md	100
Vertical permeability, md	10
Initial CH_4 in place, Billion SCF	6.177
Initial brine in place, Billion STB	0.285
Solution gas-brine-ratio, SCF/STB	21.64

6.4.2 Simulation results

The process of injecting a mixture of CO_2 and brine was simulated. The injection stream consists of 2.5 mole percent gas and 97.5 mole percent brine. This composition is close to the CO_2 saturated brine at reservoir condition. About 2.0 million metric tons (38.4 billion SCF) of CO_2 was injected in 6916 days (19 years) at a constant wellhead pressure of 2,500 psi. About 4.48 BCF of methane and 209 million barrels of brine were produced at a constant wellhead pressure of 300 psi. The amount of energy from produced methane is about 4.6 trillion BTU which is calculated from the heat of combustion of methane. Also, the amount of produced geothermal energy is about 7.1

trillion BTU. The geothermal energy is extracted by decreasing the brine temperature from 257 to 157°F. The injection and production periods were chosen based on the breakthrough time of CO_2. The results are summarized in Table 6-11.

Table 6-11: Injection and production summary for a unit cell for hydrostatically-pressured aquifer.

Injection and production periods, Days (Year)	6916 (19)
Cumulative injected CO_2, BCF (Million ton)	39.4 (2.0)
Cumulative injected brine, MMSTB	201.3
Cumulative produced CH_4, BCF	4.48
Cumulative produced brine, MMSTB	209.4
CH_4 recovery, %	73.3
Brine recovery, %	73.3
Produced CH_4 energy, BTU (Joule)	4.61E+12 (4.86E+15)
Produced thermal energy, BTU (Joule)	7.05E+12 (7.44E+15)

By dropping the pressure of brine to 50 psi, 21.69 SCF of methane can be extracted. During the production period, the aquifer pressure remains above the initial bubble point pressure of 4,700 psi. Thus, the methane content of the produced fluid is very close to the methane content of the aquifer brine. Another advantage of maintaining the aquifer pressure above the bubble point pressure is very high recovery of methane and brine. Single phase flow through the aquifer results in almost ideal displacement efficiency. Also, injected brine has lower temperature than the in-situ brine. Therefore, injected brine is more viscous and denser than the in situ brine resulting in very high sweep efficiency.

6.4.3 Analysis of energy balance for a 500 MW power plant

The strategy of injection and production from hydrostatically-pressured aquifers is the same as the one for geopressured aquifers. The results of simulations are scaled up for a 500 MW power plant. The rate of emission from a 500 MW power plant is 10,000 metric tons per day. Thus, about 1,000,000 barrels of brine per day should be injected along with CO_2. The production rate of brine is about the same 1,000,000 barrels per day. Also, 22.4 million standard cubic feet of methane is produced along with brine. About 17 injectors and 17 producers are needed to maintain the calculated injection and production rates. Table 6-12 summarizes the injection and production rates for a 500 MW power plant.

Table 6-12: Injection and production summary for a 500 MW power plant for hydrostatically-pressured aquifer.

CO_2 injection rate, Metric ton per day	10,000
Brine injection rate, STB/day	1,007,000
Brine production rate, STB/day	1,048,000
Methane production rate, MMSCF/day	22.4
Total number of injectors and producers	17

Table 6-13 shows the power needed for pressurization. The methods presented in Tables 6-5 and 6-6 are used to calculate the power for pumps and compressors. The power for compressing CO_2 to 2,500 psi is about 38 MW. The power for pumping brine is about 39 MW.

Table 6-13: Power consumption by compressors and pumps for hydrostatically-pressured aquifer.

CO_2 compression, MW	38
Brine pumping, MW	39

Table 6-14 summarizes the energy rate and net power from extracted methane and hot brine. The energy rate from produced methane calculated from heat of combustion is about 281 MW. Assuming a recovery of 47 percent, about 132 MW of net power is generated. The heat rate from extracted brine is about 448 MW. Assuming a recovery of 10%, the generated power from hot brine is about 45 MW.

Table 6-14: Gross and net power from methane and hot brine for hydrostatically-pressured aquifer.

	Gross Power	Efficiency	Equivalent Power
Energy from CH_4, MW	281	0.47	132
Energy from Brine, MW	448	0.10	45

The temperature of produced brine might not be sufficient for solvent regeneration. But, a significant amount of power can be generated from produced methane and hot brine. This power can be used to generate the pressure difference across the sides of membranes. In the membrane configuration proposed by Merkel (2010), about 16 percent of the output of power plant is consumed to enrich the CO_2 purity to more than 95 percent. Therefore, about 80 MW of power is required for the multi-stage membrane separation. Overall, the total consumed power for capture and pressurization is about 157 MW; while the total produced power is about 177 MW.

6.5 COMPARISON OF APPROACHES

In this section, results of four different approaches of coupled capture, storage, and production are compared. These approaches consist of capture by amine stripping or membrane separation and storage and production from geopressured or hydrostatically-pressured aquifers. Table 6-15 shows the energy consumption and production and the net power for all of the approaches.

Table 6-15: Energy analysis for four approaches.

Aquifer condition	Geopressured		Hydrostatic	
Capture method	Amine	Membrane	Amine	Membrane
CO_2 compression (MW)	-42	-42	-38	-38
Brine pumping (MW)	-73	-73	-39	-39
Capture (MW)	0	-80	-100	-80
CH_4 power (MW)	+235	+235	+132	+132
Geothermal power (MW)	0	+55	+45	+45
Net power (MW)	+120	+95	0	+20
Energy per ton of stored CO_2 (kWh)	+288	+228	0	+48

Overall, comparison of four approaches is summarized as follows:

- The temperature and energy from the brine produced from geopressured-geothermal aquifers is sufficient for the amine scrubbing of CO_2.
- Amine scrubbing seems to be the superior capture method for storage in geopressured-geothermal aquifers.
- Membrane separation shows better energy balance for storage in hydrostatically-pressured aquifers.

- Energy balance of approaches consist of production from geopressured aquifers are much more promising than the hydrostatically-pressured aquifers.
- Capital cost of surface facilities is much higher for geopressured aquifers since pressure and temperature of the fluids are higher.
- The cost of the wells is higher for geopressured-geothermal aquifers since depth, pressure, and temperature are higher.
- Hydrostatically-pressured aquifers are much more widespread, but the energy content is less well established.
- Site specific studies and detailed economics will be needed to determine the best strategy.

6.6 INJECTION OF FLUE GAS AND PARTIALLY SEPARATED CO_2

Achieving a CO_2 enrichment of more than 95% in the permeate stream of membranes requires very high energy and capital cost. An important question is that how does the purity of CO_2 in the permeate side effect the energy and capital cost. Is it possible to decrease the energy and capital cost by decreasing the purity of CO_2 in the processed stream? It is obvious that the presence of higher percentages of N_2 in the permeate side increases the energy and capital cost of the storage process. More energy is required to compress the additional N_2 at wellhead facilities as well as higher numbers of compressors and wells. Also, solubility of N_2 compared to CO_2 is negligible leading to occupation of a fraction of aquifer pore volume by gas. Therefore, it may be impossible to re-inject all the produced brine into the same aquifer. Disposal of the excessive water in the shallower aquifers may be a solution. However, this strategy demands cautious

consideration of environmental issues. A more practical solution for the excessive brine may be production of fresh water since the temperature of produced brine is high.

In the proposed idea for storage of partially separated CO_2, methane-saturated brine is produced from the aquifer. The dissolved methane and also economically viable geothermal energy are extracted. Then, a portion of produced brine along with a mixture of CO_2, N_2 and other components from flue gas are injected into the same aquifer. The excessive brine is injected into a shallower disposal formation or is processed to produce fresh water.

Figure 6-8 compares the solubility of CO_2, N_2 and CH_4 in brine versus pressure for a specific temperature and salinity. The solubility of CO_2 is about an order of magnitude higher than the solubility of CH_4. For example, at 10,000 psi, this ratio is about six which means that each mole of CH_4 can be substituted by six moles of CO_2 in the dissolved form. Also, the solubility of N_2 is about two-thirds of the solubility of CH_4.

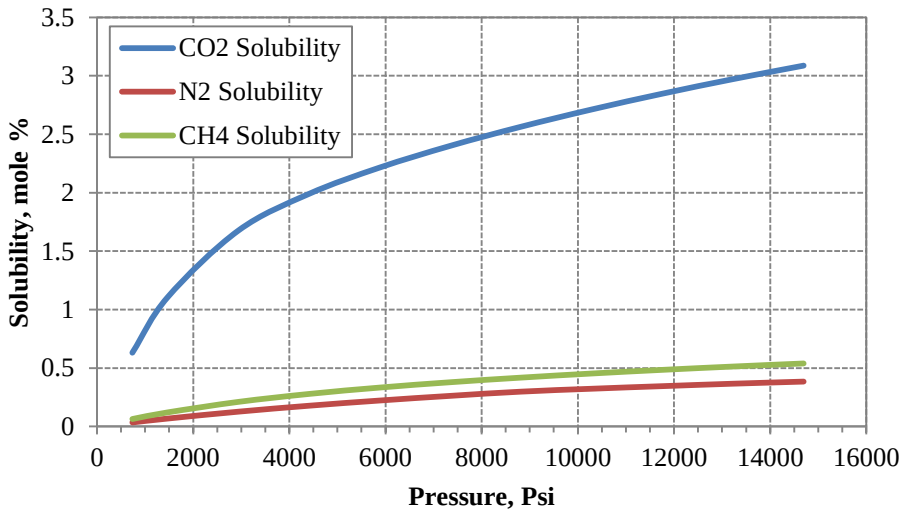

Figure 6-8: Solubility of CO_2, N_2 and CH_4 in brine (55,000 ppm) at T=302 °F.

6.6.1 Simulation model

The simulation model used in this study was similar to the one that was described in section 6.4.1. However, N_2 is added to the phase behavior model as the only impurity.

6.6.2 Simulation results

The process of injecting a mixture of CO_2, N_2 and brine was simulated. The injection stream consists of 20 mole percent gas and 80 mole percent brine. In this study, the flue gas from coal-fired power plants is simplified to 87 percent N_2 and 13 percent CO_2. It was assumed that the concentration of CO_2 is increased to 40% in a single-stage membrane process. About 1.36 million metric tons (25.8 billion SCF) of CO_2 and 1.30 million metric ton of N_2 was injected in 3072 days (8.4 years) at a constant bottomhole pressure of 6,000 psi. About, 1.62 BCF of methane and 75 million barrels of brine were produced at a constant bottomhole pressure of 4,700 psi. The amount of energy from produced methane is about 1.7 trillion BTU, which is calculated from the heat of combustion of methane. Also, the amount of produced geothermal energy is about 2.7 trillion BTU. The geothermal energy is extracted by decreasing the brine temperature from 257 to 157°F. The injection and production periods were chosen based on the breakthrough time of CO_2. The results are summarized in Table 6-16. About 35 million barrels of the produced brine were injected into the same aquifer, which means that about 53 percent of the produced brine must be disposed of or be converted to fresh water or some other use. Also, by dropping the pressure of brine to 50 psi, 21.43 SCF of methane can be extracted. During the production period, the aquifer pressure remains above the initial bubble point pressure of 4,700 psi. Thus, the methane content of the produced fluid is very close to the methane content of the aquifer brine.

Table 6-16: Injection and production summary for injection of 8% CO_2, 12% N_2, and 80% brine (mole %).

Injection and production periods, Days	3072
Cumulative injected CO_2, BCF (Million Ton)	25.8 (1.36)
Cumulative injected brine, MMSTB	35.0
Cumulative produced CH_4, BCF	1.62
Cumulative produced brine, MMSTB	75.6
Produced CH_4 energy, BTU (Joule)	1.67E+12 (1.76E+15)
Produced thermal energy, BTU (Joule)	2.65E+12 (2.79E+15)

6.6.3 Analysis of energy balance for a 500 MW power plant

The average CO_2 emission rate from a 500 MW power plant is estimated to be 10,000 metric tons per day. The capture process and pressurization are the major energy consumers. The pressurization process includes the compression of CO_2 and N_2 and pumping the brine to the wellhead pressure of injectors. About 10,000 metric tons of CO_2, 9,500 metric tons of N_2 and 258,000 barrels of brine should be pressurized from atmospheric pressure to 3,500 psi. The gross rate of produced energy based on heat of combustion of methane is about 150 MW. In this work, it is assumed that about 70 MW of power can be generated from extracted methane. The brine production rate is about 557,000 barrels. The gross rate of extractable heat from hot brine is about 238 MW. In this work, it is supposed that 25 MW of electricity can be produced. Overall, the total consumed power for capture and pressurization is about 155 MW. While, the total produced power can be about 95 MW. About 11 injectors and 11 producers are needed to maintain the required injection and production rates for a 500 MW power plant. Thus, the footprint of the project would be 22 unit cells. Also, about 299,000 barrels of

excessive brine should be disposed or be processed. Table 6-17 summarizes the injection and production rates for a 500 MW power plant. Also, Table 6-18 summarizes the energy rate and net power from extracted methane and hot brine.

Table 6-17: Injection and production summary for a 500 MW power plant for injection of 8% CO_2, 12% N_2, and 80% brine in hydrostatically-pressured aquifer.

CO_2 injection rate, Metric ton per day	10,000
N_2 injection rate, Metric ton per day	9,500
Brine injection rate, STB/day	258,000
Brine production rate, STB/day	557,000
Methane production rate, MMSCF/day	11.9
Total number of injectors and producers	22

Table 6-18: Gross and net power from methane and hot brine for hydrostatically-pressured aquifer.

	Gross Power	Efficiency	Equivalent Power
Energy from CH_4, MW	150	0.47	70
Energy from Brine, MW	238	0.105	25

The method of calculation for pressurization is the same as the one that was described in section 6.3.3. In these illustrative calculations, the efficiency of compressors and pumps are assumed to be 80%. The estimated power for compressors and pumps are 103 MW and 14 MW, respectively. The majority of energy for capture process by membrane is taken for pressurization of flue gas. In the configuration proposed by Merkel (2010), about 7.5 percent of the output of power plant is consumed to rich the 40

percent enrichment of CO_2. Therefore, about 38 MW of power is required for the single-stage membrane separation. Table 6-19 shows the power needed for pressurization and partial separation by membrane.

Table 6-19: Power consumption by compressors, pumps, and membrane for injection of 8% CO_2, 12% N_2, and 80% brine in hydrostatically-pressured aquifer.

CO_2 and N_2 compression, MW	103
Brine pumping, MW	14
Compression for partial separation, MW	38

The selection of 40 percent enrichment of CO_2 was arbitrary. The purity of CO_2 in the permeate side of the membrane effects the energy for separation, surface area of membrane, the energy for pressurization of injected fluid, pore volume for storage and number of wells. It is speculated that the 99% purity in the permeate side may not be the optimum from the point of view of total cost. To find the minimum total cost, all these parameters should be included in the calculations. In this study, the variation of energy for pressurization and pore volume versus purity of CO_2 were estimated. Figure 6-9 shows the power for pressurization of injected fluid versus purity of CO_2 for a 500 MW power plant. It is observed that most of the decline in power demand occurs from 13 percent to 40 percent. Figure 6-10 illustrates the consumed power and produced power by methane and geothermal energy versus purity of CO_2. Also, the net energy has been calculated by subtraction of consumption from production. The net energy change is very small specifically after 40 percent indicating minimal improvement in energy by further purification. Figure 6-11 shows the rate of brine production, re-injection and disposal for a 500 MW power plant. The rate of production drops drastically by improving the

concentration of CO_2 in the injected gas that results in less storage pore volume and less number of wells. However, the majority of the decline occurs between 13 percent and 40 percent.

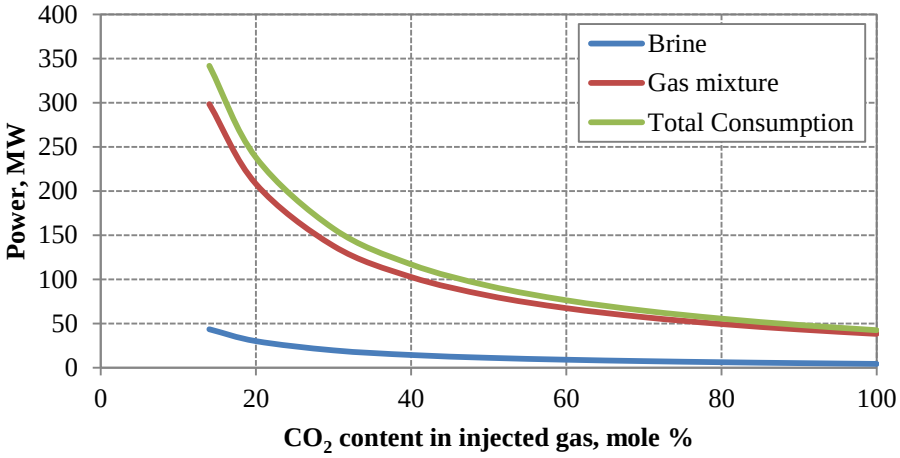

Figure 6-9: Consumed power for compression of injected gas mixture and brine (20% gas and 80% brine) for a 500MW power plant.

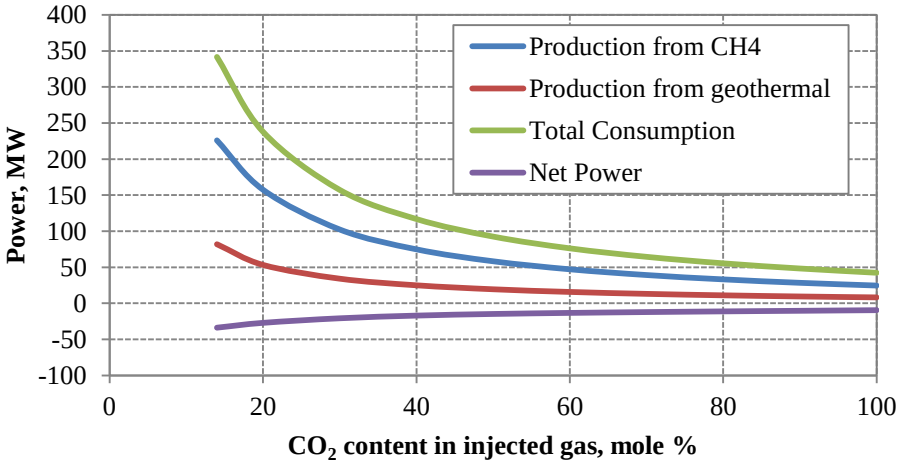

Figure 6-10: Consumed power for fluid compression and generated power from produced methane and hot brine for a 500MW power plant.

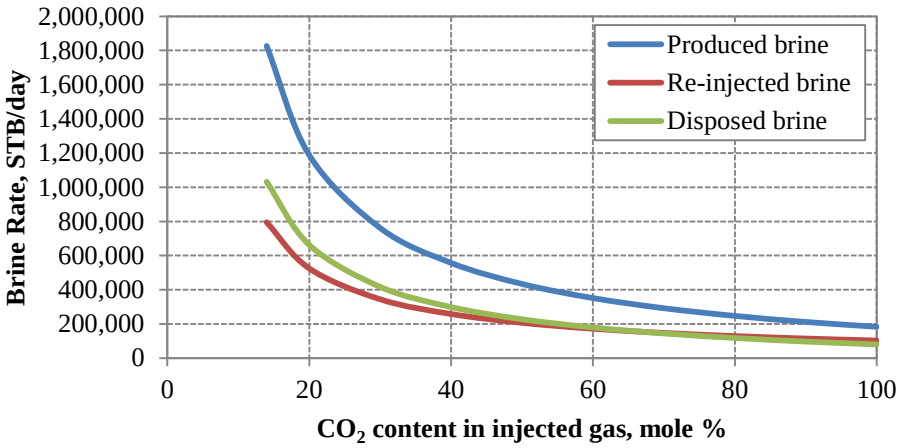

Figure 6-11: Produced, re-injected, and disposed brine for a 500MW power plant.

6.7 SUMMARY

Geologic storage of carbon dioxide in deep saline aquifers was introduced as the primary option for storage of significant amounts of CO_2 emitted from coal-fired power plants. Several studies have focused on overcoming the technical and economic challenges inhibiting this technology from becoming widespread. Extraction of brine from storage formations brings the prospects of mitigation of some of the challenges. From the economic point of view, the produced brine may convey amounts of energy comparable to the amounts required for CO_2 capture and storage processes. The success of offsetting the energy cost of capture and storage depends on the applications of the produced energy.

Geopressured-geothermal aquifers contain vast amount of dissolved methane and geothermal energy. A rough estimation indicates that the amount of produced energy exceeds the energy needed for capture and storage. It is proposed that the geothermal energy can be used in the capture process by amine scrubbing and the produced methane

can be used for pressurization of CO_2 and brine up to the wellhead pressure. In this strategy, CO_2 remains dissolved in brine. Thus, pressure buildup and CO_2 leakage will be mitigated. Also, brine is disposed into the same aquifer.

In shallower depths, where temperature of brine is not high enough to be used for chemical absorption, pressure driven separation processes can be used. The produced methane is used in compressors or vacuum pumps to generate the pressure difference for membrane process.

Review of energy analysis of four possible approaches of combined capture, storage, and production indicates that

- The energy revenue from all approaches offset all the energy cost of CO_2 capture and storage.
- The net energy gain from geopressured-geothermal aquifers is higher than from hydrostatically-pressured aquifers. The net energy gain is about 288 kWh per ton of stored CO_2 for capture by amine scrubbing and about 228 kWh by membrane separation.
- Production from hydrostatically pressured aquifers leads to about zero energy gain for capture by amine scrubbing and about 48 kWh per ton of stored CO_2 by membrane separation.
- Storage and production from geopressured-geothermal aquifers shows much better energy balance while the operating and capital cost of the process is higher for these aquifers.
- Extraction of brine from aquifers mitigates the concerns of pressure buildup, CO_2 leakage, and brine displacement. This also lowers the monitoring cost.
- Improving the enrichment of CO_2 by membrane implies drastic increase in energy and capital cost of capture by membranes. On the other hand, lower enrichment of

CO_2 requires more energy cost for pressurization of injected gas and brine. Preliminary estimations indicate that including the generated power from extracted methane and heat partially offset the energy cost of pressurization. Also, the capital cost of storage, including the compressors and pumps, number of wells and required pore volume decreases by increasing the purity of CO_2. However, most of the decrease occurs from 13 percent to 40 percent.

- Overall, the purity of CO_2 has inverse effect on the energy and capital cost of capture by membrane from one side and energy production and energy and capital cost of pressurization and storage on the other side. The minimum total cost might occur at CO_2 percentages much lower than 95%. Optimization of total cost requires careful inclusion of energy and capital cost of membrane separation and also well cost and surface facilities.

The coupling of CCS with energy production from geopressured-geothermal aquifers is a new and promising idea. There is a significant potential for offsetting the energy cost of CCS by producing large quantities of methane and geothermal energy. Determining the actual economics will of course require closer examination of CO_2 capture methods, well costs, surface facilities, the price of the produced gas, whether the geothermal energy can be used for process heat, incentives for CO_2 storage, etc. However, preliminary calculations indicate that the revenue from the energy in hot brine saturated with methane can offset much of the energy costs of CCS or even pay for it under favorable conditions such as exist along the U.S. Gulf Coast.

Chapter 7: Summary, Conclusions, and Recommendations

7.1 SUMMARY

Carbon capture and storage (CCS) is considered to be the frontier technology to significantly reduce greenhouse gas emissions. Much research has been performed on the storage of carbon dioxide in deep saline aquifers. Most of this research indicates that saline aquifers are the only viable option to store large volumes of anthropogenic CO_2 from power plants and other industrial sectors such as cement, steel, iron and natural gas processing.

Several technical and economic issues have been major impediments to the commercialization of CCS technology to date. The technical issues include pressure buildup in the aquifers, brine displacement and risk of CO_2 leakage. For conventional carbon storage, supercritical CO_2 is injected into the target aquifers. The capacity of the target aquifers is limited. Injection of CO_2 brings about local pressure buildup in vicinity of the injector leading to loss of injectivity. Also, the pore pressure may exceed the fracturing threshold of the formation. Fracturing the top seal of the formation escalates the risk of CO_2 escape from the storage formation. The bulk CO_2 occupies the pore volume around the injector and pushes the resident brine toward the neighborhood region that may pollute the fresh-water-bearing areas. If gas segregation occurs over the long term, then it will leave the CO_2 prone to escape from leaky faults or wellbores.

On the other hand, technologies considered for separating CO_2 from flue gas and injecting it into saline aquifers are energy intensive and costly. For example, it is estimated that capturing the CO_2 from coal-fired power plants and pressurizing it up to the wellhead pressure requires about a third of the power output of the power plant.

The strategy of extraction of brine from the target aquifers has been proposed to mitigate some of the technical challenges. It has been suggested that CO_2 can be dissolved into the extracted brine in surface facilities. Injection of CO_2-saturated brine mitigates the pressure buildup and risk of leakage.

In this study, the extracted brine from deep saline aquifers was considered as a source of energy to offset the energy cost of the CCS process. This energy was categorized into methane dissolved in brine and geothermal energy.

A systematic sensitivity analysis was conducted to identify the effect of different parameters on energy recovery using different development strategies and economic criteria were defined for these development strategies based on the reservoir quality. An extensive study of geopressured-geothermal aquifers of Gulf Coast as source of methane and geothermal energy was done by the US Department of Energy during the 70's and 80's. The data from this DOE study was used to determine the uncertainty of the aquifer properties and to build the reservoir models. Several reservoir simulation studies were performed using these aquifer models to find the best strategies for extraction of energy from these aquifers. The second task of this research was to couple the energy production with CO_2 storage. Two strategies were proposed for CO_2 injection. These strategies were injection of supercritical CO_2 and injection of CO_2-saturated brine. In the first strategy, methane-saturated brine is produced and supercritical CO_2 is injected to improve the energy recovery. In the second strategy, methane-saturated brine is produced and CO_2 dissolved into the extracted brine is injected into the same aquifer to improve the energy

recovery. The main questions were how much CO_2 could be stored, how much energy could be produced and how much energy could be produced per ton of stored CO_2 for each injection strategy.

The third task was to integrate the storage and production with CO_2 capture methods. Reservoir simulation models were built for both geopressured-geothermal aquifers and hydrostatically-pressured aquifers. Reservoir simulation studies were performed on the two models to quantify the amount of extractable energy per ton of stored CO_2 by injection of CO_2-saturated brine. Next, the application of the produced energy to capture and storage processes were examined. Two main capture processes were included in this study: chemical absorption by amine scrubbing and separation by membranes. Finally, an energy analysis was done for combinations of different aquifer conditions and capture processes to estimate the energy offset for each combination.

7.2 CONCLUSIONS

Based on the results presented in this dissertation, the following conclusions can be derived from this research.

- Deep saline aquifers are a very large source of energy, although the energy concentration is much lower than conventional hydrocarbon resources. Deep saline aquifers of the US Gulf Coast contain significant dissolved hydrocarbons and geothermal energy. Specifically, geopressured-geothermal aquifers accommodate vast amount of dissolved methane.

  Two strategies are capable of producing significant amounts of methane and hot brine: production by depletion to low pressures; and pressure maintenance by re-

injecting the produced brine. Pressure maintenance has the advantage of keeping the brine and gas production rates constant during the whole production period. The energy recovery factor for pressure maintenance case is much higher compared to depletion case where the recovery factor is about 3 to 5 percent. The pressure maintenance scenario requires much smaller aquifer size compared to aquifer depletion case.

Size, thickness and permeability are the most important formation parameters in production. Reservoir volume is the governing factor in production by depletion, while the product of thickness and permeability (kh) is the governing factor in production by reinjection.

Reinjection has several advantages such as increasing the sustainability of production, reducing reservoir connectivity risk, and disposal of produced brine in the same formation.

- The coupling of CO_2 geological storage with methane and geothermal energy production from geopressured-geothermal aquifers is a new and promising idea. The potential for offsetting the cost of CO_2 capture and storage by producing large quantities of valuable methane and geothermal energy is very significant.

  One-dimensional simulations demonstrate that the injected CO_2 removes all of the dissolved methane and a leading methane-rich bank forms in front of the injected CO_2. Moreover, 3-D simulations indicate that the methane bank forms in 3-D models as well. However, it is impossible to produce the entire methane bank before CO_2 breakthrough since the methane bank is spread out in 3-D space.

  Two different strategies have been introduced for injection of CO_2 and production of energy. The first strategy is to inject supercritical CO_2 and to produce methane-saturated brine. The second strategy is to inject CO_2-saturated brine. In the second

strategy, methane saturated brine is produced and CO_2 is dissolved into or co-injected with produced brine.

The strategy of injection of supercritical CO_2 is capable of storing about 8 to 10 times more CO_2 compared to strategy of injection of CO_2-saturated brine. On the other hand, about 1.5 to 2 times more energy can be produced by injecting CO_2-saturated brine. Injecting dissolved CO_2 produces a greater cost offset for the capture and storage than injecting supercritical CO_2 as well as higher energy recovery.

The strategy of injecting CO_2-saturated brine is much less vulnerable to leakage because the injected CO_2 remains dissolved for long term, while a huge CO_2 plume would be formed at the top of the aquifer by injecting supercritical CO_2. The large mobile gas phase is prone to escape from pathways to shallow formations.

The strategy of injection of CO_2-saturated brine is capable of disposing the produced brine into the same aquifer, while the produced brine in the strategy of injection of supercritical CO_2 should be disposed elsewhere. Disposing in another formation is costly and may trigger environmental issues.

When CO_2-saturated brine is injected, the amount of produced energy is about 8.27 million BTU (2,423 kWh) per ton of stored CO_2. When supercritical CO_2 is injected, the amount of produced energy is about 0.46 million BTU (133 kWh) per ton of stored CO_2.

There is a compromise between energy offset and the amount of stored CO_2 by increasing the CO_2 concentration in the injected fluid from CO_2-saturated brine to supercritical CO_2. Adding the other costs and incentives to the objective functions varies the optimum CO_2 concentration between the two limiting cases.

- Geopressured-geothermal aquifers contain vast amounts of dissolved methane and geothermal energy. A rough estimation indicates that the amount of produced energy exceeds the energy needed for capture and storage. It is proposed that the geothermal energy can be used in the capture process by amine scrubbing and the produced methane can be used for pressurization of CO_2 and brine up to the wellhead pressure. In shallower depths, where temperature of brine is not high enough to be used for chemical absorption, pressure driven separation processes can be used. The produced methane is used in compressors or vacuum pumps to generate the pressure difference for membrane process.

  A review of energy analysis of four possible approaches of combined capture, storage, and production indicates that the energy revenue from all approaches offset all the energy cost of CO_2 capture and storage. The net energy gain from geopressured-geothermal aquifers is higher than from hydrostatically-pressured aquifers. The net energy gain is about 288 kWh per ton of stored CO_2 for capture by amine scrubbing and about 228 kWh by membrane separation. Production from hydrostatically pressured aquifers leads to about zero energy gain for capture by amine scrubbing and about 48 kWh per ton of stored CO_2 by membrane separation. Storage and production from geopressured-geothermal aquifers shows much better energy balance while the operating and capital cost of the process is higher for these aquifers.

  Extraction of brine from aquifers mitigates the concerns of pressure buildup, CO_2 leakage, and brine displacement. This also lowers the monitoring cost.

  Separating CO_2 from flue gas by membranes is very costly. A lower enrichment of CO_2 costs less for the membrane separation process, but then requires more energy cost for pressurization of injected gas and brine into the aquifer.

Preliminary estimates indicate that including the generated power from extracted methane and heat partially offset the energy cost of pressurization. Also, the capital cost of storage, including the compressors and pumps, number of wells and required pore volume, decreases by increasing the purity of CO_2. However, most of the decrease occurs from 13 percent to 40 percent.

Overall, achieving the CO_2 purity of more than 95% increases the energy and capital cost of the capture. On the other hand, pressurizing and injecting the gas with higher impurity decreases the energy production and increases the energy and capital cost of pressurization and injection. The minimum total cost might occur at CO_2 percentages much lower than 95%. Optimization of total cost requires careful inclusion of energy and capital cost of membrane separation and also well cost and surface facilities.

Until now, the majority of the studies on CCS technology have been focused on two aspects: (1) the capture studies which are mainly about achieving the purer CO_2 with lower cost (2) and the storage studies which are about injecting more CO_2 with less energy consumption. However, optimization of the whole technology demands an integrated study of capture, storage and production from target aquifers.

Additional conclusions can be found at the end of each chapter of this dissertation.

7.3 RECOMMENDATIONS FOR FUTURE WORK

Some unaddressed issues in this study that might be topics for further research are presented in this chapter.

- A comprehensive uncertainty analysis was performed on formation parameters and design variables affecting the production of energy and storage of CO_2. However, there still remain several other parameters and factors to be considered for further investigation. Experimental design and response surface methods may be utilized to consider several parameters at same time.
- The majority of the reservoir models in this study were homogeneous. The results of simulations on heterogeneous cases reveal that the heterogeneity can have a considerable effect on CO_2 breakthrough. Therefore, it would be beneficial to generate several geological models to study the effect of different heterogeneity types on storage and production.
- All the reservoir models used for simulation were synthetic based on the available data from deep saline aquifers of Gulf Coast. More realistic field scale models can be generated from the data of specific studied aquifers to take into account the effect of geological elements such as barriers, faults, anticlines, channels, and surrounding aquifers. Every geological structure requires its own development scenario owing to the fact that the well placement cannot be symmetric anymore.
- In this study, CO_2 and CH_4 were the gas components included in the injected and produced streams. Most of the produced streams from power plants and other emission sources contain contaminants such as N_2, O_2, and H_2S. The purity of the CO_2 stream obtained from separation dominates the economics of the process. Allowing some percentages of impurities might significantly reduce the capture cost. An optimization study is needed to find out what type of impurities might be

tolerated to improve the economics without huge compromise in the amount of stored CO_2. On the other hand, methane is not the only component produced along with brine. Analysis of the fluids produced from the geopressured wells discloses the presence of other light hydrocarbons as well as contaminants such as CO_2 and H_2S. Another optimization is required to study the impact of the impurities and produced particles on methane revenue and operating costs.

- In this study, estimation of energy cost for CO_2 capture methods were collected from recent studies on design of capture by amine scrubbing and membrane separation. A detailed design seems to be necessary to integrate the CO_2 capture, storage, energy production and utilization of the produced energy for the consumer units.
- The criteria used to compare the strategies in this study were the energy balance. The overall economics of the process vastly depends on capital and operating costs regarding capture units, wells, turbines, pumps, heat exchangers, and etc. A comprehensive economic analysis is required to include all the cost elements in order to have a better understanding about the feasibility of the proposed ideas.
- The geopressured-geothermal aquifers of the Gulf Coast are the best well-established aquifers containing energy sources. Thus far, studies about the energy sources in shallower hydrostatic aquifers are very limited. The capital and operating costs in shallower aquifers are much lower compared to those in deep geopressured aquifers. Some of the prospective opportunities for storage and production are the shallower geothermal aquifers. These aquifers are capable of providing vast amount of geothermal energy. It is justified to locate and document these aquifers for further examination of the proposed ideas.

Appendix A: Sensitivity Analysis

Parameter space sampling is the most important step in Sensitivity Analysis and Uncertainty Assessment. The outcome of parameter space sampling is a Design for laying out a detailed simulation plan in advance of doing simulations. A well selected design maximizes the amount of "information" that can be obtained for a given amount of simulation effort.

A.1 ONE-PARAMETER-AT-A-TIME METHOD

In this method, one of the parameters is varied over the range of the samples and all other parameters are fixed at a base case condition. This procedure is performed for all the involved parameters. In this study, the base case model was introduced in section 4.3. The strategy of brine reinjection for pressure maintenance is selected for base case model. It is assumed that the maximum brine production rate is 25,000 STB/Day and the wellhead pressure of the injector is limited to 4,500 psi. Cumulative produced water and cumulative produced gas are chosen as objective functions. Simulations are performed for a quarter of the five-spot pattern. Thus, the maximum rate is set to 6,250 STB/Day. The job patterns and the results of objective functions are presented in Tables A.1 and A.2. Figures A.1 through A.4 show some of the observers throughout the 20 years for all job patterns.

Table A.1: Job patterns for One-Parameter-at-a-Time sampling method.

Job ID	Size (mi^2)	Thickness (ft)	Permeability (md)	Reinjection Ratio (%)	Skin	Tubing ID (in)
1	1	400	20	100	0	6.04
2	4	400	20	100	0	6.04
3	9	400	20	100	0	6.04
4	16	400	20	100	0	6.04
5	25	400	20	100	0	6.04
6	4	180	20	100	0	6.04
7	4	300	20	100	0	6.04
8	4	400	20	100	0	6.04
9	4	500	20	100	0	6.04
10	4	600	20	100	0	6.04
11	4	400	2	100	0	6.04
12	4	400	10	100	0	6.04
13	4	400	20	100	0	6.04
14	4	400	50	100	0	6.04
15	4	400	100	100	0	6.04
16	4	400	20	0	0	6.04
17	4	400	20	25	0	6.04
18	4	400	20	50	0	6.04
19	4	400	20	75	0	6.04
20	4	400	20	100	0	6.04
21	4	400	20	100	-4	6.04
22	4	400	20	100	-2	6.04
23	4	400	20	100	0	6.04
24	4	400	20	100	10	6.04
25	4	400	20	100	20	6.04
26	4	400	20	100	0	2.99
27	4	400	20	100	0	3.83
28	4	400	20	100	0	4.78
29	4	400	20	100	0	6.04
30	4	400	20	100	0	7.20

Table A.2: Results of objective functions and recovery factor observers for One-Parameter-at-a-Time sampling method.

Job ID	Cumulative Produced Brine (STB)	Cumulative Produced Gas (SCF)	Brine Recovery (%)	Gas Recovery (%)
0	4.53E+07	1.35E+09	11.3	7.9
1	4.47E+07	1.31E+09	44.5	29.4
2	4.53E+07	1.35E+09	11.3	7.9
3	4.57E+07	1.40E+09	5.1	3.8
4	4.57E+07	1.44E+09	2.8	2.4
5	4.57E+07	1.49E+09	1.8	1.7
6	3.33E+07	1.01E+09	18.4	12.9
7	4.51E+07	1.36E+09	15.0	10.5
8	4.53E+07	1.35E+09	11.3	7.9
9	4.54E+07	1.35E+09	9.1	6.4
10	4.56E+07	1.36E+09	7.6	5.4
11	1.13E+07	3.54E+08	2.8	2.3
12	3.76E+07	1.15E+09	9.4	6.8
13	4.53E+07	1.35E+09	11.3	7.9
14	4.53E+07	1.31E+09	11.3	7.7
15	4.54E+07	1.30E+09	11.3	7.7
16	1.32E+07	4.07E+08	3.3	2.8
17	2.13E+07	6.28E+08	5.3	4.0
18	2.94E+07	8.58E+08	7.3	5.2
19	3.73E+07	1.10E+09	9.3	6.5
20	4.53E+07	1.35E+09	11.3	7.9
21	4.53E+07	1.31E+09	11.3	7.7
22	4.53E+07	1.33E+09	11.3	7.8
23	4.53E+07	1.35E+09	11.3	7.9
24	4.52E+07	1.45E+09	11.3	8.4
25	3.81E+07	1.26E+09	9.5	7.4
26	2.40E+07	7.79E+08	6.0	4.7
27	3.68E+07	1.16E+09	9.2	6.9
28	4.52E+07	1.39E+09	11.3	8.1
29	4.53E+07	1.35E+09	11.3	7.9
30	4.52E+07	1.33E+09	11.3	7.8

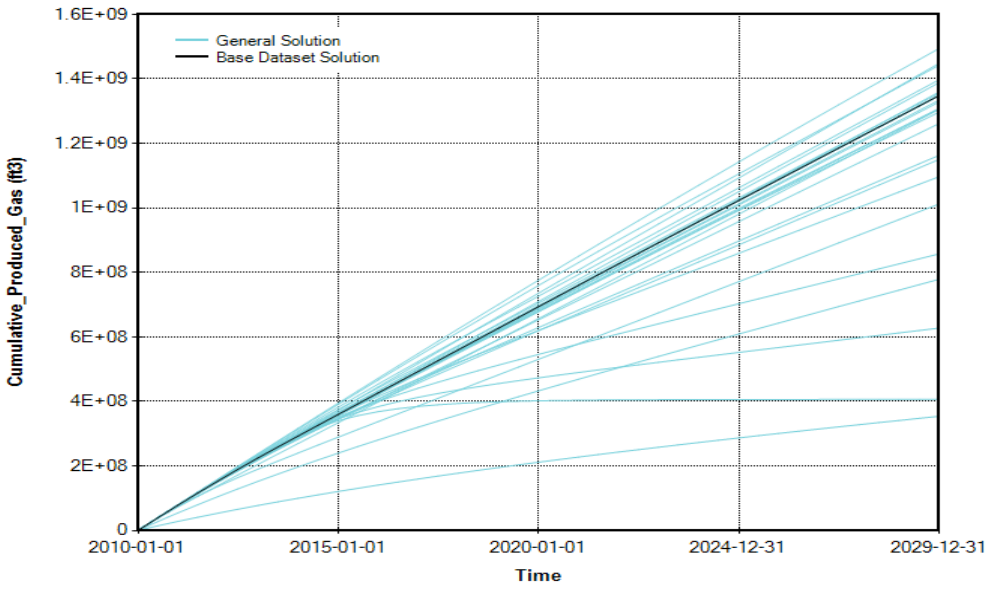

Figure A.1: Cumulative gas production throughout 20 years for all 30 samples.

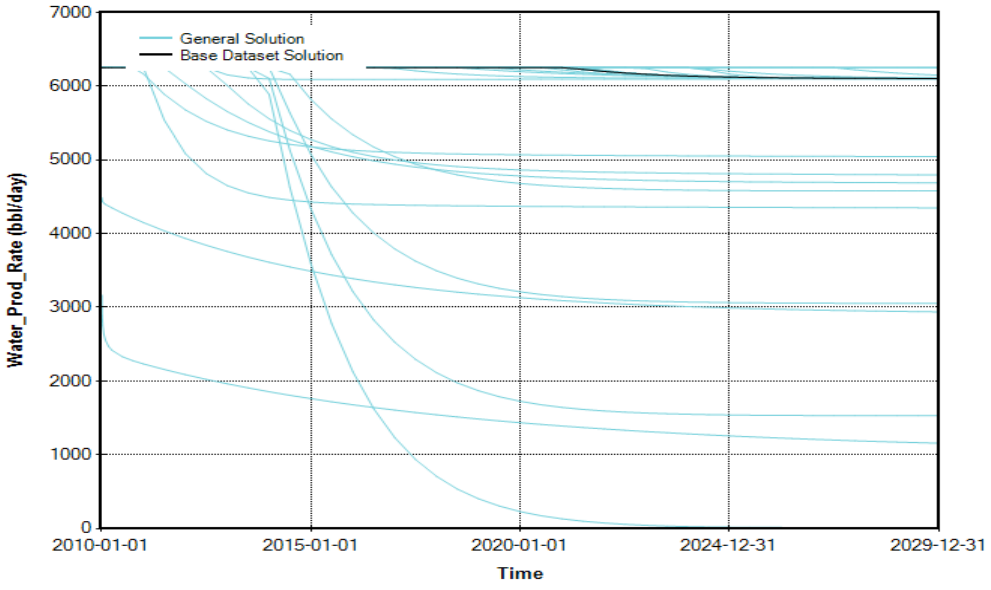

Figure A.2: Water production rate throughout 20 years for all 30 samples.

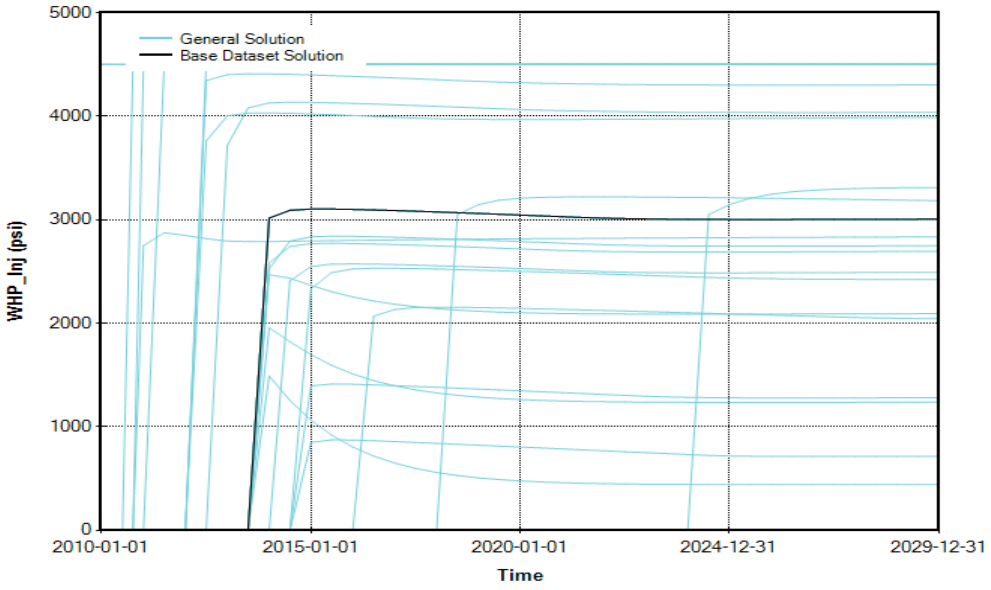

Figure A.3: Wellhead pressure of injector throughout 20 years for all 30 samples.

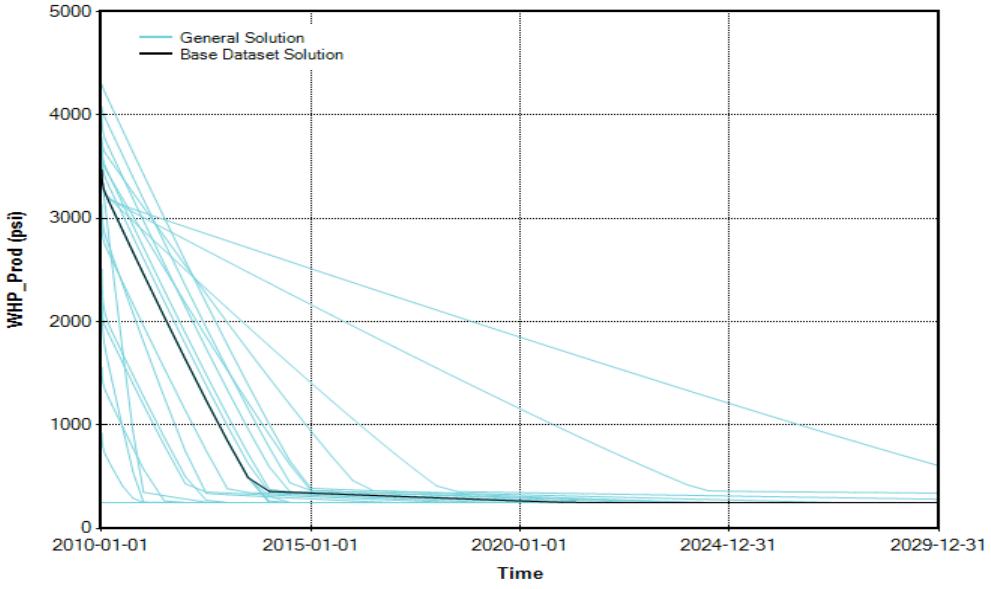

Figure A.4: Wellhead pressure of producer throughout 20 years for all 30 samples.

A.2 LATIN HYPERCUBE METHOD

Latin Hypercube is a state-of-the-art sampling method. Using Latin Hypercube, 120 job patterns are selected for a specific design. The job patterns and the results of objective functions are presented in Tables A.3 and A.4.

Table A.3: Properties of 120 job patterns for Latin Hypercube sampling method.

Job ID	Size (mi^2)	Thickness (ft)	Permeability (md)	Reinjection Ratio (%)	Skin	Tubing ID (in)
1	9	400	50	0	10	4.78
2	9	400	50	100	10	6.04
3	1	300	100	50	10	4.78
4	4	300	10	100	0	4.78
5	4	600	50	100	0	6.04
6	9	600	20	0	0	4.78
7	1	400	100	100	0	7.20
8	9	600	50	0	-4	4.78
9	9	300	100	0	-4	7.20
10	4	600	100	100	-4	6.04
11	4	300	10	0	10	7.20
12	9	300	10	50	-4	4.78
13	4	300	10	0	-4	7.20
14	9	600	20	50	-4	7.20
15	4	300	20	50	10	4.78
16	4	400	20	0	0	4.78
17	1	400	100	100	0	4.78
18	9	400	50	100	-4	7.20
19	1	400	100	50	0	7.20
20	1	600	20	100	0	4.78
21	4	600	20	50	-4	4.78
22	4	300	100	100	10	7.20
23	4	600	20	100	10	4.78
24	4	300	10	100	10	7.20
25	4	600	10	50	-4	4.78
26	9	600	10	100	-4	6.04

Job ID	Size (mi^2)	Thickness (ft)	Permeability (md)	Reinjection Ratio (%)	Skin	Tubing ID (in)
27	9	300	20	50	-4	6.04
28	1	600	10	0	0	4.78
29	1	400	100	50	10	6.04
30	9	600	50	0	10	7.20
31	4	600	50	0	10	4.78
32	9	400	10	100	-4	6.04
33	4	600	100	0	0	7.20
34	4	400	10	100	10	7.20
35	1	400	20	50	0	7.20
36	1	300	10	50	0	6.04
37	1	600	10	100	-4	6.04
38	4	400	100	100	0	4.78
39	1	300	20	100	-4	7.20
40	9	300	50	50	0	6.04
41	9	600	100	0	-4	4.78
42	1	600	20	50	10	4.78
43	1	300	20	0	0	4.78
44	1	300	20	0	0	7.20
45	4	400	20	100	10	7.20
46	9	400	100	50	-4	4.78
47	4	300	10	100	0	6.04
48	4	300	20	100	-4	7.20
49	4	400	20	50	-4	4.78
50	9	600	50	100	0	7.20
51	4	300	50	50	10	4.78
52	9	600	20	100	-4	6.04
53	1	300	50	0	10	7.20
54	4	600	20	100	0	7.20
55	1	300	20	0	10	4.78
56	4	600	10	100	0	6.04
57	4	300	50	50	-4	6.04
58	9	400	50	100	0	7.20
59	9	600	20	0	-4	6.04
60	9	300	100	50	-4	4.78
61	1	600	50	50	-4	7.20

Job ID	Size (mi^2)	Thickness (ft)	Permeability (md)	Reinjection Ratio (%)	Skin	Tubing ID (in)
62	1	600	10	0	-4	6.04
63	4	400	100	0	-4	6.04
64	1	400	50	100	-4	4.78
65	4	600	10	0	0	4.78
66	4	400	20	50	0	4.78
67	9	600	100	0	0	6.04
68	1	400	20	0	-4	6.04
69	9	300	20	0	10	6.04
70	9	300	50	100	10	7.20
71	9	400	10	100	-4	7.20
72	1	600	50	0	-4	7.20
73	4	600	10	0	10	6.04
74	9	600	100	100	-4	4.78
75	9	300	10	50	10	6.04
76	1	300	50	50	10	6.04
77	9	400	10	100	0	6.04
78	9	600	10	50	10	6.04
79	1	400	100	0	0	7.20
80	1	400	50	0	-4	7.20
81	9	600	10	100	0	7.20
82	1	400	10	0	0	4.78
83	1	300	100	50	-4	7.20
84	1	400	10	100	0	6.04
85	1	600	50	50	0	6.04
86	1	600	50	0	10	6.04
87	9	400	100	100	10	4.78
88	1	400	100	0	0	6.04
89	1	600	100	0	10	6.04
90	9	300	100	100	10	6.04
91	9	300	50	0	-4	7.20
92	1	600	10	50	0	6.04
93	9	300	10	0	10	7.20
94	4	300	100	100	-4	4.78
95	9	600	100	0	10	6.04
96	4	300	20	0	10	4.78

Job ID	Size (mi^2)	Thickness (ft)	Permeability (md)	Reinjection Ratio (%)	Skin	Tubing ID (in)
97	1	400	100	100	10	4.78
98	4	400	50	50	10	6.04
99	4	600	50	50	0	4.78
100	9	300	100	50	0	6.04
101	4	400	20	50	-4	7.20
102	4	600	50	100	10	7.20
103	1	300	50	50	-4	4.78
104	4	400	50	50	10	7.20
105	4	300	20	0	0	6.04
106	4	300	100	50	10	4.78
107	9	600	20	0	10	7.20
108	4	400	50	0	10	6.04
109	9	300	50	0	-4	6.04
110	1	400	10	0	-4	6.04
111	1	400	100	100	10	7.20
112	1	400	50	50	0	7.20
113	1	400	100	50	-4	6.04
114	1	400	10	100	0	4.78
115	4	600	20	50	0	7.20
116	9	300	20	50	-4	7.20
117	1	300	10	100	0	4.78
118	9	300	10	50	0	4.78
119	9	400	20	50	10	4.78
120	4	400	100	50	10	7.20

Table A.4: Results of objective functions and recovery factor observers for Latin Hypercube sampling method.

Job ID	Cumulative Produced Brine (STB)	Cumulative Produced Gas (SCF)	Brine Recovery (%)	Gas Recovery (%)
1	2.91E+07	9.09E+08	3.2	2.8
2	4.57E+07	1.40E+09	5.1	3.9
3	2.37E+07	6.59E+08	31.4	19.8
4	2.77E+07	8.50E+08	9.2	6.7
5	4.57E+07	1.34E+09	7.6	5.4
6	3.96E+07	1.24E+09	2.9	2.6
7	4.47E+07	1.22E+09	44.5	27.1
8	4.20E+07	1.32E+09	3.1	2.7
9	2.25E+07	6.99E+08	3.3	2.9
10	4.57E+07	1.33E+09	7.6	5.4
11	9.49E+06	2.93E+08	3.2	2.7
12	3.38E+07	1.02E+09	5.0	3.8
13	1.00E+07	2.99E+08	3.3	2.8
14	4.46E+07	1.38E+09	3.3	2.8
15	2.74E+07	8.57E+08	9.1	6.8
16	1.32E+07	4.07E+08	3.3	2.8
17	4.47E+07	1.28E+09	44.5	28.8
18	4.57E+07	1.36E+09	5.1	3.8
19	2.39E+07	6.50E+08	23.8	14.7
20	4.47E+07	1.33E+09	29.7	20.2
21	3.33E+07	9.87E+08	5.5	4.1
22	4.52E+07	1.30E+09	15.0	10.0
23	4.55E+07	1.45E+09	7.6	5.7
24	2.10E+07	6.80E+08	7.0	5.4
25	3.31E+07	9.84E+08	5.5	4.1
26	4.57E+07	1.41E+09	3.4	2.7
27	3.43E+07	1.01E+09	5.1	3.8
28	4.92E+06	1.51E+08	3.3	2.8
29	2.40E+07	6.61E+08	23.9	15.0
30	4.18E+07	1.31E+09	3.1	2.7
31	1.96E+07	6.12E+08	3.3	2.8

Job ID	Cumulative Produced Brine (STB)	Cumulative Produced Gas (SCF)	Brine Recovery (%)	Gas Recovery (%)
32	4.39E+07	1.32E+09	4.9	3.6
33	1.97E+07	6.14E+08	3.3	2.8
34	2.78E+07	9.02E+08	6.9	5.3
35	2.40E+07	6.71E+08	23.9	15.2
36	2.35E+07	6.96E+08	31.3	21.1
37	4.47E+07	1.28E+09	29.7	19.2
38	4.53E+07	1.33E+09	11.3	7.9
39	4.47E+07	1.25E+09	59.3	37.3
40	3.44E+07	1.02E+09	5.1	3.9
41	4.24E+07	1.33E+09	3.1	2.7
42	2.50E+07	7.30E+08	16.6	11.2
43	2.50E+06	7.65E+07	3.3	2.8
44	2.50E+06	7.63E+07	3.3	2.8
45	4.52E+07	1.44E+09	11.3	8.4
46	3.90E+07	1.18E+09	4.3	3.4
47	2.98E+07	9.11E+08	9.9	7.1
48	4.51E+07	1.29E+09	15.0	9.9
49	2.97E+07	8.63E+08	7.4	5.3
50	4.57E+07	1.42E+09	3.4	2.8
51	2.79E+07	8.22E+08	9.2	6.5
52	4.57E+07	1.41E+09	3.4	2.8
53	2.50E+06	7.74E+07	3.3	2.9
54	4.56E+07	1.35E+09	7.6	5.4
55	2.50E+06	7.69E+07	3.3	2.8
56	4.55E+07	1.39E+09	7.6	5.5
57	2.77E+07	7.83E+08	9.2	6.3
58	4.57E+07	1.37E+09	5.1	3.9
59	4.22E+07	1.31E+09	3.1	2.7
60	3.50E+07	1.04E+09	5.2	4.0
61	2.48E+07	6.81E+08	16.5	10.5
62	4.92E+06	1.50E+08	3.3	2.8
63	1.32E+07	4.12E+08	3.3	2.9
64	4.47E+07	1.28E+09	44.5	28.8
65	1.95E+07	5.98E+08	3.2	2.8

Job ID	Cumulative Produced Brine (STB)	Cumulative Produced Gas (SCF)	Brine Recovery (%)	Gas Recovery (%)
66	2.96E+07	8.76E+08	7.4	5.3
67	4.34E+07	1.36E+09	3.2	2.8
68	3.31E+06	1.01E+08	3.3	2.8
69	2.06E+07	6.42E+08	3.0	2.6
70	4.57E+07	1.39E+09	6.7	5.0
71	4.50E+07	1.35E+09	5.0	3.7
72	4.92E+06	1.53E+08	3.3	2.8
73	1.86E+07	5.76E+08	3.1	2.7
74	4.57E+07	1.43E+09	3.4	2.8
75	2.20E+07	7.20E+08	3.2	2.6
76	2.36E+07	6.65E+08	31.3	20.0
77	3.99E+07	1.24E+09	4.4	3.4
78	3.88E+07	1.27E+09	2.9	2.4
79	3.31E+06	1.03E+08	3.3	2.9
80	3.31E+06	1.03E+08	3.3	2.8
81	4.57E+07	1.43E+09	3.4	2.7
82	3.31E+06	1.01E+08	3.3	2.8
83	2.36E+07	6.35E+08	31.3	19.0
84	3.77E+07	1.14E+09	37.5	26.0
85	2.49E+07	6.88E+08	16.5	10.6
86	4.92E+06	1.53E+08	3.3	2.8
87	4.57E+07	1.41E+09	5.1	3.9
88	3.31E+06	1.03E+08	3.3	2.9
89	4.92E+06	1.54E+08	3.3	2.8
90	4.57E+07	1.37E+09	6.7	5.0
91	2.25E+07	6.95E+08	3.3	2.9
92	2.48E+07	7.10E+08	16.5	10.9
93	1.66E+07	5.29E+08	2.5	2.2
94	4.52E+07	1.31E+09	15.0	10.2
95	4.27E+07	1.34E+09	3.2	2.8
96	9.95E+06	3.06E+08	3.3	2.8
97	4.47E+07	1.31E+09	44.5	29.5
98	2.94E+07	8.60E+08	7.3	5.3
99	3.34E+07	9.92E+08	5.5	4.2

Job ID	Cumulative Produced Brine (STB)	Cumulative Produced Gas (SCF)	Brine Recovery (%)	Gas Recovery (%)
100	3.45E+07	1.02E+09	5.1	3.9
101	2.93E+07	8.40E+08	7.3	5.1
102	4.57E+07	1.35E+09	7.6	5.5
103	2.37E+07	6.50E+08	31.4	19.5
104	2.93E+07	8.56E+08	7.3	5.2
105	9.99E+06	3.05E+08	3.3	2.8
106	2.79E+07	8.08E+08	9.3	6.4
107	3.81E+07	1.20E+09	2.8	2.5
108	1.32E+07	4.11E+08	3.3	2.8
109	2.25E+07	6.95E+08	3.3	2.9
110	3.31E+06	9.99E+07	3.3	2.8
111	4.47E+07	1.24E+09	44.5	27.8
112	2.40E+07	6.57E+08	23.9	14.9
113	2.40E+07	6.52E+08	23.9	14.7
114	3.33E+07	1.02E+09	33.2	23.2
115	3.27E+07	9.67E+08	5.4	4.1
116	3.42E+07	1.01E+09	5.0	3.8
117	2.68E+07	8.15E+08	35.5	24.7
118	3.04E+07	9.50E+08	4.5	3.5
119	3.64E+07	1.16E+09	4.0	3.2
120	2.93E+07	8.46E+08	7.3	5.2

Appendix B: GEM Base Case Input File

Following is the GEM input file for simulating the injection of CO_2-saturated brine and production of methane and brine described in section 5.3.4. Single stars (*) are followed by keywords and double stars (**) are followed by comments.

```
**************************************************************
RESULTS SIMULATOR GEM 201100
FILENAMES OUTPUT SRFOUT RESTARTOUT INDEX-OUT MAINRESULTSOUT
*TITLE1 'Methane and Geothermal Energy Extraction'
*TITLE2 'CO2 Injection in Methane-Saturated Brine'
*TITLE3 '3D Horizontal Well Modeling'
*CASEID 'CASE 1'
*INUNIT *FIELD

*WSRF   *GRID  *TIME
*WSRF   *WELL  *TIME
*WPRN   *GRID  *TIME
*WPRN   *WELL  *TIME
*WPRN   *ITER  *NONE
*OUTPRN *GRID  *NONE
*OUTPRN *WELL  *RESERVOIR
*OUTSRF *WELL  *ZWEL 'C1'  'PROD1'
          *XWEL 'C1'  'PROD1'
          *YWEL 'C1'  'PROD1'
          *ZWEL 'CO2' 'PROD1'
          *XWEL 'CO2' 'PROD1'
          *YWEL 'CO2' 'PROD1'
          *ZWEL 'H2O' 'PROD1'
          *XWEL 'H2O' 'PROD1'
```

```
          *YWEL 'H2O' 'PROD1'

*OUTSRF *GRID  *PRES *SO *SG *SW *RHOO *RHOG *SIG *VISO *TEMP
          *Z 'C1'  *X 'C1'  *Y 'C1'
          *Z 'CO2' *X 'CO2' *Y 'CO2'
          *Z 'H2O' *X 'H2O' *Y 'H2O'

**----------------------------------------------------RESERVOIR DATA------
*GRID  CART  80  80  30
*KDIR DOWN
*DIP  0  0
*DI  CON  66
*DJ  CON  66
*DK  CON  10
*DEPTH  TOP 1 1 1  15000.00
**$ Property: NULL Blocks  Max: 1  Min: 1
**$  0 = null block, 1 = active block
*NULL CON          1
*POR  CON  0.2463
*PERMI  CON  100
*PERMJ  EQUALSI
*PERMK  EQUALSI * 0.1
**$ Property: Pinchout Array  Max: 1  Min: 1
**$  0 = pinched block, 1 = active block
*PINCHOUTARRAY CON          1
*CPOR  4.0E-06
*PRPOR  3550.0
*CROCKTYPE 1
**ROCK HEAT CAPACITY [BTU/(LB F)]
*CP-ROCK 0.25
**THERMAL CONDUCTIVITY OF ROCK AND FLUIDS [BTU/(HR LB F)]
*THCONR0 2.0
*HEAT-LOSS BOTTOM-TOP
*HLPROP 165.0 0.25 2.0
** new GEM requires END-GRID line
*END-GRID
**----------------------------------------------------FLUID COMPONENT DATA
*MODEL    PR
*NC     3   3
*COMPNAME   'CO2'   'C1'   'H2O'
*VISCOR    HZYT
```

```
*MIXVC     1.0
*VISCOEFF   0.1023   0.023364   0.058533   -0.040758   0.0093324
*EOSSET 1
*HCFLAG     0      1      0
*PCRIT          72.8          45.4          217.6
*TCRIT          304.2          190.6          647.3
*AC             .225          .008          .344
*MW             44.01         16.043        18.7300
*VSHIFT      -.075904        -.17121         .22001
*VCRIT          .094          .099          .056
*VISVC        .095190        0.092283        0.047835
*OMEGA      .457235529      .457235529      .457235529
*OMEGB  7.77960739E-02   7.77960739E-02   7.77960739E-02
*SG             .818          .3             1
*TB          -109.21        -258.61           212
*PCHOR            78            77            52
*PVC3      1.2
*BIN
 .103
 .0326    .0277
*PHASEID    DEN
*ENTHCOEF
 4.77805E+00 1.14433E-01  1.01132E-04 -2.64940E-08  3.47060E-12 -1.31400E-16
-5.58114E+00 5.64834E-01 -2.82973E-04  4.17399E-07 -1.52558E-10  1.95886E-14
-2.46342E+00 4.57392E-01 -5.25120E-05  6.45490E-08 -2.02759E-11  2.36310E-15
*TRES      302
*EOSSET 2
*VSHIFT          0.0           0.0         0.16025
*VISVC          .094          0.099        0.056213
*BIN
 0.103
 0     0
*THERMAL ON
**----------------------------------------------------ROCK FLUID----------
*ROCKFLUID
*RPT
*SWT      ** water-oil relative permeability not used in simulation
    0.000000    0.0000000    1.0000000    0.000000000
    0.050375    0.0008203    0.8400835    0.000000000
    0.100750    0.0032813    0.6973033    0.000000000
    0.151125    0.0073828    0.5708514    0.000000000
```

0.201500	0.0131250	0.4599021	0.000000000
0.251875	0.0202078	0.3636104	0.000000000
0.302250	0.0295313	0.2811098	0.000000000
0.352625	0.0401953	0.2115100	0.000000000
0.403000	0.0525000	0.1538931	0.000000000
0.453375	0.0664453	0.1073101	0.000000000
0.503750	0.0820313	0.0707757	0.000000000
0.554125	0.0992578	0.0432609	0.000000000
0.604500	0.1181250	0.0236831	0.000000000
0.654875	0.1386328	0.0108919	0.000000000
0.705250	0.1607813	0.0036447	0.000000000
0.755625	0.1845703	0.0005609	0.000000000
0.806000	0.2100000	0.0000000	0.000000000

*SLT ** liquid-gas relative permeability used in simulation

0.2000000	0.7000000	0.0000000	3.5570606
0.2500000	0.5956981	0.0002441	2.1213203
0.3000000	0.5013236	0.0019531	1.9452593
0.3500000	0.4165398	0.0065918	1.8491243
0.4000000	0.3409975	0.0156250	1.7838107
0.4500000	0.2743341	0.0305176	1.7347425
0.5000000	0.2161713	0.0527344	1.6956544
0.5500000	0.1661133	0.0837402	1.6632939
0.6000000	0.1237437	0.1250000	1.6357616
0.6500000	0.0886223	0.1779785	1.6118549
0.7000000	0.0602804	0.2441406	1.5907658
0.7500000	0.0382141	0.3249512	1.5719263
0.8000000	0.0218750	0.4218750	1.5549220
0.8500000	0.0106562	0.5363770	1.5394420
0.9000000	0.0038670	0.6699219	1.5252473
0.9500000	0.0006836	0.8239746	1.5121499
1.0000000	0.0000000	1.0000000	1.5000000

*HYSKRG 0.3085 **maximum residual gas saturation

**ROCK DENSITY [LB/CUFT]
*ROCKDEN CON 165.4340404
**----------INITIAL CONDITION---
*INITIAL
*USER_INPUT
*SW CON 0.0

```
*PRES KVAR 11000 11004 11009 11013 11018 11022 11027 11032 11036 11041
           11045 11050 11055 11059 11064 11068 11073 11077 11082 11087
           11091 11096 11100 11105 11110 11114 11119 11123 11128 11133
*ZGLOBALC 'CO2' CON 0.00000
*ZGLOBALC 'C1'   CON 0.0057300
*ZGLOBALC 'H2O' CON 0.9942700
**----------------------------------------------NUMERICAL-----------
*NUMERICAL
*DTMIN    1.0E-6
*DTMAX   100
*NORM     PRESS  2000
*NORM     SATUR  0.20
*NORM     GMOLAR 0.20
**----------------------------------------------WELL DATA-----------
*RUN
*DATE 2010 1 1
**
*AIMWELL

************INJECTORS*********************
WELL            'INJ1'
INJECTOR        'INJ1'
*IWELLBORE MODEL
  ** wdepth  wlen   rough   whtemp  bhtemp  wrad
    15290  15290  0.0001   200    200    0.25
*INCOMP       SOLVENT        0.025    0.0    0.975
*OPERATE         MAX   BHP    12000   CONT
**$        rad  geofac  wfrac  skin
*GEOMETRY  I  0.25  0.53   0.5   0.
*PERF  GEO  'INJ1'
**$ UBA       ff  Status  Connection
80  80  30    1.0   open
79  80  30    1.0   open
78  80  30    1.0   open
77  80  30    1.0   open
76  80  30    1.0   open
75  80  30    1.0   open
74  80  30    1.0   open
73  80  30    1.0   open
72  80  30    1.0   open
71  80  30    1.0   open
```

70 80 30 1.0 open
69 80 30 1.0 open
68 80 30 1.0 open
67 80 30 1.0 open
66 80 30 1.0 open
65 80 30 1.0 open
64 80 30 1.0 open
63 80 30 1.0 open
62 80 30 1.0 open
61 80 30 1.0 open
60 80 30 1.0 open
59 80 30 1.0 open
58 80 30 1.0 open
57 80 30 1.0 open
56 80 30 1.0 open
55 80 30 1.0 open
54 80 30 1.0 open
53 80 30 1.0 open
52 80 30 1.0 open
51 80 30 1.0 open
50 80 30 1.0 open
49 80 30 1.0 open
48 80 30 1.0 open
47 80 30 1.0 open
46 80 30 1.0 open
45 80 30 1.0 open
44 80 30 1.0 open
43 80 30 1.0 open
42 80 30 1.0 open
41 80 30 1.0 open
40 80 30 1.0 open
39 80 30 1.0 open
38 80 30 1.0 open
37 80 30 1.0 open
36 80 30 1.0 open
35 80 30 1.0 open
34 80 30 1.0 open
33 80 30 1.0 open
32 80 30 1.0 open
31 80 30 1.0 open
30 80 30 1.0 open

```
29  80  30    1.0   open
28  80  30    1.0   open
27  80  30    1.0   open
26  80  30    1.0   open
25  80  30    1.0   open
24  80  30    1.0   open
23  80  30    1.0   open
22  80  30    1.0   open
21  80  30    1.0   open
20  80  30    1.0   open
19  80  30    1.0   open
18  80  30    1.0   open
17  80  30    1.0   open
16  80  30    1.0   open
15  80  30    1.0   open
14  80  30    1.0   open
13  80  30    1.0   open
12  80  30    1.0   open
11  80  30    1.0   open
10  80  30    1.0   open
 9  80  30    1.0   open
 8  80  30    1.0   open
 7  80  30    1.0   open
 6  80  30    1.0   open
 5  80  30    1.0   open
 4  80  30    1.0   open
 3  80  30    1.0   open
 2  80  30    1.0   open
 1  80  30    1.0   open

**********PRODUCERS**********
*WELL  'PROD1'
*PRODUCER 'PROD1'
*PWELLBORE *MODEL
   ** wdepth  wlen   rough   whtemp  bhtemp  wrad
      15000  15000  0.0001    280    302    0.25
*OPERATE        MIN    BHP     11000    CONT
*MONITOR        MAX    M1        0.1    STOP
**$         rad  geofac  wfrac  skin
GEOMETRY  I  0.25  0.53    0.5     0.
PERF  GEO  'PROD1'
```

```
**$ UBA     ff  Status  Connection
1:80  1  1  1.0  open

*HEADITER 'INJ1' ITERATIVE
*HEADITER 'PROD1' ITERATIVE

*OPEN 'INJ1'
*OPEN 'PROD1'
*DTMAX    0.05
*DATE 2010 1 2

*DTMAX    0.1
*DATE 2010 1 5
*DTMAX    0.2
*DATE 2010 1 10
*DTMAX    0.5
*DATE 2010 1 20
*DATE 2010 2 1
*DTMAX    1
*DATE 2010 3 1
*DTMAX    2
*DATE 2010 4 1
*DTMAX    5
*DATE 2010 7 1
*DATE 2011 1 1
*DTMAX    10
*DATE 2011 7 1
*DATE 2012 1 1
*DATE 2012 7 1
*DATE 2013 1 1
*DATE 2013 7 1
*DATE 2014 1 1
*DATE 2014 7 1
*DATE 2015 1 1
*DATE 2016 1 1
*DATE 2017 1 1
*DATE 2018 1 1
*DATE 2019 1 1
*DATE 2020 1 1
*DATE 2022 1 1
*DATE 2024 1 1
```

*DATE 2026 1 1
*DATE 2028 1 1
*DATE 2030 1 1
*DATE 2032 1 1
*DATE 2034 1 1
*DATE 2036 1 1
*DATE 2038 1 1
*DATE 2040 1 1
*DATE 2042 1 1
*DATE 2044 1 1
*DATE 2046 1 1
*DATE 2048 1 1
*DATE 2049 1 1
*DATE 2050 1 1
*STOP

References

Agarwal, R. K., & Li, Y. K. (1988, December). Implementation of a simplified wellbore model in a compositional simulator. *CMG Report 88.13.C*.

Alnes, H., Eiken, O., Nooner, S., Stenvold, T., & Zumberge, M. (2011). Results from Sleipner gravity monitoring: Updated density and temperature distribution of the CO_2 plume. *Energy Procedia, 4*, 5504-5511.

Arts, R., Chadwick, A., Eiken, O., Thibeau, S., & Nooner, S. (2008). Ten years' experience of monitoring CO_2 injection in the Utsira sand at Sleipner, offshore Norway. *First Break, 26*, 65-72.

Atwater, J. E., & Holtsnider, J. T. (1991). Airborne trace organic contaminant removal using thermally regenerable multi-media layered sorbents. *SAE Transactions Journal of Aerospace, 100*, 1726-1733.

Aziz, K., Govier, G. W., & Fogarasi, M. (1972). Pressure drop in wells producing oil and gas. *Journal of Canadian Petroleum Technology, 11*(3), 38-48.

Bachu, S., Gunter, W. D., & Perkins, E. H. (1994). Aquifer disposal of CO_2: Hydrodynamic and mineral trapping. *Energy Conversion and Management,, 35*(4), 269-279.

Bates, E. D., Mayton, R. D., Ntai, I., & Davis, J. H. (2002). CO_2 capture by a task-specific ionic liquid. *Journal of American Chemical Society,, 124*(6), 926-927.

Bebout, D. G., Loucks, R., & Gregory, A. R. (1983). *Frio sandstone reservoirs in the deep subsurface along the Texas Gulf Coast: Their potential for production of geopressured geothermal energy.* Bureau of Economic Geology, The University of Texas at Austin.

Bebout, D. G., Weise, B. R., Gregory, A. R., & Edwards, M. B. (1982). *Wilcox sandstone reservoirs in the deep subsurface along the Texas Gulf Coast: Their potential for production of geopressured geothermal energy.* Report of Investigations No. 117, Bureau of Economic Geology, The University of Texas at Austin.

Bennion, B., & Bachu, S. (2008). Drainage and imbibition relative permeability relations for supercritical CO_2/brine and H2S/brine systems in intergranular sandstone, carbonate, shale, and anhydrite rocks. *SPE Reservoir Evaluation and Engineering, 11*(3), 487-496.

Benson, S. M., Hepple, R., Apps, J., Tsang, C. F., & Lippmann, M. (2007). *Lessons learned from natural and industrial analogues for storage of CO_2 in deep*

geological formations. Report LBNL-51170, Lawrence Berkeley National Laboratory.

Birkholzer, J. T., Zhou, Q., & Tsang, C.-F. (2009). Large-scale impact of CO_2 storage in deep saline aquifers: A sensitivity study on pressure response in stratified systems. *International Journal of Greenhouse Gas Control, 3*(2), 181-194.

Bounaceur, R., Lape, N., Roizard, D., Vallieres, C., & Favre, E. (2006). Membrane processes for post-combustion carbon dioxide capture: A parametric study. *Energy, 31*(14), 2556-2570.

Brooks, R. H., & Corey, A. T. (1966). Propreties of porous media affecting fluid flow. *Journal of Irrigation and Drainage Engineering, 92*, 61-88.

Bryant, S. L. (2007). Geological CO_2 storage - Can the oil and gas industry help save the planet? *Journal of Petroleum Technology, 59*(9), 98-105.

Bryant, S. L. (2013, November). The one-step carbon solution. *American Scientific, 309*(5), 72-77.

Bryant, S. L., Lakshminarasimhan, S., & Pope, G. A. (2008). Buoyancy-dominated multiphase flow and its impact on geological sequestration of CO_2. *SPE Journal, 13*(4), 447-454.

Burton, M., & Bryant, S. L. (2009). Eliminating buoyant migration of sequestered CO_2 through surface dissolution: Implementation costs and technical challenges. *SPE Reservoir Engineering and Evaluation, 12*(3), 399-407.

Chakravarti, S., Gupta, A., & Hunek, B. (2001). Advanced technology for the capture of carbon dioxide from flue gas. *Proceedings on First National Conference on Carbon Sequestration.* Washington, DC.

CMG. (2011). GEM Technical Manual. Computer Modeling Group.

Deppe, G., Tam, S. S., Young, J. S., Anderson, G. K., Le, L., & Spencer, D. F. (2002). A high pressure carbon dioxide separation process in an IGCC plant. *Proceedings of the Future Energy Systems and Technology for CO_2 Abatement*, (pp. 97-106). Antwerp, Belgium.

Dickinson, G. (1953). Geological aspects of abnormal reservoir pressure in Gulf Coast Louisiana. *Bulletin AAPG*.

Dorfman, M., & Deller, R. W. (1976). Summary of future projections of geopressured geothermal energy. *Second Geopressured Geothermal Energy Conference,*. Austin, TX.

Dorfman, M., & Kehle, R. O. (1974). Potential geothermal resources of Texas. *Geological Circular, Bureau of Economic Geology, The University of texas at Austin*.

Duan, Z., & Mao, S. (2006). A thermodynamic model for calculating methane solubility, density and gas phase composition of methane-bearing aqueous fluids from 273 to 523 K and from 1 to 2000 bar. *Geochimica et Cosmochimica Acta, 70*, 3369–3386.

Duan, Z., & Sun, R. (2003). An improved model calculating CO_2 solubility in pure water and aqueous NaCl solutions from 273 to 533 K and from 0 to 2000 bar. *Chemical Geology, 193*, 257-271.

Ennis-King, J., & Paterson, L. (2002). Engineering aspects of geological sequestration of carbon dioxide. *SPE Asia Pacific Oil and Gas Conference and Exhibition.* Melbourne, Australia.

Ennis-King, J., & Paterson, L. (2005). Role of convective mixing in the long-term storage of carbon dioxide in deep saline formations. *SPE Journal, 10*(3), 349-356.

Ennis-King, J., Preston, I., & Paterson, L. (2005). Onset of convection in anisotropic porous media subject to a rapid change in boundary conditions. *Physics of Fluids, 17*.

Esposito, A., & Augustine, C. (2011). Geopressured geothermal resource and recoverable energy estimate for the Wilcox and Frio formations, Texas. *Geothermal Resource Council Transactions, 35*.

Esposito, A., & Augustine, C. (2012). Recoverable resource estimate of identified onshore geopressured geothermal energy in Texas and Louisiana. *AAPG Annual Convention and Exhibition.* Long Beach, CA.

Ewing, T. E. (1986). *Structural styles of the Wilcox and Frio growth-fault trends in Texas: Constraints on geopressured reservoirs.* Report of Investigations No. 154, Bureau of Economic Geology, The University of Texas at Austin.

Favre, E. (2007). Carbon dioxide recovery from post-combustion processes: Can gas permeation membranes compete with absorption? *Journal of Membrane Science, 294*, 50-59.

Feron, P. H. (2002). Advanced separation processes for CO_2-capture from power stations . *Proceedings of the Conference on the Future Energy Systems and Technology for CO_2 Abatement*, (pp. 107-112). Antwerp, Belgium.

Flett, M., Gurton, R., & Taggart, I. (2004). The function of gas-water relative permeability hysteresis in the sequestration of carbon dioxide in saline formations. *SPE Asia Pacific Oil and Gas Conference and Exhibition.* Perth, Australia.

Freeman, S. A., Dugas, R., Van Wagener, D. H., Nguyen, T., & Rochelle, G. T. (2010). Carbon dioxide capture with concentrated, aqueous piperazine. *International Journal of Greenhouse Gas Control, 4*(2), 119-124.

Gale, J. (2004). Geological storage of CO_2: What do we know, where are the gaps and what more needs to be done. *Energy, 29*(9-10), 1329-1338.

Ganjdanesh, R., Bryant, S. L., Orbach, R. L., Pope, G. A., & Sepehrnoori, K. (2013a). Coupled carbon dioxide sequestration and energy production from geopressured/geothermal aquifers. *SPE Journal*, Available online.

Ganjdanesh, R., Bryant, S. L., Pope, G. A., & Sepehrnoori, K. (2013b). Making CCS pay for itself: Storage strategies in geopressured-geothermal aquifers. *Energy Procedia, 37*, 2495–2504.

Ganjdanesh, R., Bryant, S. L., Pope, G. A., Orbach, R. L., & Sepehrnoori, K. (2012). Coupled CO_2 sequestration and energy production from geopressured-geothermal aquifers. *SPE 151351, Proceedings of the First Carbon Management Technology Conference.* Orlando, FL.

Geer, E. C., & Cook, H. L. (1978). Enhanced gas recovery from geopressured aquifers. *SPE 7541, SPE Annual Fall Technical Conference.* Houston, TX.

Ghomian, Y. (2008). Reservoir simulation studies for coupled CO_2 sequestration and enhanced oil recovery. *PhD Dissertation*. The Unversity of Texas at Austin.

Ghomian, Y., Sepehrnoori, K., & Pope, G. A. (2008). Reservoir simulation of CO_2 sequestration pilot in Frio brine formation, US Gulf Coast. *Energy Journal, 33*.

Gregory, A. R., Dodge, M., Posey, J., & Morton, R. (1980). *Volume and accessibility of entrained (solution) methane in deep geopressured reservoirs-Tertiary formations of the Texas Gulf Coast.* Final Report, Bureau of Economic Geology, The University of Texas at Austin.

Griggs, J. (2005). A re-evaluation of geopressurized-geothermal aquifers as an energy source. *Workshop of Geothermal Reservoir Engineering, Stanford University.* Stanford, CA.

Gunter, W. D., Perkins, E. H., & McCann, T. J. (1993). Aquifer disposal of CO_2-rich gases: Reaction design for added capacity. *Energy Conversion and Management, 34*(9), 941-948.

Gunter, W. D., Wong, S., Cheel, D. B., & Sjostrom, G. (1998). Large CO_2 sinks: Their role in the mitigation of greenhouse gases from an international, national (Canadian) and provincial (Alberta) perspective. *Applied Energy, 61*, 209-227.

Hawkins, J. T., Benvegnu, A. J., Wingate, T. P., McKamie, J. D., Pickard, C. D., & Altum, J. T. (1996). SACROC unit CO_2 flood: Multidisciplinary team improves reservoir management and decreases operating costs. *SPE Reservoir Engineering, 11*(3), 141-148.

Herzog, H., Eliasson, B., & Karstad, O. (2000, February). Capturing greenhouse gases. *Scientific American*, 72-79.

Hesse, M. A., Tchelepi, H. A., & Orr, F. A. (2006). Scaling analysis of the migration of CO_2 in saline aquifers. *SPE Annual Technical Conference and Exhibition.* San Antonio, TX.

Hise, B. R. (1976). *Natural gas from geopressured zone: Chapter 3 of natural gas from unconventional geologic sources.* Washington, DC: National Academy of Sciences.

Ho, M. T., Allinson, G. W., & Wiley, D. E. (2008). Reducing the cost of CO_2 capture from flue gases using pressure swing adsorption. *Industrial & Engineering Chemistry Research, 47*(14), 4883-4890.

Holtz, H. M. (2002). Residual gas saturation to aquifer influx: A calculation method for 3-D computer reservoir model construction. *SPE Gas Technology Symposium*, *SPE 75502*. Calgary, Alberta, Canada.

Hosseini, S. A., Lashgari, H., Choi, J.-W., Nicot, J.-P., Lu, J., & Hovorka, S. D. (2013). Static and dynamic reservoir modeling for geological CO_2 sequestration at Cranfield, Mississippi, U.S.A. *International Journal of Greenhouse Gas Control, 18*, 449-462.

Hovorka, S. D., Benson, S. M., Doughty, C., Freifeld, B. M., Sakurai, S., Daley, T. M., et al. (2006). Measuring permanence of CO_2 storage in saline formations: The Frio experiment. *Environmental Geosciences, 13*, 105-121.

Hovorka, S. D., Meckel, T. A., & Trevino, R. H. (2013). Monitoring a large-volume injection at Cranfield, Mississippi–Project design and recommendations. *International Journal of Greenhouse Gas Control, 18*, 345-360.

IPCC. (2007). *Summary for policymakers, In climate change 2007: Mitigation of climate change. Contribution of working group III to the fourth assessment report of the intergovernmental panel on climate change, Edited by Metz, B., Davidson O. R., Bosch, P. R., Dave, R.,.* Cambridge University Press.

Isokrari, O. F. (1976). Natural gas production from geothermal geopressured aquifers. *SPE 6037, SPE Annual Fall Technical Conference.* New Orleans, LA.

Jain, L., & Bryant, S. L. (2011). Optimal design of injection/extraction wells for the surface dissolution CO_2 storage strategy. *Energy Procedia, 4*, 4299-4306.

Jessen, K., & Orr, F. M. (2003). Gas cycling and the development of miscibility in condensate reservoirs. *SPE 84070, SPE Annual Technical Conference and Exhibition.* Denver, CO.

Jessen, K., Kovscek, A. R., & Orr, F. M. (2005). Increasing CO_2 storage in oil recovery. *Energy Conversion Management, 46*(2), 293-311.

John, C. J. (1988). Geology of the Gladys McCall geopressured prospect, Cameron Parish, Louisiana. *Journal of Energy Resources Technology*, 255-261.

Jones, P. H. (1976). *Natural gas resources of the geopressured zones in the Northern Gulf of Mexico Basin: Chapter 1 of natural gas from unconventional geologic sources.* Washington, DC: National Academy of Sciences.

Juanes, R., Spiteri, E. J., Orr, F. M., & Blunt, M. J. (2006). Impact of relative permeability hysteresis on geological CO_2 storage. *Water Resources Research, 42*(12).

Killough, J. E. (1976). Reservoir simulation with history-dependent saturation functions. *SPE Journal, 16*(1), 37-48.

Knapp, R. M., Isokrari, O. F., Garg, S. K., & Pritchett, J. W. (1976). Aspects of numerical simulation of future performance of geopressured geothermal aquifers. *Second Geopressured Geothermal Energy Conference.* Austin, TX.

Knapp, R. M., Isokrari, O. F., Garg, S. K., & Pritchett, J. W. (1977). An analysis of production from geopressured geothermal aquifers. *SPE 6825, SPE Annual Fall Technical Conference.* Denver, Colorado.

Kovscek, A. R. (2002). Screening criteria for CO_2 storage in oil reservoirs. *Journal of Petroleum Science and Technology, 20*(7-8), 841-866.

Kumar, A. (2004). A simulation study of carbon dioxide sequestration in deep saline aquifers. *M.Sc. Thesis* . The University of Texas at Austin.

Kumar, A., Ozah, R., Noh, M., Pope, G. A., Bryant, S. L., Sepehrnoori, K., et al. (2005). Reservoir simulation study of CO_2 storage in deep saline aquifers. *SPE Journal, 10*, 336-348.

Lambert, M. R., Marino, S. D., Anthony, T. L., Calvin, M. W., Gutierrez, S., & Smith, D. P. (1996). Implementing CO_2 floods: No more delays . *SPE 35187, SPE Permian Basin Oil and Gas Recovery Conference.* Midland, TX.

Law, D. H.-S., & Bachu, S. (1996). Hydrogeological and numerical analysis of CO_2-disposal in deep aquifers in the Alberta sedimentary Basin. *Energy Conversion Management, 37*(6-8), 1167-1174.

Liang, Y. (2003). Carbon dioxide capture from flue gas using regenerable sodium-based sorbents. *M.Sc. Thesis*. Louisiana State University.

Littke, R., Cramer, B., Gerlin, P., Lopatin, N. V., Poelchau, H. S., Schaefer, R. G., et al. (1999). Gas generation and accumulation in the West Siberian Basin. *AAPG Bulletin, 83*, 1642-1665.

Loucks, R. G., Dodge, M. M., & Galloway, W. E. (1986). *Controls on porosity and permeability of hydrocarbon reservoirs in Lower Tertiary sandstones along the Texas Gulf Coast.* Report of Investigations No. 149, Bureau of Economic Geology, The University of Texas at Austin.

Luo, Z., & Bryant, S. L. (2010). Influence of thermo-elastic stress on CO_2 injection induced fractures during storage. *SPE International Conference on CO_2 Capture Storage, and Utilization.* New Orleans, LA.

MacDonald, R. C., Ohkuma, H., & Sepehrnoori, K. (1981). Modeling requirements for geopressured-geothermal reservoir production . *Journal of Energy Resources Technology*, 301-306.

Malik, Q. M., & Islam, M. R. (2000). CO_2 injection in the Weyburn Field of Canada: Optimization of enhanced oil recovery and greenhouse gas storage with horizontal wells. *SPE 59327, SPE/DOE Improved Oil Recovery Symposium.* Tulsa, OK.

Manrique, J. F., & Kaneko, T. (2000). Reservoir management strategies for development of gas dissolved in water (brine) reservoirs. SPE-59420-MS.

Marsden, S. S. (1979). Natural gas dissolved in brine: A major energy resource in Japan . *SPE 8355, SPE Annual Fall Technical Conference.* Las Vegas, NV.

Mathieson, A., Midgley, J., Dodds, K., Wright, I., Ringrose, P., & Saoula, N. (2010). CO_2 sequestration monitoring and verification technologies applied at Krechba, Algeria. *The Leading Edge, 29*(2), 216-221.

Matthews, C. S. (1981). Possibilities of enhancing gas production from geopressured aquifers. *SPE 9733, Society of Petroleum Engineers.*

McGuire, P. L., & Stalkup, F. I. (1995). Performance analysis and optimization of the Prudhoe Bay miscible gas project. *SPE Reservoir Engineering, 10*(2), 88-93.

Merkel, T. C., Lin, H., Wei, X., & Baker, R. (2010). Power plant post-combustion carbon dioxide capture: An opportunity for membranes. *Journal of Membrane Science, 359*, 126-139.

Mizenko, G. J. (1992). North Cross (Devonian) CO_2 flood: Status report. *SPE 24210, Eight SPE/DOE Symposium on Enhanced Oil Recovery.* Tulsa, OK.

Moberg, R., Stewart, B. D., & Stachniak, D. (2002). The IEA Weyburn CO_2 monitoring and storage project. *Greenhouse Gas Control Technologies (GHGT-6)*. Kyoto, Japan.

Nicot, J. P. (2008). Evaluation of large-scale CO_2 storage on fresh-water sections of aquifers: An example from the Texas Gulf Coast Basin. *International Journal of Greenhouse Gases Control, 2*(4), 982-993.

Nicot, J. P., Hovorka, S. D., & Choi, J. W. (2009). Investigation of water displacement following large CO_2 sequestration operations. *Energy Procedia, 1*, 4411-4418.

Nordbotten, J. M., Celia, M. A., Bachu, S., & Dahle, H. K. (2005). Semianalytical solution for CO_2 leakage through an abandoned well. *Environmental Science and Technology, 39*(2), 602-611.

Ogha, K., Sasaki, K., Deguchi, G., & Fujioka, M. (2002). Fundamental tests on carbon dioxide sequestration into coal seams. *Greenhouse Gas Control Technologies (GHGT-6).* Kyoto, Japan.

Ohkuma, H. (1986). Numerical simulation of geopressured-geothermal aquifer phenomena. *PhD dissertation*. The University of Texas at Austin.

Ohkuma, H., Knapp, R. M., & Sepehrnoori, K. (1979a). An analysis of reservoir mechanics of geopressured-geothermal aquifers. *Expanding the geothermal Frontier, V. 3*, 511-514.

Ohkuma, H., Sepehrnoori, K., Lewis, F. T., Knapp, R. M., & MacDonald, R. C. (1979b). An analysis of reservoir mechanics of geopressured-geothermal aquifers, The Brazoria County prospect. *Fourth U. S. Gulf Coast Geopressured-Geothermal Energy Conference.* Austin, TX.

Oldenberg, C. M., & Benson, S. M. (2002). CO_2 injection for enhanced gas production and carbon sequestration. *SPE 74367, SPE International Petroleum Conference and Exhibition.* Villahermosa, Mexico.

Oldenberg, C. M., Stevens, S. H., & Benson, S. M. (2004). Economic feasibility of carbon sequestration with enhanced gas recovery (CSEGR). *Energy, 29*(9-10), 1413-1422.

Orr, F. M. (2004). Storage of carbon dioxide in geologic formations. *Journal of Petroleum Technology, 56*(9), 90-97.

Oruganti, Y., & Bryant, S. L. (2009). Pressure build-up during CO_2 storage in partially confined aquifers. *Energy Procedia, 1*, 3315-3322.

Ozah, R. (2005). Numerical simulation of the storage of CO_2 and CO_2-H_2S gas mixture in deep saline aquifers. *M.Sc. Thesis*. The University of Texas at Austin.

Ozah, R., Lakshminarasimhan, S., Pope, G. A., Sepehrnoori, K., & Bryant, S. L. (2005). Numerical simulation of the storage of pure CO_2 and CO_2-H_2S gas mixtures in deep saline aquifers. *SPE 97255, SPE Annual Technical Conference and Exhibition.* Dallas, TX.

Parson, E. A., & Keith, D. W. (1998). Fossil fuels without CO_2 emissions. *Science, 282*, 1053-1054.

Pekot, L. J., & Reeves, S. R. (2002). *Modeling coal matrix shrinkage and differential swelling with CO_2 injection for enhanced coalbed methane recovery and carbon sequestration applications.* Washington, DC: Topical Report, Contract No. DE-FC26-00NT40924, US DOE.

Peneloux, A., Rauzy, E., & Freze, R. (1982). A constant correction for Redlich-Kwong-Soave volumes. *Journal of Fluid Phase Equilibria, 8*, 7-23.

Peng, D., & Robinson, D. B. (1976). A new two-constant equation of state. *Industrial and Engineering Chemistry, 15*(1), 59-64.

Plaza, J. M., Van Wagener, D. H., & Rochelle, G. T. (2010). Modeling CO_2 capture with aqueous monoethanolamine. *International Journal of Greenhouse Gas Control, 4*(2), 161-166.

Pope, G. A. (2003). *Reservoir simulation of CO_2 Storage.* Washington, DC: Final Report, Contract No. DE-FC26-01NT41145, US DOE.

Price, P. N., McKone, T. E., & Sohn, M. D. (2007). *Carbon sequestration risks and risk management.* Lawrence Berkeley National Laboratory Report, LBNL-513E.

Pruess, K. (2004). Numerical simulation of CO_2 leakage from a geologic disposal reservoir, including transitions from super- to sub-critical conditions, and boiling of liquid CO2. *SPE Journal, 9*(2), 237-248.

Pruess, K., Xu, T., Apps, J., & Garcia, J. (2003). Numerical modeling of aquifer disposal of CO_2. *SPE Journal, 8*(1), 49-60.

Quitzau, R., & Bassiouni, Z. (1981). The possible impact of the geopressured resource on conventional oil and gas exploration. *SPE 10281, SPE Annual Fall Technical Conference.* San Antonio, TX.

Quong, R., Owen, L. B., & Locke, F. E. (1982). Technical potential of methods for methane extraction from geopressured-geothermal fluids at high temperature and pressure. *Journal of Petroleum Technology, 34*(3), 504-510.

Rao, A. B., & Rubin, E. S. (2002). A technical, economic and environmental assessment of amine-based CO_2 capture technology for power plant greenhouse gas control. *Environmental Science and Technology, 36*(20), 4467-4475.

Reeves, S. R. (2001). Geological sequestration of CO_2 in deep, unmineable coalbeds: An integrated research and commercial-scale field demonstration project. *SPE 71749, SPE Annual Technical Conference and Exhibition.* New Orleans, LA.

Riney, T. D. (1988). Gladys McCall geopressured reservoir analysis. *Journal of Energy Resources Technology, 110*, 262-268.

Riney, T. D. (1991). Pleasant Bayou geopressured-geothermal reservoir analysis. *Journal of Energy Resources Technology, 114*, 315-322.

Rochana, P., Ozdogan, E., Lee, K., & Wilcox, J. (2013). Theoretical and experimental investigations of N2-selective membranes. *Energy Procedia, 37*, 1093-1103.

Rochelle, G. T. (2009). Amine scrubbing for CO_2 capture. *Science*(325), 1652-1653.

Saadatpoor, E. (2012). Local capillary trapping in geological carbon storage. *PhD Dissertation*. The University of Texas at Austin.

Salvi, S., Quattrocchi, F., Angelone, M., & Brunori, C. A. (1999). A multidisciplinary approach to earthquake research: Implementation of a geochemical geographic information system for the Gargano Site, Southern Italy. *Natural Hazard, 20*(1), 255-278.

Singh, V., Cavanagh, A., Hansen, H., Nazarian, B., Iding, M., & Ringrose, P. (2010). Reservoir modeling of CO_2 plume behaviour calibrated against monitoring data

from Sleipner, Norway. *SPE 134891, SPE Annual Technical Conference and Exhibition.* Florence, Italy.

Stein, M. H., Frey, D. D., Walker, R. D., & Pariani, G. J. (1992). Slaughter Estate Unit CO_2 flood: Comparison between pilot and field-scale performance. *Journal of Petroleum Technology, 44*(9), 1026-1032.

Stevens, S. H., Spector, D., & Riemer, P. (1998). Enhanced coalbed methane recovery using CO_2 injection: Worldwide resource and CO_2 sequestration potential. *SPE 48881, SPE International Conference and Exhibition.* Beijing, China.

Swanson, R. K., Bernard, W. J., & Osoba, J. S. (1986). A summary of the geothermal and methane production potential of U.S. Gulf Coast geopressured zones from test well data. *Journal of Petroleum Technology, 38*(12), 1365-1370.

Taggart, I. (2010). Extraction of dissolved methane in brines by CO_2 injection: Implication for CO_2 sequestration. *SPE Reservoir Evaluation Engineering, 13*(5), 791-804.

Tanner, C. S., Baxley, P. T., Crump, J. G., & Miller, W. C. (1992). Production performance of the Wasson Denver Unit CO_2 flood. *SPE 24156, Eight SPE/DOE Symposium of Enhanced Oil Recovery.* Tulsa, OK.

Tao, Q., & Bryant, S. L. (2012). Optimal control of injection/extraction wells for the surface dissolution CO_2 storage strategy. *SPE 151370, Carbon Management Technology Conference.* New Orleans, FL.

Torp, T. A., & Gale, J. (2002). Demonstrating storage of CO_2 in geological reservoirs: The Sleipner and SACS projects. *Greenhouse Gas Control Technologies (GHGT-6).* Kyoto, Japan.

Van Wagener, D. H. (2011). Stripper modeling for CO_2 removal using monoethanolamine and piperazine solvents. *PhD Dissertation*. The University of Texas at Austin.

Van Wagener, D. H., & Rochelle, G. T. (2011a). Stripper configurations for CO_2 capture by aqueous monoethanolamine. *Chemical Engineering Research and Design, 89*(9), 1639-1646.

Van Wagener, D. H., & Rochelle, G. T. (2011b). Stripper configurations for CO_2 capture by aqueous monoethanolamine and piperazine. *Energy Procedia, 4*, 1323-1330.

Van Wagener, D. H., Rochelle, G. T., & Chen, E. (2013). Modeling of pilot stripper results for CO_2 capture by aqueous piperazine. *International Journal of Greenhouse Gas Control, 12*, 280-287.

Vikas, B. (2002). Simulation of CO_2 sequestration . *M.Sc. Thesis*. The University of Texas at Austin.

Wallace, R. H., Kraemer, T. F., Taylor, R. E., & Wesselman, J. B. (1978). Assessment of geopressured geothermal resources in the Northern Gulf of Mexico Basin. *U.S. Geological Survey Circular, 790*, 132-155.

Woods, A. W., & Farcas, A. (2009). Capillary entry pressure and the leakage of gravity currents through a sloping layered permeable rock. *Journal of Fluid Mechanics, 618*, 361-379.

Wrighton, F. (1981). An economic overview of geopressured solution gas . *Fifth Geopressured Geothermal Energy Conference.* Baton Rouge, LA.

Xu, T., Apps, J. A., & Pruess, K. (2004). Numerical simulation of CO_2 disposal by mineral trapping in deep aquifers. *Applied Geochemistry, 19*(6), 917-936.

Xu, Z. K., Wang, J., Chen, W., & Xu, Y. Y. (2001). Separation and fixation of carbon dioxide using polymeric membrane contractor. *Netl Publications, 1st National Conference on Carbon Sequestration.* Washington, DC.

Zhou, Q., Birkholzer, J. T., Chin-Fu, T., & Rutqvist, J. (2008). A method for quick assessment of CO_2 storage capacity in closed and semi-closed saline formations. *International Journal of Greenhouse Gas Control, 2*(4), 626-639.

Zoback, M. D., & Gorelick, S. M. (2012). Earthquake triggering and large-scale geologic storage of carbon dioxide. *PNAS, 109*(26), 10164-10168.